DOI: 10.1002/chem.200601759

Unmasking Melon by a Complementary Approach Employing Electron Diffraction, Solid-State NMR Spectroscopy, and Theoretical Calculations—Structural Characterization of a Carbon Nitride Polymer

Bettina V. Lotsch,[a] Markus Döblinger,[a] Jan Sehnert,[b] Lena Seyfarth,[b] Jürgen Senker,*[b] Oliver Oeckler,[a] and Wolfgang Schnick*[a]

Dedicated to Professor Wolfgang Beck on the occasion of his 75th birthday

Abstract: Poly(aminoimino)heptazine, otherwise known as Liebig's melon, whose composition and structure has been subject to multitudinous speculations, was synthesized from melamine at 630 °C under the pressure of ammonia. Electron diffraction, solid-state NMR spectroscopy, and theoretical calculations revealed that the nanocrystalline material exhibits domains well-ordered in two dimensions, thereby allowing the structure solution in projection by electron diffraction. Melon ($[C_6N_7(NH_2)(NH)]_n$, plane group $p2gg$, $a=16.7$, $b=12.4$ Å, $\gamma=90°$, $Z=4$), is composed of layers made up from infinite 1D chains of NH-bridged melem ($C_6N_7(NH_2)_3$) monomers. The strands adopt a zigzag-type geometry and are tightly linked by hydrogen bonds to give a 2D planar array. The inter-layer distance was determined to be 3.2 Å from X-ray powder diffraction. The presence of heptazine building blocks, as well as NH and NH_2 groups was confirmed by ^{13}C and ^{15}N solid-state NMR spectroscopy using ^{15}N-labeled melon. The degree of condensation of the heptazine core was further substantiated by a ^{15}N direct excitation measurement. Magnetization exchange observed between all ^{15}N nuclei using a fp-RFDR experiment, together with the CP-MAS data and elemental analysis, suggests that the sample is mainly homogeneous in terms of its basic composition and molecular building blocks. Semiempirical, force field, and DFT/plane wave calculations under periodic boundary conditions corroborate the structure model obtained by electron diffraction. The overall planarity of the layers is confirmed and a good agreement is obtained between the experimental and calculated NMR chemical shift parameters. The polymeric character and thermal stability of melon might render this polymer a pre-stage of g-C_3N_4 and portend its use as a promising inert material for a variety of applications in materials and surface science.

Keywords: ab initio calculations · carbon nitrides · electron diffraction · solid-state NMR spectroscopy · solid-state structures

Introduction

The quest for binary carbon nitride C_3N_4, whose postulated material properties are believed to push the borders of ultra-hard materials, has provided a tight link between Liebig's historic work and modern materials chemistry.[1] While being re-invented in a new context in the 1980s, carbon nitride had been discussed as the ultimate de-ammonation product of a series of "ammonocarbonic acids" such as cyanamide or melamine as early as 1834.[2] All attempts to synthesize pure carbon nitride were invariably spoiled by the presence of hydrogen, yielding an amorphous, infusible material which was first obtained by Berzelius and given the name "melon" by Liebig.[2,3] As reviewed by Franklin,[3] the latter was obtained by heating to redness the yellow precipi-

[a] Dr. B. V. Lotsch, Dr. M. Döblinger, Dr. O. Oeckler, Prof. Dr. W. Schnick
Department Chemie und Biochemie
Ludwig-Maximilians-Universität
Butenandtstrasse 5–13 (D), 81377 München (Germany)
Fax: (+49) 89-2180-77440
E-mail: wolfgang.schnick@uni-muenchen.de

[b] J. Sehnert, L. Seyfarth, Prof. Dr. J. Senker
Anorganische Chemie I
Universität Bayreuth
Universitätsstrasse 30, 95447 Bayreuth (Germany)
Fax: (+49) 921-55-2788
E-mail: juergen.senker@uni-bayreuth.de

Supporting information for this article is available on the WWW under http://www.chemeurj.org/ or from the author.

tate formed by the action of chlorine on a solution of potassium or sodium thiocyanate, by heating ammonium or mercury thiocyanate, and as the final de-ammonation product on heating mixed "aquo-ammonocarbonic acids" such as ammeline or urea.[4,5] Owing to its unusual thermal stability, some doubt arose whether melon should be classified as an organic or an inorganic compound. Despite the lack of sharply defined composition, melon was assigned the empirical formula $H_3C_6N_9$, which led Redemann and Lucas to draw two alternative planar structure models based on the heptazine (cyameluric) core C_6N_7 (Scheme 1, **1a** + **1b**). Alternatively, a symmetric triangular form was proposed, whose empirical formula approaches asymptotically the limit C_3N_4 if condensations extend indefinitely (Scheme 1, **1c**).[4]

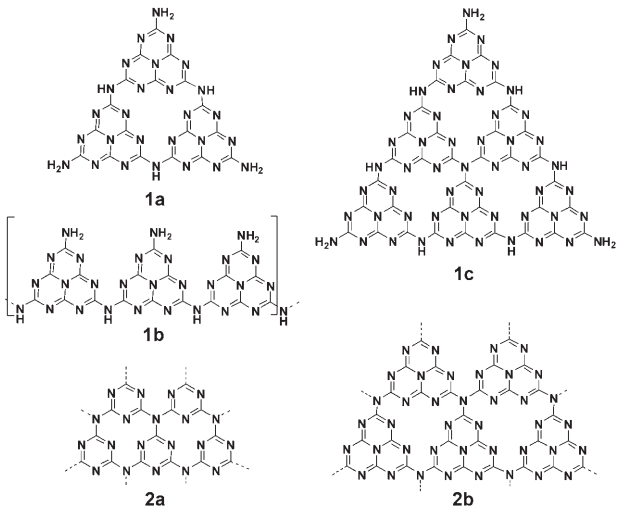

Scheme 1. Structure models proposed for melon (**1a**, **1b**) and cutouts of hypothetical structure models of graphitic carbon nitride based on triazine (**2a**) and heptazine building blocks (**2b**). The melon-derived structure "$C_{36}N_{52}H_{12}$" (**1c**) has an empirical formula intermediate between melon and g-C_3N_4.

Other structure models, including triazine-based variants, have been put forward for melon owing to the lack of detailed knowledge on the structure of its presumed monomer, melem.[6] Franklin found that the empirical composition of melon varied with the method of preparation, as he obtained samples with a hydrogen content between 1.1 and 2.0 wt%. Products with a hydrogen content of only 0.6 wt% were rationalized by assuming a mixture of several "compact" condensation products of triangular shape as for example model **1c** (Scheme 1).[3,4a] On this background, it was conjectured that "it is probably incorrect to assign any one structure to melon, for it is more than likely a mixture of molecules of different sizes and shapes. This gives rise to its amorphous character".[4a]

The gap between historic and modern carbon nitride chemistry is bridged by the hypothetical graphitic modification of C_3N_4 (g-C_3N_4), which has been calculated to be the most stable form of carbon nitride, and owing to its analogy with graphite was attributed the triazine core C_3N_3 as elementary building block (Scheme 1, **2a**).[1,7] Since then, a plethora of experimental and theoretical efforts have been made to elucidate the structure of g-C_3N_4, which failed due to the ill-defined nature of the obtained polymers.[7,8]

The search for graphitic carbon nitride typically emanates from derivatives or precursors of triazine, whose structural integrity is believed to be preserved upon thermal treatment of the starting materials. Thus, a considerable number of possible triazine-based structures—akin to graphite—has been devised and their topologies as well as their relative stabilities computed.[1d,8,10,11] For example, Kawaguchi et al. synthesized a material with the presumed formula $[(C_3N_3)_2(NH)_3]_n$ ($\equiv C_6N_9H_3$) by polycondensation of cyanuric chloride and melamine, whose electron diffraction pattern was indexed on a hexagonal cell with $a = 8.2$ Å and $d_{100} = 7.1$ Å.[7b] Demazeau et al. reported on the solvothermal synthesis of g-C_3N_4 by reacting melamine with hydrazine as a nitriding agent under supercritical conditions.[7a,g,l,o,11]

Only recently, an alternative structure model based on the heptazine nucleus emerged (**2b**, Scheme 1), reminiscent of the extensive work on melon, which still represents a highly controversial chapter in the history of C/N chemistry.[8a,12–15] Although the heptazine-based nitrogen compounds such as melem or cyameluric acid had been known for decades, the significantly less stable unsubstituted nucleus, tri-*s*-triazine, was synthesized and structurally characterized only in the 1980s.[16] Komatsu proposed polymers of melem to form upon polycondensation/pyrolysis of NH_4SCN and various heptazine derivatives.[9b,c] The as-obtained graphite-like "pseudo carbon nitrides" were classified according to their composition as "symmetric triangular forms" (cf. model **1c**, Scheme 1) or as partially condensed, irregular forms of heptazine-based polymers. In addition, the synthesis of a "cyameluric high polymer" by thermal de-ammonation of melon via a melem-dimer was postulated, affording a linear polymer composed of 42 monomers.[9d] In most cases, the X-ray powder patterns were indexed on orthorhombic unit cells ($a = 7.104$, $b = 16.190$, $c = 12.893$ Å;[9b] $a = 7.229$, $b = 21.512$, $c = 13.589$ Å).[9d] In contrast, the attempt to prepare carbon nitrides by polycondensation of melamine with the Lewis acid $ZnCl_2$ afforded a polymer with similar orthorhombic metrics, which was assigned a vacancy-network structure consisting of triazine cores.[9a]

As outlined above, the synthetic strategy that appears to be most promising to obtain reasonably well-defined carbon nitride materials includes the controlled pyrolysis of CN_xH_y precursors.[15] However, the advantage of comparatively high crystallinity usually accompanies the presence of hydrogen in the products, which at the same time seems to stabilize the structure and to function as defect site. On the other end of the experimental spectrum, high-energy techniques (ion beam sputtering, CVD, laser- or shock-wave techniques) almost exclusively afford amorphous materials with substoichiometric nitrogen content with respect to the idealized formula C_3N_4.

In this work we present the 2D structure of a material, subject to numerous speculation, that has commonly been identified with graphitic carbon nitride. We thus provide the first structural characterization of a polymeric carbon(IV) nitride based on electron diffraction and solid-state NMR spectroscopy, which at the same time resolves the controversial identity of melon.

Results and Discussion

Synthesis and characterization: A brownish polymer of the approximate composition $C_3N_{4.4}H_{1.8}$, (N: 61.2; C: 36.0; H: 1.8) determined from elemental analysis and with an average C/N ratio of 0.68 (theor. for C_3N_4: 0.75) was obtained by heating melamine (triamino-*s*-triazine) in sealed silica glass ampoules at 630 °C. Whereas at temperatures below 620 °C, melem ($C_6N_7(NH_2)_3$) was found in the products, thermolysis above 640 °C leads to rapidly increasing carbonization. It should be pointed out that heating melamine at 500 °C in an open system for several hours affords polymeric materials with different colors ranging from light yellow to dark beige. Whereas under these conditions, largely amorphous compounds are obtained, the crystallinity is significantly enhanced by pyrolyzing melamine in a closed system under an autogenous pressure of ammonia that arises from the condensation reactions. The brownish color of the as-obtained products suggests that crystallization accompanies the onset of carbonization of the sample. Small amounts of oxygen (up to 2 wt%; typically 0.5–0.7 wt%) detected in the bulk suggest that the material is prone to water absorption, as was pointed out in the literature.[17] In addition, melamine crystals were detected as impurities, which likely result from depolymerization of the product induced by ammonolysis at elevated temperatures and pressure of ammonia.[18] Possible depolymerization products other than melamine, such as dicyandiamide, were not observed as crystalline side phases; however, the presence of very small amounts of amorphous by-products such as (poly)imides below the detection level of solid-state NMR spectroscopy ($\leq$5% for CP measurements) may not entirely be excluded. Also, the comparatively harsh synthetic conditions applied in the present context likely induce heterogeneous crystallization and probably yield a broad spectrum of differently ordered domains, ranging from amorphous to nanocrystalline. Presumably, a mixture of polymers with different chain lengths is obtained, which can be considered a feature intrinsic to thermally induced polymerization processes. In this sense, the as-synthesized material, which will be referred to as "C/N/H-graphite" owing to its commonly inferred graphite-like character,[7] cannot be considered an overall homogeneous phase.

In situ temperature-programmed X-ray powder diffraction shows that the material is stable up to about 770 °C without passing through phase transitions prior to its decomposition. The observed thermal stability of this lightweight material is therefore comparable to or somewhat higher than that of aromatic polyamides and -imides.[9d]

The FTIR spectrum of C/N/H-graphite is displayed in Figure 1. Owing to obvious analogies with the vibrational spectra of melon already present in the literature,[9d,19] we will only focus on the most important results here. The well-

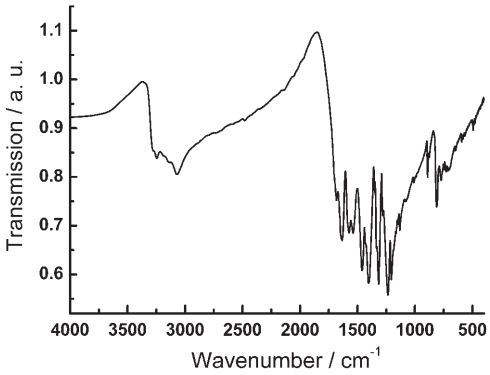

Figure 1. FTIR spectrum of melon recorded as a KBr pellet between 400 and 4000 cm^{-1}.

resolved bands indicate a fairly high degree of ordering. Whereas the sharp band at about 810 cm^{-1} can be attributed to the ring-sextant out-of-plane bending vibration characteristic of both triazine or heptazine ring systems,[13,15,20] the prominent absorption bands at 1206 and 1235 cm^{-1} and possibly 1316 cm^{-1} have been shown to be characteristic of the C–NH–C unit in melam.[19,21,22] Therefore, a similar structural motif, corresponding to either trigonal C–N(-C)–C (full condensation) or bridging C–NH–C units (partial condensation), can be inferred for the polymer. Absorption found in the N–H stretching region between 3250 and 3070 cm^{-1} proves the presence of NH and/or NH_2 groups, which are most likely integral parts of the structure.

Scanning electron microscopy images demonstrate the micro- and nanocrystalline character of the CN_xH_y material as shown in Figure 2. The morphology of the material resembles that of microcapsules, the hollow tubes and spheres with a diameter of several micrometers containing nanocrystallites. While the crystalline particles appear to be platelike, the spheres presumably result from the isotropic bulging of the particles during gas evolution in the course of condensation. Owing to the small crystallite size, structure elucidation by X-ray methods does not seem to be particularly promising.

In accordance with literature data, the X-ray diffraction pattern is indicative of a layered substance with an interlayer spacing of 3.19 Å.[7,8,14,15,24] The powder pattern resembles that of graphite, which has an interlayer spacing slightly larger than that of the carbon nitride material (3.33 Å) as shown in Figure 3. Remarkably, the strong reflection, which is commonly indexed as 002 by analogy with graphite, is sharp, whereas all *hk*0 and *h*0*l* reflections—if present at all—are weak and broadened. In addition, asymmetric shapes of the reflections ("tailing" towards higher 2θ values, as seen for the low-angle reflection at $2\theta \approx 12.6°$), are visible. These features could result from "streaking" along c^* due to

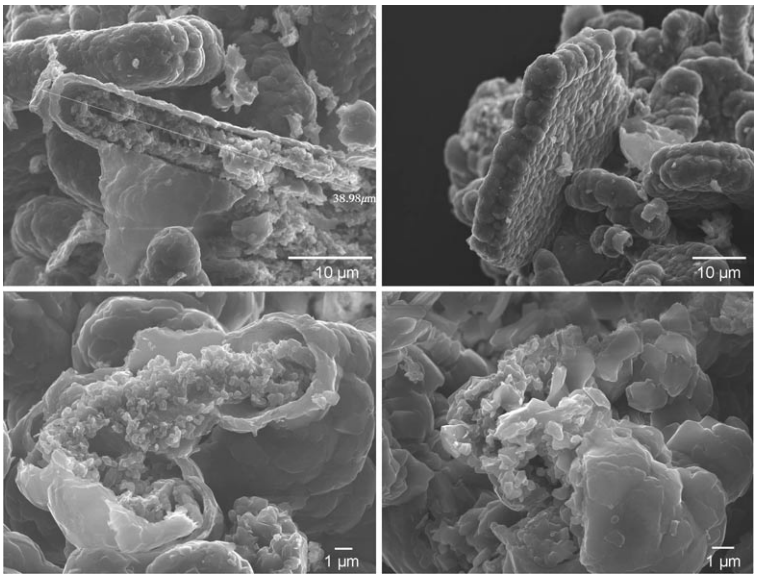

Figure 2. Scanning electron microscopy images of C/N/H-graphite, taken from various sample regions. The images reveal crystallite sizes on the nanometer- and micrometer-length scales, as well as the "porous" morphology of the sample.

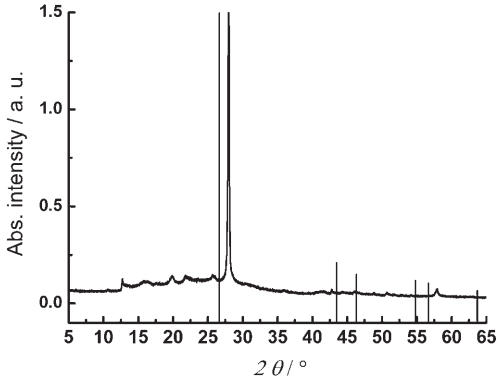

Figure 3. X-ray powder pattern ($Cu_{K\alpha 1}$ radiation) of C/N/H-graphite (continuous line) and simulation for graphite (bars). The interlayer distance (strong reflection) amounts to 3.19 Å.

2D planar disorder. However, the sharp main reflection and absence of splitting of the latter points to the layers being planar with a sharply defined interlayer spacing.

Solid-state NMR spectroscopy: Solid-state NMR spectroscopy is a valuable tool for probing the structure of semicrystalline or amorphous materials on local and intermediate length scales, as it is not dependent on the long-range order in contrast to diffraction techniques. Owing to the low sensitivity of the ^{15}N nucleus, a ^{15}N-enriched C/N/H-graphite (degree of enrichment of $\approx 25\,\%$) was synthesized starting from ^{15}N-labeled melamine.

The ^{15}N CP-MAS spectrum of the C/N/H-graphite is displayed in Figure 4 (top). The comparatively high resolution is diagnostic of a semicrystalline rather than an amorphous material. For a reliable signal assignment (as indicated in Figure 4), a CPPI (cross-polarization with polarization inversion) experiment was carried out. By evaluating the characteristic time dependence of the polarization inversion dynamics of the different ^{15}N nuclei, the number of protons covalently bonded to the latter can be ascertained. As outlined in Figure 5, three types of signals can be distinguished: The signals between $\delta = -177$ and -195 ppm, as well as the resonance at $\delta = -225$ ppm exhibit a moderate intensity loss, the continuous, slow decrease of the polarization being characteristic of tertiary nitrogen atoms. In contrast, the polarization of the signals at $\delta = -245$ and -265 ppm follows a two-step process induced by the covalently bonded protons. The intensity at the cross-over

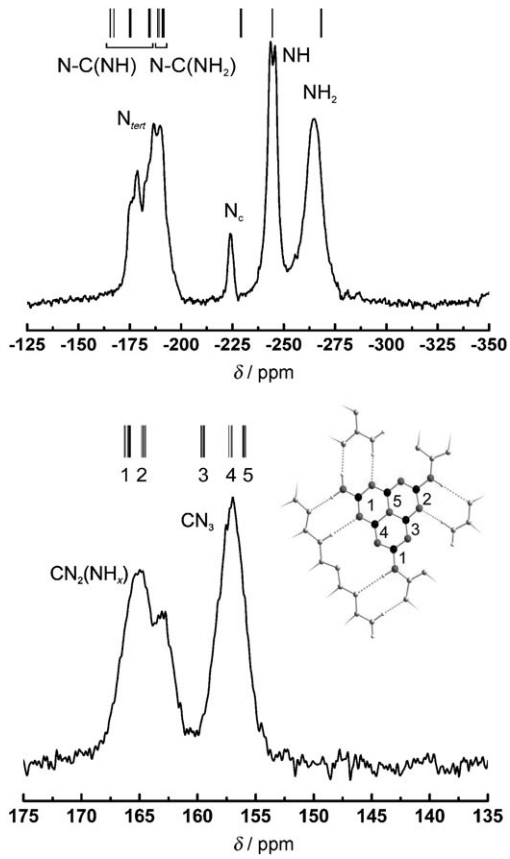

Figure 4. ^{15}N (top) and ^{13}C (bottom) CP-MAS solid-state NMR spectra of the C/N/H-graphite. The signal assignments according to ab initio calculations of the chemical shift values for the DFT-optimized cell (see inset) are indicated on top of the experimental spectra. The respective carbon sites in the structure are indicated by numbers (black: C, gray: N).

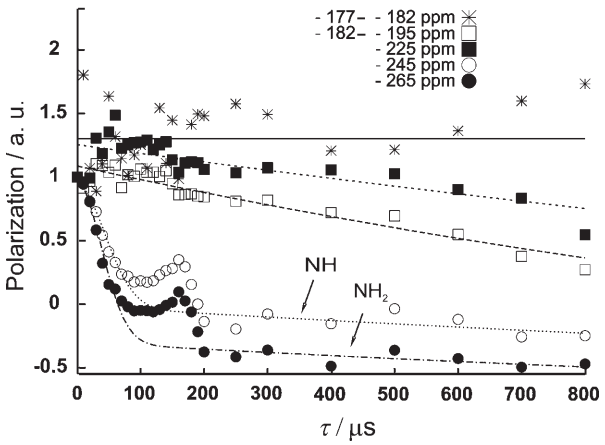

Figure 5. Evolution of the signal intensities (cf. Figure 4) during the course of a ^{15}N CPPI experiment. The polarization of the ^{15}N nuclei is given as a function of the inversion time τ_i.

between the dipolar and spin-diffusion regime is given by $[2/(n+1)]-1$ ($n=0,1,2$), thereby allowing the differentiation between NH (crossover at 0) and NH_2 (crossover at $-1/3$) nitrogen nuclei.[13,25]

Therefore, the assignment of all signals according to the proton environment of the ^{15}N nuclei is feasible. Notably, apart from tertiary nitrogen atoms expected for a fully condensed network, NH and NH_2 groups are present, which suggest the formation of an only partially condensed C/N/H network.

Information on the nature of the building blocks can be obtained from the isolated signal at $\delta=-225$ ppm in the ^{15}N spectrum. This tertiary nitrogen resonance is strongly reminiscent of the central nitrogen atom ("N_c") of the heptazine core, since it exhibits an up-field shift compared to the outer nitrogen nuclei of the ring in essentially all heptazine-based compounds studied so far.[13,26] For example, this nitrogen resonance is observed at $\delta=-234.2$ ppm for melem.[13,24] Thus, these findings furnish the first significant indication of the heptazine-based nature of the graphitic C/N/H material.

The ^{13}C CP-MAS spectrum of the product shows remarkable similarity with that of melem. In detail, two signal groups are found with peak maxima at $\delta\approx164$ and 157 ppm. In melem, two groups of carbon resonances are observed at $\delta=164.3/166.4$ and 155.1/156.0 ppm, respectively, where the low-field signals ($\delta=164$–166 ppm) were assigned to the carbon positions adjacent to the amino groups.[13,24] Based on DFT calculations, an analogous assignment of the low-field signals ($\delta=163$–165 ppm) to $CN_2(NH_x)$ and the high-field signal ($\delta=157$ ppm) to CN_3 moieties was accomplished for the C/N/H-graphite as will be discussed below. The use of different CP contact times τ_c corroborates this assignment.

To quantify the relative ^{15}N signal intensities and to draw conclusions on the degree of condensation of the presumed heptazine core, an experiment using direct excitation of the ^{15}N nuclei was carried out (Figure 6). In this experiment, the magnetization transfer from the abundant protons to the ^{15}N nuclei is circumvented, thereby rendering the signal intensities independent of the number of protons in spatial proximity. Owing to the very long relaxation time of the ^{15}N nuclei, a recycle delay between successive scans of 8 h had to be applied to ensure total magnetization recovery before each scan. Comparatively long relaxation times are diagnostic of well-ordered materials. Owing to the isotopic enrichment of melon, 16 scans were sufficient to acquire a spectrum with a reasonable signal-to-noise ratio. As depicted in Figure 6, the signal intensities show significant variations as compared to the CP-MAS spectrum in Figure 4. As expected, the tertiary nitrogen resonances gained intensity at the expense of the protonated nitrogen signals. A quantitative fit of the relative intensities indicates a ratio of the four signal groups N_{tert}:N_c:NH:NH_2 roughly corresponding to 7:1:1:1. In particular, the equal intensities of N_c, NH, and NH_2 suggests a degree of condensation approximately corresponding to that expected for melon (6:1:1:1, cf. **1a** + **1b**, Scheme 1). To sum up, evidence of only one single type of building block—heptazine—is provided by the CP-MAS and direct excitation spectra. Since atom connectivities and, hence, local structural motifs dominate the chemical shift of the nuclei, this missing spread in chemical shift values renders the presence of triazine ring systems highly unlikely. In addition, DFT calculations of the chemical shift parameters of fully condensed triazine- and heptazine-based C_3N_4 systems suggest that the chemical shift range expected for triazine-based structures would spread out way downfield as compared to the observed data, for both planar and corrugated structures.[27] This adds to the above evidence that the C/N/H-graphite is composed of heptazine rather than triazine building blocks. Accordingly, the somewhat higher intensity observed for N_{tert} may result from the admixture of minor, heptazine-based side phases exhibiting a slightly higher degree of condensation (cf. for instance structure **1c**, Scheme 1). The line width observed in the NMR spectra is slightly increased (by a factor of about 2) as compared to typical line widths of crystalline molecular compounds. This is indicative of varying chemical environments of the heptazine nuclei, which depend on the orientation of the adjacent layers as determined by the local stacking sequence. Similar

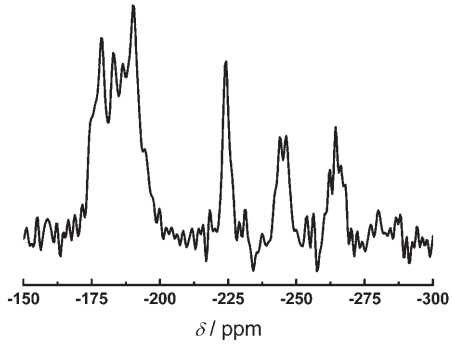

Figure 6. ^{15}N direct excitation spectrum using a recycle delay of 8 h as estimated from a ^{15}N T_1 measurement to ensure a total recovery of the magnetization. Number of scans: 16; spinning frequency: 9 kHz.

effects may be induced by different polymer lengths, which give rise to slightly altered local magnetic fields at the sites of nuclei in the vicinity of chain or layer terminations. In contrast, for a completely amorphous material the line widths should be increased by a factor of 10 to 20.

A fp-RFDR experiment was carried out to probe the homonuclear, through-space magnetization transfer between the ^{15}N nuclei. It can therefore be considered as a sensor for spatial proximities of the nuclei in the sample. By selectively exciting the NH_2 signal, the time dependence of the magnetization transfer to the surrounding ^{15}N nuclei (other than NH_2) was monitored by successively varying the mixing time in small intervals. Figure 7 (top spectra) outlines the

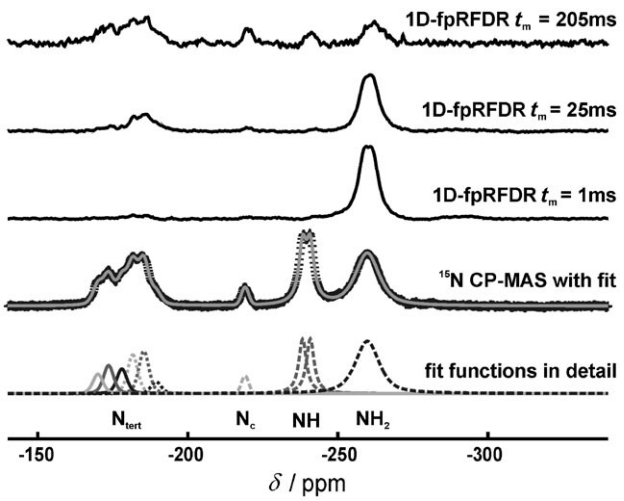

Figure 7. ^{15}N CP-MAS spectrum of the C/N/H-graphite and the corresponding overall fit (gray line; 2nd spectrum from bottom). Individual resonances of the fits (cf. Figure 8) (bottom), and 1D-fpRFDR spectra for mixing times $t_m = 1$, 25, 205 ms.

1D-RFDR spectra obtained for three mixing times ($t_m = 1$, 25, and 205 ms) corresponding to short, intermediate and long periods of magnetization transfer. Whereas for $t_m =$ 1 ms no magnetization transfer to the other nitrogen nuclei is visible, exchange commences at $t_m = 25$ ms for the high-field part of the tertiary nitrogen signals, which is visible by the growing intensity of the latter. Very weak signals can also be distinguished for the N_c and NH resonances. For long mixing times, all initial resonances are observable, which indicates a dipolar exchange of magnetization among the NH_2 nitrogen and *all* other ^{15}N nuclei in the sample. This observation is confirmed by the build-up curves (see Figure S4 in the Supporting Information), which trace the increase of magnetization at the tertiary and NH nitrogen nuclei and the concomitant loss of signal intensity at the selectively excited NH_2 nitrogen atoms. Build-up is fastest for the tertiary ^{15}N nuclei from $\delta = -195$ to -187 ppm, which therefore represent the closest neighbors of the NH_2 group. This finding is in agreement with the ab initio ^{15}N chemical shift parameters calculated for the DFT-optimized cell based on the structure solution from electron diffraction, as will be detailed below (see also Figure 4). This exchange behavior suggests homogeneity of the sample in a regime up to 30 Å. Note that the coexistence of different domains is thus limited to different stacking variants and possibly heptazine-based structural isomers, which do not give rise to additional signals in the 1D CP-MAS spectrum as outlined above. Summing up, this experiment suggests that all ^{15}N nuclei are in spatial neighborhoods and no structurally distinct phases are detectable by ^{15}N NMR spectroscopy.

Electron diffraction: Electron diffraction (ED) can provide structural insights into nanometer-sized materials. The dimensions of the C/N/H-graphite particles can be estimated to amount to 50–200 nm by transmission electron microscopy (TEM, Figure 8). In the diffraction mode, the presence of domains (Figure 9) of varying crystallinity is evident, as can

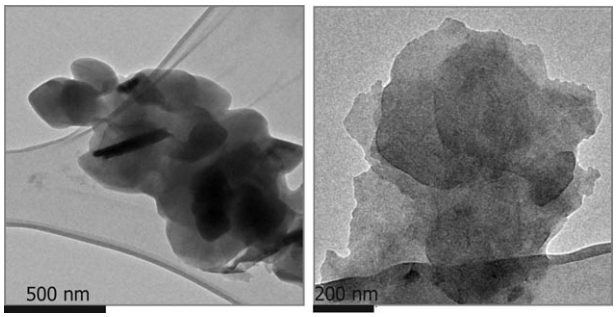

Figure 8. TEM images of the C/N/H-graphite on a carbon coated copper grid, showing the platelike nano- and microcrystals.

be seen by the asymmetric peak shapes and diffuse scattering, the latter being either intrinsic or due to amorphous cover layers. In agreement with the platelike character of the crystallites, the preferred orientation is such that most diffraction patterns are taken along the [001] zone axis, other zone axes are hardly accessible. As indicated by the X-ray powder patterns, varying degrees of "streaking" along c^* are observable (Figure 10, right), resulting from planar defects or possibly turbostratic stacking disorder. Nevertheless, SAED patterns of crystalline domains with perfect pe-

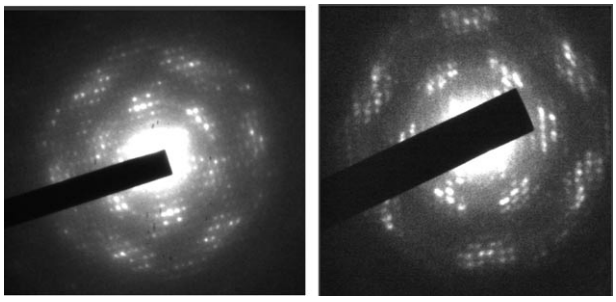

Figure 9. Selected area electron diffraction (SAED) patterns of the *hk*0 plane (zone axis [001]) of the C/N/H-graphite. All patterns exhibit different degrees of diffuse scattering and are indicative of partial disorder and/or thick sample sizes.

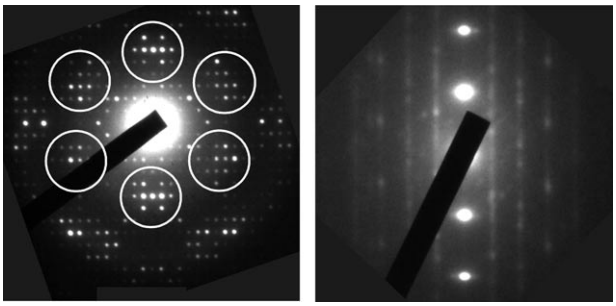

Figure 10. Left: Electron diffraction pattern of the *hk*0 plane (zone axis [001]). The pseudo-hexagonal intensity distribution is indicated by white circles. Merging the reflection groups contained in the circles (shown exemplarily; the same applies for all reflection groups) into one single spot would generate a diffraction image similar to that of graphite. Right: SAED pattern viewed perpendicular *c**. Whereas the 00*l* reflections are clearly visible, "diffuse bars" are observed parallel to *c** with a non-discrete intensity distribution ("streaking").

riodicity at least in two dimensions can be obtained, which are unaffected by the stacking disorder (Figure 10, left).

The commonly claimed graphite-like character of this material, which has led to the assumption that it is related to graphitic carbon nitride, is associated with the pseudo-hexagonal intensity distribution in the *hk*0 plane. Groups of strong reflections can be correlated with reflections of graphite with respect to their symmetry as well as the encoded distance information (Figure 10, left). Indexing the *hk*0 patterns yields a rectangular mesh with cell parameters $a=16.7$, $b=12.4$ Å. These values are similar to those determined by Komatsu from X-ray powder patterns ($a=7.104$ ($\equiv$ 2c), $b=16.190$ ($\equiv$ a), $c=12.893$ Å ($\equiv$ b)) given the layer spacing of 3.2 Å.[9b] Taking advantage of a number of beneficial factors, such as the planarity of the layers, the light atom structure, and large unit cell (small structure factors, minimum multiple scattering), the structure was solved in projection based on the electron diffraction data. Owing to the small sample thickness, the kinematical approximation $I_{hkl} \propto |F_{hkl}|^2$ could be used. Evaluation of the observed absences in the base plane (*h*0: $h=2n+1$; 0*k*: $k=2n+1$) allows for the plane group *p*2*gg*. Strong reflections remain sufficiently strong to find phase relationships using direct methods,[28a] and, thus, a figure of merit of 20.06% was obtained by employing SIR-97[29] for structure solution. Reducing the symmetry to *p*2 and introducing the mirror planes as a twin law yields better residuals. However, the data/parameter ratio obtained is very low. Therefore, the improvement of the residuals is not significant and is accompanied by an unreasonable distortion of the heptazine rings. Upon regularizing the heptazine units, the residuals again increase, so that the twin approach does not lead to a real improvement.

All carbon and nitrogen atoms could be located with reasonable bond angles and distances. Upon refinement (208 reflections, 46 parameters), *R*1 was 26.44%. As reflection intensities are affected by dynamical diffraction, better residuals have not been obtained; however, they lie in the range usually reported for refinements based on electron diffraction data.[28] After refinement, the difference Fourier synthesis has no significant maxima, which can be demonstrated by arbitrarily removing one atom from the structure model. The removed atom then yields by far the highest difference Fourier peak. The bond length precision after refinement is 0.045 Å, within this experimental error (neglecting systematic errors), the distances and angles calculated are reasonable within a 2σ interval. Crystallographic data are summarized in Table 1.[31]

Table 1. Crystallographic data of the structure solution and refinement of melon based on ED data.

formula	$C_6N_9H_3$
M_w [g mol^{-1}]	201
plane group	*p*2*gg*
instrument type	JEOL 2011 TEM
instrument details	single tilt holder, TVIPS CCD camera (F114)
incident radiation energy [kV]	200
d_{min} [Å]	0.65
a [Å]	16.7[a]
b [Å]	12.4[a]
layer distance along *c* [Å]	3.2[b]
symmetry-independent reflections	208
number of parameters	46
*R*1	26.44%
R_{rim}[29]	40.2%

[a] The error for determination of the lattice parameters from ED is estimated to be $\approx$5%. [b] Determined from X-ray powder diffraction.

To countercheck the consistency of the structure model, kinematical SAED diffraction patterns based on the structural parameters were calculated. The simulation of the *hk*0 plane is shown in Figure 11 (right), together with experimental patterns used for structure solution. The patterns agree well, although the experimental intensity distribution deviates slightly from the *mm*2 symmetry of the plane group. Note however, that the symmetry of the precession patterns is significantly less violated.

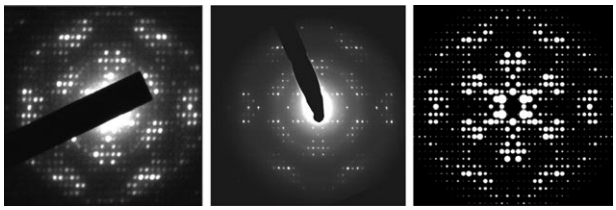

Figure 11. Experimental (left, middle) *hk*0 diffraction patterns, from which the structure solution in projection was accomplished. The left diffraction pattern was recorded under "static" conditions and its intensities merged with a second pattern (not shown); the middle pattern was recorded by using the precession technique.[27g,30] Right: Simulation of an SAED pattern of the 0th layer based on the proposed structural model, assuming ideal kinematical scattering of electrons.

The 2D projection of the crystal structure is displayed in Figure 12. The layers comprise infinite chains of "melem-monomers" condensed via N(H) bridges, thereby forming a

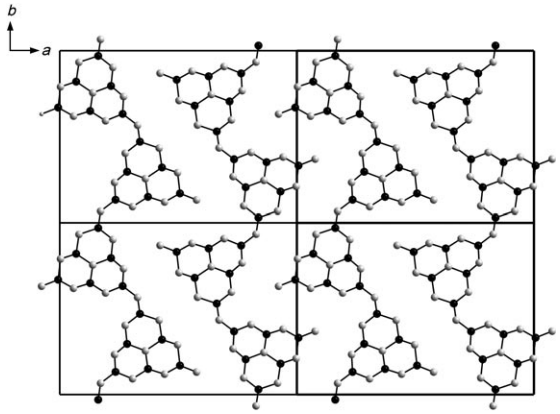

Figure 12. Projection of the structure of melon. Hydrogen atoms and molecular fragments from adjacent strands are omitted for clarity; black: C, gray: N.

closely packed two-dimensional array. The heptazine strands are arranged in a zigzag-type fashion, allowing close N···N contacts of 3.1–3.4 Å between adjacent strands, which are bridged by medium strong hydrogen bonds between the ring-nitrogen atoms and the NH and NH_2 groups, respectively. Covalent interactions within the heptazine backbone and formation of a delocalized π system seem to play a pivotal role in fixing the planar geometry of the strands. Van der Waals-type interactions between the layers are likely to contribute significantly to the overall stabilization of the system; however, they appear to be largely unselective toward a particular kind of stacking sequence.

As the structure is built up from infinite 1D chains instead of 2D atomic arrays it does not represent any structure model postulated for hypothetical g-C_3N_4. In contrast, it corresponds to the "polymer" structure model proposed for melon (**1b**, Scheme 1),[3,4,9b] whose existence has therefore been substantiated. Detailed statements on the structure of the melon strands are now possible, as for instance the zigzag-type arrangement of the heptazine motifs as well as the close packing of the chains leading to a tightly hydrogen-bonded 2D array. Furthermore, the alternative structure model postulated for melon, which is based on a triangular-shaped trimer of melem (**1a**, Scheme 1), can be discarded at least in the present case. However, this does not in principle disavow the existence of this structural isomer of melon.

The structure solution presented above allows the unique determination of the 2D structure of melon, and is in full agreement with the spectroscopic data presented above. However, the stacking disorder of the bulk sample seems to impede a comprehensive 3D approach, as due to the disorder it may not seem straightforward that the projection yields the structure of a single layer. Nevertheless, possible interpretations of the structure projection will be delineated in the following.

As a starting basis, we assume that the 2D projection delineated above is only compatible with some sort of AAA… type stacking. Given the fact that X-ray powder patterns, theoretical calculations (see below), and the expected planarity of heptazine cores and amide/imide moieties[7a–c,8,14] indicate overall planarity of the layers, the maximum symmetry of a 3D structure in the case of eclipsed layers is given by space group *Pbam*. However, theoretical calculations (see below) suggest a lateral displacement of adjacent layers to be far more likely. These displacements become favorable, since π-stacking interactions usually require a slight displacement of adjacent layers to prevent repulsion of the negatively polarized π orbitals.[32] The above requirements can be met by considering layer-offsets in which *p*2*gg* symmetry is retained in the projections. In other words, it is reasonable to assume monoclinic 3D symmetry, which implies that the layers are laterally shifted along either *a* or *b* with a monoclinic angle $\neq$ 90° and an AAA… type of stacking. When viewed along [001], the associated diffraction patterns are very similar to those obtained for an orthorhombic setting. Therefore, the structure can alternatively be solved in the $P2_1/a$ space group (cell setting $a = 12.4$, $b = 16.7$ Å, β between 92 and 115°, layers shifted along the *a* axis). Note that a layer offset along the *b* axis has the same negligible effect on the structure solution. Apart from slight distortions of the heptazine building blocks for $\beta \neq 90°$, the structure projection of eclipsed layers using orthorhombic and monoclinic variants, respectively, are hardly distinguishable. Other ordered models, such as those with an ABA… layer sequence, are incompatible with the experimental data; however, alternative explanations might be considered.

It seems unlikely that the thickness of the sample corresponds to only a few layers, which would yield 2D scattering and lead to an interpretation of the diffraction pattern in terms of a section through diffuse streaks along *c**. However, in the case of statistically shifted (but not rotated) layers, without any periodicity of the stacking sequence (cf. powder diagram, Figure 3), the *z* component of Patterson vectors is lost, and the *hk*0 section would be likewise representative of interatomic distances only perpendicular to *c*. In other words, a structure determination would yield the structure of a single layer. Diffraction patterns like that shown in Figure 10 (right) might corroborate this situation;[33] however, it is impossible to ascertain the exact zone axis orientation. Therefore, we can conclude that the true situation is to be found between the borderline cases outlined here.

Theoretical calculations: Theoretical calculations were used as an independent verification of the structure model obtained from electron diffraction. To this end, complementary calculations were carried out based on three different computational methods. Both a single chain comprising nine heptazine molecules, as well as an array of six chains containing six heptazine monomers each were optimized by using the PM3 method.[34,35]

Energy minimization reveals that the single zigzag chain as found by ED already possesses a stable molecular arrangement in the gas phase. Its geometry after optimization is outlined in Figure 13 (right). As an alternative, the classically proposed straight melon chain bends upon energy minimization as demonstrated in Figure 13 (left). The tendency

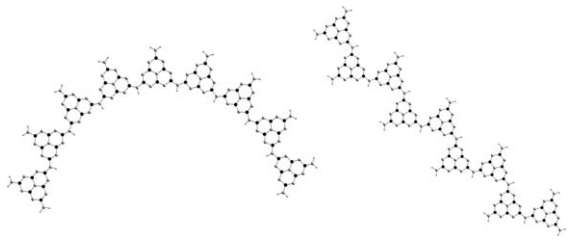

Figure 13. PM3-optimized polymeric models of melon. Left: "Classical" model of an initially linear (starting geometry) melon chain with identical alignment of the heptazine monomers. The linear chain bends upon energy minimization. Right: Zigzag chain of melon as obtained from ED. Gray: N; black: C; gray: H; the positions of the latter are empirically fitted.

of a pair of NH-bridged heptazine rings to bend apart is also visible in the linear zigzag arrangement, whereby the alternating curvatures about every NH bridge compensate, yielding an overall linear array. When assembling six zigzag chains into a 2D arrangement according to the structure proposed by ED, a planar oligomer is obtained upon optimization, which is highly stabilized by a tight hydrogen-bonding network (compare Figure 14).

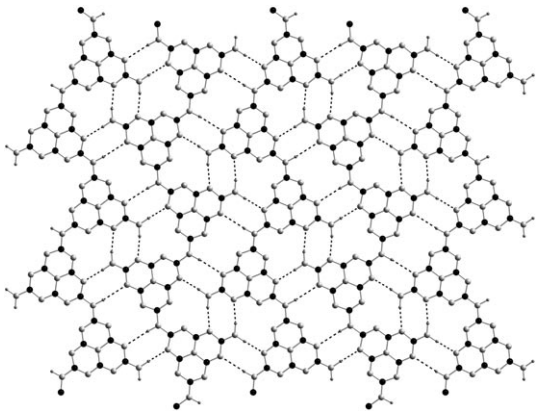

Figure 14. Planar cluster of melon after geometry optimization under periodic boundary conditions using CASTEP. The hydrogen positions are empirically fitted and the hydrogen-bonding network is indicated by black dots. Gray: N; black: C; gray: H.

To calculate the NMR chemical shift parameters for a single layer of melon, the latter was further optimized by using DFT (Figure 14).[36] The periodicity of the PM3-optimized core region of the above planar oligomer allowed the extraction of the *a*/*b* cell parameters and the establishment of a rectangular unit mesh. Although symmetry restrictions were not applied during structure optimization, a planar structure with a rectangular mesh was retained. Whereas the resulting *b* axis matches the value found by calculations at the PM3 level, the *a* axis is slightly elongated as outlined in Table 2. The overestimation of the *a* axis can be rationalized by the poor description of dispersion forces in hydrogen-bonding networks obtained by using DFT. Furthermore, attempts to optimize an orthorhombic unit cell with an interlayer spacing of 3.2 Å does not lead to a minimum on the energy surface. This renders orthorhombic metrics associated with an AAA… stacking extremely unlikely.

Table 2. Experimental and calculated lattice parameters for the structure of melon obtained from ED and different theoretical approaches.

Method	*a* [Å]	*b* [Å]	Interlayer distance [Å]
CASTEP[a]	17.1	12.8	(4.43)[a]
PM3[b]	16.6	12.7	
DREIDING	16.7–16.8	12.8	3.2–3.4
TEM/XRD	16.7[c]	12.4[c]	3.2[d]

[a] Constrained during geometry optimization. [b] Cluster of 36 hepatazine units arranged in six planar zigzag chains. [c] Estimated error ≈5%. [d] X-ray powder diffraction.

An overall description including dispersion interactions between individual layers is possible based on force field methods.[37,38] The *a* and *b* axes are in excellent agreement with the values calculated by using PM3 and CASTEP (Table 2). For an eclipsed layer arrangement, which is considered to be energetically unfavorable in terms of interlayer van der Waals interactions, the repulsive inter-planar forces are maximized, and a layer distance of 3.4 Å is obtained. In contrast, for layer arrangements exhibiting an offset stacking—not complying with orthorhombic metrics—cells with interlayer distances of 3.2 Å were found, as observed in the experiment.

For the DFT-optimized unit mesh, ab initio ^{13}C and ^{15}N NMR chemical shift parameters were calculated. As demonstrated in Figure 4, the calculated ^{13}C and ^{15}N chemical shifts are in good agreement with those in experimental spectra and confirm the overall signal assignments extracted from the CPPI experiment. The ^{13}C chemical shift range is reproduced by the calculations; in the theoretical ^{15}N spectrum, the resonance of the central nitrogen atom is slightly shifted towards higher field; the same tendency is observed for the NH and NH_2 groups. The calculated chemical shifts also allow one to distinguish between tertiary nitrogen atoms bonded to different NH_x groups, since they are directly affected by the surrounding NH (low-field shift) and NH_2 moieties (high-field shift), respectively. These observations match well with the results from the 1D fp-RFDR NMR experiment and confirm the structure model derived from the ED experiments.

Conclusion

The above results shed light on the long-standing debate concerning the identity of Liebig's inert compound "melon", whose structure has now been proven for the first time. The 2D structure of melon reveals the heptazine molecular building blocks and polymeric nature of this important CN_x precursor. Owing to the weak attractive interlayer forces, the "bulk" 3D structure is intrinsically affected by inherent planar defects associated with translations of the layers. Different energetically similar stacking modes with various translational layer offsets are likely to contribute to the

overall 3D structure.[39] This feature adds to the special importance of understanding the 2D arrangement of the molecular building blocks.

Considering the fact that melon is composed of planar layers built up by a carbon(IV) nitride core (heptazine units), this compound may be considered as a "defective g-C_3N_4" material, whose graphite-like topology may in fact result from the presence of network terminations in the form of NH and NH_2 groups. These function as triggers for strain release in such a way that buckling of the sheets is prevented. As has recently been noted,[14b] melon (in that work called g-C_3N_4) may therefore be considered a promising functional material in catalysis or surface science, and at the same time represent a pre-stage of graphitic carbon nitride. Along the same lines, the recently synthesized sp^3-hybridized carbon nitride imide $C_2N_2(NH)$, which represents a formal pre-stage of 3D C_3N_4, can be considered the high-pressure analogue of melon.[40]

However, the existence of melon highlights characteristic differences between graphite and "graphitic" carbon nitride materials, and in doing so, demonstrates that the analogy between the two systems is clearly limited both with respect to chemical and structural aspects. Given the fact that essentially all attempts to prepare g-C_3N_4 from hydrogen-containing precursors yield materials with similar structural features and hydrogen contents, we hypothesize that the products of the frequently claimed syntheses of graphitic carbon nitride have in fact rather been polymers such as melon or related compounds.[7,14,11,9a–c] We can thus add the first direct evidence to the ongoing debate on the structure of the hypothetical g-C_3N_4, that triazine-based models, which are still predominantly being discussed in the literature, should henceforward be assessed very critically. Therefore, the present work may stimulate a careful re-evaluation of commonly accepted paradigms about the existence and structure of graphitic carbon nitride.

Experimental Section

Synthesis of melon: Pyrolyses of melamine were carried out in sealed silica glass ampoules under vacuum at temperatures between 560 and 600 °C, or predominantly under dry argon at temperatures between 620 and 640 °C. Typically, melamine (230 mg, 1.83×10^{-3} mol; ≥ 99 %, Fluka) was transferred into a thick-walled silica glass tube ($\varnothing_{ext.}$ 15 mm, $\varnothing_{int.}$ 11 mm), from which water had been removed by thorough heating and evacuation. The tube was sealed by using a hydrogen burner at a length of about 120 mm. The ampoule was then placed in a vertical tube furnace and heated (1 K min^{-1}) to 630 °C, at which temperature the sample was held for 12 to 36 h. The cooling rates did not notably affect the crystallinity of the products, so that the furnace was typically switched off and the sample was allowed to cool down to room temperature over several hours. The sample was then isolated by carefully breaking the ampoule, upon which a significant amount of HCN and ammonia was released. The yield of brownish residue typically amounted to 38–57 %; approximately 8–10 % were recovered from the top of the ampoule in the form of a brown sublimate mixed together with long, needle-shaped melamine crystals. To purify the residue and eliminate melamine and—present to only a small extent—melem crystals, the product (≈80–100 mg) was transferred into a Duran ampoule (pre-dried in vacuo under heating), which was sealed off under an atmosphere of argon and heated to temperatures around 600 °C (1 K min^{-1}) for at least 12 h. Alternatively, admixtures of the starting material melamine were removed by sublimation using a cold finger integrated into a glass tube. Upon purification, the brownish material lightened up, thereby changing its color into reddish-brown.

^{15}N-enriched melamine was prepared according to the procedure introduced by Jürgens et al.[13,24] Sodium tricyanomelaminate $Na_3[C_6N_9]$ was prepared by heating sodium dicyanamide $Na[N(CN)_2]$ (2 g; ≥ 96 %, Fluka) to 500 °C (5 K min^{-1}) in a quartz tube under pressure equalization and subsequently reacting the as-obtained material (742.5 mg, $2.78\ 10^{-3}$ mol) with $^{15}NH_4Cl$ (183 mg, 3.36×10^{-3} mol, ≥ 98 %, Cambridge Isotopes) in a Duran tube (length: 160 mm, $\varnothing_{ext.}$: 26 mm, $\varnothing_{int.}$: 24 mm) at 470 °C (1 K min^{-1}) for 12 h.[13,24] The raw material was further purified by sublimation (1 Pa, 220 °C).

General techniques: Elemental analyses were performed by using a commercial C, H, N elemental analyzer system Vario EL (Elementar Analysensysteme GmbH).

XRD measurements were performed on a Stoe-Stadi P diffractometer. High-temperature in situ X-ray diffraction was carried out on a STOE Stadi P powder diffractometer (Ge(111)-monochromated $Mo_{K\alpha1}$ radiation, $\lambda = 70.093$ pm) with an integrated furnace using unsealed quartz capillaries ($\varnothing$ 0.5 mm) as sample containers.

FTIR measurements were carried out on a Bruker IFS 66v/S spectrometer. Spectra of the samples were recorded by utilizing KBr pellets (1 mg sample, 500 mg KBr, hand press with press capacity 10 kN) in an evacuated cell equipped with a DLATGS detector at ambient conditions between 400 and 4000 cm^{-1}.

Scanning electron microscopy was performed on a JEOL JSM-6500F equipped with a field emission gun at an acceleration voltage of 10 kV. Samples were prepared by putting the powder specimen on adhesive conductive pads and subsequently coating them with a thin conductive carbon film.

Solid-state NMR spectroscopy: ^{13}C and ^{15}N CP-MAS solid-state NMR spectra were recorded at ambient temperature on the conventional impulse spectrometers DSX Avance 500 (Bruker) and DSX Avance 400 (Bruker) operating at a proton resonance frequency of 500 MHz and 400 MHz, respectively. The samples were contained in 4-mm ZrO_2 rotors, which were mounted in standard double-resonance MAS probes (Bruker). The ^{13}C and ^{15}N signals were referenced with respect to TMS and nitromethane, respectively. Data collection of all experiments was performed applying broadband proton decoupling using a TPPM sequence.[41] For the CP MAS spectra of both nuclei a ramped cross-polarization sequence was employed where the ^{1}H pulse amplitude was decreased linearly by 50 %. Contact times between 10 ms and 20 ms were used and the recycle delay was chosen to allow a nearly complete magnetization recovery optimized via ^{1}H spin-lattice relaxation experiments. The spinning frequencies ν_{rot} varied between 7 and 12 kHz. To determine the number of covalently bonded protons to the nitrogen atoms, a ^{15}N CPPI[25] (cross-polarization combined with polarization inversion) experiment was performed ($\nu_{rot} = 6$ kHz). The polarization inversion behavior was probed by varying the inversion time from 0.2 to 800 μs (28 spectra), with an initial contact time of 2 ms. ^{15}N direct excitation spectra were acquired with three back-to-back 90° pulses to eliminate unwanted contributions from the probe and ringing effects.[42] The nutation frequency and the recycle delay were adjusted to 75 kHz and 28800 s (= 8 h) (estimated from a ^{15}N T_1 measurement) to ensure a total recovery of the magnetization. A total amount of 16 scans was collected and the spinning frequency was set to 9 kHz. To probe homonuclear ^{15}N connectivities and distances, selective excitation fp-RFDR experiments were performed by using a XY-16 phase cycle.[42] For the fp-RFDR mixing block active rotor synchronization was applied with $\nu_{rot} = 15$ kHz. The length of the soft 180° pulse in the middle of each rotor period was adjusted according to $p(180°) = 0.3\cdot1/\nu_{rot}$ corresponding to a nutation frequency of 25 kHz. To ensure a selective excitation of the ^{15}N resonance of the NH_2 groups a CP sequence with a short CP contact time (90 μs) was followed by a comb of two 90° pulses (3.4 μs) on-resonant on the NH_2-signal with an interpulse spacing τ between 280 μs and 340 μs corresponding to $\tau =$

$^1/_4(\nu(NH)-\nu(NH_2))^{-1}$. The short contact time excites only NH and NH_2 resonances significantly. Afterwards the comb of 90° pulses allows one to dephase the magnetization of the off-resonant resonance while preserving the magnetization of the on-resonant one.

Electron diffraction/transmission electron microscopy: ED and TEM measurements were carried out on a JEOL 2011 instrument equipped with a tungsten cathode operating at 200 kV. The images were recorded using a TVIPS CCD camera (F114). The sample was finely dispersed by sonication in ethyl alcohol suspension for 30 minutes, and a small amount of the suspension was subsequently dispersed on a copper grid coated with holey carbon film. The grids were mounted on a single tilt holder with a maximum tilt angle of 30° and subsequently transferred to the microscope. Suitable crystallites were singled out among those yielding diffraction patterns of main poles, typically with the zone axis [001] aligned along the electron beam. The selected-area aperture was adapted in each case to the size of the selected thin crystalline domains. Precession experiments were conducted by using a FEI Tecnai 12 transmission electron microscope with a LaB_6 cathode, operating at 120 kV and equipped with a Spinning Star precession interface (NanoMEGAS). A precession angle of approximately 1.5° was applied. The images were recorded on a TVIPS 2k CCD camera (F224HD) with a dynamic range exceeding 25000:1. Reflection intensities were extracted by using the ELD program package;[44] for simulation of the kinematical diffraction patterns the program JSV1.08 Lite[45] was employed. Calculation of the electron diffraction patterns was done using the programs VEC[46] and JEMS.[47] In principle, it is possible to solve a structure provided the strong reflections remain sufficiently strong to find phase relationships using direct methods.[28a] To quantify all strong *hk*0 reflections, intensities of two *hk*0 diffraction patterns were merged, yielding a dataset of 208 independent reflections. Evaluation of the observed absences in the base plane (*h*0: $h=2n+1$; 0*k*: $k=2n+1$) indicates the presence of the plane group *p*2*gg*. Owing to the lack of detailed three-dimensional information, the structure was solved by using the space groups $P2_12_12$ or *Pbam*, which correspond to the plane group *p*2*gg* in (001) projection. The most probable solution as found by SIR-97[29a] had a figure of merit of 20.06 %.[29b] The heptazine molecular unit was obtained without prior fixation of parameters. Refinement of the ED data for calculation of Fourier maps was done with the program SHELX-97,[48] using the electron form factors as given by Doyle and Turner.[49]

Calculations: In the cluster approach the semiempirical PM3 method[34] was used for structure optimization with the Gaussian03 program package.[35] The input structures were created from the ED structure solution with hydrogen added to the NH and NH_2 groups. DFT calculations under periodic boundary conditions were performed with the MS Modelling 4.0 package by Accelrys. The input cell was created in orthorhombic symmetry from a cutout in the core region of the PM3-optimized structure. For the CASTEP[36] calculations the PBE functional and ultrasoft pseudopotentials were taken with sampling over 6 k-points. In the structure optimization of the input cell an energy cutoff of 280 eV was used. To ensure that the dispersion interaction between neighboring layers become negligible, a constrained slab of 4.43 Å along the *c* axis was introduced. NMR parameters were calculated with a cutoff of 350 eV for the optimized cell. For a core cutout of the PM3-optimized cluster the Hirschfeld charges were determined with the $DMol^3$ program, the PBE functional and the DNP basis set.[38] These partial charges were used in flexible body structure optimizations of the input cell with the Dreiding force field.[37] By default, 1,4-intramolecular electrostatic interactions were excluded from the energy evaluation.

Acknowledgements

We gratefully acknowledge financial support that was granted from the Deutsche Forschungsgemeinschaft (DFG) (projects SCHN 377/12–1 and SE 1417/2–1), Fonds der Chemischen Industrie (FCI), the BMBF, and the Studienstiftung des Deutschen Volkes (scholarships for B. V. Lotsch). We gratefully acknowledge NanoMEGAS and TVIPS for providing us with their equipment and for experimental support to obtain the precession pattern, especially I. Daberkow and J. Portillo. We also thank Prof. E. Rössler (University of Bayreuth) for making available his NMR equipment, and Mrs. C. Buhtz for her support with the data analysis.

[1] a) M. L. Cohen, *Phys. Rev. B* **1985**, *32*, 7988; b) A. Y. Liu, M. L. Cohen, *Science* **1989**, *245*, 841; c) C.-M. Sung, M. Sung, *Mater. Chem. Phys.* **1996**, *43*, 1; d) D. M. Teter, R. J. Hemley, *Science* **1996**, *271*, 53.
[2] J. Liebig, *Ann. Pharm.* **1834**, *10*, 10.
[3] E. C. Franklin, *J. Am. Chem. Soc.* **1922**, *44*, 486.
[4] a) C. E. Redemann, H. J. Lucas, *J. Am. Chem. Soc.* **1940**, *62*, 842; b) L. Pauling, J. H. Sturdivant, *Proc. Natl. Acad. Sci. USA* **1937**, *23*, 615.
[5] B. Bann, S. A. Miller, *Chem. Rev.* **1958**, *58*, 131.
[6] a) L. Costa, G. Camino, G. Martinasso, *Polym. Prepr. Am. Chem. Soc. Div. Polym. Chem.* **1989**, *30*, 531; b) H. May, *J. Appl. Chem.* **1959**, *9*, 340.
[7] a) I. Alves, G. Demazeau, B. Tanguy, F. Weill, *Solid State Commun.* **1999**, *109*, 697; b) Kawaguchi, K. Nozaki, *Chem. Mater.* **1995**, *7*, 257; c) E. G. Gillan, *Chem. Mater.* **2000**, *12*, 3906; d) Q. Guo, Y. Xie, X. Wang, S. Lv, T. Hou, X. Liu, *Chem. Phys. Lett.* **2003**, *380*, 84; e) J. L. Zimmermann, R. Williams, N. Khabashesku, J. L. Margrave, *Nano Lett.* **2001**, *1*, 731; f) M. Todd, J. Kouvetakis, T. L. Groy, D. Chandrasekhar, D. J. Smith, P. W. Deal, *Chem. Mater.* **1995**, *7*, 1422; g) H. Montigaud, B. Tanguy, G. Demazeau, I. Alves, S. Courjault, *J. Mater. Sci.* **2000**, *35*, 2547; h) V. N. Khabashesku, J. L. Zimmerman, J. L. Margrave, *Chem. Mater.* **2000**, *12*, 3264; i) J. Kouvetakis, A. Bandari, M. Todd, B. Wilkens, *Chem. Mater.* **1994**, *6*, 811; j) D. R. Miller, D. C. Swenson, E. G. Gillan, *J. Am. Chem. Soc.* **2004**, *126*, 5372; k) D. R. Miller, J. Wang, E. G. Gillan, *J. Mater. Chem.* **2002**, *12*, 2463; l) S. Courjault, B. Tanguy, G. Demazeau, *C. R. Acad. Sci. Ser. IIc: Chim.* **1999**, *2*, 487; m) Z. H. Zhang, K. Leinenweber, M. Bauer, L. A. J. Garvie, P. F. McMillan, G. H. Wolf, *J. Am. Chem. Soc.* **2001**, *123*, 7788; n) Q. Guo, Y. Xie, X. J. Wang, S. Zhang, T. Hou, S. Lv, *Chem. Commun.* **2004**, *1*, 26; o) H. Montigaud, B. Tanguy, G. Demazeau, I. Alves, M. Birot, J. Dunogues, *Diamond Relat. Mater.* **1999**, *8*, 1707.
[8] a) E. Kroke, M. Schwarz, *Coord. Chem. Rev.* **2004**, *248*, 493; b) S. Muhl, J. M. Mendez, *Diamond Relat. Mater.* **1999**, *8*, 1809; c) T. Malkow, *Mater. Sci. Eng. A* **2001**, *302*, 311; d) M. C. dos Santos, F. Alvarez, *Phys. Rev. B* **1998**, *58*, 13 918.
[9] a) T. Komatsu, *J. Mater. Chem.* **2001**, *11*, 799; b) T. Komatsu, *J. Mater. Chem.* **2001**, *11*, 802; c) T. Komatsu, T. Nakamura, *J. Mater. Chem.* **2001**, *11*, 474; d) T. Komatsu, *Macromol. Chem. Phys.* **2001**, *202*, 19.
[10] D. T. Vodak, K. Kim, L. Iordanidis, P. G. Rasmussen, A. J. Matzger, O. M. Yaghi, *Chem. Eur. J.* **2003**, *9*, 4197.
[11] G. Demazeau, *J. Mater. Chem.* **1999**, *9*, 15.
[12] E. Kroke, M. Schwarz, E. Horath-Bordon, P. Kroll, B. Noll, A. D. Norman, *New J. Chem.* **2002**, *26*, 508.
[13] B. Jürgens, E. Irran, J. Senker, P. Kroll, H. Müller, W. Schnick, *J. Am. Chem. Soc.* **2003**, *125*, 10 288.
[14] a) M. Groenewolt, M. Antonietti, *Adv. Mater.* **2005**, *17*, 1789; b) F. Goettmann, A. Fischer, M. Antonietti, A. Thomas, *Angew. Chem.* **2006**, *118*, 4579; *Angew. Chem. Int. Ed.* **2006**, *45*, 4467.
[15] a) B. V. Lotsch, W. Schnick, *Chem. Mater.* **2005**, *17*, 3976; b) B. V. Lotsch, W. Schnick, *Chem. Mater.* **2006**, *18*, 1891.
[16] a) R. S. Hosmane, M. A. Rossman, N. J. Leonard, *J. Am. Chem. Soc.* **1982**, *104*, 5497; b) A. M. Halpern, M. A. Rossman, R. S. Hosmane, N. J. Leonard, *J. Phys. Chem.* **1984**, *88*, 4324; c) M. Shahbaz, S. Urano, P. R. LeBreton, M. A. Rossman, R. S. Hosmane, N. J. Leonard, *J. Am. Chem. Soc.* **1984**, *106*, 2805.
[17] D. D. Cubicciotti, W. M. Latimer, *J. Am. Chem. Soc.* **1948**, *70*, 3509.
[18] C. Grundmann, A. Kreutzberger, *J. Am. Chem. Soc.* **1955**, *77*, 6559.
[19] a) A. I. Finkel'shtein, N. V. Spiridova, *Russ. Chem. Rev.* **1964**, *33*, 400; b) A. I. Finkel'shtein, *Opt. i Spektr.* **1959**, *6*, 17.
[20] a) M. K. Marchewka, *Bull. Korean Chem. Soc.* **2004**, *25*, 466; b) M. K. Marchewka, *J. Chem. Res. Synop.* **2003**, 518; c) P. J. Larkin,

M. P. Makowski, N. B. Colthoup, *Spectrochim. Acta* **1999**, *55*, 1011; d) W. Jeremy-Jones, W. J. Orville-Thomas, *Trans. Faraday Soc.* **1959**, *55*, 193; e) E. N. Boitsov, A. I. Finkel'shtein, *Russ. Chem. Rev.* **1962**, *31*, 712.

[21] a) M. Takimoto, *Kogyo Kagaku Zasshi* **1961**, *64*, 1452; b) M. Takimoto, *Kogyo Kagaku Zasshi* **1964**, *85*, 168.

[22] B. V. Lotsch, W. Schnick, *Chem. Eur. J.* DOI: 10.1002/chem.200601291.

[23] V. V. Khorosheva, A. I. Finkel'shtein, *Zh. Fiz. Khim.* **1962**, *36*, 1055.

[24] B. Jürgens, Ph. D. thesis, University of Munich (Germany), Shaker, Aachen, **2004**.

[25] C. Gervais, F. Babonneau, J. Maquet, C. Bonhomme, D. Massiot, E. Framery, M. Vaultier, *Magn. Reson. Chem.* **1998**, *36*, 407.

[26] a) A. Sattler, Diploma thesis, University of Munich (Germany), **2005**; b) A. Sattler, L. Seyfarth, J. Senker, W. Schnick, *Z. Anorg. Allg. Chem.* **2005**, *631*, 2545.

[27] J. Sehnert, K. Bärwinkel, J. Senker, *J. Phys. Chem. B*, **2007**, submitted.

[28] a) T. E. Weirich, X. Zou, R. Ramlau, A. Simon, G. L. Cascarano, C. Giacovazzo, S. Hovmöller, *Acta Crystallogr. Sect. A* **2000**, *56*, 29; b) T. E. Weirich, R. Ramlau, A. Simon, S. Hovmöller, X. Zou, *Nature* **1996**, *382*, 144; c) U. Kolb, G. N. Matveeva, *Z. Kristallogr.* **2003**, *218*, 259; d) T. E. Weirich, J. Portillo, G. Cox, H. Hibst, S. Nicolopoulos, *Ultramicroscopy* **2006**, *106*, 164; e) D. L. Dorset, C. J. Gilmore, *Acta Crystallogr. Sect. A* **2000**, *56*, 62; f) D. L. Dorset, *Z. Kristallogr.* **2003**, *218*, 458; g) R. Vincent, P. A. Midgeley, *Ultramicroscopy* **1994**, *53*, 271.

[29] a) A. Altomare, M. C. Burla, M. Camalli, G. L. Cascarano, C. Giacovazzo, A. Guagliardi, A. G. G. Moliterni, G. Polidori, R. Spagna, *J. Appl. Crystallogr.* **1999**, *32*, 115; b) A. Altomare, G. L. Cascarano, C. Giacovazzo, A. Guagliardi, *J. Appl. Crystallogr.* **1993**, *26*, 343.

[30] M. S. Weiss, *J. Appl. Crystallogr.* **2001**, *34*, 130.

[31] The structure solution was verified by using precession intensity data. Owing to their robustness with respect to sample misalignment and less pronounced dynamical effects, the data quality obtained under otherwise identical experimental conditions can be improved. Accordingly, R_{rim} is 20% and the straightforward structure solution has a figure of merit of 19.5%. The structure refinement (184 independent reflections, no. of reflections/parameter ≈ 6, $d_{min.}$ 0.78 Å) was less successful due to the large sample thickness, which gives rise to stronger dynamical effects (cf. Figure 11, middle).

[32] a) C. Janiak, *J. Chem. Soc. Dalton Trans.* **2000**, 3885; b) C. A. Hunter, J. M. Sanders, *J. Am. Chem. Soc.* **1990**, *112*, 5525.

[33] a) J. M. Cowley, *Acta Crystallogr.* **1961**, *14*, 920; b) J. M. Cowley, A. Goswami, *Acta Crystallogr.* **1961**, *14*, 1071.

[34] J. J. P. Stewart, *J. Comput. Chem.* **1989**, *10*, 221.

[35] Gaussian 03, Revision C.02, M. J. Frisch, G. W. Trucks, H. B. Schlegel, G. E. Scuseria, M. A. Robb, J. R. Cheeseman, J. A. Montgomery, Jr., T. Vreven, K. N. Kudin, J. C. Burant, J. M. Millam, S. S. Iyengar, J. Tomasi, V. Barone, B. Mennucci, M. Cossi, G. Scalmani, N. Rega, G. A. Petersson, H. Nakatsuji, M. Hada, M. Ehara, K. Toyota, R. Fukuda, J. Hasegawa, M. Ishida, T. Nakajima, Y. Honda, O. Kitao, H. Nakai, M. Klene, X. Li, J. E. Knox, H. P. Hratchian, J. B. Cross, V. Bakken, C. Adamo, J. Jaramillo, R. Gomperts, R. E. Stratmann, O. Yazyev, A. J. Austin, R. Cammi, C. Pomelli, J. W. Ochterski, P. Y. Ayala, K. Morokuma, G. A. Voth, P. Salvador, J. J. Dannenberg, V. G. Zakrzewski, S. Dapprich, A. D. Daniels, M. C. Strain, O. Farkas, D. K. Malick, A. D. Rabuck, K. Raghavachari, J. B. Foresman, J. V. Ortiz, Q. Cui, A. G. Baboul, S. Clifford, J. Cioslowski, B. B. Stefanov, G. Liu, A. Liashenko, P. Piskorz, I. Komaromi, R. L. Martin, D. J. Fox, T. Keith, M. A. Al-Laham, C. Y. Peng, A. Nanayakkara, M. Challacombe, P. M. W. Gill, B. Johnson, W. Chen, M. W. Wong, C. Gonzalez, and J. A. Pople, Gaussian, Inc., Wallingford CT, **2004**.

[36] M. D. Segall, P. J. D. Lindan, M. J. Probert, C. J. Pickard, P. J. Hasnip, S. J. Clark, M. C. Payne, *J. Phys. Condens. Matter* **2002**, *14*, 2717.

[37] S. L. Mayo, B. D. Olafson, W. A. Goddard III, *J. Phys. Chem.***1990**, *94*, 8897.

[38] a) B. Delley, *J. Chem. Phys.* **1990**, *92*, 508; b) B. Delley, *J. Chem. Phys.* **2000**, *113*, 7756.

[39] J. E. Lowther, *Phys. Rev. B*, **1999**, *59*, 11683.

[40] E. Horvath-Bordon, R. Riedel, P. F. McMillan, P. Kroll, G. Miehe, P. A. van Aken, A. Zerr, P. Hoppe, O. Shebanova , I. McLaren, S. Lauterbach, E. Kroke, R. Boehler, *Angew. Chem.* **2007**, *119*, 1498; *Angew. Chem. Int. Ed.* **2007**, *46*, 1476 .

[41] A. E. Bennett, C. Rienstra, M. Auger, K. V. Lakshmi, R. G. Griffin, *J. Chem. Phys.* **1995**, *103*, 6951.

[42] S. Zhang , X. Wu , M. Mehring, *Chem. Phys. Lett.* **1990**, *173*, 481.

[43] Y. Ishii, *J. Chem. Phys.* **2001**, *114*, 8473.

[44] a) X. D. Zou, Y. Sukharev, S. Hovmöller, *Ultramicroscopy* **1993**, *49*, 147; b) X. D. Zou, Y. Sukharev, S. Hovmöller, *Ultramicroscopy* **1993**, *52*, 436.

[45] S. Weber, *Java Structure Viewer*, v1.08, 1999.

[46] Z. H. Wan, Y. D. Liu, Z. Q. Fu, Y. Li, T. Z. Cheng, F. H. Li, H. F. Fan, *Z. Kristallogr.* **2003**, *218*, 308.

[47] P. A. Stadelmann, *Ultramicroscopy* **1987**, *21*, 129.

[48] G. M. Sheldrick, SHELX-97, Programs for the solution and the refinement of crystal structures, University of Göttingen, Göttingen (Germany), **1997**.

[49] P. A. Doyle, P. S. Turner, *Acta Crystallogr. A* **1968**, *24*, 390.

Received: December 7, 2006
Published online: April 5, 2007

Unmasking Melon by a Complementary Approach Employing Electron Diffraction, Solid-State NMR and Theoretical Calculations - Structural Characterization of a Carbon Nitride Polymer

Bettina V. Lotsch[*], Markus Döblinger,[#] Jan Sehnert,[**] Lena Seyfarth,[**] Jürgen Senker,[**] O. Oeckler, Wolfgang Schnick*

I. Electron Diffraction

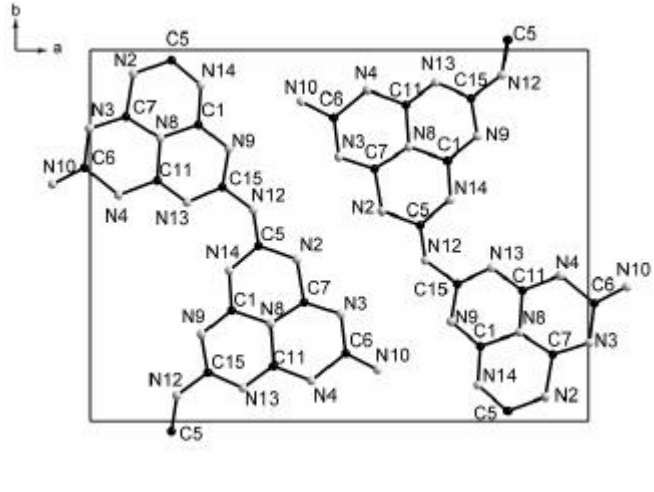

Figure S1. Numbering scheme for the atoms contained in the unit cell of melon.

Table S1. Bond lengths (in Å) of melon with estimated standard deviations in parentheses.

C(1) - N(8)	1.38(5)	C(5) - N(14)	1.31(5)
C(1) - N(9)	1.28(4)	C(6) - N(10)	1.22(5)
C(1) - N(14)	1.31(5)	C(7) - N(8)	1.35(5)
N(2) - C(5)	1.35(4)	N(8) - C(11)	1.42(5)
N(2) - C(7)	1.45(4)	N(9) - C(15)	1.30(4)
N(3) - C(6)	1.31(5)	C(11) - N(13)	1.25(4)
N(3) - C(7)	1.28(5)	N(12) - C(15)	1.30(4)
N(4) - C(6)	1.47(4)	N(13) - C(15)	1.29(4)
N(4) - C(11)	1.37(5)		

Table S2. Bond angles (in °) of melon with estimated standard deviations in parentheses.

N(9) - C(1) - N(8)	121(3)	C(7) - N(8) - C(1)	128(3)
N(14) - C(1) - N(8)	112(3)	C(11) - N(8) - C(1)	113(3)
N(14) - C(1) - N(9)	125(3)	C(11) - N(8) - C(7)	117(3)
C(7) - N(2) - C(5)	119(2)	C(15) - N(9) - C(1)	119(3)
C(7) - N(3) - C(6)	115(3)	N(8) - C(11) - N(4)	115(3)
C(11) - N(4) - C(6)	119(2)	N(13) - C(11) - N(4)	123(3)
N(14) - C(5) - N(2)	120(3)	N(13) - C(11) - N(8)	121(3)
N(4) - C(6) - N(3)	121(2)	C(15) - N(13) - C(11)	120(3)
N(10) - C(6) - N(3)	124(3)	C(5) - N(14) - C(1)	126(3)
N(10) - C(6) - N(4)	114(3)	N(12) - C(15) - N(9)	116(3)
N(3) - C(7) - N(2)	118(2)	N(13) - C(15) - N(9)	122(3)
N(8) - C(7) - N(2)	112(2)	N(13) - C(15) - N(12)	120(3)
N(8) - C(7) - N(3)	129(3)		

II. Ab initio Calculations

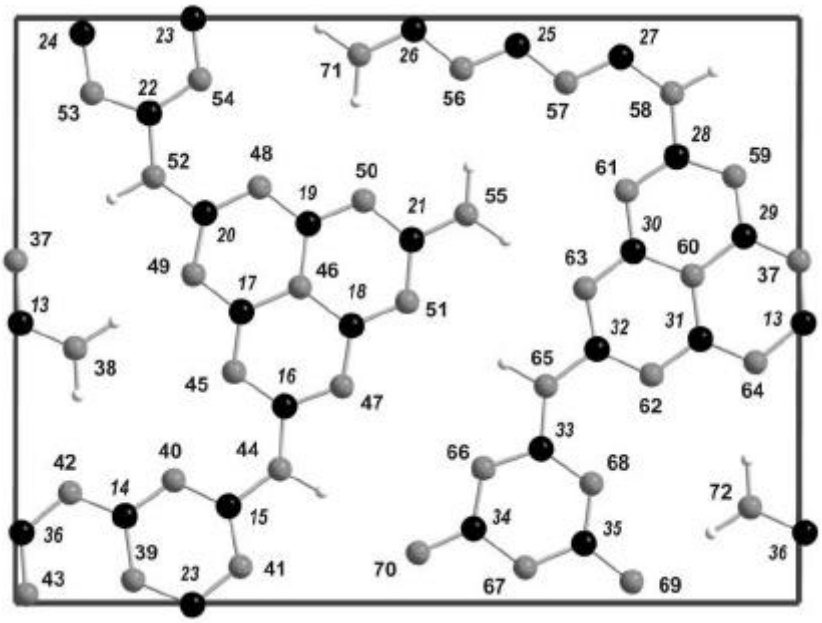

Figure S2. Numbering scheme for NMR parameters calculated with CASTEP (see Table S5).

Table S3. Summary of the ab initio NMR parameters obtained by calculations with CASTEP (for atom numbering see Figure S1). Since no internal referencing was performed during the calculations only shift differences can be discussed. To allow a better comparison with the experimental data all isotropic shift values presented here were corrected by a constant value.

	No.	σ / ppm	δ / ppm	η		No.	σ / ppm	δ / ppm	η
N	**54**	-165,1	295,2	0,65	**C**	**16**	166,6	-127,7	0,88
N	**47**	-165,3	295,4	0,66	**C**	**22**	166,5	-127,8	0,88
N	**66**	-166,9	293,2	0,64	**C**	**28**	166,3	-127,7	0,88
N	**59**	-167,1	293,1	0,65	**C**	**33**	166,2	-127,7	0,88
					C	**13**	166,2	133,2	0,07
N	**40**	-174,5	318,1	0,66	**C**	**36**	166,1	133,4	0,08
N	**57**	-174,5	317,2	0,66	**C**	**26**	166,1	133,4	0,07
N	**48**	-174,8	318,1	0,65					
N	**53**	-174,9	326,6	0,64	**C**	**15**	165,1	-125,1	0,92
N	**45**	-174,9	326,5	0,63	**C**	**20**	165,0	-124,8	0,93
N	**61**	-175,2	326,2	0,63	**C**	**27**	164,9	-125,0	0,93
N	**68**	-175,2	326,3	0,63	**C**	**32**	164,8	-124,7	0,94
N	**62**	-175,4	316,9	0,65					
					C	**35**	160,0	112,1	0,94
N	**69**	-184,0	253,5	0,51	**C**	**30**	159,9	112,3	0,93
N	**63**	-184,3	253,9	0,52	**C**	**23**	159,8	111,5	0,96
N	**41**	-184,7	253,7	0,51	**C**	**17**	159,7	111,6	0,95
N	**49**	-184,9	254,4	0,52					
					C	**18**	157,6	-112,4	0,86
N	**50**	-188,4	260,3	0,56	**C**	**24**	157,4	-112,3	0,86
N	**56**	-188,7	261,1	0,56	**C**	**29**	157,4	-113,3	0,83
N	**42**	-188,7	260,4	0,56	**C**	**34**	157,3	-113,2	0,82
N	**64**	-189,2	260,8	0,56					
					C	**25**	156,4	-108,2	0,94
N	**37**	-190,5	261,7	0,58	**C**	**14**	156,3	-108,8	0,93
N	**70**	-190,9	260,9	0,58	**C**	**19**	156,2	-109,1	0,92
N	**51**	-191,3	262,1	0,57	**C**	**31**	156,2	-108,5	0,93

N	**43**	-191,6	261,1	0,57
N	**67**	-228,9	218,6	0,01
N	**39**	-229,3	217,8	0,01
N	**60**	-229,4	217,9	0
N	**46**	-229,6	217,7	0,01
N	**65**	-244,4	-107,1	0,01
N	**58**	-244,4	-107,2	0,01
N	**44**	-244,5	-106,7	0,01
N	**52**	-244,6	-106,7	0,01
N	**38**	-268,1	-113,8	0,21
N	**72**	-268,3	-113,9	0,21
N	**71**	-268,5	-113,5	0,2
N	**55**	-268,7	-113,3	0,19

III. Solid State NMR Spectroscopy

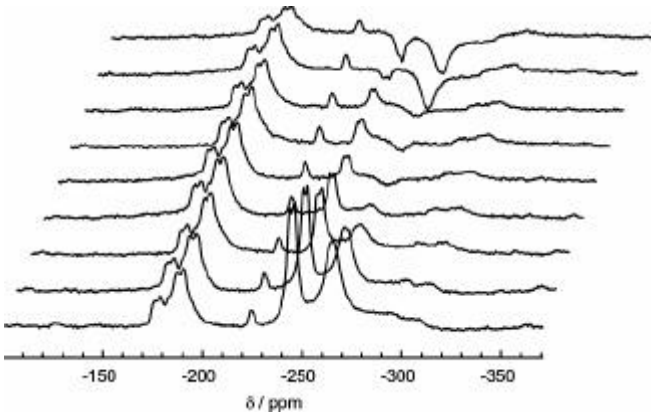

Figure S3. ^{15}N CPPI spectrum of melon. The polarization inversion behavior was monitored by varying the inversion time from 0.2 to 800 µs (front to back). Contact time t_c: 2 ms, spinning frequency n_{rot}: 6 kHz.

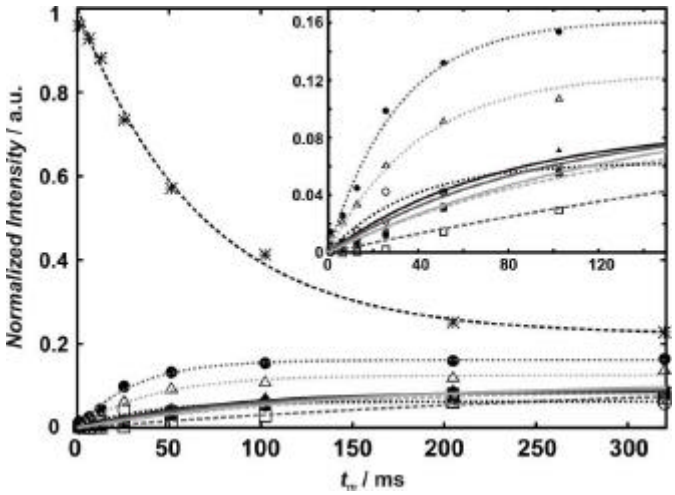

Figure S4. ^{15}N fp-RFDR curves after selective excitation of the NH_2 nuclei. Plot of all magnetization transfer curves, including the magnetization loss of the NH_2 nuclei. An enlarged plot of the magnetization build-up at the tertiary and NH nitrogen atoms is depicted in the inset. * NH_2; ? NH; ¦ N_c; ? N_{tert} (-195 ppm); ? (-191 ppm); ? (-187 ppm); ? (-182 ppm); ∇ (-179 ppm) ? (-177 ppm).

CHEMISTRY OF MATERIALS

Article

pubs.acs.org/cm

Structural Investigation of Graphitic Carbon Nitride via XRD and Neutron Diffraction

Federica Fina,[†] Samantha K. Callear,[‡] George M. Carins,[†] and John T. S. Irvine*[,†]

[†]School of Chemistry, University of St. Andrews, St. Andrews, KY16 9ST Scotland, United Kingdom

[‡]ISIS Neutron and Muon Facility, STFC, Rutherford Appleton Laboratory, Harwell Oxford, Didcot OX11 0QX, United Kingdom

Supporting Information

ABSTRACT: Graphitic carbon nitride (g-C_3N_4) has, since 2009, attracted great attention for its activity as a visible-light-active photocatalyst for hydrogen evolution. Since it was synthesized in 1834, g-C_3N_4 has been extensively studied both catalytically and structurally. Although its 2D structure seems to have been solved, its 3D crystal structure has not yet been confirmed. This study attempts to solve the 3D structure of graphitic carbon nitride by means of X-ray diffraction and of neutron scattering. Initially, various structural models are considered and their XRD patterns compared to the measured one. After selecting possible candidates as g-C_3N_4 structure, neutron scattering is employed to identify the best model that describes the 3D structure of graphitic carbon nitride. Parallel chains of tri-s-triazine units organized in layers with an A−B stacking motif are found to describe the structure of the synthesized graphitic carbon nitride well. A misalignment of the layers is favorable because of the decreased $\pi-\pi$ repulsive interlayer interactions.

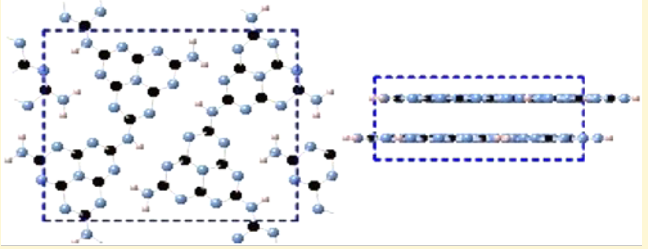

INTRODUCTION

Graphitic carbon nitride (g-C_3N_4) is one of several allotropes of the carbon nitrides family. It was synthesized for the first time by Berzelius and named "melon" by Liebig in 1834.[1] It is a polyconjugated semiconductor composed of carbon and nitrogen atoms and it is characterized by a layered graphitic-like structure.[2] The fully polymerized form of g-C_3N_4, characterized by a C:N ratio of 0.75, cannot be practically obtained. Therefore, the material presents a hydrogen content of 1−2%, which varies depending on the synthesis procedure.[3] Graphitic carbon nitride can be easily synthesized via solid state synthesis from cheap materials such as melamine, it is insoluble in most solvents and shows great stability in extreme conditions (pH 0 and 14).[2,4] Because of these characteristics, it has recently attracted great attention for different catalytic applications, in particular photocatalysis for hydrogen evolution from water.[2,4] Even though widely studied as a catalyst, to date, the g-C_3N_4 crystal structure has not been fully solved. The first examples of structural investigation date back to the early 20th century.[5−7] Since then, two main 2D structures have been suggested: a triazine-based (Figure 1a)[8−11] and a tri-s-triazine-based one (Figure 1b).[12−15] Many investigations have been carried out in order to confirm which of the two structures could describe g-C_3N_4.[12,13,16−20] By 2009,[16,19] with the aid of electron diffraction,[16,19,20] and solid-state nuclear magnetic resonance,[16] the 2D structure of g-C_3N_4 synthesized by thermal condensation of small organic polymers was considered solved. The structure of g-C_3N_4 was confirmed as a tri-s-triazine-based polymeric structure.[16,19] However, because of the highly disordered character of the material an accurate description of its 3D structure had only been suggested.[20,21]

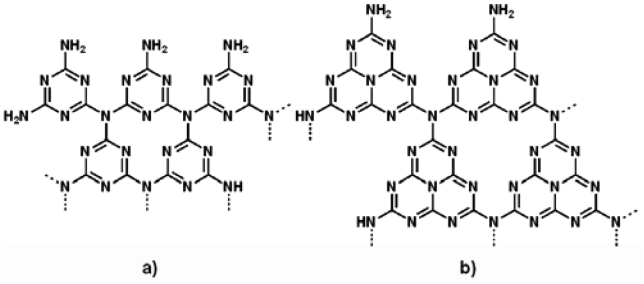

Figure 1. Structures considered representative of g-C_3N_4: (a) triazine based and (b) tri-s-triazine based.

To the best of our knowledge, the most recent work on the 3D structure of g-C_3N_4 is that of Tyborski et al.[21] In their work, X-ray diffraction modeling is employed to solve the structure of graphitic carbon nitride. However, because of the lack of long-range order in the material that prevents proper structure refinement, conventional X-ray diffraction alone is not sufficient. On the other hand, total scattering data, which incorporates information from the diffuse scattering regarding short-range order, can provide additional information useful for the structure determination of g-C_3N_4.

Received: February 2, 2015
Revised: March 9, 2015
Published: March 23, 2015

DOI: 10.1021/acs.chemmater.5b00411
Chem. Mater. 2015, 27, 2612−2618

Neutrons interact with the nuclei of the atoms instead of the electrons and can therefore offer complementary information to XRD analysis regarding the atomic structure of materials.[22] Additionally, neutron scattering is very sensitive to hydrogen and other light elements such as carbon. Because of the opposite sign of the scattering lengths of H and D,[23] negative peaks are produced in the first case and positive in the second. A comparison of labeled and not-labeled materials allows for direct identification of atomic correlations involving hydrogen. Neutron scattering can therefore be a suitable analytical technique for g-C_3N_4 and can offer complementary information to the XRD analysis. In the present work, we employ structural models proposed in the literature, we create some new ones and generate their theoretical XRD patterns. These are then compared to the measured XRD pattern of the synthesized graphitic carbon nitride. After narrowing down the possible crystal structures, the most promising ones are compared with the results from the neutron scattering analysis. It is found that the material synthesized for this study is best described by tri-s-triazine layers with an offset in their alignment. To the best of our knowledge, no report of neutron scattering on g-C_3N_4 exists in the literature, and this work brings the structural characterization of this active catalyst a step forward.

EXPERIMENTAL SECTION

Material Synthesis. Graphitic carbon nitride was synthesized by thermal polycondensation of Melamine (Sigma-Aldrich, 99.9%) at 500 °C for 15 h. The precursor was placed in a closed alumina crucible and heated to temperature with a rate of 5 °C/min. After the synthesis, it was ground to fine powder. To synthesize the deuterated g-C_3N_4, we applied the same synthetic procedures, but melamine-d_6 was employed as the starting material.

Photocatalytic Performance Evaluation. Measurement of the photocatalytic hydrogen evolution were performed in a custom-made photocatalytic reactor with top irradiation through a quartz window. In a typical experiment, 0.1 g of catalyst (1 g L^{-1}) were suspended in 100 mL of a 10 v.% solution of triethanolamine (TEOA)[2] employed as sacrificial agent. The inner atmosphere was purged with argon gas to remove any trace of air. Top irradiation was carried out with a 250 W iron-doped metal halide ultraviolet−visible lamp (≥290 nm; UV Light Technology Limited) with a cutoff filter (≥420 nm; borosilicate-coated glass, UQG Optics Ltd.) to block UV irradiations. Hydrogen evolution was monitored for an experimental duration of 20 h using a gas chromatograph (Agilent 3000 micro gas chromatograph).

X-ray Diffraction. The microstructure was investigated by powder X-ray Diffraction (XRD) using an Empyrean PANalytical series 2 diffractometer with a Cu Kα radiation source (λ = 1.5406 Å). The theoretical patterns of the modeled structures were generated using the software FullProf. In order to remove all symmetry operators during the generation of the theoretical patterns, the space group *P*1 is employed as a mere processing tool.

Neutron Scattering. The neutron scattering measurements were performed using NIMROD (InterMediate Range Order Diffractometer) at the ISIS Neutron and Muon Facility, Rutherford Appleton Laboratory, U.K.. Graphitic carbon nitride was packed into a flat plate TiZr container that was chosen because of the opposite sign of the scattering length of the two elements, giving an overall null scattering.[24] The container had a wall thickness of 1 mm and an inner aperture of 1 mm. The beam size was 3 cm × 3 cm. A Vanadium plate was used as a standard to normalize the data. Measurements of the background and container were also collected and used to correct the raw data. The data normalisation and corrections were carried out using GudrunN.[24] PDFGui was employed to generate calculated PDFs of the crystal structures using scale and damping factors that were fitted to the experimental data. The atomic positions, lattice parameters and isotropic displacement parameters were inputted as per the crystal structure data and were kept fixed.[25] PDFGui outputs a residual curve (the difference between the model and the data) and also the weighted *R*-factor (R_w) which is a measure of how accurately the model represents the data (the smaller the value the better the fit).

Elemental Analysis and Density Measurement. The elemental analysis was acquired with Carlo Erba Flash 2000 elemental analyzer, configured for wt % CHN. Density measurements were carried out with a Micromeritics, AccuPyc 1340 gas pycnometer.

RESULTS

Photocatalytic Performance. Graphitic carbon nitride is tested for photocatalytic hydrogen evolution under visible light. Triethanolamine (TEOA) is employed as sacrificial agent to promote the production of hydrogen. The material without the aid of a cocatalyst shows an evolution rate at the steady state of less than 1 μmol h^{-1} under the described conditions. However, after loading of 1 wt % platinum as the cocatalyst the performance reaches a rate of 22 μmol h^{-1}. This results are consistent with what has been reported in the literature for graphitic carbon nitride,[2] showing that the material subject of this study is an active photocatalyst for hydrogen evolution.

XRD Analysis. The X-ray diffraction pattern of g-C_3N_4 synthesized by thermal polycondensation of melamine is illustrated in Figure 2. The characteristic peaks associated

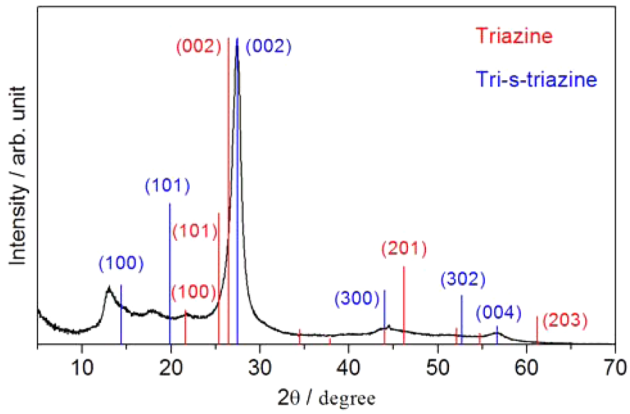

Figure 2. Theoretical patterns for fully polymerized triazine and tri-s-triazine based g-C_3N_4 respectively. Triazine unit-cell parameters: $a = b$ = 4.7420 Å, c = 6.7205 Å, $\alpha = \beta = 90°$, $\gamma = 120°$; tri-s-triazine unit-cell parameters: $a = b$ = 7.113 Å, c = 6.490 Å, $\alpha = \beta = 90°$, $\gamma = 120°$.

with g-C_3N_4 can be identified.[2,14] The main peak at 2θ = 27.4° is reported as the (002) plane, equivalent to a *d*-spacing of 0.326 nm. This is usually ascribed to the distance between the layers of the graphitic material.[2,14] The peak at 2θ = 13.00° is attributed to the (100) plane, with a *d*-spacing of 0.680 nm. This is due to the intralayer *d*-spacing.[2,14]

The measured XRD pattern is initially compared to the crystal structure proposed by Teter and Hemley[8] in 1996 (Figure 2). Even though a fully polymerized g-C_3N_4 (C:N ratio of 0.75) cannot be obtained, we still assess it for completeness. The proposed structure describes layers of triazine units with a 3D A-B stacking organization and it is characterized by a hexagonal unit cell ($a = b$ = 4.7420 Å, c = 6.7205 Å, $\alpha = \beta$ = 90°, γ = 120°) with space group $P\bar{6}m2$. Compared to the measured pattern, the (002) reflection is shifted toward lower angles meaning a larger *d*-spacing in between the layers; in addition the (100) reflection is significantly shifted compared to that of our g-C_3N_4, corresponding to an intralayer *d*-spacing of 0.411 nm. A similar result was obtained by Tyborski et al.[21] for their polymeric carbon nitride (PCN) synthesized from

DOI: 10.1021/acs.chemmater.5b00411
Chem. Mater. 2015, 27, 2612−2618

dicyandiamide by double calcination step.[21] The PCN described in their paper is characterized by a more pronounced (100) reflection compared to the material subject of this investigation.

To take into account a fully polymerized tri-s-triazine-based g-C_3N_4, a structure is generated starting from the unit cell proposed by Teter and Hemley. The new unit-cell parameters are $a = b = 7.113$ Å, $c = 6.490$ Å, $\alpha = \beta = 90°$, $\gamma = 120°$. The parameter c is chosen to match the interlayer spacing of the measured pattern. The theoretical pattern generated from the tri-s-triazine structure is compared to the measured pattern in Figure 2. The same reflections seen for the triazine-based structure are present but with a shift toward lower angles. The (100) reflection, being at $2\theta = 14.38°$ (0.615 nm), does not yet match the measured one. On the other hand its relative intensity is 0.18, very close to the experimental value, $I_{100}/I_{002} = 0.19$. The offset of the (100) reflection and the presence of a strong (101) reflection at $2\theta = 19.86°$ do not make this a suitable model.

Elemental analysis of the synthesized material reveals a hydrogen content of 1.5 wt % and a C:N ration of 0.68. These values confirm a partially polymerized structure. Models of partially polymerized g-C_3N_4 can be obtained by removing tri-s-triazine units from the network. With this approach, depending on which units are removed, many different structural models can be generated. Figure 3 compares two different structures:

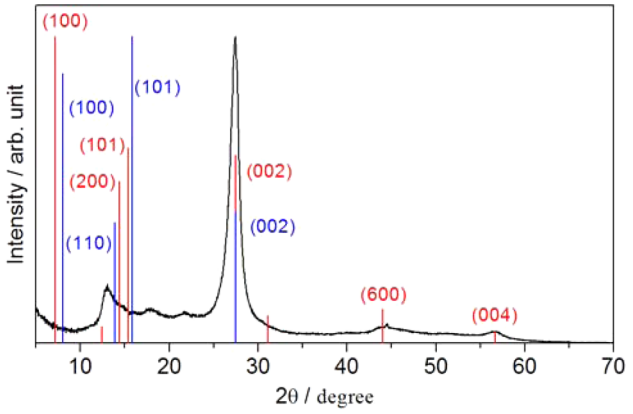

Figure 3. Theoretical XRD patterns for two different partially polymerized graphitic carbon nitride: Döblinger et al.[19] (blue, $a = b = 12.77$ Å, $c = 6.49$ Å, $\alpha = \beta = 90°$, and $\gamma = 120°$) and this study (red, $a = b = 13.9246$ Å, $c = 6.49$ Å, $\alpha = \beta = 90°$, and $\gamma = 120°$).

one proposed by Döblinger et al.,[19] and one created for this study (atomic coordinates in Table S1 in the Supporting Information). The structure proposed by Döblinger et al.,[19] after an electron diffraction study, is characterized by a hexagonal unit cell with cell parameters as follow: $a = b = 12.77$ Å, $c = 6.49$ Å, $\alpha = \beta = 90°$, and $\gamma = 120°$. The partially polymerized structure created for this study is also characterized by hexagonal unit cell ($a = b = 13.9246$ Å, $c = 6.49$ Å, $\alpha = \beta = 90°$, and $\gamma = 120°$) and it is obtained from the tri-s-triazine structure previously discussed. Both 3D structures are considered with an A-B stacking configuration. Figure 3 shows the theoretical patterns. In both cases, the peaks at low angles are more intense than the (002) reflection. This indicates that these structures also cannot be considered representative of the synthesized graphitic carbon nitride.

An alternative tri-s-triazine structure has been proposed by Lotsch et al.[16,20] after carrying out an electron diffraction study. The structure is composed of parallel chains of tri-s-triazine units (Figure 4 inset) and the authors refer to it as "melon".[16]

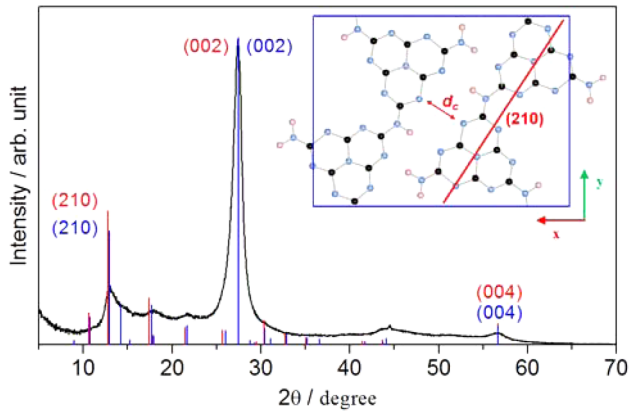

Figure 4. XRD theoretical patterns of Melon as proposed by Lotsch et al. (red, $a = 16.7$ Å, $b = 12.4$ Å, $c = 6.49$ Å, $\alpha = \beta = \gamma = 90°$, space group: $P2_12_12$) and the modified version of this investigation (blue, $a = 16.4$ Å, b = 12.4 Å, $c = 6.49$ Å, $\alpha = \beta = \gamma = 90$ °C). Inset: structure of melon.

This nomenclature will be employed in the present study to distinguish this and similar structures from other tri-s-triazine models; while the synthesized material will still be referred to as g-C_3N_4. The unit cell of Melon is characterized by an orthorhombic geometry and an A-A staking of the layers. The XRD theoretical pattern of this structure is shown in Figure 4. The unit cell parameter c was chosen to match the (002) reflection ($a = 16.7$ Å, $b = 12.4$ Å, $c = 6.49$ Å, $\alpha = \beta = \gamma = 90°$, space group: $P2_12_12$). The theoretical pattern generated by this structure is very similar to the measured one. Two major reflections are observed at $2\theta = 12.78°$ and $2\theta = 27.46°$. The reflection at $2\theta = 12.78°$ is now assigned to the $(210)_{orthorhombic}$ plane rather than the $(100)_{hexagonal}$ because of the different geometry of the unit cell. However, this reflection is shifted of 0.17° toward lower angles compared to the measured one, and its intensity relative to the (002) reflection (I_{210}/I_{002}) is 0.44, whereas the experimental value is 0.19. The material employed by Lotsch et al.[16,20] was synthesized by thermal polycondensation of melamine, as in the present work, but the reaction is carried out in a sealed ampule. This will generate a material with a higher level of crystallinity, which could justify the small differences in the XRD patterns. This structure is therefore employed as starting point for further improvement. Initially it can be modified to move the peak in the desired position. This can be achieved by "shrinking" the unit cell or by reducing the distance, dc (Figure 4 inset), between the polymeric chains. The first approach was applied by Tyborski et al.;[21] however, this method causes a contraction of the aromatic network resulting in C═N bond too short.[26,27] The second approach does not affect the aromatic network and therefore is chosen for this investigation. The structure is now described by a unit cell of parameters: $a = 16.4$ Å, b = 12.4 Å, $c = 6.49$ Å, $\alpha = \beta = \gamma = 90$ °C (for atomic coordinates, see Table S2 in the Supporting Information). The theoretical pattern for the modified Melon is illustrated in Figure 4. All of the experimental reflections find an equivalent in the theoretical pattern. The position of the $(210)_{orthorhombic}$ reflection, as

DOI: 10.1021/acs.chemmater.5b00411
Chem. Mater. 2015, 27, 2612−2618

expected, matches that of the measured peak. However, its relative intensity is 0.37, still too high.

The modified melon structure can be further modified to achieve a better match to the real structure. The angles of the orthorhombic unit cell can be increased or decreased to simulate a structural shift of the layers. This would affect the $(210)_{orthorhombic}$ reflection which is associated with the alignment of the aromatic layers. Tyborski et al.[21] investigated the effect that modifying the angle γ has on the XRD pattern.[21] However, an increase or decrease of this angle would produce a distortion of the aromatic units placed on the *ab* planes, rather than a shift of the layers. This is an example of the molecular constraints posed by the structure of graphitic carbon nitride. Here, only α and β will be modified to investigate the effect of a shift of the layers but maintaining a nominal A-A stacking. The new unit cell will now have a monoclinic geometry. While changing one of the angles, the parameter *c* is adjusted to retain the distance between the layers constant at a value of 2θ = 27.4°. Figure 5 illustrates the effect that a change in one of the

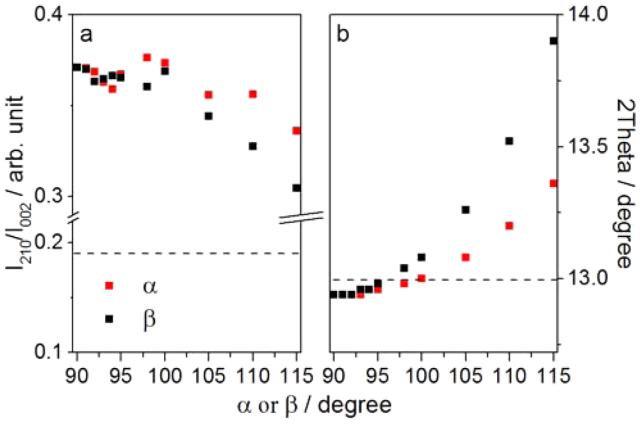

Figure 5. Effect of α and β on the relative intensity (I_{210}/I_{002}) and the position of the (210) reflection. Dashed lines represents the experimental values.

angles has on the position and the relative intensity of the $(210)_{monoclinic}$ reflection. The effects produced by varying α or β are found to be very similar. In both cases the intensity slightly decreases from the original 0.37 to ~0.30. The decrease is greater for β (0.30 for β = 115°) than for α (0.34 for α = 115°) but in both cases this value still remains too high compared to that of g-C_3N_4 (I_{210}/I_{002} = 0.19). Changing the angle also has an effect on the position of the peak by shifting it toward higher 2θ. After remaining nearly the same for both α and β up to 95°, the change is the largest for β = 115° with 2θ = 13.90°. The effects of the angles below 90 °C have also been investigated and they were found mirroring the behavior of $\alpha(\beta) > 90°$. The optimum value of α and β can be found between 82 and 98°.

A different approach is that of actually shifting the layers retaining the orthorhombic geometry and introducing an A-B stacking configuration. Lotsch[20] considered three different shifts in her electron diffraction study but concluded that for her material those models did not match the experimental electron diffraction patterns. Here, the different synthesis method applied probably results in a different structure, and therefore the proposed shifts are used to generate the XRD theoretical patterns (Figure 6).

The first shift, A, is random along both the *x* and *y* directions (0.124, −0.244) the second, B, is along the diagonal of the cell

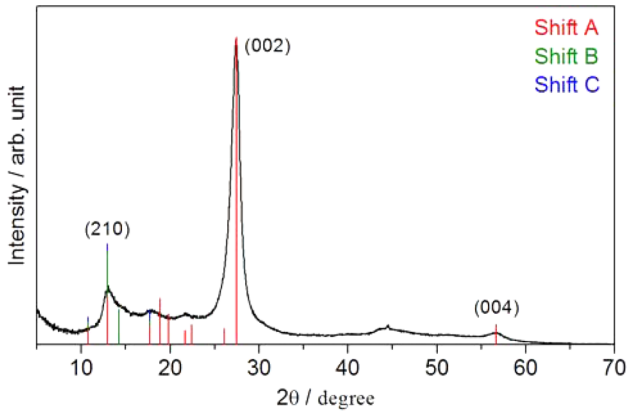

Figure 6. Theoretical XRD patterns of three modified melon structure with shifted layers. Shift A, (0.124, −0.244); shift B, (0.072, 0.054); shift C, (0.000, 0.109).

(0.072, 0.054) and the third, C, is along the *y* axis (0.000, 0.109). The theoretical pattern of modified Melon with shifted layers are compared in Figure 6. While no major differences in the peak position can be observed between the patterns, the relative intensities of some of the reflections, especially the (200) and (210), are found to vary significantly. The reflection (200) has an I_{200}/I_{002} intensity of 0.05, 0.07, and 0.09 for shifts A, B and C, respectively. For the (210) reflection, the I_{210}/I_{002} is 0.16 for shift A, 0.30 for shift B, and 0.33 for shift C. While shift B and shift C are only marginally decreased, Shift A is in good agreement with the experimental value (0.19), making it the most promising model. A summary of the models and their parameters can be found in Table S3 in the Supporting Information.

The measured pattern was indexed with the software HighScore Plus to investigate the level of symmetry of the structure. The suggested unit cell is characterized by orthorhombic geometry in agreement with the orthorhombic cell considered for the melon structure. It was also found that the highest level of symmetry that justifies all the reflections of the experimental pattern is described by the space group *Cmmm* (Figure S1 in the Supporting Information).

Neutron Scattering Analysis. The structure factor, $F(Q)$, measured for the graphitic carbon nitride (g-C_3N_4H, Figure S2 in the Supporting Information) is in good agreement with the XRD pattern, showing the $(210)_{orthorhombic}$ and the $(002)_{orthorhombic}$ reflections. From the Fourier transform of the structure factor, the differential correlation function, $D(r)$, is obtained (Figure 7). The $D(r)$ can be divided into three main sections (I, II, and III, Figure 7). Area I includes the distances from 0 to3 Å, these are atomic correlations within the layers of the graphitic carbon nitride materials, more specifically, within a tri-s-triazine unit. Examples are the N−H bond at about 1 Å and the C═N bond at 1.33 Å. The second area (II) can be found between 3 and 6 Å, where the interlayer distances contribute to the signal, for example the interlayer *d*-spacing at 3.25 Å. In this area long intra-planar distances can also be found, for instance the distance between the N_3 and the N_{12} (Figure 7-inset) of ~4.7 Å. Systematic ripples observed above 6 Å (III) can be attributed to the same moieties found in area II repeated in space. Therefore, from this point on, only areas I and II will be discussed in more detail.

Hydrogen and deuterium have scattering lengths of opposite sign[23] that in a D(r) plot will translate in negative peaks for

DOI: 10.1021/acs.chemmater.5b00411
Chem. Mater. 2015, 27, 2612−2618

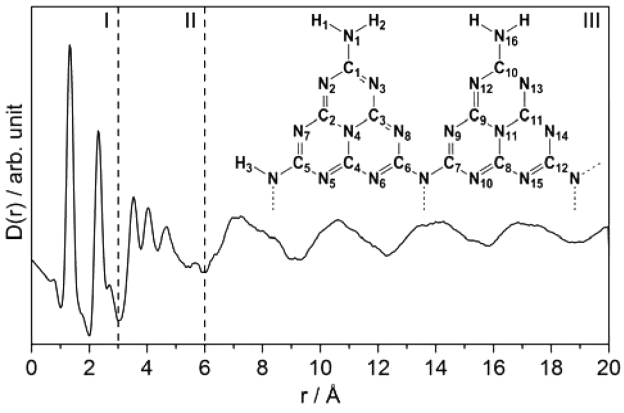

Figure 7. $D(r)$ of graphitic carbon nitride (g-C_3N_4H). Inset: tri-s-triazine units.

hydrogen and positive peaks for deuterium. Figure 8 compares the differential correlation functions of hydrogenated and

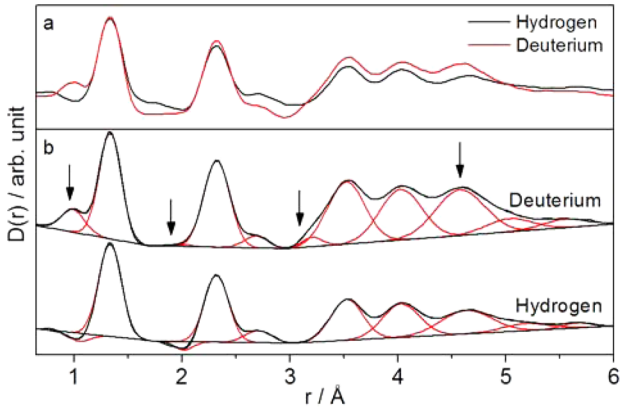

Figure 8. (a) Direct comparison and (b) peak fitting of the $D(r)$ of graphitic carbon nitride and of the deuterated analogue.

deuterated graphitic carbon nitride. The most evident effect of isotopic labeling is visible at 1 Å which corresponds to the N−H bond distance.[26] This appears in the form of a negative peak for the graphitic carbon nitride and positive for the labeled version (Figure 8). At 2 Å a less pronounced effect of the labeling is visible. This peak is assigned to the second-neighbor distance H-(N)-C (from H_1 to C_1 in Figure 7). Less obvious differences can be noticed at longer distances: at ∼3.2 Å in the form of a small shoulder and at ∼4.6 Å as a change in the peak intensity. The shoulder at ∼3.2 Å can be associated with the distance between the hydrogen from an amino group to the first nitrogen encountered in the aromatic ring (H_3 to N_5 in Figure 7). The peak at ∼4.6 Å is more difficult to assign to any specific atomic correlation due to the large amount of possible atomic pairs at this and similar distances.

Fitting the data with Gaussian functions for each peak shows that the first positive peak is centred at 1.33 Å, which is thought due to be due to the partial double bond in the aromatic network, C=N.[26−28] The high symmetry of the peak (Figure 8) suggests the absence of a component at 1.41 Å which would indicate the presence of a Csp^2-Nsp^3 correlation[28] for the C−N bonds bridging the tri-s-triazine units. Instead the data suggest that the bridging nitrogen atoms feature a sp^2 hybridization resulting in a shorter bond. At 2.32 Å the second-neighbor correlation for carbon and nitrogen atoms (C_2 to C_4 and N_4 to N_8, Figure 7 inset) is present. The small peak at 2.68 Å is due to the correlation between mirroring carbon and nitrogen atoms in the aromatic ring (N_2 to C_3). The interlayer d-spacing in the XRD for the (002) is reported at 3.26 Å. In the differential pair correlation functions $D(r)$, however, no isolated peak is seen at 3.26 Å, the first well defined peak in this region appears instead at 3.52 Å which is the correlation between atoms such as N_1 and C_3 (Figure 7 inset). Due to the broad nature of the peaks the correlation at 3.26 Å is not clearly visible which is typical for structures with inter-layer disorder, e.g. graphite, as the disordered nature of the layers results in a broad peak. Instead the interlayer correlations can be seen as periodic oscillations at high r values − these show the interlayer spacing to be 3.25 Å.

Figure 9 compares the experimental correlation function to the theoretical D(r) of the structures selected after the X-ray

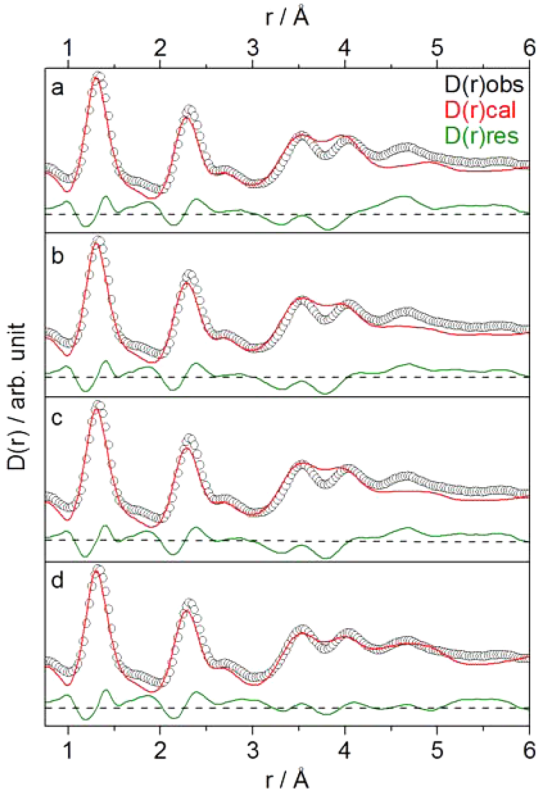

Figure 9. Comparison between the calculated $D(r)$ and the observed $D(r)$ for the g-C_3N_4H. The residual represents the difference between the two curves. (a) Modified melon, (b) $\alpha = 98°$, (c) $\beta = 98°$, and (d) shift A.

diffraction investigation: the modified Melon, the structures with α and $\beta \neq 90°$ and the structure with shifted layers (shift A). After generating the theoretical D(r) plots the peak areas compared to the area of the C−N peak at 1.33 Å ($A_{peak}/A_{1.33}$) are used to compare the different structures, together with the R_w values. The modeling of an amorphous material is less accurate at large distances (section III in Figure 7). For this reason, here the R_w values are given for the shorter range, 0−6 Å.

The calculated $D(r)$ of the modified version of Melon well matches the measured one up to 3 Å (Figure 9a). Above this value it cannot be considered satisfactory. Table 1 shows the relative peak areas of the theoretical pattern. The ratio $A_{2.1}/A_{1.33}$ = 1.23 is comparable to that of the measured $D(r)$ (1.25).

DOI: 10.1021/acs.chemmater.5b00411
Chem. Mater. 2015, 27, 2612−2618

Table 1. Summary of the Normalized Peak Areas As Obtained from the Gaussian Fitting of the $D(r)$ from g-C_3N_4Hx Prepared From Melamine Fired at 500 °C for 15 h

	$A_{peak}/A_{1.33}$				
r (Å)	g-C_3N_4	melon	α = 98°	β = 98°	shift A
1.03	0.07	0.15	0.14	0.15	0.15
2.07	0.14	0.09	0.09	0.09	0.08
2.1	1.25	1.23	1.24	1.23	1.29
2.72	0.14	0.12	0.12	0.12	0.15
3.52	0.63	0.64	0.69	0.65	0.67
4.03	0.59	0.72	0.60	0.64	0.61
4.62	0.77	0.39	0.54	0.64	0.8
5.14	0.20	0.05	0.06	0.02	0.23
R_w		0.41	0.40	0.40	0.32

However, the relative peak area of the correlation at 1.03 Å is higher than the measured value suggesting a higher content of N−H bonds in the modeled structure compared to the real structure. Another difference is found at 4.62 Å. This feature is found significantly lower ($A_{4.62}/A_{1.33}$ = 0.39) than the experimental value of 0.77. In addition, the correlation at 5.14 Å appears almost missing with an $A_{5.14}/A_{1.33}$ = 0.05. The R_w for this model is found to be 0.41.

Among the models with modified α and β, the angles 92, 95, and 98° were employed to generate the theoretical D(r). Among them the models with α or β of 98° produced the best result (Table 1 and Table S4 in the Supporting Infomration). The theoretical D(r) of the two models are illustrated in Figure 9b and Figure 9c. The results for both structures are very similar. In both cases an R_w of 0.40 is obtained. Even though an angle different from 90° brings to a small increase in the ratio $A_{4.62}/A_{1.33}$, now equal to 0.54 for α and 0.64 for β, this remain too small if compared to the experimental value. Similarly, the correlation at 5.14 Å is still found with a low relative peak area (0.06 for α and 0.02 for β).

When an actual shift of the layers (Shift A) is introduced in the structure, the R_w decreases to a value of 0.32 (Table 1). The calculated $D(r)$ for the structure is presented in Figure 9d. It readily be seen that the calculated D(r) well matches the observed $D(r)$. Even though an excess of N−H bonds is still present ($A_{1.03}/A_{1.33}$ = 0.15) all the other correlations have relative areas that match those of the measured $D(r)$. In particular in the region of the interlayer interactions, the correlations at 4.62 and 5.14 Å are now characterized by values which are very close to the experimental ones.

To account for a higher level of polymerization than that of Melon a mixed phase is also considered. The modeled structure with shifted layers is taken as main phase and a fully polymerized tri-s-triazine structure with A-B stacking is added to the model. In order to find the composition of the mixture, this was refined until constant R_w. The lowest achievable R_w of 0.27 was obtained for a mixture of 70% of shifted melon and 30% of the fully polymerized structure.

■ DISCUSSION

After an initial investigation by XRD followed by a neutron diffraction study, the following observations can be made. The structure of g-C_3N_4 calculated by Teter and Hemley and officially recognized does not describe the photoactive material (g-C_3N_4) obtained by calcination of small organic molecules, in the specific melamine. The interlayer d-spacing of Teter and Hemley's structure is too large (0.336 nm) compared to that of the synthesized material (0.326 nm). Furthermore, the theoretical pattern does not justify the peak observed at ∼13°. A tri-s-triazine-based structure produces a XRD pattern similar to the measured one suggesting that indeed the structure is based on the tri-s-triazine building block.

The removal of some of the tri-s-triazine units from the polymeric network, in order to introduce hydrogen atoms, does not bring an improved result. Too many reflections at low angles are present, making these partially polymerized structures not representative of the here synthesized material. However, the structure proposed by Lotsch et al.,[16,20] melon, produces a theoretical XRD pattern that well matches the experimental one in terms of peak position with only a small shift of the $(210)_{orthorhombic}$ reflection. The structure consists of parallel chains of tri-s-triazine units and can be classified as partially polymerized. The elemental composition ($C_{2.88}N_{4.32}H_{1.44}$) of melon and the C:N ratio (0.67) are coherent with those measured for the material synthesized for this study ($C_{2.88}N_{4.23}H_{1.51}$ and 0.68).

Because of the close match of the XRD pattern and the similar atomic composition, this structure is employed here as a starting point for further modifications. This can be justified by the different synthetic method employed by Lotsch et al.,[16,20] which generates a more ordered structure. To bring the position of the (210) reflection to the desired value the unit-cell parameter a is decreased by moving the chains closer to each other. The position of the (210) reflection of the modified-Melon matches the position of the experimental one. However, the relative intensity is too high compared to the measured peak. The intensity of this reflection is most likely linked to 3D structural features that can be affected by the synthesis method. In fact, Tyborski et al. after a double calcination step obtained a peak at ∼13° that is more intense and defined than that of the g-C_3N_4 synthesized for this study. An example of structural effect is a shift of the aromatic layers. A misalignment of the layers can affect the intensity of the (210) reflection. A shift of the layers is simulated by changing the angle α or β in the unit cell, which will become monoclinic. A change in one of these angles shows that it is possible to decrease the intensity of the (210) reflection but also move the reflection toward higher angles. The optimum range for both angles is found to be between 82 and 98°.

To introduce a shift in the layers, the vectors proposed by Lotsch are applied on the atomic coordinates of the modified melon. Indeed shifting the layers produces a decrease in the intensity of the (210) reflection is shift A, offset stacking of the layers is thermodynamically favorable. The aromatic layers are surrounded by π clouds. If the layers are perfectly aligned this will create repulsive forces. However, an offset between the layers minimizes the $\pi-\pi$ interlayer interactions, making the structure more stable and therefore more likely to be formed during the thermal polycondensation process. Shift A is the most successful model because it brings the tri-s-triazine units of a layer to be in between two tri-s-triazine units of an adjacent layer, creating an optimum A-B configuration that minimizes the repulsion of the layers (Figure S3a in the Supporting Information). These results are confirmed by the neutron diffraction analysis that shows that among the considered models, Shift A produces a calculated D(r) that best matches the measured one.

To account for the lower amount of N−H bonds found in the measured $D(r)$ compared to the calculated ones, a mixture of shifted Melon and a fully polymerized tri-s-triazine structure

DOI: 10.1021/acs.chemmater.5b00411
Chem. Mater. 2015, 27, 2612−2618

was considered. A marginally better R_w is obtained when 30% of the fully polymerized structure is added as a secondary phase. This high amount is however surprising since the atomic composition for the modeled melon ($C_{2.88}N_{4.32}H_{1.44}$) is found coherent with the values measured for the synthesized material ($C_{2.88}N_{4.23}H_{1.51}$). Therefore, it can be assumed that the peak at 1.03 Å is artificially affected by the correction for inelastic scattering characteristic of hydrogen atoms.

CONCLUSIONS

In conclusion, the structure of a photocatalytically active graphitic carbon nitride synthesized via polycondensation of melamine was investigated by mean of XRD and neutron diffraction. In both cases modeled structures were employed to generate calculated patterns and plots. These were then compared to the measured ones. Starting from proposed structural models for graphitic carbon nitride, we reduced to one the number of 3D configurations that can describe the structure of our catalyst. From the resultsm it can be concluded that graphitic carbon nitride obtained from calcination of melamine in a closed system is a tri-s-triazine-based polymer organized in layers at a distance of 0.326 nm. These layers, however, are not aligned with an A-A configuration but present an offset with respect to each other. This A-B configuration sees tri-s-triazine of adjacent layers being alternated. This minimizes the repulsive forces of the π clouds of adjacent layers. We believe that this work, by using neutron diffraction for the first time on graphitic carbon nitride, provides important insights on the 3D structure of photoactive g-C_3N_4 synthesized via thermal polycondensation of melamine.

ASSOCIATED CONTENT

Supporting Information

Atomic coordinates, graphical information, additional neutron diffraction summary. This material is available free of charge via the Internet at http://pubs.acs.org.

AUTHOR INFORMATION

Corresponding Author

*E-mail: jtsi@st-andrews.ac.uk. Tel: +44 (0)1334 463817.

Author Contributions

F.F. wrote the manuscript and carried out the XRD and neutron diffraction modeling. S.K.C. was the instrument scientist for the neutron scattering experiment. G.M.C. helped in the preparation of the samples and in the acquisition of the data. F.F and J.T.S.I. designed the experiments. All authors have given approval to the final version of the manuscript.

Notes

The authors declare no competing financial interest.

ACKNOWLEDGMENTS

We thank EPSRC for support through the EPSRC/NSF chemistry programme and the Royal Society for a Wolfson Merit award.

REFERENCES

(1) Liebig, J. *Ann. Pharm.* **1834**, *10* (1), 1−47.
(2) Wang, X.; Maeda, K.; Thomas, A.; Takanabe, K.; Xin, G.; Carlsson, J. M.; Domen, K.; Antonietti, M. *Nat. Mater.* **2009**, *8* (1), 76−80.
(3) Thomas, A.; Fischer, A.; Goettmann, F.; Antonietti, M.; Muller, J.-O.; Schlogl, R.; Carlsson, J. M. *J. Mater. Chem.* **2008**, *18* (41), 4893−4908.
(4) Wang, Y.; Wang, X.; Antonietti, M. *Angew. Chem., Int. Ed.* **2012**, *51* (1), 68−89.
(5) Franklin, E. C. *J. Am. Chem. Soc.* **1922**, *44* (3), 486−509.
(6) Pauling, L.; Sturdivant, J. H. *Proc. Natl. Acad. Sci. U.S.A.* **1937**, *23* (12), 615−620.
(7) Redemann, C. E.; Lucas, H. J. *J. Am. Chem. Soc.* **1940**, *62* (4), 842−846.
(8) Teter, D. M.; Hemley, R. J. *Science* **1996**, *271*, 53−55.
(9) Matsumoto, S.; Xie, E. Q.; Izumi, F. *Diamond Relat. Mater.* **1999**, *8* (7), 1175−1182.
(10) Kawaguchi, M.; Nozaki, K. *Chem. Mater.* **1995**, *7* (2), 257−264.
(11) Gillan, E. G. *Chem. Mater.* **2000**, *12* (12), 3906−3912.
(12) Kroke, E.; Schwarz, M. *Coord. Chem. Rev.* **2004**, *248* (5−6), 493−532.
(13) Jürgens, B.; Irran, E.; Senker, J.; Kroll, P.; Müller, H.; Schnick, W. *J. Am. Chem. Soc.* **2003**, *125* (34), 10288−10300.
(14) Yan, S. C.; Li, Z. S.; Zou, Z. G. *Langmuir* **2009**, *25* (17), 10397−10401.
(15) Groenewolt, M.; Antonietti, M. *Adv. Mater.* **2005**, *17* (14), 1789−1792.
(16) Lotsch, B. V.; Döblinger, M.; Sehnert, J.; Seyfarth, L.; Senker, J.; Oeckler, O.; Schnick, W. *Chem. − Eur. J.* **2007**, *13* (17), 4969−4980.
(17) Lotsch, B. V.; Schnick, W. *Chem. Mater.* **2006**, *18* (7), 1891−1900.
(18) Lotsch, B. V.; Schnick, W. *Chem. Mater.* **2005**, *17* (15), 3976−3982.
(19) Döblinger, M.; Lotsch, B. V.; Wack, J.; Thun, J.; Senker, J.; Schnick, W. *Chem. Commun.* **2009**, *12*, 1541−1543.
(20) Lotsch, B. V. PhD Thesis, Ludwig-Maximilian University of Munich, Munich, Germany, 2006.
(21) Tyborski, T.; Merschjann, C.; Orthmann, S.; Yang, F.; Lux-Steiner, M.-C.; Schedel-Niedrig, T. *J. Phys.: Condens. Matter* **2013**, *25* (39), 395402.
(22) Keen, D. *J. Appl. Crystallogr.* **2001**, *34* (2), 172−177.
(23) Sears, V. F. *Neutron News* **1992**, *3* (3), 26−37.
(24) Soper, A. K.; Science; Council, T. F. *GudrunN and GudrunX: Programs for Correcting Raw Neutron and X-ray Diffraction Data to Differential Scattering Cross Section*; Science & Technology Facilities Council: Swindon, U.K., 2011.
(25) Farrow, C. L.; Juhas, P.; Liu, J. W.; Bryndin, D.; Božin, E. S.; Bloch, J.; Proffen, T.; Billinge, S. J. L. *J. Phys.: Condens. Matter* **2007**, *19* (33), 335219.
(26) Lide, D. R. *CRC Handbook of Chemistry and Physics*, 71st ed.; CRC Press, Boca Raton, FL, 1990.
(27) Kroke, E.; Schwarz, M.; Horath-Bordon, E.; Kroll, P.; Noll, B.; Norman, A. D. *New J. Chem.* **2002**, *26* (5), 508−512.
(28) Allen, F. H.; Kennard, O.; Watson, D. G.; Brammer, L.; Orpen, A. G.; Taylor, R. *J. Chem. Soc., Perkin Trans. 2* **1987**, No. 12, S1−S19.

DOI: 10.1021/acs.chemmater.5b00411
Chem. Mater. 2015, 27, 2612−2618

Supplementary Information

Structural investigation of graphitic carbon nitride *via* XRD and Neutron Diffraction

Federica Fina[†], Samantha K. Callear[‡], George M. Carins[†], John T. S. Irvine[†]*

[†] School of Chemistry, University of St Andrews, St Andrews, KY16 9ST, Scotland, United Kingdom

[‡] ISIS Neutron and Muon Facility, STFC, Rutherford Appleton Laboratory, Harwell Oxford, Didcot OX11 0QX, United Kingdom

ATOMIC COORDINATES

Table S1 Atomic coordinates of the partially polymerized g-C_3N_4. Unit cell parameters: *a* = b = 13.924 Å, *c* = 6.49 Å, α = β = 90 °, γ = 120 °.

Atom	x	y	z
C1	0.6111	0.55555	0.75
C2	0.6111	1.05555	0.75
C3	1.1111	0.55555	0.75
C4	0.6111	0.7222	0.75
C5	0.6111	1.2222	0.75
C6	1.1111	0.7222	0.75
C7	0.6111	0.88889	0.75
C8	0.6111	1.38889	0.75
C9	1.1111	1.38889	0.75
C10	0.77777	1.38889	0.75
C11	1.27777	0.88889	0.75
C12	1.27777	1.38889	0.75
C13	0.94443	1.38889	0.75
C14	1.44443	0.88889	0.75
C15	1.44443	1.38889	0.75
C16	0.94443	0.55555	0.75
C17	1.44443	0.55555	0.75
C18	1.44443	1.05555	0.75
H1	1.12644	1.25287	0.75
H2	1.12644	0.87356	0.75
H3	0.74711	0.87356	0.75
N1	0.5	0.5	0.75
N2	0.5	1	0.75
N3	1	0.5	0.75
N4	0.5	0.66667	0.75
N5	0.5	1.16667	0.75
N6	1	0.66667	0.75
N7	0.5	0.83333	0.75
N8	0.5	1.33333	0.75

N9	1	1.33333	0.75
N10	0.66667	0.5	0.75
N11	0.66667	1	0.75
N12	1.16667	0.5	0.75
N13	0.66667	0.83333	0.75
N14	0.66667	1.33333	0.75
N15	1.16667	0.83333	0.75
N16	1.16667	1.33333	0.75
N17	0.83333	0.5	0.75
N18	1.33333	0.5	0.75
N19	1.33333	1	0.75
N20	0.66667	0.66667	0.75
N21	0.66667	1.16667	0.75
N22	1.16667	0.66667	0.75
N23	0.83333	1.33333	0.75
N24	1.33333	0.83333	0.75
N25	1.33333	1.33333	0.75

Table S2 Atomic coordinates of the modified Melon with closer chains. Unit cell parameters: *a* = 16.4 Å, b = 12.4 Å, *c* = 6.49 Å, α = β = γ = 90 °.

Atom	x	y	z
C1	0.3448	0.472	0.25
C2	0.6552	0.528	0.25
C3	0.22159	0.798	0.25
C4	0.77841	0.202	0.25
C5	0.26945	0.63	0.25
C6	0.73055	0.37	0.25
C7	0.13605	0.648	0.25
C8	0.86395	0.352	0.25
C9	0.98716	0.683	0.25
C10	0.01284	0.317	0.25
C11	0.07292	0.82	0.25
C12	0.92708	0.18	0.25
C13	0.83442	0.028	0.25
C14	0.16558	0.972	0.25
C15	0.7112	0.702	0.25
C16	0.2888	0.298	0.25
C17	0.75906	0.87	0.25
C18	0.24094	0.13	0.25
C19	0.62567	0.852	0.25
C20	0.37433	0.148	0.25
C21	0.47801	0.817	0.25
C22	0.52199	0.183	0.25
C23	0.56253	0.68	0.25

C24	0.43747	0.32	0.25
H1	0.87494	0.8891	0.25
H2	0.12506	0.1109	0.25
H3	0.38533	0.6109	0.25
H4	0.61467	0.3891	0.25
H5	0.91649	0.5576	0.25
H6	0.08351	0.4424	0.25
H7	0.40734	0.9424	0.25
H8	0.59266	0.0576	0.25
H9	0.35826	0.8217	0.25
H10	0.64174	0.1783	0.25
H11	0.86741	0.6783	0.25
H12	0.13259	0.3217	0.25
N1	0.14216	0.762	0.25
N2	0.85784	0.238	0.25
N3	0.08819	0.935	0.25
N4	0.91181	0.065	0.25
N5	0.22668	0.904	0.25
N6	0.77332	0.096	0.25
N7	0.28269	0.733	0.25
N8	0.71731	0.267	0.25
N9	0.19817	0.588	0.25
N10	0.80183	0.412	0.25
N11	0.05765	0.608	0.25
N12	0.94235	0.392	0.25
N13	0.99734	0.788	0.25
N14	0.00266	0.212	0.25
N15	0.3336	0.568	0.25
N16	0.6664	0.432	0.25
N17	0.92097	0.638	0.25
N18	0.07903	0.362	0.25
N19	0.63178	0.738	0.25
N20	0.36822	0.262	0.25
N21	0.57781	0.565	0.25
N22	0.42219	0.435	0.25
N23	0.71629	0.596	0.25
N24	0.28371	0.404	0.25
N25	0.7723	0.767	0.25
N26	0.2277	0.233	0.25
N27	0.68778	0.912	0.25
N28	0.31222	0.088	0.25
N29	0.54726	0.892	0.25
N30	0.45274	0.108	0.25
N31	0.4882	0.712	0.25

N32	0.5118	0.288	0.25
N33	0.82321	0.932	0.25
N34	0.17679	0.068	0.25
N35	0.41182	0.862	0.25
N36	0.58818	0.138	0.25

Table S3 List of the key parameters for the investigated structural models. Fully polymerized structures are indicated with "f.p.", while partially polymerized structure with "p.p.".

Structure		Cell geometry	a (Å)	b (Å)	c (Å)	α, β, γ (°)	$(210)_{ortho}$ or $(100)_{hexa}$ 2θ (°)	Δ2θ (°)	I_{210}/I_{002} I_{100}/I_{002}
g-C_3N_4	-	-	-	-	-	-	*13.00*	-	*0.19*
Teter & Hemley	f.p.	hexagonal	4.7420	4.7420	6.7205	90, 90, 120	21.62	8.62	0.11
Tri-*s*-triazine	f.p.	hexagonal	7.1130	7.1130	6.4900	90, 90, 120	14.38	1.38	0.18
Döblinger	p.p.	hexagonal	12.77	12.77	6.49	90, 90, 120	8.00	5.00	2.05
Tri-*s*-triazine	p.p.	hexagonal	13.9246	13.9246	6.49	90, 90, 120	7.18	5.82	1.64
Lotsch	p.p.	orthorhombic	16.7	12.4	6.49	90, 90, 90	12.78	0.22	0.44
Melon	p.p.	orthorhombic	16.4	12.4	6.49	90, 90, 90	12.94	0.06	0.37
α = 98 °	p.p.	orthorhombic	16.4	12.4	6.567	98, 90, 90	12.98	0.02	0.38
β = 98 °	p.p.	orthorhombic	16.4	12.4	6.567	90, 98, 90	13.04	0.04	0.36
Shift A	p.p.	orthorhombic	16.4	12.4	6.49	90, 90, 90	12.94	0.06	0.16
Shift B	p.p.	orthorhombic	16.4	12.4	6.49	90, 90, 90	12.94	0.06	0.30
Shift C	p.p.	orthorhombic	16.4	12.4	6.49	90, 90, 90	12.94	0.06	0.33

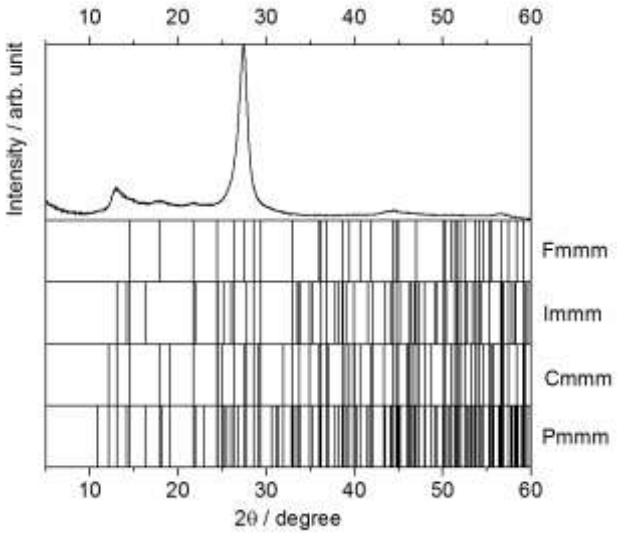

Figure S1 Results of the indexing of the experimental XRD pattern.

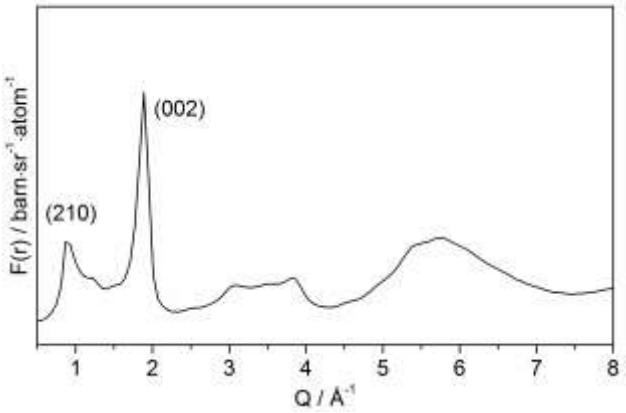

Figure S2 Structure factor of graphitic carbon nitride.

Table S4 Summary of the normalized peak areas as obtained from the Gaussian fitting of the D(r) plots.

	A_{peak}/A_{II}				
r (Å)	C_3N_4	α = 92 °	α = 95 °	β = 92 °	β = 95 °
1.03	0.07	0.15	0.15	0.16	0.15
2.07	0.14	0.09	0.09	0.09	0.09
2.1	1.25	1.23	1.23	1.23	1.22
2.72	0.14	0.12	0.12	0.12	0.12
3.52	0.63	0.66	0.66	0.67	0.65
4.03	0.59	0.68	0.66	0.65	0.67
4.62	0.77	0.41	0.52	0.40	0.49
5.14	0.20	0.06	0.02	0.08	0.04
Rw	-	0.41	0.41	0.41	0.41

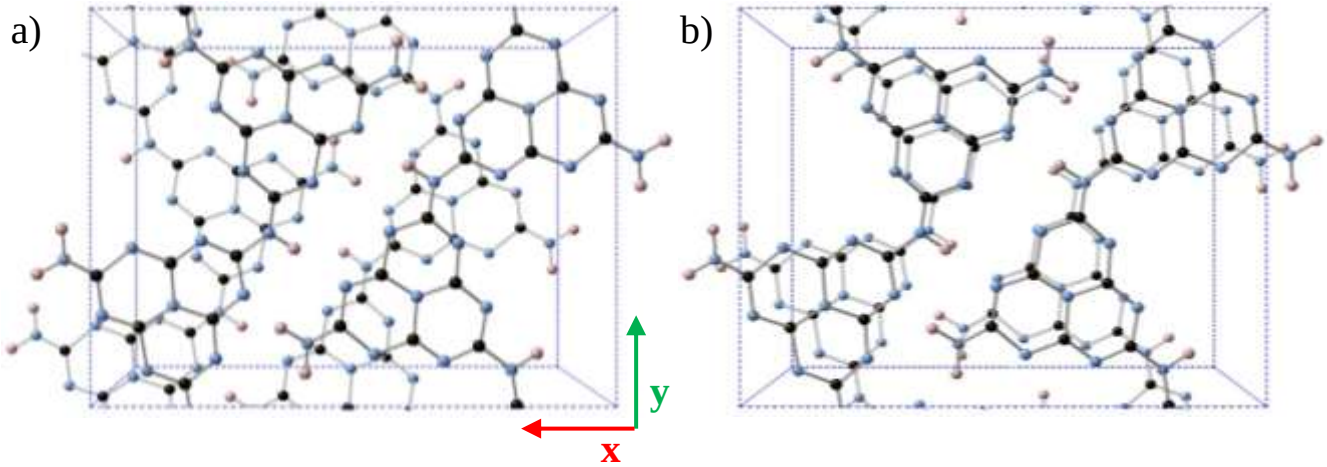

Figure S3 Representation of the crystal structure of a) modified Melon with randomly shifted layers and b) original modified Melon.

CHEMISTRY OF MATERIALS

Article

pubs.acs.org/cm

Thermodynamic Equilibria in Carbon Nitride Photocatalyst Materials and Conditions for the Existence of Graphitic Carbon Nitride g-C_3N_4

Tiago Botari,[†,¶] William Paul Huhn,[†] Vincent Wing-hei Lau,[‡] Bettina V. Lotsch,[‡,§] and Volker Blum*[,†]

[†]Department of Mechanical Engineering and Materials Science, Duke University, Durham, North Carolina 27708, United States
[‡]Max Planck Institute for Solid State Research, Heisenbergstraße 1, 70569 Stuttgart, Germany
[¶]Applied Physics Department, State University of Campinas, Campinas-SP 13083-970, Brazil
[§]Department of Chemistry, University of Munich, Butenandtstraße 5-13, 81377 Munich, Germany

Supporting Information

ABSTRACT: We quantify the thermodynamic equilibrium conditions that govern the formation of crystalline heptazine-based carbon nitride materials, currently of enormous interest for photocatalytic applications including solar hydrogen evolution. Key phases studied include the monomeric phase melem, the 1D polymer melon, and the hypothetical hydrogen-free 2D graphitic carbon nitride phase "g-C_3N_4". Our study is based on density functional theory including van der Waals dispersion terms with different experimental conditions represented by the chemical potential of NH_3. Graphitic carbon nitride is the subject of a vast number of studies, but its existence is still controversial. We show that typical conditions found in experiments pertain to the polymer melon (2D planes of 1D hydrogen-bonded polymer strands). In contrast, equilibrium synthesis of heptazine (h)-based g-h-C_3N_4 below its experimentally known decomposition temperature requires much less likely conditions, equivalent to low NH_3 partial pressures around 1 Pa at 500 °C and around 10^3 Pa even at 700 °C. A recently reported synthesis of triazine (t)-based g-t-C_3N_4 in a salt melt is interpreted as a consequence of the altered local chemical environment of the C_3N_4 nanocrystallites.

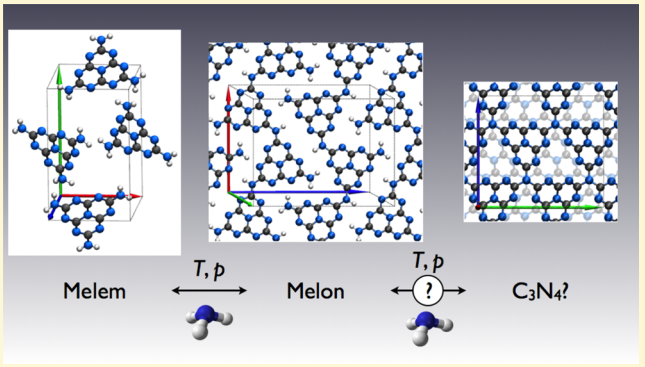

INTRODUCTION

Graphitic carbon nitride materials are subject to enormous recent attention as materials for catalysis,[1] particularly for photocatalytic hydrogen evolution.[2−5] Even though the first characterizations date back to at least the 1830s,[6] the nature and even the existence of completely H-free crystalline polymeric C−N compounds continue to be subject of intense debate.[7−9] Past synthesis and characterization efforts revealed triazine[8,9] (t) C_3N_3 units and heptazine[7] (h) C_6N_7 units as the most important building blocks. Some of the most important related compounds are illustrated in Figure 1:

(i) The NH_2 terminated heptazine monomer melem (a), its dimer, a likely reaction intermediate (b),[10] and the confirmed crystalline form of monomeric melem (c).[11,12]

(ii) Melon (d−f), a 1D heptazine polymer that crystallizes in two-dimensional (2D) hydrogen-bonded planes stacked three-dimensionally in nanocrystalline platelets.[13−15]

(iii) g-t-C_3N_4 (g−i), a possible periodic triazine-based equivalent of heptazine-based g-C_3N_4[16−19] recently reported to have been successfully synthesized in a salt melt.[8,9]

(iv) g-h-C_3N_4 (j−l), a much discussed but still hypothetical hydrogen-free layered C−N phase of heptazine units connected via triply bonded N atoms.[20] This structure is often portrayed as 2D but exhibits a significant long-range corrugation in first-principles simulations[21,22] accompanied by the bridging N atoms adopting a more sp^3-like local geometry.

Remarkably, despite overwhelming follow-up attention to the seminal paper on C−N compound-based water splitting,[2] the basic (intrinsic) atomistic mechanisms behind the catalytic activity and how to control them remain poorly understood. Heptazine-based g-h-C_3N_4, subject to a host of theoretical studies (e.g., refs 20 and 23−28), remains elusive in experiments.[9,29] Note that g-h-C_3N_4 was originally modeled as the 1D polymer melon,[2] although a large number of subsequent papers used the fully condensed, stoichiometric C_3N_4 in their discussion. For instance, out of 12 journal papers on C−N materials[30−41] that appeared on Google Scholar in a time frame of 3 weeks prior to submission of the present manuscript, five[31,35−38] show images of g-h-C_3N_4, five others use the term g-C_3N_4 as an apparent fact without further discussion of the atomic structure,[32−34,39,40] and only two[30,41] pay heed to the actual, more complex phase space of polymeric

Received: March 8, 2017
Revised: April 27, 2017
Published: April 28, 2017

DOI: 10.1021/acs.chemmater.7b00965
Chem. Mater. 2017, 29, 4445−4453

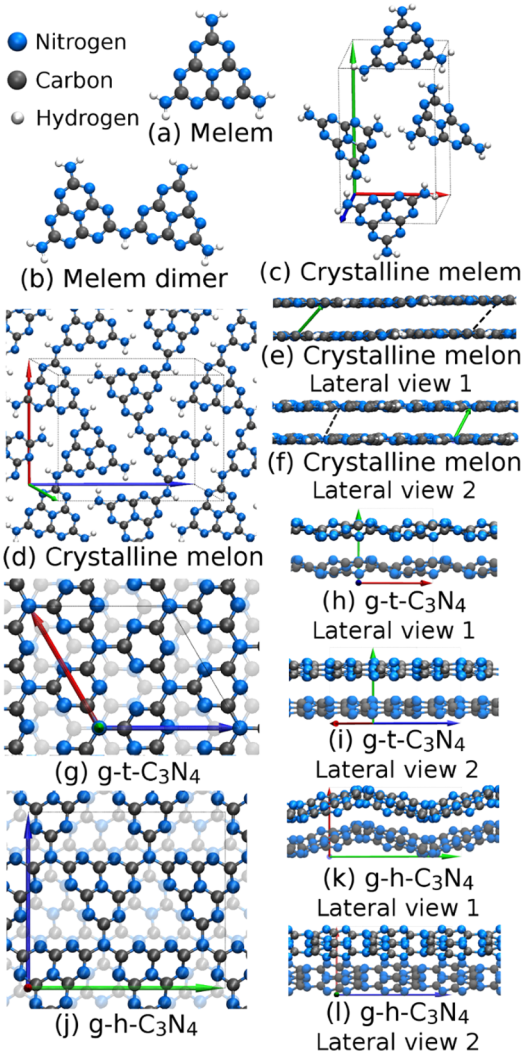

Figure 1. Key C−N-based compounds considered in this work. (a) Melem molecule ($C_6N_7(NH_2)_3$). (b) Melem dimer.[10] (c) Unit cell of crystalline melem[11] (see Table S3). (d−f) Shifted single plane (SSP) stacked monoclinic model of the crystalline form of the 1D polymer melon (Table S4) viewed from three different angles. (g−i) Crystal structure model of g-t-C_3N_4 viewed from three different angles (Table S7). (j−l) Crystal structure model of g-h-C_3N_4 viewed from three different angles (Table S6). In subfigures (g) and (j), the second layer in each unit cell is shown lightly shaded.

carbon nitride. Instead, the (nano)crystalline phase reached during conventional syntheses[7] appears to be melon.[13] On the other hand, g-t-C_3N_4 triazine (with the same formal composition as heptazine-based g-h-C_3N_4) could be synthesized as reported recently[8,9] but in a very different reaction environment. Here, the procedure used for the synthesis of the triazine-based g-t-C_3N_4, employing a LiCl/KCl salt melt, yields as the majority phase the lithium/chloride-intercalated poly(triazine imide) (PTI).[42,43] Structurally, this is the *incompletely* condensed g-t-C_3N_4, also discussed in ref 22 and shown in Figure S3, whereas the fully condensed g-t-C_3N_4 appears to be a minor phase formed at the interface of the salt melt.[43] If so, this formation process could be related to earlier work by chemical vapor deposition based on hydrogen-free, triazine-based precursors that were also reported to yield hydrogen-free g-t-C_3N_4.[44,45] First-principles studies found that g-t-C_3N_4 is *less* stable than the heptazine-based g-h-C_3N_4.[20,25] Still, if the triazine-based phase can be synthesized under some conditions, it is not clear why the heptazine-based phase cannot. In addition, even the H-containing crystalline phases, which can be made (crystalline melem and melon), show little or no activity for photochemical hydrogen evolution by themselves,[10] supporting the idea that interfaces, disorder, defects, and/or accidentally inserted functionalities during synthesis play a major role in the observed activity.[3,10] For instance, under-reacted oligomeric melon species were implicated as potentially active,[10] and specific chemical modifications can dramatically enhance this activity.[46,47] In fact, melon obtained under certain synthesis conditions may well itself be an oligomeric phase.

The key motivation for this paper is to provide a quantitative understanding of the structure and relative stability of the basic C−N phases under different reaction conditions, needed to arrive at a rational, reductionist understanding and control of the specific mechanisms governing activity. Specifically, we quantify the relative stability of the most important C−N phases discussed in the literature by an ab initio thermodynamic approach.[48] We deliberately restrict the analysis to the already large space of structure models discussed in the literature as a first perimeter, creating a sound base for future extensions, e.g., by including defects or targeted chemical modifications. A key result is that the heptazine-based g-C_3N_4 phase cannot be stable at conditions pertaining to conventional syntheses, at least not for the structures suggested in the literature so far. This observation emerges as a simple consequence of the thermodynamic equilibrium conditions connecting the different phases. Our approach is based on the fact that the different phases described above are all connected by simple reaction equilibria that involve the release of NH_3. Therefore, the emergence of each phase at different conditions can be related to the NH_3 chemical potential as the critical quantity that characterizes the reaction environment. Experimentally, species other than NH_3 (such as CNH or C_2N_2) are only released during transformations of C−N compounds at high temperature.[42] They are usually taken to be indicative of the materials' decomposition, justifying our focus on NH_3 as the gas-phase species connecting different triazine- or heptazine-based phases. Our analysis also allows us to place oligomeric intermediates[10] in the context of the confirmed stable phases, showing that they are indeed close to equilibrium and should be considered to explain the observed chemical stability range of melon.

METHODS

Background. The standard route to synthesize C−N compounds is rather straightforward.[7] A commercially available C−N-containing substance, e.g., melamine ($C_3N_3(NH_2)_3$), is heated for an extended period of time at a defined temperature in an open[10] or closed vessel. The synthesis can then be rationalized as a continued condensation during which NH_3 units are removed and escape:

Melamine ⇆ melem (per heptazine unit)

$$2C_3N_3(NH_2)_3 \rightleftarrows C_6N_7(NH_2)_3 + 2NH_3 \quad (1)$$

Melem ⇆ melon

$$C_6N_7(NH_2)_3 \rightleftarrows C_6N_7(NH)(NH_2) + NH_3 \quad (2)$$

Melon ⇆ g-[t/h]-C_3N_4

$$C_6N_7(NH)(NH_2) \rightleftarrows C_6N_8 + NH_3 \quad (3)$$

The formation of crystalline melem following eq 1 was reported at T = 450 °C for 5 h in a closed ampule;[11] other procedures in an open vessel have been reported,[49] although we found that the product

DOI: 10.1021/acs.chemmater.7b00965
Chem. Mater. 2017, 29, 4445−4453

obtained contains higher condensates such as oligomers.[46] Melon formation, eq 2, was reported for a range of conditions[7] in opened (e.g., lidded crucible) or closed vessels (sealed quartz ampule), including T = 490 °C for 4 days (opened vessel),[50] T = 500 °C for 15 h (opened vessel),[15] T = 550 °C for 12 h (opened vessel),[10] and T = 630 °C for 12 h (closed vessel).[13] It is worth noting that, because of the release of ammonia, these syntheses are often associated with rather high ammonia pressures. For instance, differential scanning calorimetry in ref 11 needed to be carried out in steel pressure crucibles "because conventional alumina crucibles burst due to evolution of ammonia," and pressures up to 12 bar are reported in salt-melt triazine-based g-t-C_3N_4 synthesis.[8]

The resulting C−N-based materials are reported to decompose at temperatures around T = 680−700 °C.[42] However, the formation of gaseous decomposition fragments other than NH_3 has been observed at temperatures as low as T = 480 °C (CNH) and T = 550 °C (C_2N_2),[42] i.e., typical formation conditions of melon may already overlap with the onset of decomposition of some intermediate fractions of the material. Interestingly, well-defined crystalline phases of melamine-melem adducts have also been synthesized "at temperatures ranging from 350 to 400°C with reaction times of at least 7 days,"[51] potentially providing a lower-temperature limit to the formation range of crystalline melem. The corresponding structure models are shown in Figure 2. As mentioned above, however, the formation of g-h-C_3N_4, eq 3, has never to our knowledge been unambiguously confirmed in any synthesis.

Computational Approach. All first-principles calculations in this work were carried out using density-functional theory (DFT) including correction terms for long-range dispersion interactions. We employed the highly accurate[52] all-electron electronic structure code FHI-aims[53−55] with "tier2" basis sets and "tight" numerical settings.

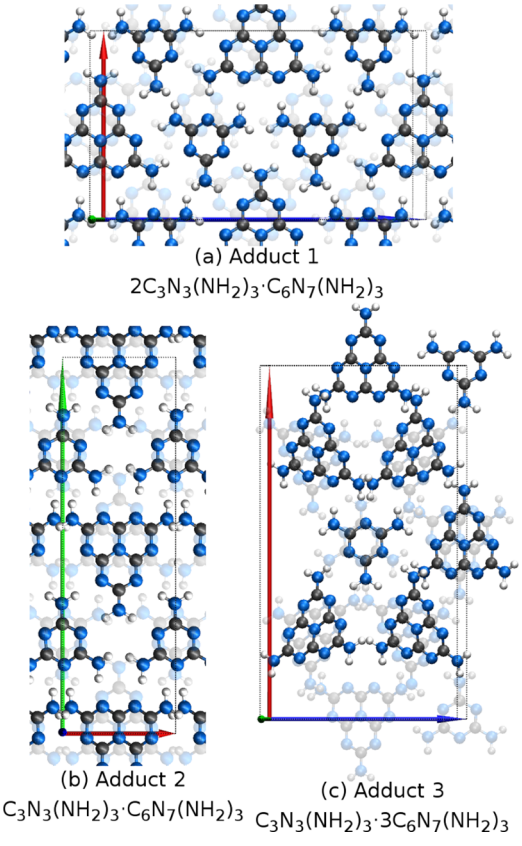

Figure 2. Crystal structure models of three melamine-melem adduct phases proposed in ref 51 using unit cell parameters and atomic positions determined by first-principles relaxations in this work (Table S7).

With these settings, conformational energy hierarchies of complex hydrogen-bonded systems are converged to a few meV per hydrogen bond.[53] All atomic positions and unit cell parameters were fully relaxed[56] to local minima (residual energy gradients: 5×10^{-3} eV/Å or below) of the PBE[57] semilocal density functional with the Tkatchenko−Scheffler (TS)[58] pairwise van der Waals correction. Because van der Waals bonding plays a significant role in these systems, we validated our key results against a recent, extensively benchmarked[59−61] many-body dispersion (MBD)[62] approach. Furthermore, the PBE part of the functional was checked by substituting, for a few key compounds, the hybrid HSE06 functional[63] in a recent linear-scaling periodic implementation[64,65] using "intermediate" basis settings, as documented in Table S1. The corresponding density functionals are referred to as PBE+TS, PBE+MBD, and HSE06+MBD below.

For our analysis of the chemical equilibria between different C−N phases, we surveyed and compared the different structure models put forth in the literature (experiment and theory), as well as different candidate structures of our own. Within DFT-PBE+TS, the key geometry parameters of the fully optimized structures (local minima of the potential energy surface) agree well with earlier experimental findings[11,13−15] (see Supporting Information (SI) for details: Table S3 for crystalline melem, Tables S4 and S5 for data related to different models of melon, Table S6 for g-h-C_3N_4, Table S7 for g-t-C_3N_4, and Table S8 for melamine-melem adduct phases).

We can relate the formation equilibria (eqs 1−3) to the temperature and NH_3 partial pressure under reaction conditions using first-principles total energy calculations for all involved phases. The finite-temperature and pressure properties of NH_3 are represented by chemical potential μ_{NH_3}. In a gas phase environment, μ_{NH_3} can be related to the NH_3 partial pressure p_{NH_3} and to T using its experimentally known form $\mu_{NH_3}(p,T)$. Specifically, we employ a parametrized ideal-gas expression for $\mu_{NH_3}(p,T)$ (SI, eqs S1−S3 and Table S2),[66] which is in excellent agreement with available thermochemical data in the literature[67−69] (Figure S1). Importantly, because μ_{NH_3} is an abstract quantity, it can be used to reflect any other near-equilibrium NH_3 reservoir as well, including NH_3 exchanged with and/or solvated in a salt melt.[8]

We can quantify the equilibria (eqs 1−3) in terms of their approximate Gibbs free energy differences based on the total energies of the lowest-energy structures of each phase referenced to the energy of a melem molecule and to μ_{NH_3}

$$\Delta G^{\text{melem,cryst.}} = G^{\text{melem,cryst.}} - G^{\text{melem,mol.}} \quad (4)$$

$$\Delta G^{\text{melon}} = G^{\text{melon}} - (G^{\text{melem,mol.}} - \mu_{NH_3}) \quad (5)$$

$$\Delta G^{\text{g-}C_3N_4} = G^{\text{g-}C_3N_4} - (G^{\text{melem,mol.}} - 2\mu_{NH_3}) \quad (6)$$

The energies $G^{\text{melem,cryst.}}$, G^{melon}, and $G^{\text{g-}C_3N_4}$ are taken per unit of melem/heptazine in accordance with eqs 2 and 3. The subtracted energy of molecular melem, $G^{\text{melem,mol.}}$, thus acts as a common offset, leaving μ_{NH_3} as the only experimental variable. Because all relevant phases except for NH_3 are solids, by far the largest dependence on external conditions (temperature, pressure and partial pressures, NH_3 reservoir) enters through μ_{NH_3}. We therefore approximate G for all solid phases by their DFT-calculated total energies E, omitting their smaller temperature and pressure dependence (particularly the vibrational contribution). Likewise, effects of the reaction environment (gas-phase or salt melt) and kinetic effects (barriers and/or kinetically necessary intermediates) are not yet included. Although it is hard (if not impossible) to treat the latter factors conclusively from first-principles alone, they will be considered qualitatively in the discussion below. Finally, we note that synthesis paths are possible that start with precursors other than melamine, e.g., cyanamide, dicyanamide, urea, or thiourea. However, our analysis covers the thermodynamic (near-)equilibrium regime. Thus, as long as the reaction leads to one of the intermediates of the governing reactions (eqs 1−3), i.e., melamine,

DOI: 10.1021/acs.chemmater.7b00965
Chem. Mater. 2017, 29, 4445−4453

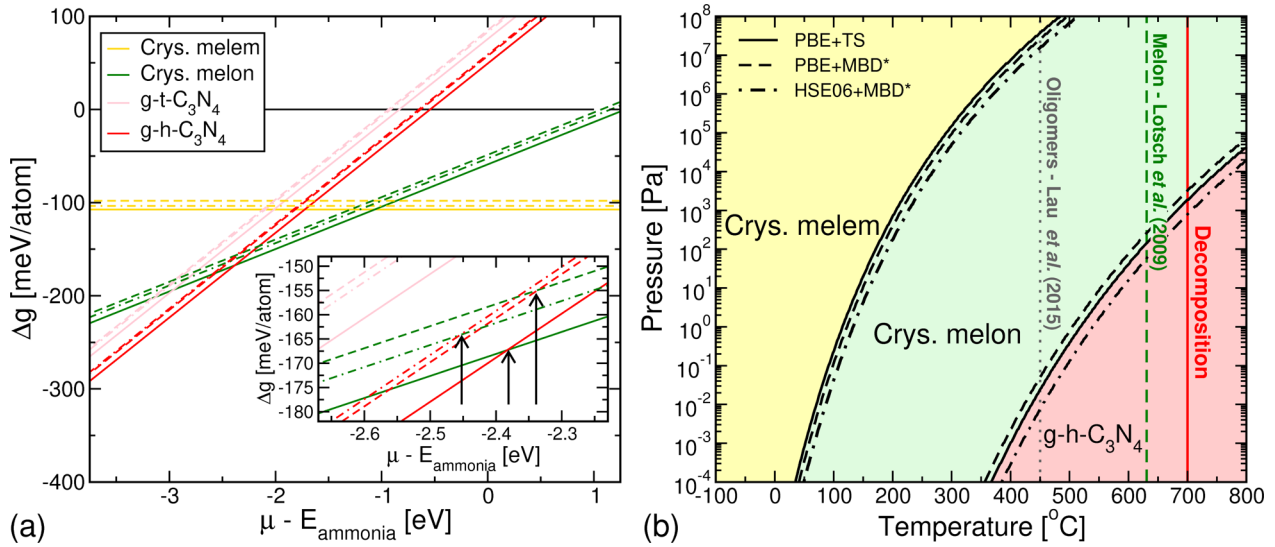

Figure 3. (a) Calculated Gibbs free energies per atom, Δg, for crystalline melem, melon (lowest-energy SSP stacked model, see Table S4), and the lowest-energy model of g-t-C_3N_4[22] and g-h-C_3N4[21,22] as a function of the ammonia chemical potential μ_{NH_3}. The isolated melem molecule is taken as the reference compound (zero line). Results are provided for three different density functionals, PBE+TS, PBE+MBD, and HSE06+MBD, for the lowest-energy geometries at the PBE+TS level of theory. (b) Calculated temperature/NH_3 partial pressure phase diagram based on $\mu_{NH_3}(p,T)$ (SI, eqs S1−S3, Table S2, and Figure S1) comparing three phases: crystalline melem, crystalline melon, and g-h-C_3N^4. Different colored areas indicate where a given phase has the lowest Δg. Phase boundaries are drawn for all three density functionals considered. Experimental conditions referenced are from refs 10 and 13.

melem, melon, or g-h-C_3N_4, our conclusions are independent of the starting point and kinetic paths to reach one of those products. We do, however, believe that different synthesis starting points may leave behind different defect moieties in the product that may affect its practical catalytic properties. We demonstrated the effect of such potential moieties, e.g., related to cyanamide or urea, in two different recent studies.[46,47]

RESULTS AND DISCUSSION

Structure of Phases Considered. For melon, the parameter that emerges from experimental XRD with the highest degree of certainty is the interplanar spacing d = 3.19[13]−3.26 Å[14,15] of successive 2D hydrogen-bonded planes characterized by a sharp powder diffraction peak. Although different authors agree on the in-plane arrangement of heptazine polymer strands in 3D melon, different stacking sequences of 2D planes have been put forward.[13,15,70] Specifically, stacks of individual, laterally shifted planes (here referred to as "shifted single plane" (SSP) with monoclinic unit cells) and orthorhombic AB stackings of pairs of planes are summarized in refs 15 and 70. For the monoclinic SSP and orthorhombic AB structure models, we tested grids of different interplanar registries as starting points for full DFT-PBE+TS geometry optimizations. The lowest total energy per lateral melon unit cell (72 atoms) is obtained for SSP stacking (see Table S4 for structural details) with a predicted interplanar distance d = 3.20 Å. There are, however, several other energetically indistinguishable SSP-stacked local minimum structures. Furthermore, AB-stacked geometries are not much higher in energy, i.e., $\Delta E \lesssim 0.10$ eV per unit cell or ∼1−2 meV/atom for a model similar to that in ref 70 (Table S5).

The AB stacked model remains nearly orthorhombic in our simulations. In Figure S2, we compare published experimental powder X-ray diffraction (PXRD) data with simulated PXRD data for the fully optimized structure models obtained in this work. There is considerable variation already between experimental data obtained from different syntheses.[13,15] However, some features are reproduced in both experiments, for instance, the low-angle diffraction peak at around 2θ = 13°, which indicates a slightly better match of the orthorhombic AB-stacked computational model. One main finding from our analysis of SSP- and AB-stacked models of melon with different interplanar stacking relationships is that there are local energy minima with almost equivalent total energies in line with earlier analyses as well.[71] It is thus likely that small local variations in experimental conditions would lead to locally different stacking relationships in different melon platelets. Shifts between successive planes with similar probabilities for different shift directions could also lead to an overall stacking that is more similar to the orthorhombic case and thus to the experimental PXRD. Because the total energies of the different low-energy melon models are similar[71] and their stoichiometries are identical, this local structural difference will not affect the overall phase equilibria between stoichiometrically different phases examined in this work.

For the g-h-C_3N_4 and g-t-C_3N_4 phases, we considered planar arrangements as well as arrangements that allowed for longer-ranged corrugation, specifically, the significantly corrugated g-h-C_3N_4 and g-t-C_3N_4 model of refs 21 and 22. In our calculations (DFT-PBE+TS), these corrugated models are lower in total energy than essentially planar models by 44 meV/atom (g-h-C_3N_4) and 54 meV/atom (g-t-C_3N_4), i.e., by rather sizable amounts. In addition, there is a large space of further long-range corrugated models that could conceivably yield even lower energy structures, which we did not explore. However, it is clear that at least the idealized g-h-C_3N_4 structure cannot be truly 2D in nature. The g-t-C_3N_4 model of ref 22 remains somewhat more planar; although we tried a g-t-C_3N_4 model with a similarly large long-range corrugation as the heptazine-based compound, for triazine, this larger corrugation did not yield a lower total energy than that of the model of ref 22. Regarding the exact nature of the corrugation, the main total

DOI: 10.1021/acs.chemmater.7b00965
Chem. Mater. 2017, 29, 4445−4453

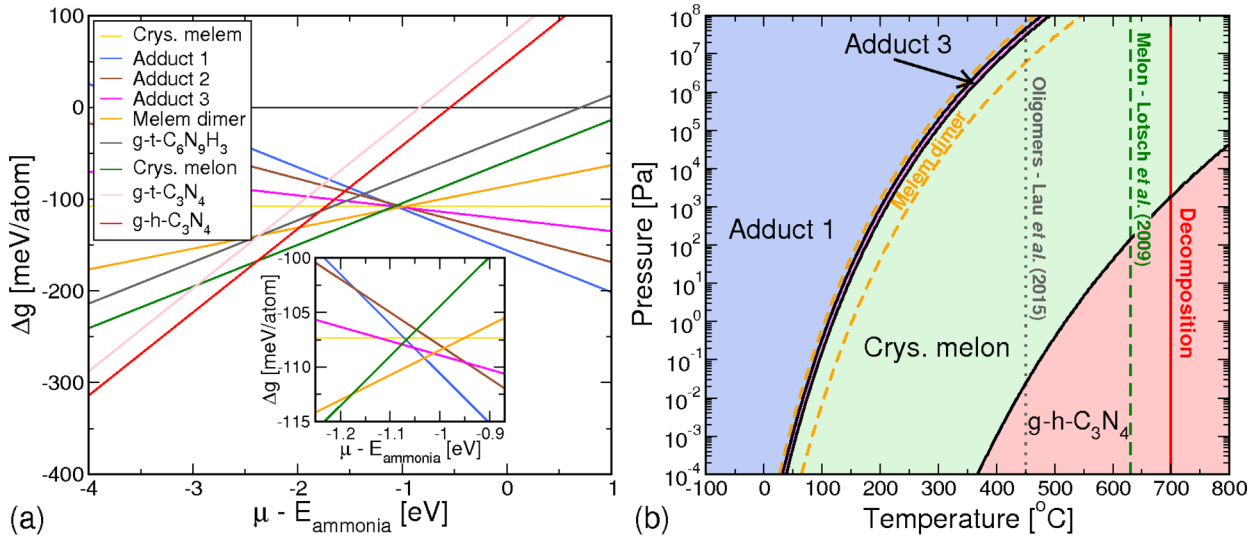

Figure 4. Gibbs free energies and phases as in Figure 3 but reflecting a wider space of potential intermediate phases. Results are provided for the PBE+TS density functional. (a) Calculated Gibbs free energies per atom, Δg, for the melamine-melem adduct structures 1−3 of Figure 2, crystalline melem, the lowest-energy SSP stacked model of melon, g-t-C_3N_4, g-h-C_3N4, and a hypothetical melem dimer phase as a function of the ammonia chemical potential μ_{NH_3}. Additionally, a suggested crystalline PTI compound g-t-$C_6N_9H_3$[22] (see Figure S3 and Table S9), reportedly achieved in the chemical environment of a salt melt,[8,9] is included but found to be unstable in the present analysis. The reference compound (zero line) is molecular melem. μ_{NH_3} is given with reference to the calculated total energy per atom of an NH_3 molecule. (b) Calculated temperature/NH_3 partial pressure phase diagram based on $\mu_{NH_3}(p,T)$. In DFT-PBE+TS, the melamine-melem adduct phases 1 and 3 are slightly more stable than crystalline melem up to the stability range of melon. A hypothetical melem dimer phase could have a narrow stability range of its own. T = 450 °C is marked to indicate the melem oligomer synthesis temperature used in ref 10.

energy term(s) associated with nonplanarity (compared to purely planar models) are likely already included in the structure models of refs 21 and 22, which we considered in our work.

Thermodynamic Equilibria. Figure 3 summarizes the predicted phase equilibria for the restricted space of the three key phases in the C−N system and assesses their dependence on the level of theory used (PBE+TS, PBE+MBD, and HSE06+MBD). To clarify the essential trends related to melon and g-h-C_3N_4, Figure 3(a) is limited to Δg (i.e., ΔG/atom) for crystalline melem, crystalline melon (SSP stacked), and for the corrugated heptazine-based g-h-C_3N_4 and triazine-based g-t-C_3N_4 structure models as a function of μ_{NH_3} and is evaluated at the PBE+TS equilibrium structures. Molecular melem is used as a common reference (energy zero). Compared to the energy scale that distinguishes different equilibrium phases in Figure 3(a), the differences between the different functionals cancel to a large extent, i.e., total-energy differences based on the PBE+TS functional provide a reliable description in this case. The transition between different phases is marked by the crossing points of different curves in Figure 3(a); the equilibrium μ_{NH_3} varies by only 0.05 eV (melem/melon) and by 0.12 eV (melon/g-h-C_3N_4) between different functionals. g-t-C_4N_3 is found to be higher in energy than g-h-C_3N_4 by 0.04 eV/atom in both PBE+TS and PBE+MBD, a rather notable difference, although still in a range that could be overturned by changes to the chemical environment (such as intercalation of ions from a salt melt). The structures used reflect the lowest-energy known corrugated structure models for each phase,[21,22] which are lower in energy by ∼0.04−0.06 eV/atom than their smaller-scale less-corrugated counterparts (Tables S6 and S7). We note that, in principle, even lower-energy structure models cannot be ruled out if a very different corrugated model for g-t-C_4N_3 or g-h-C_3N_4 could be found. Although our present work is restricted to relating existing models suggested in the literature to one another, the energy differences between the existing flat and corrugated models suggest that the resulting uncertainty will not exceed a few tens of meV/atom at most. We also note, however, that other extensive first-principles structure searches have targeted the more general space of C_3N_4 compounds, for instance, the recent searches reported in refs 72 and 73. These studies also cover different, denser, three-dimensionally bonded C_3N_4 phases that could become stable at much higher hydrostatic pressure (not the same as the partial pressure of ammonia, the relevant quantity in our present work). However, for the pressure range of interest in the present work, these composition-specific structure searches also do not reveal any significant lower-energy structural alternatives to the corrugated g-h-C_3N_4 structure considered in our work. To verify this finding, we recomputed fully optimized structures and DFT-PBE+TS total energies for the C_3N_4 structures reported in Table 1 of the Supporting Information accompanying the paper by Pickard et al.,[73] confirming that no significantly lower-energy compounds than g-h-C_3N_4 were found. Details are given in Table S11 and the accompanying text in the SI of the present work.

Using the known shape of $\mu_{NH_3}(p,T)$ for gas-phase ammonia and assuming a direct or indirect equilibrium with gas-phase $\mu_{NH_3}(p,T)$, Figure 3(a) can be converted to an NH_3 temperature−pressure phase diagram, shown in Figure 3(b). In the restricted space of phases considered in Figure 3(a), the key finding is the broad stability area of melon for common synthesis temperatures and even rather low ammonia partial pressures, consistent with the literature. g-h-C_3N_4, on the other hand, cannot become the stable phase even at very high

DOI: 10.1021/acs.chemmater.7b00965
Chem. Mater. 2017, 29, 4445−4453

synthesis temperatures unless the NH_3 partial pressure in the system is very low. For example, $p_{NH_3} < 50$ Pa would have to be maintained so that g-C_3N_4 could form at $T \approx 600$ °C, a temperature very close to the known overall decomposition temperature of the material.[42] Even lower p would be required at lower temperatures. The common synthesis route—by pyrolysis in an atmosphere that produces NH_3 and thus encourages a non-negligible NH_3 partial pressure under all circumstances—is thus an impractical if not impossible synthesis path for g-h-C_3N_4. For common synthesis conditions, particularly in a closed ampule, our calculations based on the presently known C−N compound structure models thus rule out an effective synthesis of g-h-C_3N_4. Only a different system geometry, much lower in total energy than even the heavily corrugated geometries considered in the literature so far,[21,22] could change this picture. On the basis of our present findings, the only viable pathways to H-free g-h-C_3N_4 would require very low ammonia partial pressures. This could, perhaps, be achieved by synthesis in a very low-pressure environment, such as a dynamically pumped vacuum, assuming that other degradation paths of the material can be avoided.

The overall melon synthesis conditions reported in the literature ($T \approx 500$−630 °C[10,13,15,51]) agree well with the melon stability range identified in Figure 3(b) at reasonable NH_3 partial pressures of 10^3−10^6 Pa. In particular, the apparent difficulty of synthesizing g-h-C_3N_4 at high temperatures, below the overall decomposition temperature of C−N materials, is consistent with the extent of the predicted stability range of melon. However, the low-temperature limit of melon stability, bounded by melem-like compounds, is also of interest, not least because of the potential existence of oligomeric melem species in this range with greater activity than that of crystalline melon.[10]

In Figure 4, we refine the schematic picture given in Figure 3 by adding additional C−N compound phases, including H, that have been reported in the literature. Because all three levels of theory considered in this work were shown to be nearly equivalent above, we only show the PBE-TS level of theory in Figure 4; Figure S4 shows that practically no changes occur if PBE+MBD is used instead.

First, we turn to the three crystalline melamine-melem "adduct" phases reported in the literature[51] and shown in Figure 2. Interestingly (inset of Figure 4a), the enlarged phase space shows that crystalline melem, crystalline melon, and the three adduct phases all cross in a narrow chemical potential range very close to one another with estimated Gibbs free energies only a few meV/atom apart. Regarding the lowest-energy phases at the PBE+TS level of theory, the "Adduct 1" and "Adduct 3" phases could be thermodynamically stable according to Figure 4a, whereas both "Adduct 2" and crystalline melem would remain narrowly unstable. However, for the low energy differences at issue here, either kinetic factors or entropic terms (vibrations or phonons, which were not considered in this work) or both may easily change the stability balance, rendering the calculated energetic balance of all four phases ("Adducts 1−3" and crystalline melem) consistent with past experimental observations. As a further key point, neither crystalline phase impacts the observed stability range of melon in a significant way.

Second, we consider the approximate stability of experimentally observed melem oligomer intermediates that have been shown to occur as synthesis intermediates.[10] Crystal structures (if they exist) for oligomeric melem are not known, such that a precise total energy assessment on equal footing with the remaining compounds covered in Figure 4 is not possible. We can, however, look at related compounds to arrive at a lower limit estimate of the total energy of a melem oligomer. In Figure 4, we focus on the melem dimer (see Figure 1b) as the simplest example. To estimate the energy of a melem dimer embedded in a solid phase, we take the calculated total energy of isolated dimerized melem and add the known energy gain (per atom) of crystal formation from isolated monomeric melem. A solid orange line in Figure 4a and dashed orange lines in Figure 4b indicate the relative energy and stability range of a melem dimer in this approximation. The approximate temperature/pressure range of melem dimer formation, calculated in this way, includes a temperature range from slightly below the crossover line between crystalline "Adduct 3" and crystalline melon to approximately 50 °C higher than that line. Oligomers beyond dimers are expected to extend to somewhat higher temperatures, qualitatively well in line with the experimentally found synthesis conditions of previously observed melem oligomers.[10]

We note that additional, high-pressure C−N-based compounds have not just been predicted computationally[72,73] but that a H-containing, tetrahedrally bonded phase of composition C_2N_3H (same composition as melon) with a defective wurtzite structure has also been synthesized experimentally at very high hydrostatic pressure and temperature ($p > 27$ GPa, $T > 1500$ °C).[74,75] Although these conditions are outside the range covered in our phase diagrams (Figures 3 and 4), the existence of this and potentially other similar phases is entirely consistent with our findings.

A final crystal structure suggested in the literature for PTI,[22,43] labeled g-t-$C_6N_9H_3$ (same stoichiometry as melon, see Figure S3 and Table S9), is included in Figure 4a for completeness but is not energetically competitive.

Evidently, triazine-based crystalline g-t-C_3N_4 cannot appear as a stable phase in Figures 3 and 4 because its total energy is found to be above that of the heptazine-based compound g-h-C_3N_4. However, the triazine-based compound can apparently be synthesized, albeit under the very different conditions of a salt melt under high ammonia pressure and $T = 600$ °C.[8] This g-t-C_3N_4 formation is reported to occur in equilibrium with a high-pressure NH_3 gas phase in an ampule at 600 °C,[8] i.e., fundamentally the same thermodynamic conditions as considered in our work. We note that the NH_3 chemical potential itself is well-defined by way of the equilibrium with its gas phase. Unless a very different triazine-based structure than the one considered here and in past works exists, it seems unlikely that this relatively large discrepancy could be explained by uncertainties in the level of theory used (different levels of DFT or temperature and pressure dependence of ΔG of the solid phases). The observed stability of g-t-C_3N_4, if correct, would thus have to be related to the immediate environment of a salt melt, introducing ions in close proximity to or perhaps even intercalated into the C−N compound formed.[43] The chemical difference between a H/C/N-rich environment (gas phase) and a hot salt melt environment is likely drastic and could well destabilize heptazine units completely, as is observed in the formation of triazine-based g-t-C_3N_4. A detailed theoretical assessment of this environment, however, would not be easy and is certainly beyond the confines of the current work.

DOI: 10.1021/acs.chemmater.7b00965
Chem. Mater. 2017, 29, 4445−4453

CONCLUSIONS

In conclusion, our calculations show that crystalline, heptazine-based graphitic carbon nitride (g-h-C_3N_4) cannot be stable over melon under common synthesis conditions (e.g., contact with a high-pressure NH_3 phase in a closed ampule at T = 600−700 °C) below the experimentally observed decomposition range of C−N-based materials. Extremely low NH_3 partial pressures approaching the high-vacuum range would have to be guaranteed to reach g-h-C_3N_4 below the decomposition temperature by a conventional synthesis approach. Because the recent observation of triazine-based g-t-C_3N_4 is not in line with theoretical stability estimates of crystals of both phases and because this synthesis also happens in indirect contact with a high-pressure NH_3 phase in a closed ampule, we speculate that this occurrence of a hydrogen-free C−N is because of the contact with the very different chemical environment of a hot salt melt. The dominant phase(s) formed under common reaction conditions should be H-containing, NH-bridged heptazine-based phases like melon, the proper starting point for further atomistic studies of this class of materials, and its activity.

ASSOCIATED CONTENT

Supporting Information

The Supporting Information is available free of charge on the ACS Publications website at DOI: 10.1021/acs.chemmater.7b00965.

Details of the computational settings used for the first-principles calculations and complete chemical potential expressions used for NH_3; structure models for all C−N-based materials discussed in this paper; unit cells and optimized atomic coordinates at the DFT-PBE+TS level of theory for the atomic structure models of all major phases discussed in this work; these structures, as well as associated input and output files of the FHI-aims code, can also be found as ASCII files at the NOMAD repository with the permanent digital object identifier DOI: 10.17172/NOMAD/2017.04.20-1 (PDF)

AUTHOR INFORMATION

Corresponding Author

*E-mail: volker.blum@duke.edu.

ORCID

Bettina V. Lotsch: 0000-0002-3094-303X

Volker Blum: 0000-0001-8660-7230

Notes

The authors declare no competing financial interest.

ACKNOWLEDGMENTS

T.B. acknowledges support by Grant 2014/11986-7, São Paulo Research Foundation (FAPESP). Support from a seed grant by Duke University's Energy Initiative is gratefully acknowledged. B.V.L. thanks the Deutsche Forschungsgemeinschaft (Grant LO1801/1-1) for financial support.

REFERENCES

(1) Zhu, J.; Xiao, P.; Li, H.; Carabineiro, S. A. C. Graphitic Carbon Nitride: Synthesis, Properties, and Applications in Catalysis. *ACS Appl. Mater. Interfaces* **2014**, *6*, 16449−16465.

(2) Wang, X.; Maeda, K.; Thomas, A.; Takanabe, K.; Xin, G.; Carlsson, J. M.; Domen, K.; Antonietti, M. A metal-free polymeric photocatalyst for hydrogen production from water under visible light. *Nat. Mater.* **2009**, *8*, 76−80.

(3) Wang, Y.; Wang, X.; Antonietti, M. Polymeric Graphitic Carbon Nitride as a Heterogeneous Organocatalyst: From Photochemistry to Multipurpose Catalysis to Sustainable Chemistry. *Angew. Chem., Int. Ed.* **2012**, *51*, 68−89.

(4) Marschall, R. Semiconductor Composites: Strategies for Enhancing Charge Carrier Separation to Improve Photocatalytic Activity. *Adv. Funct. Mater.* **2014**, *24*, 2421−2440.

(5) Liu, J.; Liu, Y.; Liu, N.; Han, Y.; Zhang, X.; Huang, H.; Lifshitz, Y.; Lee, S.-T.; Zhong, J.; Kang, Z. Metal-free efficient photocatalyst for stable visible water splitting via a two-electron pathway. *Science* **2015**, *347*, 970−974.

(6) von Liebig, J. On some nitrogen compounds. *Annalen der Pharmacie* **1834**, *10*, 1−47.

(7) Schwarzer, A.; Saplinova, T.; Kroke, E. Tri-s-triazines (s-heptazines)−From a "mystery molecule" to industrially relevant carbon nitride materials. *Coord. Chem. Rev.* **2013**, *257*, 2032−2062.

(8) Algara-Siller, G.; Severin, N.; Chong, S. Y.; Björkman, T.; Palgrave, R. G.; Laybourn, A.; Antonietti, M.; Khimyak, Y. Z.; Krasheninnikov, A. V.; Rabe, J. P.; Kaiser, U.; Cooper, A. I.; Thomas, A.; Bojdys, M. J. Triazine-Based Graphitic Carbon Nitride: a Two-Dimensional Semiconductor. *Angew. Chem. Int. Ed.* **2014**, *53*, 7450−7455.

(9) Kroke, E. gt-C 3N 4-The First Stable Binary Carbon(IV) Nitride. *Angew. Chem. Int. Ed.* **2014**, *53*, 11134−11136.

(10) Lau, V. W.-h.; Mesch, M. B.; Duppel, V.; Blum, V.; Senker, J.; Lotsch, B. V. Low-Molecular-Weight Carbon Nitrides for Solar Hydrogen Evolution. *J. Am. Chem. Soc.* **2015**, *137*, 1064−1072.

(11) Jürgens, B.; Irran, E.; Senker, J.; Kroll, P.; Müller, H.; Schnick, W. Melem (2,5,8-Triamino-tri-s-triazine), an Important Intermediate during Condensation of Melamine Rings to Graphitic Carbon Nitride: Synthesis, Structure Determination by X-ray Powder Diffractometry, Solid-State NMR, and Theoretical Studies. *J. Am. Chem. Soc.* **2003**, *125*, 10288−10300.

(12) Sattler, A.; Schnick, W. Zur Kenntnis der Kristallstruktur von Melem C6N7(NH2)3. *Z. Anorg. Allg. Chem.* **2006**, *632*, 238−242.

(13) Lotsch, B. V.; Döblinger, M.; Sehnert, J.; Seyfarth, L.; Senker, J.; Oeckler, O.; Schnick, W. Unmasking Melon by a Complementary Approach Employing Electron Diffraction, Solid-State NMR Spectroscopy, and Theoretical Calculations−Structural Characterization of a Carbon Nitride Polymer. *Chem. - Eur. J.* **2007**, *13*, 4969−4980.

(14) Tyborski, T.; Merschjann, C.; Orthmann, S.; Yang, F.; Lux-Steiner, M. C.; Schedel-Niedrig, T. Crystal structure of polymeric carbon nitride and the determination of its process-temperature-induced modifications. *J. Phys.: Condens. Matter* **2013**, *25*, 395402.

(15) Fina, F.; Callear, S. K.; Carins, G. M.; Irvine, J. T. S. Structural Investigation of Graphitic Carbon Nitride via XRD and Neutron Diffraction. *Chem. Mater.* **2015**, *27*, 2612−2618.

(16) Teter, D. M.; Hemley, R. J. Low-Compressibility Carbon Nitrides. *Science* **1996**, *271*, 53−55.

(17) Ortega, J.; Sankey, O. F. Relative stability of hexagonal and planar structures of hypothetical C3N4 solids. *Phys. Rev. B: Condens. Matter Mater. Phys.* **1995**, *51*, 2624−2627.

(18) Alves, I.; Demazeau, G.; Tanguy, B.; Weill, F. On a new model of the graphitic form of C3N4. *Solid State Commun.* **1999**, *109*, 697−701.

(19) Lowther, J. E. Relative stability of some possible phases of graphitic carbon nitride. *Phys. Rev. B: Condens. Matter Mater. Phys.* **1999**, *59*, 11683−11686.

(20) Kroke, E.; Schwarz, M.; Horath-Bordon, E.; Kroll, P.; Noll, B.; Norman, A. D. Tri-s-triazine derivatives. Part I. From trichloro-tri-s-triazine to graphitic C3N4 structures. *New J. Chem.* **2002**, *26*, 508−512.

(21) Gracia, J.; Kroll, P. Corrugated layered heptazine-based carbon nitride: the lowest energy modifications of C3N4 ground state. *J. Mater. Chem.* **2009**, *19*, 3013−3019.

(22) Melissen, S.; le Bahers, T.; Steinmann, S. N.; Sautet, P. Relationship between Carbon Nitride Structure and Exciton Binding

DOI: 10.1021/acs.chemmater.7b00965
Chem. Mater. 2017, 29, 4445−4453

Energies: A DFT Perspective. *J. Phys. Chem. C* **2015**, *119*, 25188−25196.
(23) Huda, M. N.; Turner, J. A. Morphology-dependent optical absorption and conduction properties of photoelectrochemical photocatalysts for H_2 production: A case study. *J. Appl. Phys.* **2010**, *107*, 123703.
(24) Guo, Y.; Yang, J.; Chu, S.; Kong, F.; Luo, L.; Wang, Y.; Zou, Z. Theoretical and experimental study on narrowing the band gap of carbon nitride photocatalyst by coupling a wide gap molecule. *Chem. Phys. Lett.* **2012**, *550*, 175−180.
(25) Xu, Y.; Gao, S.-P. Band gap of C_3N_4 in the GW approximation. *Int. J. Hydrogen Energy* **2012**, *37*, 11072−11080.
(26) Du, A.; Sanvito, S.; Li, Z.; Wang, D.; Jiao, Y.; Liao, T.; Sun, Q.; Ng, Y. H.; Zhu, Z.; Amal, R.; Smith, S. C. Hybrid Graphene and Graphitic Carbon Nitride Nanocomposite: Gap Opening, Electron−Hole Puddle, Interfacial Charge Transfer, and Enhanced Visible Light Response. *J. Am. Chem. Soc.* **2012**, *134*, 4393−4397.
(27) Butchosa, C.; Guiglion, P.; Zwijnenburg, M. A. Carbon Nitride Photocatalysts for Water Splitting: A Computational Perspective. *J. Phys. Chem. C* **2014**, *118*, 24833−24842.
(28) Ruan, L.-W.; Zhu, Y.-J.; Qiu, L.-G.; Yuan, Y.-P.; Lu, Y.-X. First principles calculations of the pressure affection to g-C3N4. *Comput. Mater. Sci.* **2014**, *91*, 258−265.
(29) Mansor, N.; Miller, T. S.; Dedigama, I.; Jorge, A. B.; Jia, J.; Brazdova, V.; Mattevi, C.; Gibbs, C.; Hodgson, D.; Shearing, P. R.; Howard, C. A.; Cora, F.; Shaffer, M.; Brett, D. J.; McMillan, P. F. Graphitic Carbon Nitride as a Catalyst Support in Fuel Cells and Electrolyzers. *Electrochim. Acta* **2016**, *222*, 44−57.
(30) Yang, P.; Ou, H.; Fang, Y.; Wang, X. A Facile Steam Reforming Strategy to Delaminate Layered Carbon Nitride Semiconductors for Photoredox Catalysis. *Angew. Chem. Int. Ed.* **2017**, *56*, 3992−3996.
(31) Xu, X.; Liu, Y.; Zhu, Y.; Fan, X.; Li, Y.; Zhang, F.; Zhang, G.; Peng, W. Fabrication of a Cu2O/g-C3N4/WS2 Triple-Layer Photocathode for Photoelectrochemical Hydrogen Evolution. *ChemElectroChem* **2017**, DOI: 10.1002/celc.201700014.
(32) Yuan, Y.; Huang, G.-F.; Hu, W.-Y.; Xiong, D.-N.; Zhou, B.-X.; Chang, S.; Huang, W.-Q. Construction of g-C3N4/CeO2/ZnO ternary photocatalysts with enhanced photocatalytic performance. *J. Phys. Chem. Solids* **2017**, *106*, 1−9.
(33) Zhang, Q.; Wang, H.; Chen, S.; Su, Y.; Quan, X. Three-dimensional TiO2 nanotube arrays combined with g-C3N4 quantum dots for visible light-driven photocatalytic hydrogen production. *RSC Adv.* **2017**, *7*, 13223−13227.
(34) Liu, J.; Zhao, D.; Li, L.; Weng, M.; Zhang, C.; Zhang, S.; Zhu, J.; Feng, Y.; Shih, K.; Huang, W. Rational Design of Mini-size Carbon Nitride Nanosheets with Double Excitation- and pH-Dependent Fluorescence Behaviors for Two-photon Cell Imaging. *Chem. - Asian J.* **2017**, *12*, 835.
(35) Ong, W.-J.; Putri, L. K.; Tan, Y.-C.; Tan, L.-L.; Li, N.; Ng, Y. H.; Wen, X.; Chai, S.-P. Unravelling charge carrier dynamics in protonated g-C3N4 interfaced with carbon nanodots as co-catalysts toward enhanced photocatalytic CO2 reduction: A combined experimental and first-principles DFT study. *Nano Res.* **2017**, *10*, 1−24.
(36) Li, S.; Wang, Z.; Wang, X.; Sun, F.; Gao, K.; Hao, N.; Zhang, Z.; Ma, Z.; Li, H.; Huang, X.; Huang, W. Orientation controlled preparation of nanoporous carbon nitride fibers and related composite for gas sensing under ambient conditions. *Nano Res.* **2017**, *10*, 1710−1719.
(37) Liu, Q.; Peng, Y.-J.; Xu, J.-C.; Ma, C.; Li, L.; Mao, C.-J.; Zhu, J.-J. Label-free electrochemiluminescence aptasensor for highly sensitive detection of acetylcholinesterase based on Au nanoparticles functionalized g-C3N4 nanohybrid. *ChemElectroChem* **2017**, DOI: 10.1002/celc.201700035.
(38) Li, J.-X.; Ye, C.; Li, X.-B.; Li, Z.-J.; Gao, X.-W.; Chen, B.; Tung, C.-H.; Wu, L.-Z. A Redox Shuttle Accelerates O2 Evolution of Photocatalysts Formed In Situ under Visible Light. *Adv. Mater.* **2017**, 1606009.
(39) Zhu, C.; Jiang, Z.; Chen, L.; Qian, K.; Xie, J. L-cysteine-assisted synthesis of hierarchical NiS2 hollow spheres supported carbon nitride as photocatalysts with enhanced lifetime. *Nanotechnology* **2017**, *28*, 115708.
(40) Vo, V.; Thi, X. D. N.; Jin, Y.-S.; Thi, G. L.; Nguyen, T. T.; Duong, T. Q.; Kim, S.-J. SnO2 nanosheets/g-C3N4 composite with improved lithium storage capabilities. *Chem. Phys. Lett.* **2017**, *674*, 42−47.
(41) Savateev, A.; Pronkin, S.; Willinger, M. G.; Antonietti, M.; Dontsova, D. Towards Organic Zeolites and Inclusion Catalysts: Heptazine Imide Salts Can Exchange Metal Cations in the Solid State. *Chem. - Asian J.* **2017**, 1.
(42) Bojdys, M. J. *On new allotropes and nanostructures of carbon nitrides*. Ph.D. thesis, Universität Potsdam, Potsdam, Germany, 2009.
(43) Wirnhier, E.; Döblinger, M.; Gunzelmann, D.; Senker, J.; Lotsch, B. V.; Schnick, W. Poly(triazine imide) with intercalation of lithium and chloride ions [(C3N3)2(NH(x)Li(1-x))3·LiCl]: a crystalline 2D carbon nitride network. *Chem. - Eur. J.* **2011**, *17*, 3213−21.
(44) Kouvetakis, J.; Todd, M.; Wilkens, B.; Bandari, A.; Cave, N. Novel Synthetic Routes to Carbon-Nitrogen Thin Films. *Chem. Mater.* **1994**, *6*, 811−814.
(45) Todd, M.; Kouvetakis, J.; Groy, T. L.; Chandrasekhar, D.; Smith, D. J.; Deal, P. W. Novel Synthetic Routes to Carbon Nitride. *Chem. Mater.* **1995**, *7*, 1422−1426.
(46) Lau, V. W.-h.; Moudrakovski, I.; Botari, T.; Weinberger, S.; Mesch, M. B.; Duppel, V.; Senker, J.; Blum, V.; Lotsch, B. V. Rational design of carbon nitride photocatalysts by identification of cyanamide defects as catalytically relevant sites. *Nat. Commun.* **2016**, *7*, 12165.
(47) Lau, V. W.-h.; Yu, V. W.-z.; Ehrat, F.; Botari, T.; Moudrakovski, I.; Simon, T.; Duppel, V.; Medina, E.; Stolarczyk, J.; Feldmann, J.; Blum, V.; Lotsch, B. V. Urea-Modified Carbon Nitrides: Enhancing Photocatalytic Hydrogen Evolution by Rational Defect Engineering. *Adv. Energy Mater.* **2017**, 1602251.
(48) Reuter, K.; Scheffler, M. Composition, structure, and stability of RuO2 (110) as a function of oxygen pressure. *Phys. Rev. B: Condens. Matter Mater. Phys.* **2001**, *65*, 035406.
(49) Schwarzer, A.; Böhme, U.; Kroke, E. Use of Melem as a Nucleophilic Reagent to Form the Triphthalimide C6N7(phthal)3 − New Targets and Prospects. *Chem. - Eur. J.* **2012**, *18*, 12052−12058.
(50) Sattler, A.; Schnick, W. On the Formation and Decomposition of the Melonate Ion in Cyanate and Thiocyanate Melts and the Crystal Structure of Potassium Melonate, K3[C6N7(NCN)3]. *Eur. J. Inorg. Chem.* **2009**, *2009*, 4972−4981.
(51) Sattler, A.; Pagano, S.; Zeuner, M.; Zurawski, A.; Gunzelmann, D.; Senker, J.; Müller-Buschbaum, K.; Schnick, W. Melamine-Melem Adduct Phases: Investigating the Thermal Condensation of Melamine. *Chem. - Eur. J.* **2009**, *15*, 13161−13170.
(52) Lejaeghere, K.; et al. Reproducibility in density functional theory calculations of solids. *Science* **2016**, *351*, aad3000.
(53) Blum, V.; Gehrke, R.; Hanke, F.; Havu, P.; Havu, V.; Ren, X.; Reuter, K.; Scheffler, M. Ab initio molecular simulations with numeric atom-centered orbitals. *Comput. Phys. Commun.* **2009**, *180*, 2175−2196.
(54) Havu, V.; Blum, V.; Havu, P.; Scheffler, M. Efficient integration for all-electron electronic structure calculation using numeric basis functions. *J. Comput. Phys.* **2009**, *228*, 8367−8379.
(55) Ren, X.; Rinke, P.; Blum, V.; Wieferink, J.; Tkatchenko, A.; Sanfilippo, A.; Reuter, K.; Scheffler, M. Resolution-of-identity approach to Hartree−Fock, hybrid density functionals, RPA, MP2 and GW with numeric atom-centered orbital basis functions. *New J. Phys.* **2012**, *14*, 053020.
(56) Knuth, F.; Carbogno, C.; Atalla, V.; Blum, V.; Scheffler, M. All-electron formalism for total energy strain derivatives and stress tensor components for numeric atom-centered orbitals. *Comput. Phys. Commun.* **2015**, *190*, 33−50.
(57) Perdew, J. P.; Burke, K.; Ernzerhof, M. Generalized Gradient Approximation Made Simple. *Phys. Rev. Lett.* **1996**, *77*, 3865−3868.
(58) Tkatchenko, A.; Scheffler, M. Accurate Molecular van der Waals Interactions from Ground-State Electron Density and Free-Atom Reference Data. *Phys. Rev. Lett.* **2009**, *102*, 073005.

DOI: 10.1021/acs.chemmater.7b00965
Chem. Mater. 2017, 29, 4445−4453

(59) Rossi, M.; Chutia, S.; Scheffler, M.; Blum, V. Validation challenge of density-functional theory for peptides-example of Ac-Phe-Ala5-LysH(+). *J. Phys. Chem. A* **2014**, *118*, 7349−7359.
(60) Schubert, F.; Rossi, M.; Baldauf, C.; Pagel, K.; Warnke, S.; von Helden, G.; Filsinger, F.; Kupser, P.; Meijer, G.; Salwiczek, M.; Koksch, B.; Scheffler, M.; Blum, V. Exploring the conformational preferences of 20-residue peptides in isolation: Ac-Ala_{19}-Lys + H^+ vs. Ac-Lys-Ala_{19} + H^+ and the current reach of DFT. *Phys. Chem. Chem. Phys.* **2015**, *17*, 7373−7385.
(61) Tkatchenko, A. Current Understanding of van der Waals Effects in Realistic Materials. *Adv. Funct. Mater.* **2015**, *25*, 2054−2061.
(62) Ambrosetti, A.; Reilly, A. M.; DiStasio, R. A., Jr.; Tkatchenko, A. Long-range correlation energy calculated from coupled atomic response functions. *J. Chem. Phys.* **2014**, *140*, 18A508.
(63) Heyd, J.; Scuseria, G. E.; Ernzerhof, M. Erratum: "Hybrid functionals based on a screened Coulomb potential" [J. Chem. Phys. 118, 8207 (2003)]. *J. Chem. Phys.* **2006**, *124*, 219906.
(64) Levchenko, S. V.; Ren, X.; Wieferink, J.; Johanni, R.; Rinke, P.; Blum, V.; Scheffler, M. Hybrid functionals for large periodic systems in an all-electron, numeric atom-centered basis framework. *Comput. Phys. Commun.* **2015**, *192*, 60−69.
(65) Ihrig, A. C.; Wieferink, J.; Zhang, I. Y.; Ropo, M.; Ren, X.; Rinke, P.; Scheffler, M.; Blum, V. Accurate localized resolution of identity approach for linear-scaling hybrid density functionals and for many-body perturbation theory. *New J. Phys.* **2015**, *17*, 093020.
(66) McQuarrie, D. *Statistical Mechanics*; University Science Books, 2000.
(67) NIST-JANAF Table − Ammonia. http://kinetics.nist.gov/janaf/html/H-083.html (accessed Sept. 13, 2016).
(68) Chase, M. W. *NIST-JANAF Themochemical Tables*, 4th ed.; J. Phys. Chem. Ref. Data, **1998**; Vol. *Monograph 9*.
(69) Haar, L.; Gallagher, J. S. Thermodynamic properties of ammonia. *J. Phys. Chem. Ref. Data* **1978**, *7*, 635.
(70) Chamorro-Posada, P.; Vázquez-Cabo, J.; Sánchez-Arévalo, F. M.; Martín-Ramos, P.; Martín-Gil, J.; Navas-Gracia, L. M.; Dante, R. C. 2D to 3D transition of polymeric carbon nitride nanosheets. *J. Solid State Chem.* **2014**, *219*, 232−241.
(71) Seyfarth, L.; Seyfarth, J.; Lotsch, B. V.; Schnick, W.; Senker, J. Tackling the stacking disorder of melon-structure elucidation in a semicrystalline material. *Phys. Chem. Chem. Phys.* **2010**, *12*, 2227−2237.
(72) Dong, H.; Oganov, A. R.; Zhu, Q.; Qian, G.-R. The phase diagram and hardness of carbon nitrides. *Sci. Rep.* **2015**, *5*, 9870.
(73) Pickard, C. J.; Salamat, A.; Bojdys, M. J.; Needs, R. J.; McMillan, P. F. Carbon nitride frameworks and dense crystalline polymorphs. *Phys. Rev. B: Condens. Matter Mater. Phys.* **2016**, *94*, 094104.
(74) Horvath-Bordon, E.; Riedel, R.; McMillan, P. F.; Kroll, P.; Miehe, G.; van Aken, P. A.; Zerr, A.; Hoppe, P.; Shebanova, O.; McLaren, I.; Lauterbach, S.; Kroke, E.; Boehler, R. High-Pressure Synthesis of Crystalline Carbon Nitride Imide, C2N2(NH). *Angew. Chem. Int. Ed.* **2007**, *46*, 1476−1480.
(75) Salamat, A.; Woodhead, K.; McMillan, P. F.; Cabrera, R. Q.; Rahman, A.; Adriaens, D.; Corà, F.; Perrillat, J.-P. Tetrahedrally bonded dense C_2N_3H with a defective wurtzite structure: X-ray diffraction and Raman scattering results at high pressure and ambient conditions. *Phys. Rev. B: Condens. Matter Mater. Phys.* **2009**, *80*, 104106.

DOI: 10.1021/acs.chemmater.7b00965
Chem. Mater. 2017, 29, 4445−4453

Supporting Information: Thermodynamic Equilibria in Carbon Nitride Photocatalyst Materials and Conditions for the Existence of Graphitic Carbon Nitride g-C_3N_4

Tiago Botari,[†,¶] William Paul Huhn,[†] Vincent Wing-hei Lau,[‡] Bettina V. Lotsch,[‡,§] and Volker Blum[*,†]

†*Department of Mechanical Engineering and Materials Science, Duke University, Durham, NC 27708, USA*

‡*Max Planck Institute for Solid State Research Heisenbergstraße 1, 70569 Stuttgart, Germany*

¶*Applied Physics Department, State University of Campinas, Campinas-SP, 13083-970, Brazil*

§*Department of Chemistry, University of Munich, Butenandtstraße 5-13, 81377 Munich, Germany*

E-mail: volker.blum@duke.edu

May 6, 2017

All-Electron Electronic Structure Calculations and Numeric Atom-Centered Basis Sets Employed

All the electronic structure calculations reported in this work were carried out using the FHI-aims all-electron electronic structure code.[1–6] Fully relaxed structure models for each compound were obtained by combining the semilocal PBE[7] density functional with the Tkatchenko-Scheffler (TS)[8] correction to account for long-range dispersion (van der Waals) interactions, abbreviated as "DFT-PBE+TS". In addition, the hybrid density functional HSE06[9] and a recent many-body dispersion correction[10] were also included to validate the results obtained. The basis sets used for "tight" settings are standard in FHI-aims, see, e.g., Ref.[1] The basis sets employed for "intermediate" settings are given in Table S1 for completeness. The auxiliary basis function listed together with each basis set is not used to expand the generalized Kohn-Sham orbitals. It only enters the construction of the resolution-of-identity basis for the two-electron screened Coulomb operator as described in Ref.[5] We used the atomic ZORA approximation to correct the electronic energy to account for relativistic effects[1] (note that any relativistic effects are minor in the case of the light elements at issue here).

Atomic coordinates for the final DFT-PBE+TS relaxed structures of the different phases are included in FHI-aims' human-readable `geometry.in` format with this submission. This format is also supported by a variety of viewer programs (e.g., jmol) and can be converted to other structure file format types using the OpenBabel tool. Additionally, these structures, as well as associated input and output files of the FHI-aims code, can also be found as ASCII files at the NOMAD repository with the permanent digital object identifier DOI:10.17172/NOMAD/2017.04.20-1 .

Table S1: FHI-aims "intermediate" basis settings used in the hybrid HSE06 functional calculations. The minimal basis consists of the free-atom core and valence radial functions (these radial functions are here determined for the PBE generalized-gradient density functional). Additional basis functions are included following the "tiers" or levels of basis functions described in Ref.[1] H(nl, z) denotes a hydrogen-like basis function for the bare Coulomb potential z/r, where n is the radial quantum number and l is the angular quantum number. The complete "first tier" and a single function from the "second tier" of basis functions for each element is included. The auxiliary basis set employed to express the Coulomb operator using a resolution-of-identity formalism[3] is augmented by additional higher angular momentum functions as described in detail in Ref.[5] Each radial function is confined to within r_{outer}=6 Å from its nucleus, and all grid and Hartree potential related parameters remain the same as the standard "tight" settings used in FHI-aims.

	H	C	N
Minimal basis	1s	[He] + 2s 2p	[He] + 2s 2p
"First tier"	H(2s, 2.1)	H(2p, 1.7)	H(2p, 1.8)
	H(2p, 3.5)	H(3d, 6.0)	H(3d, 6.8)
		H(2s, 4.9)	H(3s, 5.8)
"Second tier"	H(1s, 0.85)	H(4f, 9.8)	H(4f, 10.8)
Auxiliary only	H(3d, 7.0)	H(5g,14.4)	H(5g,16.0)

Tabulated Gas-Phase Chemical Potential of Ammonia (NH_3)

To connect the theoretical results with the experimental synthesis conditions, we employed the known temperature (T) and pressure (P) dependence of the chemical potential for the ammonia gas. Specifically, we used the polyatomic ideal gas approximation fitted to experimental data, substituting the first-principles calculated total energy of an isolated NH_3 molecule, E_{ammonia}, for the total-energy part of the chemical potential $\mu(T, P)$. The chemical potential is then (Ref.[11] and applying the Legendre transformation $G = H + PV$) given by:

$$\begin{aligned}\mu(T,P) - E_{ammonia} = & - kT\{\ln\left[\left(\frac{2\pi m_T kT}{h^2}\right)^{3/2}\frac{kT}{P}\right] \\ & + \ln\left(\frac{1}{\sigma}\sqrt{\frac{\pi T^3}{\theta_{r,1}\theta_{r,2}\theta_{r,3}}}\right) \\ & - \sum_i^{3N-6}\ln\left(1-e^{\frac{\theta_{\nu,i}}{T}}\right)\}, \end{aligned} \tag{S1}$$

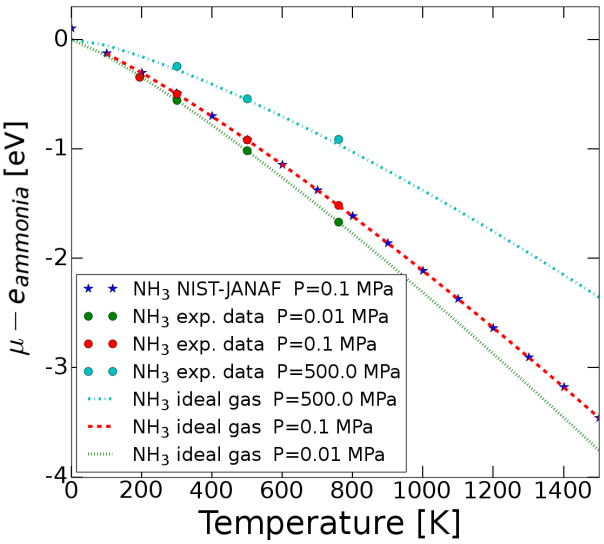

Figure S1: Comparison of the ideal-gas chemical potential expression Eq. (S1) used in this work (taken from Ref.[11] and labelled "ideal gas;" parameters given in Table S2) to available thermochemical reference data for P=0.01 MPa, 0.1 MPa, and 500 MPa, respectively. The reference data are taken from the NIST-JANAF table[12,13] and from the thermodynamic analysis of Haar and Gallagher[14] (labelled "exp. data") as described in the text.

where k is the Boltzmann constant, m_T the total mass of the ammonia molecule, h is the Planck constant, $\sigma = 3$ and $N = 4$ for ammonia molecule. $\theta_{r,i}$ with $i = 1..3$ is the rotational temperature, and $\theta_{\nu,i}$ is the vibrational temperature. The rotational temperature is defined by

$$\theta_{r,i} = \frac{\hbar}{2I_i K_b} \ , \tag{S2}$$

where I_i is one of the three inertia momentum of the molecule. The vibrational temperature can be defined as

$$\theta_{\nu,i} = \frac{\hbar \nu_i}{K_b} \ , \tag{S3}$$

where ν_i is the normal mode of vibration of the molecule. The $\theta_{r,i}$ and $\theta_{\nu,i}$ used in this work were obtained from Ref.;[15] their values are reproduced in table S2.

To verify the accuracy of this chemical potential expression, we compare the chemical potential $\mu(T, P)$ (equation S1) with the data available in the literature, specifically the NIST-JANAF Thermochemical Tables[12,13] for P = 0.1MPa and the pressure-dependent thermochemical reference data by Haar and Gallagher.[14] A didactic work explaining how

to use the NIST-JANAF Thermochemical Tables can be found in Ref.[16] Specifically, we obtained the Gibbs free energy G for $P = 0.1$MPa from the tabulated values of $-[G^o - H^o(T_r)]/T$ and $H^o - H^o(T_r)$, where H indicates the enthalpy and the overscore ^{o} indicates the conditions $P^o = 0.1\ MPa$ and $T_r = 298.15\ K$. These values can be related to $\mu(T, P^o) - e_{\text{ammonia}}$ (per NH_3 molecule) using the expression

$$\begin{aligned} \mu(T, P^o) - E_{\text{ammonia}} &= -\left[\frac{G^o - H^o(T_r)}{T}\right] \times T \\ - \quad & [H + H^o(T_r)] \ , \end{aligned} \tag{S4}$$

where $G^o = G(T, P^o)$, $H = H(T = 0, P^o)$, $H^o = H(T, P^o)$, $H^o(T_r) = H(T_r, P^o)$ and we used $G(T = 0, P^o) = H(T = 0, P^o)$. The resulting comparison is shown in Figure S1 for a wide range of temperatures and for pressures P=0.01 MPa, 0.1 MPa, and 500 MPa, respectively, showing the excellent validity of the parameterized ideal gas expression Eq. (S1) over the entire range of T and P relevant in this work.

Table S2: Rotational and vibrational temperatures for the ammonia gas, obtained from Ref.[11] and Ref.[15] [d]: states with double degeneracy.

Ro-vibrational Temperatures	[K]
$\theta_{r,1}$	4800
$\theta_{r,2}$	1360
$\theta^d_{r,3}$	4880
$\theta^d_{r,4}$	2330
$\theta_{\nu,1}$	13.6
$\theta_{\nu,2}$	13.6
$\theta_{\nu,3}$	8.92

Table S3: Unit cell parameters of crystalline melem determined in experiment (Ref.[17]) and by a total-energy minimization of atomic positions and unit cell parameters in this work, using DFT-PBE+TS. †Distance calculated from simulated XRD.

Structure	a [Å]	b [Å]	c [Å]	α	β	γ	interplanar distance [Å]
XRD[17]	7.399	8.653	13.382	90.0°	99.912°	90.0°	3.27
PBE+TS	7.593	8.435	13.540	90.0°	101.7°	90.0°	3.28†

Structure Model, Total Energies and Calculated Crystallographic Parameters for Isolated and Crystalline Melem

The structure optimization for bulk melem (the heptazine monomer terminated with -NH_2 groups, see Figures 1(a) and 1(c) of the main paper) used the known crystal structure published in Ref.[17] as a starting point. The unit cell parameters before and after structure optimization using the DFT-PBE+TS density functional are summarized in Table S3.

Structure Models, Total Energies and Calculated Crystallographic Parameters for Crystalline Melon

Table S4 summarizes the experimental literature results pertaining to "single shifted plane" (SSP) stacked models of the crystal structure of melon, as well as the minimum-energy DFT-PBE+TS geometry obtained in this work. In Table S5, we alternatively consider orthorhombic A-B stacked models as starting points, as suggested on the basis of XRD in Ref.,[18] and as suggested on the basis of semiempirical PM6 calculations in Ref.[19] DFT-PBE+TS optimizations of both structures (this work) are also given.

Regarding the interlayer distances obtained in different experimental references, we note that there is a known dependence on the synthesis conditions. Chamorro-Posada *et al.* find that the interlayer distance decreases with increasing annealing temperature, from 3.27 Å (500°C) to 3.19 Å (700°C). A dependence on synthesis conditions is also observed in other studies.[20,21] Buckling of the melon layers has also been discussed in the literature.[21] Our calculations do not show any evidence of the buckling considered in that reference.

The stacking registries between subsequent melon planes are not safely known, much less settled, from diffraction theory. The XRD structure model discussed in Ref.[21] assumes unshifted ("A-A") stacking of successive planes but deviates significantly from other studies regarding the lateral unit cell parameters. The XRD study by Fina and coworkers[18] discusses both an orthorhombic SSP stacking (90° unit cell angles, no registry of successive planes) and an orthorhombic "A-B" stacked model where there is a registry shift between successive planes. Their model termed "shift A" is in good agreement with their XRD data and included in Table S5.

Our theoretical analysis shows that an orthorhombic A-A stacking is locally unstable. Successive layers shift dramatically, leading to the final structure included in Table S4. The structure shown is the minimum-energy structure reached in separate relaxations of 16 different starting structures, using a 4×4 grid of different initial structures with interplanar registries between 0 and 0.5 along the a and b axes. Several different local minima are iden-

Table S4: Unit cell parameters of experimental models of SSP-stacked monoclinic melon,[19,21,22] compared to the DFT-PBE+TS fully-relaxed structure (this work). The "PBE+TS" result is obtained by a local structure optimization, starting from a hypothetical unstable orthorhombic stacking of successive planes. The final shifts between successive planes amount to $x_{f,a}$=0.175 and $x_{f,b}$=−0.131 in fractional units of a and b, respectively. Using a 4×4 grid of different initial structures with interplanar registries between 0 and 0.5 along the a and b axes, we did not find a lower-energy SSP stacked arrangement of melon planes. From among the XRD lattice parameter estimates according to reference[19] we quote the sample with the highest crystallinity (synthesis at T=700°C).

Structure	a [Å]	b [Å]	c [Å]	α	β	γ	interplanar distance [Å]
Electron diffraction[22]	16.7	12.4	3.2	90°	90°	90°	3.2 (XRD)
Electron diffraction[22]	16.7	12.4	–	90°	92-115°	90°	3.2 (XRD)
TEM (a,b), XRD (c)[19]	16.6	13.4	–	–	–	–	3.19
XRD[21]	16.2	12.1	3.275	90°	90°	87-90°	3.26-3.275
PBE+TS	16.67	12.69	4.63	111.0°	51.0°	90°	3.20

tified, but energetically, all remain within 5 meV/atom of one another. This indicates that more than one registry shift between different planes may be found in actual (experimental) nanoplatelets of stacked melon planes.

Interestingly, the unit cell angles of the orthorhombic A-B cells are locally stable, i.e., do not deviate much from their starting values α=β=90°. However, the registry shifts of DFT-PBE+TS local energy minima differ noticeably from the reports in Refs.[18,19] The DFT-PBE+TS predicted total energies are also approximately 0.1 eV per melon unit area (72 atoms) above that found for the final structure starting from A-A models. From a total energy point of view, the registry-shifted non-orthorhombic unit cell arrangement (SSP) is more favorable.

A comparison of simulated XRD patterns for the lowest-energy DFT-PBE+TS predicted SSP stacked and AB stacked structure models of Tables S4 and S5, respectively, and scanned experimental XRD data from Refs.[22] and[19] is shown in Figure S2. The comparison shows that experimental XRD scans can vary; a clear distinction between the SSP stacked and the AB stacked model is not possible based on this data alone.

Table S5: Unit cell parameters of literature models of AB-stacked orthorhombic melon[18,19] and fully relaxed DFT-PBE+TS geometries resulting from energy minimization (this work). "Init. A-B shift" defines the interplanar shift used in the starting structure of the DFT-PBE+TS relaxations. ΔE refers to the DFT-PBE+TS energy per unit cell of a single melon plane (72 atoms), using the optimized SSP stacked model in Table S4 as a reference (energy zero). The model of Chamorro-Posada et al.[19] refers to a calculated structure model based on the semiempirical PM6 model Hamiltonian (Fig. 4 in Ref.[19]) that compares reasonably well to TEM and X-ray powder diffraction experiments in Ref.[19] A-B shifts (in fractional coordinates of a and b) were measured from a scan of their Figure 4 and are therefore approximate. All unit cell parameters were included as free parameters during the DFT-PBE+TS optimization.

	Init. A-B shift		Final A-B shift		Final unit cell parameters							
Source	$x_{i,a}$	$x_{i,b}$	$x_{f,a}$	$x_{f,b}$	a [Å]	b [Å]	c [Å]	α	β	γ	d [Å]	ΔE [eV]
XRD[18]			0.124	-0.244	16.4	12.4	6.49	90	90	90	3.245	–
PBE+TS	0.124	-0.244	0.168	-0.149	16.66	12.68	6.59	78.8	85.6	90.0	3.22	+0.063
Theory (PM6)[19]	–	–	0.167	0.135	17.26	13.16	6.46	90.23	92.36	90.03	3.23	–
PBE+TS	0.2	0.15	0.173	0.117	16.66	12.69	6.44	89.4	89.7	90.0	3.22	+0.089

Structure Models, Total Energies and Calculated Crystallographic Parameters for g-h-C_3N_4

Final calculated geometric parameters for all g-h-C_3N_4 structures investigated here can be found in table S6. We confirm that the significantly buckled, large-unit-cell structure models of Refs.[23,24] are much lower in energy than planar arrangements (the planarity of which is due to a much smaller supercell size in the calculations).

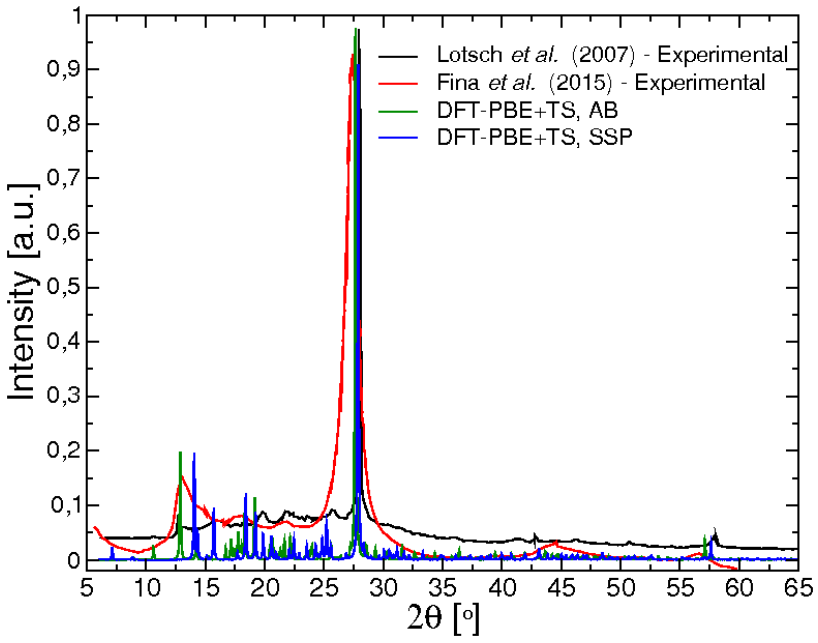

Figure S2: Powder X-ray diffraction (PXRD) scans for polymeric melon. Black line: Experimental data adapted from Lotsch *et al.*, Ref.,[22] Figure 3. Red line: Experimental data adapted from Fina *et al.*, Ref.,[18] Figure 3. Green line: Simulated PXRD for the AB stacked, DFT-PBE+TS optimized structure model, using the suggested orthorhombic AB stacked structure proposed by Fina *et al.*[18] as the initial structure. Blue line: Simulated PXRD for the SSP stacked melon structure model, with optimized coordinates using DFT-PBE+TS, that yields the lowest total energy in this work. As mentioned in the main text, different shifts between successive planes energetically close to one another and could also lead to an overall stacking that is more similar to the orthorhombic case and thus to the experimental PXRD.

Structure Models, Total Energies and Calculated Crystallographic Parameters for g-t-C_3N_4

Final calculated geometric parameters for all g-t-C_3N_4 structures investigated here can be found in Table S7. The models include AB- and ABC-stacked models from Ref.[26] as well as a larger unit cell model from Ref.[24] The lowest-energy triazine-based model in Table S7 is *higher* by Δe=0.043 eV/atom than the overall lowest-energy heptazine-based model in Table S6.

Table S6: Computed parameters of the g-h-C_3N_4 structure models considered in this work. Structure models reflecting different unit cell sizes and different interplanar arrangements are shown. For each structure model, the number of atoms per unit cell, N, is given. The structures labelled as "initial" are experimental XRD structures. For each structure, the unit cell parameters and internal (atomic) coordinates were optimized using DFT-PBE+TS. All calculations used "tight" settings. The two largest unit-cell models (Gracia *et al.* 2009 and Melissen *et al.* 2015) reveal significantly buckled structures. The local minima corresponding to them in DFT-PBE+TS are the same (lattice vectors are interchanged). Their much lower total energies, compared to the more constrained, small-cell planar models, show that g-h-C_3N_4 will not exist as an effectively 2D material of stacked planes. The energy difference Δe between planar and buckled models is reported in eV/atom, not per supercell.

Structure	N	Method	a [Å]	b [Å]	c [Å]	α	β	γ	Δe [$eV/atom$]
Tyborski *et al.* 2013 SSP[25]	14	Initial	6.95	6.95	3.275	90	90	120	
	14	PBE+TS	6.91	6.95	4.10	92.5	112.7	119.8	0.055
Tyborski *et al.* 2013 AB[25]	28	Initial	6.60	6.60	6.55	90	90	120	
	28	PBE+TS	6.96	6.94	6.79	90.6	90.0	120.1	0.044
Gracia *et al.* 2009[23]	224	Initial	13.31	23.74	7.92	90	90	90	
	224	PBE+TS	13.32	23.78	7.05	90.0	90.1	90.0	0.000
Melissen *et al.* 2015[24]	112	Initial	11.84	6.75	13.25	90	90	90	
	112	PBE+TS	11.89	7.05	13.33	90.0	90.0	90.0	0.000

Crystalline Melamine-Melem Adduct Phases

Experimental and DFT-PBE+TS calculated unit cell parameters for the experimentally reported, crystalline melamine-melem adduct phases reported in Ref.[27] are summarized in Table S8. The corresponding structures are shown in Figure 2 in the main paper.

Table S7: Computed parameters of all g-t-C_3N_4 structure models investigated in this work. Structures reflecting different unit cell sizes and different interplanar arrangements are shown. For each structure model, the number of atoms per unit cell is given. The structure labelled as "initial" are structure models suggested in Refs.[26] and.[24] For each structure, the unit cell parameters and internal (atomic) coordinates were optimized using the DFT-PBE+TS density-functional. All calculations used "tight" settings.

Structure	N	Method	a [Å]	b [Å]	c [Å]	α	β	γ	Δe $[eV/atom]$
Algarra-Siller *et al.* 2014 AB[26]	14	Initial	4.70	4.69	6.76	87.5	95.4	119.9	
	14	PBE+TS	4.70	4.69	6.87	84.8	92.7	119.9	0.058
Algarra-Siller *et al.* 2014 ABC[26]	21	Initial	5.04	5.04	9.87	90	90	120	
	21	PBE+TS	4.70	4.69	10.13	88.3	93.6	119.9	0.054
Melissen *et al.* 2015[24]	42	Initial	7.96	7.96	6.76	90	90	120	
	42	PBE+TS	7.99	7.99	6.96	90.0	90.0	120.0	0.00

Table S8: Computational parameters for melamine-melem adduct phases, following the experimental structure models of Sattler *et al.*[27] For each structure, the chemical formula and number of atoms per unit cell is given. The structure labelled as "initial" are experimental XRD structures. For each structure, the unit cell parameters and internal (atomic) coordinates were optimized using the DFT-PBE+TS density functional. N is the number of atoms per unit cell contained in each model. All calculations used "tight" settings.

Structure	Chemical Formula	N	Method	a [Å]	b [Å]	c [Å]	α	β	γ
Sattler *et al.* (2009)[27] "Adduct 1"	$2C_3N_3(NH_2)_3{\cdot}C_6N_7(NH_2)_3$	208	Initial	21.53	12.60	6.85	90.0	94.8	90.0
		208	PBE+TS	21.50	12.56	6.83	90.0	97.6	90.0
Sattler *et al.* (2009)[27] "Adduct 2"	$C_3N_3(NH_2)_3{\cdot}C_6N_7(NH_2)_3$	148	Initial	7.33	7.48	24.92	90.0	90.0	90.0
		148	PBE+TS	7.35	7.46	24.81	90.0	89.1	90.0
Sattler *et al.* (2009)[27] "Adduct 3"	$C_3N_3(NH_2)_3{\cdot}3C_6N_7(NH_2)_3$	324	Initial	14.37	25.81	8.16	90.0	94.6	90.0
		324	PBE+TS	14.36	25.71	8.23	90.0	94.8	90.0

Poly(triazine imide) Phase g-$C_6N_9H_3$

A poly(triazine imide) crystal structure g-t-$C_6N_9H_3$ was experimentally suggested in Ref.[28] and further pursued in Ref.[24] We included this structure in our analysis by performing a full DFT-PBE+TS structure optimization. The suggested structure is shown in Fig. S3 and its unit cell parameters are summarized in Table S9. We find this structure to be energetically unstable compared to melon.

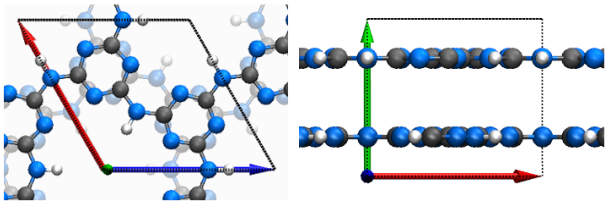

(a) g-t-$C_6N_9H_3$ Front view (b) g-t-$C_6N_9H_3$ Lateral view

Figure S3: Suggested crystal structure models of poly(triazine imide), PTI, g-t-$C_6N_9H_3$, following Ref.,[24] using unit cell parameters and atomic positions determined by DFT-PBE+TS structure optimization in this work (see Table S9).

Table S9: Computed parameters for the PTI phase, g-t-$C_6N_9H_3$. The structure labelled as "initial" is the structure proposed in Ref.[24] The unit cell parameters and internal (atomic) coordinates were optimized using the DFT-PBE+TS density functional.

Structure	N	Method	a [Å]	b [Å]	c [Å]	α	β	γ
Melissen *et al.* (2015)[24]	36	Initial	8.56	8.56	6.51	90.0	90.0	120.0
	36	Opt. PBE+TS	8.62	8.62	6.68	90.1	90.0	120.0

Temperature-Pressure Phase Diagrams

In addition to the temperature-pressure phase diagrams included in the main text (Figures 3 and 4), in Table S10 we give the predicted crossing chemical potentials of the Gibbs free energies (per atom) of the key phases crystalline melem, melon, and of the hypothetical g-h-C_3N_4 phase as they emerge from three different functionals: DFT-PBE+TS, DFT-PBE+MBD, and DFT-HSE06+MBD. In all cases, the equilibrium geometries obtained at the DFT-PBE+TS level of theory were used.

In Figure S4, we show the predicted equilibrium phase diagram including all phases considered in this paper, but evaluated at the DFT-PBE+MBD level of theory. Equilibrium geometries obtained at the DFT-PBE+TS level of theory were used. The differences to the corresponding phase diagram in Figure 4 of the main text are minor.

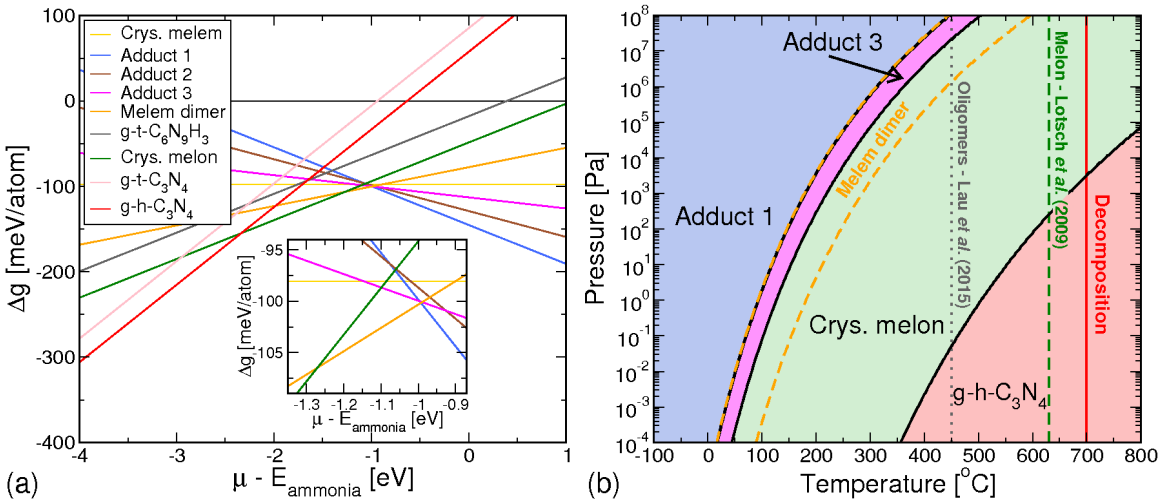

Figure S4: Gibbs free energies reflecting the same space of phases as Figure 4 of the main paper, but evaluated at the DFT-PBE+MBD level of theory. (a) Calculated Gibbs free energies Δg per atom for the different phases as in Figure 4 of the main paper. (b) Calculated temperature-pressure phase diagram as described for Figure 4 in the main paper.

Additional C_3N_4 Structure Candidates Identified by Pickard et al. 2016

In Ref.,[29] Pickard *et al.* used an extensive, *ab initio* random structure search based on the PBEsol[30] density functional of the compound space associated with the composition C_3N_4. As a result, Pickard *et al.* identified specific sets of energetically competitive structures in different hydrostatic pressure ranges, covering low pressure (p=0) as well as other ranges spanning up to p=400 GPa that are not relevant for our work. (Note that hydrostatic pressure is distinct from the NH_3 partial pressure that appears in our main paper's Figures 3

Table S10: Predicted chemical potentials for the crossing points of the Gibbs free energy for crystalline melem to melon and melon to g-C_3N_4 in Figure 3 in the main text. † DFT-PBE+TS predicted equilibrium geometries were used for DFT-PBE+MBD and HSE06+MBD.

	$\mu_{\text{melem (cr.) - melon}}$	$\mu_{\text{melon - g-h-heptazine}}$
PBE@TS	-1.06 eV	-2.38 eV
PBE@MBD †	-1.08 eV	-2.34 eV
HSE06@MBD †	-1.11 eV	-2.45 eV

and 4.) Their search at p=0 revealed ten alternative compounds of composition C_3N_4 that are energetically competitive with the lowest-energy layered corrugated g-h-C_3N_4 prototype considered in the present work. These structures are summarized in Table I of the Supplementary Information document accompanying Ref.[29] and their PBEsol-optimized geometries are also provided with that reference.

We compared the energetic stability of these ten alternative compounds to the structures considered in our own work. Since the different density functionals employed will yield different lowest-energy geometries and energetic hierarchies, we fully relaxed each of the structures reported by Pickard *et al.* using the methodology employed in our paper, i.e., the DFT-PBE+TS approach and tight settings in the FHI-aims code. The resulting energy hierarchies are compared in Table S11 below. Using the description based on PBE+TS, no structure emerges that is significantly lower in energy than the layered heptazine-based g-h-C_3N_4. A single structure, labelled "C3N4-Pca21-hept" by Pickard *et al.* and in Table S11, is found to be energetically competitive with g-h-C_3N_4 within 1 meV/atom. The C3N4-Pca21-hept structure is also based on bridged heptazine units, but in this case interlinked in three dimensions. Since its energy is predicted to be practically identical to g-h-C_3N_4, this additional structure would not alter any of the key conclusions of our work even if it could exist, since it would still be equally difficult to synthesize at any but the lowest NH_3 partial pressures.

Table S11: Relative total energies per atom (Δe) of the energetically competitive C_3N_4 structures suggested by Pickard *et al.*[29] The g-h-C_3N_4 structure suggested by Melissen *et al.*[24] appears with the label "C3N4-Pbca-hept" and is chosen as the reference (zero energy). The original energy hierarchy of Pickard *et al.*,[29] using the PBEsol functional, is given in the middle column. The right column reports the energy hierarchy of the same compounds, but for fully relaxed unit cells and atomic positions based on the PBE+TS density functional as used throughout the present work.

Structure	Δe [eV/atom] (PBEsol)	Δe (PBE+TS) [eV/atom]
C3N4-Cc-hept	−0.001	+0.016
C3N4-Fdd2-hept	−0.001	+0.016
C3N4-Pbca-hept	0.000	0.000
C3N4-Pca21-hept	+0.001	−0.001
C3N4-P43212	+0.015	+0.048
C3N4-Fdd2	+0.021	+0.028
C3N4-Pna21	+0.026	+0.036
C3N4-P64	+0.029	+0.040
C3N4-P63cm	+0.044	+0.043
C3N4-R3m	+0.128	+0.095
C3N4-alpha	+0.163	+0.235

Geometries Used for Total Energy Calculations

In this section, we provide the geometries used in this paper for total energy calculations. The geometries presented are fully relaxed (atomic position + unit cell parameters) by the FHI-aims all-electron code using PBE+TS until residual energy gradients were $5{\cdot}10^{-3}$ eV/Å or lower (see main text for more details.) Initial geometries used were taken from the citations listed for each geometry. Geometries are presented in the format of geometry.in for FHI-aims calculations, but they may be easily converted to any other format using the free and open source Open Babel tool (http://openbabel.org). To copy these geometry files directly from the PDF, we recommend that Adobe Acrobat be used; on Mac OS X, the default Preview program will mangle the text.

Additionally, these structures, as well as associated input and output files of the FHI-aims code, can also be found as ASCII files at the NOMAD repository with the permanent digital object identifier DOI:10.17172/NOMAD/2017.04.20-1 .

Melem molecule

```
# Botari et al. 2017, Figure 1a
# Melem molecule, C6N10H6
# Final structure after total-energy minimisation of atomic position and
#   unit cell parameters using DFT-PBE+TS.
atom      -3.42317585     -2.01929451      0.00500333 N
atom      -2.25980151     -1.33296202      0.00327540 C
atom      -2.36894067      0.00987994     -0.00102478 N
atom      -1.22948341      0.69463653     -0.00275112 C
atom      -0.00002009      0.00003999     -0.00004746 N
atom       0.01316633     -1.41200252      0.00443574 C
atom      -1.13731468     -2.07802983      0.00606847 N
atom       1.17588485     -2.05643417      0.00697370 N
atom       2.28427264     -1.29054209      0.00505425 C
atom       2.36830806      0.05409697      0.00082228 N
atom       1.21626910      0.71745436     -0.00180134 C
atom      -1.23101332      2.02400417     -0.00697917 N
atom      -0.02448466      2.62353926     -0.00839955 C
atom       1.19300670      2.04661351     -0.00604259 N
atom      -0.03704988      3.97420091     -0.01273011 N
atom       3.46028328     -1.95499922      0.00768390 N
atom      -3.40108537     -3.02890277      0.00828674 H
atom       0.83911567      4.47634360     -0.01398876 H
atom      -0.92242214      4.45993411     -0.01467248 H
atom       3.45704647     -2.96484516      0.01111479 H
atom       4.32362072     -1.43110595      0.00661332 H
atom      -4.29616045     -1.51163140      0.00309932 H
```

Melem dimer

```
# Botari et al. 2017, Figure 1b
# Melem dimer molecule, C12N19H9 (Lau et al., 2015)
# Final structure after total-energy minimisation of atomic position and
#   unit cell parameters using DFT-PBE+TS.
atom      -3.88474666     -0.10297299     -0.13828725 C
atom      -3.15958633     -1.21433771      0.10177365 N
atom      -2.04473729     -1.04739278      0.80353926 C
atom      -1.68427180      0.24022406      1.24963417 N
atom      -2.50933153      1.34674170      0.94895881 C
atom      -3.62156640      1.16161056      0.24537158 N
atom      -2.15926696      2.55633767      1.37504382 N
atom      -1.01389581      2.63470741      2.07920037 C
atom      -0.16888545      1.63618291      2.41125399 N
atom      -0.50072292      0.42178288      1.99530411 C
atom      -1.25650096     -2.07944539      1.09507786 N
atom      -0.14728238     -1.80512699      1.81185256 C
atom       0.27275798     -0.62984500      2.27430259 N
atom      -0.66396428      3.86518059      2.50811434 N
atom       0.18649204      3.97734229      3.04152316 H
atom      -1.25766813      4.65291439      2.29109565 H
atom      -5.01581723     -0.28076382     -0.85276504 N
atom       0.58913939     -2.95011087      2.05088791 N
atom       1.77365431     -3.20709029      2.71523843 C
atom       2.44468771     -2.21519420      3.29612422 N
atom       3.57787877     -2.55542394      3.91431211 C
atom       3.99288075     -3.90357396      3.92031365 N
atom       3.21129822     -4.88353069      3.27557448 C
atom       2.08556950     -4.51846594      2.66655838 N
atom       3.60512945     -6.15162174      3.28334654 N
atom       4.76026485     -6.41300779      3.92826472 C
atom       5.56991611     -5.54746069      4.56934733 N
atom       5.19057655     -4.27368286      4.57152738 C
atom       4.31856079     -1.63984650      4.52338082 N
atom       5.44589658     -2.08122500      5.11975929 C
atom       5.91929402     -3.34080050      5.17648326 N
atom       6.18989696     -1.13914241      5.73569721 N
atom       5.15380582     -7.70395738      3.93134474 N
atom      -5.26193214     -1.20909608     -1.16548991 H
atom      -5.59900136      0.51684680     -1.06202345 H
atom       0.16905659     -3.78486484      1.64874909 H
atom       7.04515078     -1.40874243      6.20041634 H
atom       5.87765192     -0.17856437      5.72217821 H
atom       4.58383117     -8.39541431      3.46533477 H
atom       6.01178738     -7.95816977      4.39968086 H
```

Crystalline Melem

```
# Botari et al. 2017, Figure 1c, Table S3
# Crystalline melem, C24N40H24 (Jurgens et al., 2003)
# Final structure after total-energy minimisation of atomic position and
#   unit cell parameters using DFT-PBE+TS.
lattice_vector      7.59277418      0.02724456     -0.07857521
lattice_vector     -0.03677268      8.43507335      0.00326444
lattice_vector     -2.61229162     -0.01915560     13.28607773
atom       4.72023686      1.67079068      5.88372549 C
atom       3.85197827      7.81910447      5.98570510 C
atom       5.00095672      0.36041487      7.91342835 C
atom       3.63346568      0.70651805      4.12484383 C
atom       4.17827725      6.64026253      7.91082611 C
atom       5.79049331      2.50331462      7.74674630 C
atom       4.54493681      0.46839692      6.58983704 N
atom       4.24101091      1.79455497      4.65357151 N
atom       3.40830574      7.94226085      4.73886919 N
atom       3.68311506      6.68262415      6.65256469 N
atom       4.78417862      7.65654182      8.57049834 N
atom       5.62693184      1.37608383      8.49019969 N
atom       5.36841806      2.67294653      6.46539715 N
atom       3.18200732      0.82125563      2.87019713 N
atom       4.05650928      5.50401392      8.59497209 N
atom      -1.17413362      3.49006858      8.40174136 N
atom       3.14489514      1.75165331      2.43622294 H
atom       2.64943800      0.04721672      2.48143120 H
atom       3.62373474      4.70125143      8.15768503 H
atom       4.51944888      5.41652441      9.50803126 H
atom      -1.07095455      3.47463484      9.43090260 H
atom      -0.97086256      4.34181721      7.85264252 H
atom       1.53329541      5.88188776      0.68292795 C
atom       0.22264245      6.77245955      7.32685994 C
atom       3.41038159      2.56121342     12.52708892 C
atom       2.38309515      3.60179596      0.58198891 C
atom       1.09138316      0.62396627      7.22443710 C
atom       2.56048270      4.84127260     12.62817909 C
atom      -1.34828558      4.55261345     11.93767430 C
atom      -0.05808913      8.08262241      5.29701727 C
atom       6.29192864      3.89038058      1.27241297 C
atom       2.62707472      4.92403858      2.44109877 C
atom       1.30982247      7.73677581      9.08546674 C
atom       2.31649605      3.51911537     10.76901885 C
atom      -0.54458062      2.40388133     11.94109287 C
atom       0.76495003      1.80264043      5.29923178 C
atom       5.48813530      6.03908029      1.26915717 C
atom      -2.15558139      6.68859881     12.10665624 C
atom      -0.84771257      5.93973386      5.46402883 C
atom       7.09921559      1.75437742      1.10330896 C
atom      -0.89393258      4.66255030     13.26176802 N
atom       0.39843874      7.97459906      6.62041102 N
atom       5.83747613      3.78047084     -0.05163521 N
atom       2.01128815      6.00803425      1.91330054 N
```

```
atom       0.70194013      6.64880341      8.55699351 N
atom       2.93235986      2.43511914     11.29672747 N
atom       2.82493355      3.72683815      1.82926940 N
atom       1.53506420      0.50093974      8.47128736 N
atom       2.11866918      4.71630384     11.38088635 N
atom      -0.05058014      2.44852001     13.19970851 N
atom       1.26024731      1.76036291      6.55745030 N
atom       4.99414406      5.99450479      0.01053272 N
atom      -1.15864489      3.41601051     11.28262589 N
atom       0.15866793      0.78642470      4.63980343 N
atom       6.10232250      5.02695430      1.92753113 N
atom      -1.98204148      5.56393060     11.36162027 N
atom      -0.68437912      7.06699942      4.72053397 N
atom       6.92570908      2.87903244      1.84838738 N
atom       0.87724289      6.87953493      0.10214968 N
atom      -0.42592083      5.77036580      6.74548123 N
atom       4.06653513      1.56356672     13.10776478 N
atom       3.07707714      5.04129141      3.69603247 N
atom       1.76146988      7.62209351     10.34005146 N
atom       1.86637435      3.40187285      9.51413876 N
atom      -0.41276613      1.26986915     11.25509840 N
atom       0.88692009      2.93875490      4.61490499 N
atom       5.35620407      7.17301891      1.95524733 N
atom       4.79965931      7.72492091     11.45312836 N
atom       6.11813030      4.95254451      4.80849957 N
atom       0.14362982      0.71791896      1.75698119 N
atom       3.10765411      5.97219917      4.12959340 H
atom       1.79866771      6.69171666     10.77403434 H
atom       1.83580738      2.47099243      9.08051820 H
atom       3.61766341      4.27206329      4.08327839 H
atom       2.29420715      8.39612424     10.72861499 H
atom       1.32585354      4.17113766      9.12689361 H
atom       0.02649271      0.47002057     11.69127208 H
atom       1.32014448      3.74140801      5.05195037 H
atom       4.91664194      7.97279283      1.51922777 H
atom      -0.87497815      1.17979986     10.34174871 H
atom       0.42402426      3.02623683      3.70181288 H
atom       5.81813457      7.26301226      2.86874887 H
atom       4.69651507      7.71021071     10.42406460 H
atom       6.01500543      4.96817978      3.77933989 H
atom       0.24666615      0.73262467      2.78604292 H
atom       4.58913098      8.57419553     12.00308275 H
atom       5.91445158      4.10088734      5.35756105 H
atom       0.35433689     -0.13131661      1.20702098 H
```

SSP-Stacked Monoclinic Melon

```
# Botari et al. 2017, Figure 1d, Table S4
# SSP-stacked monoclinic melon, C24N36H12, (Lotsch et al., 2007)
# Final structure after total-energy minimisation of atomic position and
#   unit cell parameters using DFT-PBE+TS.
lattice_vector     16.66324800      0.05154531      0.22272649
lattice_vector     -0.03390614     12.68910832      0.01689128
lattice_vector      2.87456551     -1.65516224      3.23371340
atom_frac       0.28287058      0.73411309     -0.01614892 N
atom_frac       0.71713099      0.26588557      0.01613995 N
atom_frac       0.77769556      0.76481677      0.00963698 N
atom_frac       0.22230259      0.23518463     -0.00962620 N
atom_frac       0.34077844      0.56551208     -0.03910780 N
atom_frac       0.65922385      0.43448601      0.03909417 N
atom_frac       0.83041805      0.93127600      0.01560453 N
atom_frac       0.16958307      0.06872325     -0.01561008 N
atom_frac       0.00164449      0.78094642     -0.01682850 N
atom_frac       0.99835758      0.21905210      0.01681694 N
atom_frac       0.49160914      0.72194529      0.03661198 N
atom_frac       0.50839070      0.27805473     -0.03661161 N
atom_frac       0.14153796      0.75649187     -0.01222986 N
atom_frac       0.85846469      0.24350617      0.01221494 N
atom_frac       0.63642496      0.74368524      0.01276126 N
atom_frac       0.36357208      0.25631705     -0.01274432 N
atom_frac       0.92586211      0.62875757     -0.02198473 N
atom_frac       0.07413637      0.37124359      0.02199344 N
atom_frac       0.41937095      0.86985739      0.01075494 N
atom_frac       0.58062730      0.13014404     -0.01074516 N
atom_frac       0.05977860      0.60588572     -0.01450504 N
atom_frac       0.94022136      0.39411436      0.01450546 N
atom_frac       0.55307004      0.89482860      0.01956893 N
atom_frac       0.44692694      0.10517367     -0.01955194 N
atom_frac       0.22780740      0.90281817     -0.00708949 N
atom_frac       0.77219491      0.09718007      0.00707679 N
atom_frac       0.72208876      0.59900197      0.02114115 N
atom_frac       0.27790932      0.40099946     -0.02113028 N
atom_frac       0.20030044      0.58094435     -0.03745827 N
atom_frac       0.79970554      0.41905122      0.03742349 N
atom_frac       0.69192851      0.91491817      0.00642017 N
atom_frac       0.30806308      0.08508822     -0.00637177 N
atom_frac       0.08526070      0.92741316     -0.01082729 N
atom_frac       0.91474172      0.07258511      0.01081399 N
atom_frac       0.57366378      0.57824898      0.05133830 N
atom_frac       0.42633798      0.42174935     -0.05134940 N
atom_frac       0.99688739      0.67326505     -0.01729919 C
atom_frac       0.00311277      0.32673488      0.01729841 C
atom_frac       0.48872691      0.82783187      0.02562123 C
atom_frac       0.51127151      0.17216930     -0.02561249 C
atom_frac       0.27109992      0.62739374     -0.03300725 C
atom_frac       0.72890344      0.37260369      0.03298779 C
atom_frac       0.76283688      0.86960352      0.01018134 C
atom_frac       0.23715975      0.13039904     -0.01016171 C
```

```
atom_frac       0.13297304      0.64607555     -0.01985765 C
atom_frac       0.86702974      0.35392237      0.01984175 C
atom_frac       0.62665923      0.85298466      0.01316366 C
atom_frac       0.37333596      0.14701901     -0.01313618 C
atom_frac       0.34757811      0.45703541     -0.03734898 C
atom_frac       0.65242246      0.54296396      0.03734523 C
atom_frac       0.83839724      0.03907010      0.01030425 C
atom_frac       0.16160471      0.96092851     -0.01031483 C
atom_frac       0.21846344      0.79888079     -0.01161550 C
atom_frac       0.78153886      0.20111746      0.01160255 C
atom_frac       0.71358744      0.70138450      0.01214331 C
atom_frac       0.28640986      0.29861756     -0.01212790 C
atom_frac       0.07374128      0.82346884     -0.01118591 C
atom_frac       0.92626119      0.17652940      0.01117222 C
atom_frac       0.56500143      0.67988138      0.03434189 C
atom_frac       0.43499819      0.32011878     -0.03434025 C
atom_frac       0.39499232      0.60555111     -0.04282870 H
atom_frac       0.60501002      0.39444686      0.04281496 H
atom_frac       0.88229654      0.89214898      0.02529915 H
atom_frac       0.11770617      0.10784921     -0.02531322 H
atom_frac       0.12478654      0.32566437      0.02420386 H
atom_frac       0.07719648      0.45187277      0.02070105 H
atom_frac       0.87521228      0.67433655     -0.02419705 H
atom_frac       0.92280173      0.54812854     -0.02069111 H
atom_frac       0.58241466      0.05046011     -0.00294497 H
atom_frac       0.63090321      0.17674337     -0.00720742 H
atom_frac       0.41758250      0.94954219      0.00296103 H
atom_frac       0.36909632      0.82325713      0.00720998 H
```

AB-stacked Orthorhombic Melon

```
# Botari et al. 2017, Table S5
# AB-stacked orthorhombic melon, C48N72H24, (Fina et al., 2015)
# Final structure after total-energy minimisation of atomic position and
# unit cell parameters using DFT-PBE+TS.
lattice_vector     16.65699573     -0.00989518     -0.02342442
lattice_vector      0.01827571     12.68019465     -0.01026847
lattice_vector      0.52034437      1.28166596      6.44432607
atom_frac       0.31900554      0.41361917      0.27427408 C
atom_frac       0.63699114      0.49120734      0.24473991 C
atom_frac       0.19447802      0.75379620      0.26075071 C
atom_frac       0.76219157      0.15381353      0.23814207 C
atom_frac       0.24384929      0.58509590      0.26103303 C
atom_frac       0.71298245      0.32256166      0.23667247 C
atom_frac       0.10885793      0.60386341      0.24039364 C
atom_frac       0.84934987      0.30657649      0.22996139 C
atom_frac       0.97359167      0.63166937      0.22845823 C
atom_frac      -0.01538857      0.27865278      0.24424618 C
atom_frac       0.05068006      0.77965737      0.24267880 C
atom_frac       0.90694544      0.12905126      0.24296854 C
atom_frac       0.81918520     -0.00808508      0.23657952 C
atom_frac       0.13776282      0.91565569      0.25934188 C
atom_frac       0.69419937      0.65453897      0.23346421 C
atom_frac       0.26163236      0.25196204      0.27706755 C
atom_frac       0.74344492      0.82281166      0.23548873 C
atom_frac       0.21272974      0.08407561      0.27196435 C
atom_frac       0.60733449      0.80478622      0.24929431 C
atom_frac       0.34841733      0.10081177      0.26923528 C
atom_frac       0.47121978      0.77688207      0.26315750 C
atom_frac       0.48470272      0.12805822      0.25853341 C
atom_frac       0.54884393      0.62781676      0.25716343 C
atom_frac       0.40672974      0.27666771      0.26723710 C
atom_frac       0.86581547      0.84328918      0.23290251 H
atom_frac       0.09086832      0.06481527      0.26046048 H
atom_frac       0.36632844      0.56366908      0.26880097 H
atom_frac       0.59059838      0.34125431      0.25254097 H
atom_frac       0.89941062      0.50719078      0.22118683 H
atom_frac       0.05892248      0.40307253      0.24809218 H
atom_frac       0.39643520      0.90148246      0.26770627 H
atom_frac       0.55987002      0.00342267      0.25222431 H
atom_frac       0.34835954      0.77483228      0.26901823 H
atom_frac       0.60811638      0.13132265      0.24382933 H
atom_frac       0.85074053      0.63422446      0.22051654 H
atom_frac       0.10668460      0.27532861      0.26286579 H
atom_frac       0.11813372      0.71240153      0.24859819 N
atom_frac       0.83936366      0.19632604      0.23773062 N
atom_frac       0.06183135      0.88310761      0.24840885 N
atom_frac       0.89564333      0.02538448      0.23889001 N
atom_frac       0.20438886      0.85671221      0.26512890 N
atom_frac       0.75238637      0.05048046      0.23603872 N
atom_frac       0.25796855      0.68884877      0.27001744 N
atom_frac       0.69848467      0.21742498      0.24034844 N
```

```
atom_frac       0.17327406      0.54078377      0.24366401 N
atom_frac       0.78495855      0.36960175      0.22588355 N
atom_frac       0.03702905      0.56381314      0.22971885 N
atom_frac       0.92164135      0.34769881      0.22884142 N
atom_frac       0.97802981      0.73864122      0.23315225 N
atom_frac      -0.02045103      0.17002836      0.25260089 N
atom_frac       0.31242073      0.52317907      0.27003731 N
atom_frac       0.64431050      0.38269736      0.24400614 N
atom_frac       0.90188482      0.58818176      0.22118766 N
atom_frac       0.05586305      0.32177468      0.25366898 N
atom_frac       0.61698383      0.69579805      0.24472303 N
atom_frac       0.33883225      0.20995231      0.27075493 N
atom_frac       0.56051197      0.52337247      0.26061099 N
atom_frac       0.39548570      0.38054407      0.26829691 N
atom_frac       0.70429901      0.55120050      0.22906410 N
atom_frac       0.25180538      0.35516755      0.28224751 N
atom_frac       0.75821336      0.71851607      0.22859426 N
atom_frac       0.19794674      0.18832518      0.27650627 N
atom_frac       0.67177228      0.86773557      0.24521565 N
atom_frac       0.28421756      0.03783869      0.27235465 N
atom_frac       0.53479270      0.84507813      0.25800792 N
atom_frac       0.42106147      0.05993545      0.26383026 N
atom_frac       0.47582036      0.66907155      0.26534786 N
atom_frac       0.47994682      0.23523254      0.26103078 N
atom_frac       0.81221215      0.88377262      0.23335769 N
atom_frac       0.14435874      0.02377545      0.26518159 N
atom_frac       0.39937145      0.82088728      0.26645413 N
atom_frac       0.55686631      0.08450235      0.25082871 N
atom_frac       0.48689918      0.26491327      0.75511430 C
atom_frac       0.80488219      0.34248670      0.72570508 C
atom_frac       0.36169786      0.60230325      0.76174860 C
atom_frac       0.92941124      0.00231414      0.73918615 C
atom_frac       0.41090736      0.43355588      0.76321913 C
atom_frac       0.88003987      0.17101545      0.73888865 C
atom_frac       0.27453824      0.44953470      0.76998751 C
atom_frac       1.01502995      0.15224522      0.75955948 C
atom_frac       1.13927445      0.47745287      0.75575248 C
atom_frac       0.15029349      0.12443489      0.77155079 C
atom_frac       0.21694255      0.62705968      0.75697579 C
atom_frac       1.07320759     -0.02355045      0.75729727 C
atom_frac       0.98612627     -0.15954747      0.74061843 C
atom_frac       0.30470414      0.76420155      0.76331367 C
atom_frac       0.86225428      0.50414205      0.72294013 C
atom_frac       0.42969106      0.10158153      0.76638580 C
atom_frac       0.91115742      0.67202952      0.72802929 C
atom_frac       0.38044593     -0.06668904      0.76434275 C
atom_frac       0.77547188      0.65530394      0.73065925 C
atom_frac       0.51655690     -0.04865780      0.75047990 C
atom_frac       0.63918777      0.62806270      0.74129414 C
atom_frac       0.65267131     -0.02075633      0.73663843 C
atom_frac       0.71716022      0.47944903      0.73263785 C
atom_frac       0.57504762      0.12830766      0.74265447 C
atom_frac       1.03301842      0.69128806      0.73952368 H
atom_frac       0.25807369     -0.08717488      0.76701875 H
```

```
atom_frac       0.53329144      0.41486578      0.74732813 H
atom_frac       0.75756130      0.19244498      0.73109306 H
atom_frac       1.06496001      0.35303041      0.75194702 H
atom_frac       0.22447684      0.24891215      0.77882938 H
atom_frac       0.56402328      0.75270373      0.74755671 H
atom_frac       0.72745624     -0.14535885      0.73212023 H
atom_frac       0.51577379      0.62480433      0.75596467 H
atom_frac       0.77553031     -0.01871052      0.73083048 H
atom_frac       1.01719870      0.48077430      0.73718363 H
atom_frac       0.27314431      0.12188012      0.77948221 H
atom_frac       0.28452490      0.55978718      0.76220055 N
atom_frac       1.00575436      0.04370630      0.75135820 N
atom_frac       0.22824482      0.73072859      0.76103727 N
atom_frac       1.06205671     -0.12700148      0.75157280 N
atom_frac       0.37150338      0.70563823      0.76383459 N
atom_frac       0.91950152     -0.10060164      0.73480208 N
atom_frac       0.42540556      0.53869402      0.75952682 N
atom_frac       0.86592029      0.06726053      0.72991753 N
atom_frac       0.33893080      0.38651274      0.77403683 N
atom_frac       0.95061633      0.21533069      0.75623361 N
atom_frac       0.20224534      0.40840834      0.77115369 N
atom_frac       1.08685584      0.19229049      0.77028730 N
atom_frac       1.14433761      0.58607977      0.74737091 N
atom_frac       0.14585685      0.01746519      0.76683696 N
atom_frac       0.47957949      0.37342109      0.75587316 N
atom_frac       0.81146811      0.23293227      0.72988587 N
atom_frac       1.06802101      0.43432883      0.74636276 N
atom_frac       0.22199926      0.16791966      0.77884589 N
atom_frac       0.78505715      0.54616345      0.72913161 N
atom_frac       0.50690707      0.06032608      0.75509655 N
atom_frac       0.72840309      0.37557008      0.73160370 N
atom_frac       0.56337900      0.23275047      0.73922378 N
atom_frac       0.87208053      0.40092935      0.71782422 N
atom_frac       0.41959180      0.20491939      0.77079982 N
atom_frac       0.92593837      0.56777418      0.72353983 N
atom_frac       0.36567698      0.03760226      0.77128263 N
atom_frac       0.83967060      0.71826964      0.72760460 N
atom_frac       0.45211964     -0.11160291      0.75452654 N
atom_frac       0.70282882      0.69618497      0.73601433 N
atom_frac       0.58909888     -0.08894885      0.74175640 N
atom_frac       0.64394385      0.52088768      0.73881690 N
atom_frac       0.64807032      0.08705320      0.73445854 N
atom_frac       0.97952889      0.73233026      0.73480368 N
atom_frac       0.31167801     -0.12765431      0.76652098 N
atom_frac       0.56702499      0.67162278      0.74896451 N
atom_frac       0.72451921     -0.06476265      0.73336086 N
```

```
# Botari et al. 2017, Table S5
# AB-stacked orthorhombic melon, C48N72H24, (Chamorro-Posada et al., 2014)
# Final structure after total-energy minimisation of atomic position and
# unit cell parameters using DFT-PBE+TS.
  lattice_vector        16.66028137        0.00537857        0.00000000
  lattice_vector         0.00000000       12.69414409        0.00000000
  lattice_vector         0.03468552        0.06241465        6.43993638
       atom_frac         0.29258206        0.75237012       -0.00291975  N
       atom_frac         0.73341160        0.28056453       -0.00566293  N
       atom_frac         0.79303870        0.78037434       -0.00366285  N
       atom_frac         0.23275573        0.25226041       -0.00142781  N
       atom_frac         0.34643993        0.58641945       -0.00253983  N
       atom_frac         0.67981913        0.44616871       -0.00374676  N
       atom_frac         0.84694221        0.94606146       -0.00465399  N
       atom_frac         0.17881829        0.08657967       -0.00064680  N
       atom_frac         0.01098378        0.79853514       -0.00194284  N
       atom_frac         1.01497317        0.23344226       -0.00337393  N
       atom_frac         0.51161436        0.73376737       -0.00220706  N
       atom_frac         0.51432199        0.29835068       -0.00277308  N
       atom_frac         0.15172467        0.77370629       -0.00215719  N
       atom_frac         0.87412050        0.25859787       -0.00371052  N
       atom_frac         0.65235156        0.75854225       -0.00233798  N
       atom_frac         0.37352138        0.27365679       -0.00131880  N
       atom_frac         0.93466237        0.64691941       -0.00223907  N
       atom_frac         0.09201646        0.38469451       -0.00285292  N
       atom_frac         0.43474834        0.88516521       -0.00005844  N
       atom_frac         0.59071924        0.14662118       -0.00246164  N
       atom_frac         0.06983307        0.62332746       -0.00212739  N
       atom_frac         0.95658463        0.40855421       -0.00209230  N
       atom_frac         0.57011292        0.90872799       -0.00120225  N
       atom_frac         0.45548518        0.12305880       -0.00038245  N
       atom_frac         0.23876772        0.91959480       -0.00192475  N
       atom_frac         0.78695844        0.11302800       -0.00628367  N
       atom_frac         0.73959604        0.61294848       -0.00320492  N
       atom_frac         0.28653657        0.41958696       -0.00199699  N
       atom_frac         0.20646096        0.60170831       -0.00227372  N
       atom_frac         0.81999385        0.43073929       -0.00222038  N
       atom_frac         0.70666730        0.93084936       -0.00277758  N
       atom_frac         0.31890333        0.10157891        0.00040557  N
       atom_frac         0.09546268        0.94446622       -0.00112692  N
       atom_frac         0.93022402        0.08815341       -0.00457716  N
       atom_frac         0.59635309        0.58808969       -0.00314287  N
       atom_frac         0.42983969        0.44422537       -0.00251574  N
       atom_frac         1.00637625        0.69100808       -0.00212281  C
       atom_frac         0.01991698        0.34068949       -0.00275397  C
       atom_frac         0.50675022        0.84103977       -0.00122451  C
       atom_frac         0.51905377        0.19046285       -0.00183333  C
       atom_frac         0.27788175        0.64738580       -0.00255733  C
       atom_frac         0.74833923        0.38498775       -0.00391088  C
       atom_frac         0.77812038        0.88499603       -0.00367264  C
       atom_frac         0.24719356        0.14752662       -0.00052272  C
       atom_frac         0.14210935        0.66428159       -0.00219469  C
       atom_frac         0.88394358        0.36769728       -0.00260556  C
       atom_frac         0.64240451        0.86783721       -0.00206277  C
```

```
atom_frac         0.38326726        0.16411100       -0.00039410  C
atom_frac         0.35333993        0.47805636       -0.00232426  C
atom_frac         0.67279279        0.55465853       -0.00331601  C
atom_frac         0.85380997        0.05506919       -0.00522743  C
atom_frac         0.17169308        0.97813653       -0.00124147  C
atom_frac         0.22867757        0.81596773       -0.00232094  C
atom_frac         0.79695978        0.21646369       -0.00528523  C
atom_frac         0.72929952        0.71615249       -0.00297435  C
atom_frac         0.29637228        0.31614699       -0.00154623  C
atom_frac         0.08381394        0.84044901       -0.00175618  C
atom_frac         0.94176716        0.19183396       -0.00389229  C
atom_frac         0.58472268        0.69186828       -0.00257294  C
atom_frac         0.44120601        0.34035479       -0.00220396  C
atom_frac         0.40009400        0.62659588       -0.00246985  H
atom_frac         0.62627458        0.40567154       -0.00416095  H
atom_frac         0.90075662        0.90567111       -0.00423196  H
atom_frac         0.12521922        0.12703354       -0.00113619  H
atom_frac         0.14303175        0.33834944       -0.00283056  H
atom_frac         0.09512414        0.46556796       -0.00260719  H
atom_frac         0.88381580        0.69274995       -0.00273303  H
atom_frac         0.93174597        0.56633079       -0.00254399  H
atom_frac         0.59370015        0.06588266       -0.00197903  H
atom_frac         0.64174438        0.19223757       -0.00371408  H
atom_frac         0.43217127        0.96608386       -0.00021679  H
atom_frac         0.38380511        0.83904284       -0.00096175  H
atom_frac         0.46581072        0.86836007        0.50014536  N
atom_frac         0.90664150        0.39655380        0.49794080  N
atom_frac         0.96646688        0.89666116        0.49690302  N
atom_frac         0.40617977        0.36854820        0.49859605  N
atom_frac         0.51939917        0.70275460        0.49822250  N
atom_frac         0.85278360        0.56250456        0.49752742  N
atom_frac         1.02040249        1.06234275        0.49613961  N
atom_frac         0.35227809        0.20286150        0.49965573  N
atom_frac         0.18424483        0.91547923        0.49875822  N
atom_frac         1.18823834        0.35038949        0.49726671  N
atom_frac         0.68490044        0.85056822        0.49734197  N
atom_frac         0.68760286        0.41515772        0.49667293  N
atom_frac         0.32509982        0.89032950        0.49844601  N
atom_frac         1.04749741        0.37521795        0.49726392  N
atom_frac         0.82570099        0.87526518        0.49635657  N
atom_frac         0.54686587        0.39037984        0.49685435  N
atom_frac         1.10720248        0.76422708        0.49806921  N
atom_frac         0.26456020        0.50200590        0.49745977  N
atom_frac         0.60850121        1.00229400        0.49681872  N
atom_frac         0.76447706        0.26377263        0.49454133  N
atom_frac         0.24263477        0.74037264        0.49706499  N
atom_frac         1.12938893        0.52559707        0.49709451  N
atom_frac         0.74373671        1.02586211        0.49497077  N
atom_frac         0.62910765        0.24019608        0.49566380  N
atom_frac         0.41225996        1.03589766        0.50087491  N
atom_frac         0.96045533        0.22932685        0.49724919  N
atom_frac         0.91268403        0.72933492        0.49739607  N
atom_frac         0.45962490        0.53597249        0.49812690  N
atom_frac         0.37922595        0.71818681        0.49686212  N
```

```
atom_frac         0.99276164         0.54721649         0.49719828  N
atom_frac         0.88031886         1.04734333         0.49466894  N
atom_frac         0.49255327         0.21807654         0.49739115  N
atom_frac         0.26899411         1.06076889         0.49988212  N
atom_frac         1.10375920         0.20445691         0.49650498  N
atom_frac         0.76938160         0.70469400         0.49737663  N
atom_frac         0.60286823         0.56083743         0.49755535  N
atom_frac         1.17930103         0.80823263         0.49793627  C
atom_frac         0.19284523         0.45791833         0.49729670  C
atom_frac         0.68016849         0.95845595         0.49635110  C
atom_frac         0.69246793         0.30788488         0.49570189  C
atom_frac         0.45088077         0.76393732         0.49845438  C
atom_frac         0.92134136         0.50153719         0.49753621  C
atom_frac         0.95202597         1.00139452         0.49585627  C
atom_frac         0.42109877         0.26392666         0.49849955  C
atom_frac         0.31527494         0.78122987         0.49739485  C
atom_frac         1.05711245         0.48464061         0.49718791  C
atom_frac         0.81595453         0.98481232         0.49530700  C
atom_frac         0.55681519         0.28108544         0.49659434  C
atom_frac         0.52642548         0.59426436         0.49794135  C
atom_frac         0.84588284         0.67086555         0.49741081  C
atom_frac         1.02752998         0.17078571         0.49661515  C
atom_frac         0.34540780         1.09385590         0.50018989  C
atom_frac         0.40226433         0.93246245         0.49987615  C
atom_frac         0.97054389         0.33295411         0.49745920  C
atom_frac         0.90284975         0.83277467         0.49686837  C
atom_frac         0.46992047         0.43276832         0.49776734  C
atom_frac         0.25745084         0.95708963         0.49906366  C
atom_frac         1.11540819         0.30847502         0.49703936  C
atom_frac         0.75801873         0.80856703         0.49702812  C
atom_frac         0.61449502         0.45705743         0.49704200  C
atom_frac         0.57294673         0.74324779         0.49855519  H
atom_frac         0.79912911         0.52232990         0.49730744  H
atom_frac         1.07399987         1.02188443         0.49673881  H
atom_frac         0.29846489         0.24325332         0.49942924  H
atom_frac         0.31540358         0.45617008         0.49811091  H
atom_frac         0.26747698         0.58259467         0.49764835  H
atom_frac         1.05618808         0.81057491         0.49824566  H
atom_frac         1.10409655         0.68335399         0.49770603  H
atom_frac         0.76706436         0.18285547         0.49476928  H
atom_frac         0.81540868         0.30991509         0.49550210  H
atom_frac         0.60551380         1.08303089         0.49635622  H
atom_frac         0.55748230         0.95666428         0.49804647  H
```

g-t-C3N4

```
# Botari et al. 2017, Table S7
# AB-stacked g-t-C3N4, C6N8 (Algarra-Siller et al., 2014)
# Final structure after total-energy minimisation of atomic position and
#   unit cell parameters using DFT-PBE+TS.
lattice_vector      4.70069939      0.00000000      0.00000000
lattice_vector     -2.33762920      4.06415428      0.00000000
lattice_vector     -0.32172291      0.53774178      6.84034285
atom       1.96448393      1.06840348     -0.01066227 C
atom      -1.92638861      1.90381467      3.40941078 C
atom       0.71149265      0.34743933     -0.01117199 N
atom       1.52155985      1.18302626      3.40917954 N
atom      -0.83882518      1.24626331      2.99283141 N
atom       1.94025878      2.34018604      0.39997242 N
atom       4.18162448      1.05997778     -0.13080939 C
atom       3.07181900      2.98937248      0.10765306 C
atom       0.29366123      1.89883618      3.28315109 C
atom       1.52291683     -0.23864188      3.53435500 C
atom       0.33315094      3.20386623      3.40739127 N
atom      -1.94789195      3.17454685      3.82634298 N
atom       3.05135055      0.40793167     -0.42113808 N
atom       4.22137442      2.36684247     -0.01307789 N
```

```
# Botari et al. 2017, Table S7
# ABC-stacked g-t-C3N4, C9N12 (Algarra-Siller et al., 2014)
# Final structure after total-energy minimisation of atomic position and
#   unit cell parameters using DFT-PBE+TS.
lattice_vector      4.69781316      0.00002360      0.00010656
lattice_vector     -2.33479021      4.06480202      0.00011006
lattice_vector     -0.63832573     -0.02472736     10.10691356
atom       1.92426731      0.98087489     -0.02473639 C
atom      -1.97405443      1.82533956      3.40238940 C
atom       0.67073685      0.26066967     -0.02091308 N
atom       1.47148904      1.10645892      3.39591085 N
atom      -0.88798106      1.16886419      2.98161715 N
atom       1.90076487      2.25102991      0.39178730 N
atom       4.13935648      0.97400919     -0.14692439 C
atom       3.03058682      2.90195907      0.09598435 C
atom       0.24547718      1.82123649      3.26495860 C
atom       1.47087950     -0.31526078      3.51535195 C
atom       0.28398489      3.12796507      3.37740104 N
atom      -1.99385135      3.09716223      3.81906091 N
atom       3.01034816      0.32161672     -0.43586585 N
atom       4.17945976      2.28140657     -0.03543877 N
atom      -0.39828063      1.22602488      6.61311070 C
atom      -0.39598619      2.64877265      6.73293563 N
atom      -2.75500139      2.71275196      7.15539962 N
atom      -1.62386999      3.36236318      6.86052289 C
atom      -3.84212078      3.36993372      6.73856231 C
atom      -1.58397591      4.66929315      6.74231892 N
atom      -3.86347208      4.63939223      6.31981179 N
```

```
# Botari et al. 2017, Figure 1g-i, Table S7
# g-t-C3N4, C18N24 (Melissen et al., 2015)
# Final structure after total-energy minimisation of atomic position and
#   unit cell parameters using DFT-PBE+TS.
lattice_vector      7.98784112      0.00082267      0.02456840
lattice_vector     -3.99488837      6.91742280     -0.01444598
lattice_vector     -0.02043882      0.00275991      6.95549285
atom      -2.56922089      6.88468727      0.34156293 C
atom      -0.70345956      3.36289363      6.52926989 C
atom       4.68886045      3.52556783      3.45501191 C
atom      -0.00067381     -0.00023538      0.50859123 N
atom       3.85081273      0.06639565      6.30049894 N
atom      -0.00156583      2.30827123      6.91878928 N
atom       4.10902057      4.54953010      4.08419857 N
atom      -0.01837305      4.61403682      6.37405682 N
atom       3.98568689      2.30727122      3.45338289 N
atom      -0.68513035      1.25080127      0.34859881 C
atom       3.25184158      5.69929104      0.35966088 C
atom      -3.26269571      5.69994641      3.81703067 C
atom       2.55798782      6.88659496      3.83498869 C
atom       0.67539023      1.25228758      3.83096030 C
atom       1.40700025      4.64680332      6.53558261 C
atom      -0.76015906      5.83260082      6.52886077 C
atom       0.73360224      5.83134616      3.05544111 C
atom       0.67748512      3.36164328      3.05616662 C
atom      -1.43317996      4.64512043      3.04885593 C
atom       2.57903142      2.30713856      3.44924466 C
atom       4.68919489      1.08912400      3.45604750 C
atom       3.27099933      1.09041077      6.92964360 C
atom       3.27074201      3.52688128      6.92867233 C
atom       5.38073906      2.30884334      6.93534314 C
atom      -0.00959392      0.00109136      3.98628588 N
atom       5.98039732      3.32096245      6.30560252 N
atom       2.09720011      3.53820371      6.29360354 N
atom       5.86633584      3.53712364      2.82731878 N
atom       4.11364292      0.06500910      2.82317670 N
atom       1.98296450      3.31914734      2.81586430 N
atom       1.96763839      5.78306508      6.92424165 N
atom      -2.02621836      5.75118987      6.91225606 N
atom       1.99727000      5.75028185      3.44664754 N
atom      -0.02650526      2.30696539      3.44162138 N
atom      -1.99655808      5.78133804      3.43384780 N
atom       1.97941159      1.29500229      4.07900597 N
atom       5.86270818      1.07785466      4.09113099 N
atom       2.11398603      1.07614097      0.60188272 N
atom       3.86676617      4.54818980      0.60609696 N
atom       5.99719760      1.29407384      0.61326983 N
atom      -0.00684468      4.61261851      2.89631663 N
atom       3.97410494      2.30875477      6.93116907 N
```

g-h-C3N4

```
# Botari et al. 2017, Table S6
# SSP-stacked g-h-C3N4, C6N8 (Tyborski et al., 2013)
# Final structure after total-energy minimisation of atomic position and
#   unit cell parameters using DFT-PBE+TS.
lattice_vector      6.91046138      0.00000000      0.00000000
lattice_vector     -3.45726493      6.02655054      0.00000000
lattice_vector     -1.57981738     -1.11367662      3.61612377
atom      -0.03923652     -0.00923313      0.01724802 N
atom       2.22157366      0.15594030     -0.60545689 N
atom       4.56006345     -0.00005964     -0.48869244 N
atom       3.46260898      1.99872512      0.06831920 N
atom       1.21410530      0.72734793      0.04341479 C
atom       3.42692613      0.67435955     -0.35808921 C
atom      -1.13187551      2.02731979     -0.26438772 N
atom       2.30538982      3.98365982      0.57708448 N
atom      -2.30261188      4.01858690     -0.04781639 N
atom       1.22347728      1.88682393      0.71135317 N
atom       5.67794637      0.69548798     -0.23260022 C
atom       3.43716129      4.58978512      0.18043997 C
atom       4.65584324      2.69957576     -0.07014651 C
atom       2.30152470      2.65670250      0.46932976 C
```

```
# Botari et al. 2017, Table S6
# AB-stacked g-h-C3N4, C12N16 (Tyborski et. al, 2013)
# Final structure after total-energy minimisation of atomic position and
#   unit cell parameters using DFT-PBE+TS.
lattice_vector      6.95860672      0.00000000      0.00000000
lattice_vector     -3.47896341      6.00059594      0.00000000
lattice_vector     -0.00564178     -0.08853351      6.78740722
atom       0.02886405      1.01974246       0.00007674 N
atom       2.50363419      4.97704592       0.64937539 N
atom       3.50756121      2.98870256      -0.00230895 N
atom       1.16666541      0.92027479       3.45621693 N
atom       0.01254381      2.94100685       3.39120860 N
atom       3.49100708      0.97200968       3.39353856 N
atom       1.22351220      3.00047967       0.56569747 N
atom       2.29656508      2.95274601       3.95921072 N
atom       1.26114729      1.70721451       0.19820970 C
atom       3.50794976      1.60371851       0.00078935 C
atom       0.01204014      1.55595936       3.39459311 C
atom       2.25887741      1.65949625       3.59169039 C
atom      -1.12566590      6.96860253       0.06251434 N
atom      -1.16622767      2.99995821      -0.56696415 N
atom       4.49548983     -1.07130550       4.04300482 N
atom       4.68629244      2.95236390       2.82704934 N
atom       4.66307747      0.96876216      -0.05703419 N
atom       4.51341789      4.97722030      -0.65277412 N
atom      -0.99306166      4.92954939       2.74055800 N
atom      -1.14318433      0.92105416       3.33727361 N
atom       5.75462221      1.70721203      -0.19734835 C
atom       3.50851424      5.56061217      -0.00157156 C
atom       4.64071159      3.66970569      -0.42845124 C
atom       2.37528630      3.66988083       0.42570407 C
atom       1.14487680      3.62219413       3.81917430 C
atom      -1.12064899      3.62208391       2.96532316 C
atom       3.49076013     -0.48770829       3.39187468 C
atom       4.72398054      1.65950040       3.19659981 C
```

```
# Botari et al. 2017, Table S6
# g-h-C3N4, C96N128 (Gracia et al., 2009)
# Final structure after total-energy minimisation of atomic position and
#   unit cell parameters using DFT-PBE+TS.
lattice_vector     13.32349453     -0.00011888      0.00397442
lattice_vector      0.00044690     23.77632760      0.00277934
lattice_vector     -0.00919644     -0.00232748      7.04877485
atom       2.20207240      2.75158908     -0.03294889 C
atom       8.85438042      2.74912568      7.08692600 C
atom       2.20231064     14.63974296     -0.03091769 C
atom       8.85446096     14.63735585      7.08890938 C
atom       5.62420117      8.60396609      5.96866259 C
atom      12.29427722      8.60598293      1.08869391 C
atom       5.62439972     20.49200490      5.97071949 C
atom      12.29442657     20.49427141      1.09084055 C
atom       4.35180451      2.65992540      5.96735395 C
atom      11.02185363      2.66187507      1.08760216 C
atom       4.35191903     14.54815032      5.96912309 C
atom      11.02199601     14.54995435      1.08946416 C
atom       1.12032724      8.69339843      7.08462963 C
atom       7.79156791      8.69561113     -0.03037465 C
atom       1.12054247     20.58150375      7.08690566 C
atom       7.79169466     20.58376334     -0.02816279 C
atom       2.19747265      9.13546502      3.49235390 C
atom       8.85922603      9.13546029      3.56259429 C
atom       2.19780886     21.02366862      3.49453457 C
atom       8.85936486     21.02362256      3.56487746 C
atom       5.62869105      3.28108198      2.44385803 C
atom      12.28968857      3.28077521      4.61252579 C
atom       5.62893457     15.16939740      2.44580013 C
atom      12.28988608     15.16882223      4.61449953 C
atom       4.35626555      9.22512007      2.44363444 C
atom      11.01731726      9.22490136      4.61246333 C
atom       4.35649069     21.11324356      2.44558774 C
atom      11.01757595     21.11310330      4.61449681 C
atom       1.12483032      3.19138636      3.55948719 C
atom       7.78671114      3.19133363      3.49388023 C
atom       1.12502392     15.07958917      3.56144000 C
atom       7.78687108     15.07945340      3.49602343 C
atom       1.32206545      0.81387917      0.72477617 C
atom       7.97501205      0.81152389      6.32819314 C
atom       1.32224164     12.70192486      0.72634297 C
atom       7.97513590     12.69988921      6.32972031 C
atom       4.44840342      6.70084879      6.22169472 C
atom      11.11882837      6.70278967      0.83495791 C
atom       4.44855338     18.58896829      6.22392974 C
atom      11.11896926     18.59100501      0.83733538 C
atom       5.52716847      0.75663111      6.22089497 C
atom      12.19758054      0.75883307      0.83408239 C
atom       5.52730511     12.64485601      6.22236033 C
atom      12.19774225     12.64695042      0.83550365 C
atom       2.00035437      6.75577848      6.32672704 C
atom       8.67089079      6.75783443      0.72795475 C
atom       2.00051265     18.64386773      6.32907009 C
```

```
atom       8.67100867     18.64603022      0.73035343 C
atom       1.31748576     11.07306563      4.25031506 C
atom       7.97965472     11.07329270      2.80469480 C
atom       1.31778525     22.96136408      4.25213943 C
atom       7.97988814     22.96133230      2.80650241 C
atom       4.45297182      5.18418458      2.69714315 C
atom      11.11425417      5.18401254      4.35914140 C
atom       4.45318107     17.07241044      2.69935112 C
atom      11.11445988     17.07213612      4.36144055 C
atom       5.53174206     11.12829010      2.69761997 C
atom      12.19303638     11.12802594      4.35944161 C
atom       5.53198504     23.01640322      2.69928661 C
atom      12.19330727     23.01621683      4.36115579 C
atom       2.00491274      5.12916206      2.80207710 C
atom       8.66630575      5.12900652      4.25223420 C
atom       2.00511909     17.01743421      2.80431134 C
atom       8.66648021     17.01708733      4.25458943 C
atom       3.50516120      0.75644585      0.16810588 C
atom      10.15793286      0.75422215      6.88534373 C
atom       3.50532485     12.64450500      0.16963511 C
atom      10.15806794     12.64253861      6.88682582 C
atom      13.14075733      6.69811077      6.88750101 C
atom       6.48801095      6.70065925      0.17056103 C
atom      13.14090646     18.58624641      6.88985885 C
atom       6.48815371     18.58880625      0.17282374 C
atom       3.50055305     11.13062143      3.69363604 C
atom      10.16255783     11.13058338      3.36197275 C
atom       3.50083668     23.01889172      3.69539129 C
atom      10.16280066     23.01862665      3.36374211 C
atom      13.14536478      5.18656836      3.36294590 C
atom       6.48342127      5.18648693      3.69477711 C
atom      13.14556502     17.07480184      3.36520719 C
atom       6.48362024     17.07462949      3.69700785 C
atom       3.19854170      4.59436736      6.20307465 C
atom       9.86873184      4.59637170      0.85195048 C
atom       3.19872411     16.48255452      6.20524161 C
atom       9.86884544     16.48450749      0.85423491 C
atom       0.12398524     10.54059078      0.84920447 C
atom       6.77735162     10.53839948      6.20488024 C
atom       0.12422428     22.42884333      0.85110600 C
atom       6.77756000     22.42643349      6.20666929 C
atom       3.20308418      7.29059586      2.67913016 C
atom       9.86427147      7.29043788      4.37629282 C
atom       3.20334120     19.17876782      2.68138744 C
atom       9.86444336     19.17861358      4.37867517 C
atom       0.11925829      1.34642365      4.37257009 C
atom       6.78158690      1.34647609      2.67988037 C
atom       0.11944449     13.23448700      4.37411909 C
atom       6.78178102     13.23475476      2.68153177 C
atom       1.13540702      2.08273946      0.37324084 N
atom       7.78789844      2.08012782      6.68054810 N
atom       1.13564819     13.97090256      0.37523051 N
atom       7.78797108     13.96839958      6.68243050 N
atom       4.56362671      7.88015711      5.61461301 N
```

```
atom      11.23353985      7.88210798      1.44216688 N
atom       4.56378827     19.76822638      5.61676879 N
atom      11.23369680     19.77039686      1.44442431 N
atom       5.41261391      1.93612236      5.61397011 N
atom      12.08239279      1.93795084      1.44149721 N
atom       5.41270001     13.82440372      5.61556218 N
atom      12.08257478     13.82597550      1.44312902 N
atom       2.18695889      8.02465802      6.67820759 N
atom       8.85800700      8.02655301      0.37602423 N
atom       2.18716601     19.91272120      6.68056409 N
atom       8.85810888     19.91474949      0.37841418 N
atom       1.13085046      9.80422996      3.89869956 N
atom       7.79270068      9.80442569      3.15624649 N
atom       1.13119548     21.69243615      3.90086368 N
atom       7.79284403     21.69259030      3.15847247 N
atom       4.56822448      4.00504555      2.08977583 N
atom      11.22893224      4.00455955      4.96607298 N
atom       4.56844290     15.89334894      2.09184059 N
atom      11.22917171     15.89260830      4.96823476 N
atom       5.41704992      9.94902075      2.09030041 N
atom      12.07785570      9.94871569      4.96650143 N
atom       5.41725449     21.83708498      2.09208885 N
atom      12.07815756     21.83696019      4.96834097 N
atom       2.19145881      3.86014682      3.15312181 N
atom       8.85323011      3.86020518      3.90044651 N
atom       2.19165650     15.74837510      3.15517741 N
atom       8.85337055     15.74826868      3.90279116 N
atom       2.17386121      4.06456491      6.85446344 N
atom       8.84450960      4.06676391      0.19964075 N
atom       2.17414795     15.95273935      6.85675694 N
atom       8.84459178     15.95497093      0.20189792 N
atom       5.75159141      9.89262928      5.63934597 N
atom      12.42124712      9.89472377      1.41784500 N
atom       5.75184104     21.78059925      5.64117853 N
atom      12.42140091     21.78307437      1.41974102 N
atom       4.22486188      3.94874331      5.63840847 N
atom      10.89455210      3.95044799      1.41717453 N
atom       4.22496575     15.83700103      5.64035928 N
atom      10.89467211     15.83847195      1.41933752 N
atom       1.14852172     10.01100057      0.19741779 N
atom       7.80147376     10.00863784      6.85721608 N
atom       1.14883394     21.89910401      0.19958806 N
atom       7.80159696     21.89677221      6.85924583 N
atom       2.17850231      7.82018015      3.33081651 N
atom       8.84027148      7.82008399      3.72369036 N
atom       2.17885253     19.70837006      3.33319291 N
atom       8.84034700     19.70826824      3.72621489 N
atom       5.75594798      1.99247309      2.11439225 N
atom      12.41664789      1.99198038      4.94148429 N
atom       5.75623298     13.88086112      2.11604949 N
atom      12.41682360     13.87995220      4.94316318 N
atom       4.22930327      7.93637787      2.11446440 N
atom      10.88995614      7.93626744      4.94186430 N
atom       4.22950911     19.82448270      2.11657023 N
```

```
atom      10.89020163     19.82449807      4.94406622 N
atom       1.14373210      1.87605910      3.72072716 N
atom       7.80561371      1.87598525      3.33256671 N
atom       1.14394281     13.76423919      3.72244418 N
atom       7.80571618     13.76411040      3.33452121 N
atom       0.82227429      6.13112861      6.21489318 N
atom       7.49265120      6.13348890      0.83975632 N
atom       0.82241943     18.01921470      6.21728328 N
atom       7.49276251     18.02167641      0.84210598 N
atom       4.65516095     12.02177445      7.00810085 N
atom      11.32623182     12.02445126      0.04851210 N
atom       4.65497823      0.13365749      7.00666859 N
atom      11.32610282      0.13619780      0.04716097 N
atom       5.31986778      6.07798570      7.00845683 N
atom      11.99091168      6.07999661      0.04891072 N
atom       5.32001353     17.96611935      7.01070766 N
atom      11.99105122     17.96815910      0.05132127 N
atom       2.50028162     12.07719273      0.83802468 N
atom       9.15337819     12.07564752      6.21749590 N
atom       2.50013091      0.18923740      0.83661372 N
atom       9.15323336      0.18719104      6.21614084 N
atom       0.82688057      5.75391406      2.69044336 N
atom       7.48813271      5.75352198      4.36396570 N
atom       0.82709401     17.64223340      2.69280115 N
atom       7.48830782     17.64160232      4.36628734 N
atom       4.65988075     23.63926853      3.48523719 N
atom      11.32175069     23.63903531      3.57446577 N
atom       4.65958096     11.75105523      3.48358727 N
atom      11.32150930     11.75095165      3.57279010 N
atom       5.32445085      5.80685322      3.48406484 N
atom      11.98638269      5.80702124      3.57331135 N
atom       5.32466029     17.69501427      3.48632975 N
atom      11.98657343     17.69521739      3.57564444 N
atom       2.49583338     23.58607061      4.36393792 N
atom       9.15808232     23.58574228      2.69464504 N
atom       2.49554877     11.69770266      4.36226727 N
atom       9.15781644     11.69780739      2.69300658 N
atom       3.18850909      6.01596339      6.08278341 N
atom       9.85877716      6.01789760      0.97263006 N
atom       3.18866019     17.90411347      6.08504075 N
atom       9.85891099     17.90607417      0.97506342 N
atom       0.13408569     11.96209430      0.97003158 N
atom       6.78733003     11.96000097      6.08455988 N
atom       0.13392663      0.07405088      0.96880339 N
atom       6.78716911      0.07167046      6.08325197 N
atom       3.19308159      5.86904213      2.55842418 N
atom       9.85422705      5.86886345      4.49688999 N
atom       3.19328967     17.75725936      2.56070120 N
atom       9.85441655     17.75698943      4.49927424 N
atom       0.12969164     23.70119548      4.49590712 N
atom       6.79202390     23.70126108      2.56179905 N
atom       0.12942813     11.81290631      4.49432282 N
atom       6.79177399     11.81322611      2.56031357 N
atom       3.35107452      2.04981573      6.72505662 N
```

```
atom      10.02179250      2.05204626      0.32891064 N
atom       3.35123403     13.93795115      6.72680222 N
atom      10.02191596     13.94025639      0.33067009 N
atom      13.29490402      7.99605124      0.33074194 N
atom       6.62420346      7.99395135      6.72729528 N
atom      13.29506811     19.88422560      0.33298705 N
atom       6.62436643     19.88205701      6.72946140 N
atom       3.35559786      9.83502724      3.20154101 N
atom      10.01730191      9.83489567      3.85382449 N
atom       3.35587320     21.72323399      3.20347933 N
atom      10.01752091     21.72303143      3.85583898 N
atom      13.29029936      3.89083482      3.85465765 N
atom       6.62869811      3.89090003      3.20262701 N
atom      13.29049353     15.77899208      3.85671417 N
atom       6.62891489     15.77909185      3.20471944 N
```

```
# Botari et al. 2017, Fig. 1j-l, Table S6
# g-h-C3N4, C48N64 (Melissen et al., 2015)
# Final structure after total-energy minimisation of atomic position and
#   unit cell parameters using DFT-PBE+TS.
lattice_vector     11.88855852      0.01455290      0.00702318
lattice_vector     -0.00843232      7.04793709     -0.01557983
lattice_vector     -0.00790974      0.02958365     13.32452928
atom      11.65750590      5.34809051      6.12137793 C
atom       5.62457315      6.38152446      2.68449830 C
atom       9.72013838      4.59014537      7.00191971 C
atom       3.72090762      6.12833266      3.85934418 C
atom       9.66342813      5.14134122      4.81742924 C
atom       1.61362361      6.14632323      5.10796641 C
atom      10.98838842      4.94394976      7.18864270 N
atom       4.89961935      6.73657244      3.74394738 N
atom       1.08407975      5.49636439      6.13370158 N
atom       6.91298315      6.71196127      2.55751036 N
atom       3.14917555      6.14230710      7.48510652 N
atom       9.04342974      5.34822620      3.65757790 N
atom       3.03503876      6.26848316      5.11853407 N
atom      10.95843277      5.63513679      4.96203133 N
atom       6.15513135      1.76396004     12.78834678 C
atom       0.21803240      1.79766985      0.53262236 C
atom       5.71267428      5.27494763      7.19045633 C
atom       0.21417799      1.74422764      7.19502085 C
atom       5.71654487      5.32838342      0.52805261 C
atom      11.65364133      5.29465877     12.78377863 C
atom       6.15899240      1.81734678      6.12593485 C
atom       0.30357571      0.70071995      9.35624958 C
atom       6.24841603      2.86111671      3.96483731 C
atom      11.56678165      4.24128874     10.62723706 C
atom       6.24709763      0.71080701     10.63189907 C
atom      11.56810647      6.39160426      3.96015096 C
atom       5.62329118      4.23121646      9.35159885 C
atom       0.30490014      2.85104311      2.68915837 C
atom       8.09936948      2.49619497      0.34330016 C
atom       2.14935284      1.07017168     12.97995612 C
atom       3.77449886      6.02813467      6.30762363 C
atom       2.15154634      2.50216660      6.31447606 C
atom       3.77230692      4.59613932     12.97309881 C
atom       9.72232054      6.02215717      0.33644095 C
atom       8.09717577      1.06416314      7.00877932 C
atom       2.20585431      0.95913144     10.53220980 C
atom       8.15269470      2.60736914      2.79111409 C
atom       9.66390114      4.48981061      9.45013508 C
atom       8.15077711      0.96398754      9.45706471 C
atom       9.66582773      6.13319640      2.78418940 C
atom       3.71897136      4.48496135     10.52528417 C
atom       2.20777695      2.60251607      3.86626276 C
atom       8.15076747      1.96485902     11.48588260 C
atom       2.21263897      1.60164906      1.83743507 C
atom       3.71658655      5.47682549      8.49205779 C
atom       2.20825558      1.95098096      8.49896865 C
atom       3.72090152      5.12747283      1.83051523 C
```

```
atom       9.65904389      5.49068433     11.47895837 C
atom       8.15512977      1.61550925      4.82436001 C
atom       4.31165200      0.94669132     11.78339908 C
atom      10.25993754      2.62496418      1.54241866 C
atom       7.55814704      4.46666516      8.19902393 C
atom      10.25805736      0.94599952      8.20843538 C
atom       7.56002449      6.14564272      1.53300353 C
atom       1.61173760      4.46736354     11.77398506 C
atom       4.31353324      2.62563857      5.11737054 C
atom       6.83087874      2.14328425      0.53006450 N
atom       0.88022270      1.41997170     12.79169545 N
atom       5.04382759      5.67743575      6.12240254 N
atom       0.88330012      2.14835121      6.12775222 N
atom       5.04079520      4.94905553     12.78633465 N
atom      10.99144894      5.67235284      0.52470376 N
atom       6.82782953      1.41481097      7.19398665 N
atom       1.02728044      0.35038273     10.41811818 N
atom       6.97251213      3.21324880      2.90383001 N
atom      10.84394974      3.88444343      9.56694073 N
atom       6.97206329      0.35574816      9.57246108 N
atom      10.84440338      6.74194283      2.89828147 N
atom       4.89916314      3.87908297     10.41258511 N
atom       1.02772836      3.20788194      3.74945922 N
atom       4.83997291      1.60122762     12.80685221 N
atom      10.79106561      1.97172004      0.51959275 N
atom       7.02822151      5.11530678      7.17264813 N
atom      10.78760294      1.59596042      7.18270138 N
atom       7.03170207      5.49110806      0.50954945 N
atom       1.08060744      5.12060086     12.79681440 N
atom       4.84344756      1.97695841      6.14372718 N
atom      10.90388031      0.38425324      9.23622591 N
atom       4.95920020      3.18896473      4.09035122 N
atom       0.96729154      3.89946933     10.74871648 N
atom       4.95868950      0.38036752     10.75889145 N
atom       0.96780319      6.70806701      4.08017316 N
atom       6.91249963      3.90334957      9.22606733 N
atom      10.90438886      3.19286092      2.56768212 N
atom       2.78122649      0.93168134      0.83413422 N
atom       8.71653721      2.63620594     12.48985878 N
atom       9.09648089      4.47444127      5.82370358 N
atom       8.72252624      0.95000953      5.83130409 N
atom       9.09045087      6.16064714     12.48226113 N
atom       3.15513715      4.45612153      0.82654021 N
atom       2.77520536      2.61787613      7.49269098 N
atom       8.77213946      1.75282524     10.32769667 N
atom       2.83209297      1.81518673      2.99637391 N
atom       3.09571266      5.26842915      9.65117013 N
atom       2.82825379      1.74409939      9.65881969 N
atom       3.09954226      5.33949733      2.98871018 N
atom       9.03958816      5.27714430     10.32002104 N
atom       8.77597006      1.82390068      3.66522561 N
atom       2.89022365      0.82457038     11.79282001 N
atom       8.83822843      2.74361431      1.53131438 N
atom       8.97986614      4.34798030      8.19013486 N
```

```
atom       8.83664113      0.82383627      8.19787262 N
atom       8.98145277      6.26776136      1.52357998 N
atom       3.03344408      4.34871639     11.78508579 N
atom       2.89181585      2.74434036      5.12626063 N
atom       6.85557935      1.47172993     11.63112828 N
atom       0.91644096      2.09163231      1.69063715 N
atom       5.01298354      4.98622311      8.34901313 N
atom       0.91324786      1.45718922      8.35437099 N
atom       5.01607986      5.62061693      1.68525924 N
atom      10.95524588      5.00070707     11.62575264 N
atom       6.85875773      2.10613756      4.96743925 N
```

Crystalline Melamine-Melem Adduct Phases

```
# Botari et al. 2017, Figure 2a, Table S8
# Crystalline melamine-melem, adduct 1, C48N88H72 (Sattler et al., 2009)
# Final structure after total-energy minimisation of atomic position and
#   unit cell parameters using DFT-PBE+TS.
lattice_vector     21.49609797     -0.00247677     -0.00051728
lattice_vector      0.00785440     12.56261888      0.00267455
lattice_vector     -0.90513249     -0.00504008      6.77363735
atom      21.29259293      5.23477323      1.57096151 N
atom      22.43499991      3.16694674      1.60440230 N
atom      23.65061727      5.25337923      1.44948799 N
atom      22.50671482      7.26122897      1.44908417 N
atom      24.72458851      3.25226144      1.76294321 N
atom      21.31140881      9.21968444      1.56440619 N
atom      21.28324205      3.82745845      1.56379053 C
atom      22.51213308      5.92949471      1.48524812 C
atom      23.57630502      3.90332979      1.60524418 C
atom      21.30627164      7.88868178      1.56915221 C
atom      24.73728895      2.21877809      1.85435656 H
atom      25.60031598      3.76392138      1.59114629 H
atom      22.20605401      9.73221982      1.47762672 H
atom      20.12457754      3.18280072      1.51977090 N
atom      18.93582839      5.27861204      1.71580729 N
atom      20.10122172      7.27319325      1.69425460 N
atom      17.83103809      3.28525820      1.45054214 N
atom      20.08088946      5.94192578      1.66257781 C
atom      18.98985357      3.92825101      1.56129708 C
atom      17.80567581      2.24671532      1.42132330 H
atom      16.96547849      3.80252692      1.64763493 H
atom      20.42505774      9.74386215      1.66541850 H
atom      10.51014819     11.51717313      1.81828837 N
atom      11.67679502      9.46458521      1.86980347 N
atom      12.86707167     11.55960511      1.67509346 N
atom      11.70303269     13.55485517      1.69651490 N
atom      13.97029286      9.56553463      1.94120076 N
atom      10.49413776     15.50206472      1.82638867 N
atom      10.51858599     10.10980916      1.82499933 C
atom      11.72241276     12.22356907      1.72771136 C
atom      12.81207180     10.20929426      1.82941248 C
atom      10.49834155     14.17106164      1.82133962 C
atom      13.99425599      8.52684371      1.96980103 H
atom      14.83612976     10.08259548      1.74460470 H
atom      11.38077874     16.02552251      1.72515242 H
atom       9.36643633      9.44992772      1.78325008 N
atom       8.15215352     11.53708209      1.93872655 N
atom       9.29739555     13.54431840      1.94082196 N
atom       7.07697097      9.53686776      1.62314426 N
atom       9.29108659     12.21258949      1.90389424 C
atom       8.22563180     10.18704804      1.78206261 C
atom       7.06322637      8.50357064      1.53092951 H
atom       6.20126905     10.04866101      1.79483308 H
atom       9.59979411     16.01523017      1.91389526 H
```

```
atom      20.83860816      7.31793583      4.95890841 N
atom      19.67180929      9.37043528      4.90885939 N
atom      18.48176327      7.27528119      5.10373185 N
atom      19.64590102      5.28012148      5.08060560 N
atom      17.37823086      9.26945071      4.83981599 N
atom      20.85482363      3.33303018      4.94973951 N
atom      20.83013080      8.72525510      4.95248745 C
atom      19.62642534      6.61140235      5.04997865 C
atom      18.53660093      8.62566380      4.95006991 C
atom      20.85054497      4.66402741      4.95515592 C
atom      17.35418458     10.30814168      4.81130195 H
atom      16.51260686      8.75222064      5.03683589 H
atom      19.96825582      2.80945524      5.05069238 H
atom      21.98224210      9.38525108      4.99346522 N
atom      23.19656486      7.29814993      4.83717488 N
atom      22.05140861      5.29087303      4.83540879 N
atom      24.27183779      9.29845930      5.15180240 N
atom      22.05767812      6.62259574      4.87255926 C
atom      23.12308249      8.64818297      4.99379399 C
atom      24.28574713     10.33175450      5.24397202 H
atom      25.14748179      8.78673986      4.97984138 H
atom      21.74925029      2.81988369      4.86285400 H
atom      10.04875593      1.03793345      5.20303749 N
atom       8.90646440      3.10578829      5.16834054 N
atom       7.69071088      1.01944432      5.32323040 N
atom       8.83453626     -0.98845890      5.32506949 N
atom       6.61702282      3.02044244      5.00788940 N
atom      10.02983141     -2.94696790      5.21019332 N
atom      10.05816129      2.44519419      5.21001934 C
atom       8.82918519      0.34327342      5.28838756 C
atom       7.76516159      2.36943148      5.16686127 C
atom      10.03503014     -1.61596785      5.20539346 C
atom       6.60449919      4.05391208      4.91643697 H
atom       5.74112952      2.50897030      5.17947852 H
atom       9.13518413     -3.45945034      5.29762353 H
atom      11.21680386      3.08982950      5.25491023 N
atom      12.40562460      0.99400088      5.05983932 N
atom      11.24014782     -1.00056527      5.08068190 N
atom      13.51027705      2.98726283      5.32648909 N
atom      11.26053228      0.33069387      5.11225586 C
atom      12.35154880      2.34435437      5.21446527 C
atom      13.53547929      4.02581347      5.35566649 H
atom      14.37592150      2.46997476      5.12967778 H
atom      10.91609554     -3.47124796      5.10863135 H
atom       4.07700087      1.67855142      5.82835327 N
atom       2.89800609     -0.35415622      5.39217842 N
atom       1.87527044      1.76069890      4.89877916 N
atom       3.06412632      3.69121789      5.38930968 N
atom       5.04020946     -0.35093000      6.28234091 N
atom       0.78830434     -0.22337305      4.47996337 N
atom       2.99140502      2.34172120      5.37306192 C
atom       3.97760925      0.33246459      5.81310220 C
atom       1.88973722      0.41176864      4.93080865 C
atom       3.71281277      4.07592591      6.08602162 H
```

```
atom       2.20872686      4.22993586      5.19151182 H
atom       5.94814992      0.11871454      6.21828976 H
atom       5.08254623     -1.34984563      6.10190649 H
atom       0.69347542     -1.24653191      4.55450867 H
atom       0.11876698      0.30765997      3.93920263 H
atom      14.83644890      7.93084619      5.79845959 N
atom      13.67550436      5.89024602      5.35259834 N
atom      12.55499694      7.99334095      5.07823286 N
atom      13.73947854      9.93155413      5.55569909 N
atom      15.87120405      5.90561500      6.09318383 N
atom      11.49914493      5.99246846      4.60790599 N
atom      13.69690845      8.58324765      5.47735690 C
atom      14.76790142      6.58403501      5.72672799 C
atom      12.60798909      6.64585918      5.02963440 C
atom      14.41817736     10.31143547      6.22851802 H
atom      12.86999007     10.46390560      5.41347724 H
atom      16.76710100      6.39474103      6.01195652 H
atom      15.92524484      4.91442174      5.87636566 H
atom      11.40349979      4.99161734      4.84616800 H
atom      10.64234569      6.53182558      4.63498018 H
atom       5.31694781      7.96110597      4.33099105 N
atom       6.49380446      5.92725452      4.76694844 N
atom       7.51854399      8.04085781      5.26142268 N
atom       6.33206890      9.97257392      4.77068714 N
atom       4.35177295      5.93242369      3.87673200 N
atom       8.60322898      6.05538492      5.67993354 N
atom       6.40318812      8.62303440      4.78671856 C
atom       5.41492837      6.61490264      4.34604419 C
atom       7.50268298      6.69198965      5.22902488 C
atom       5.68405117     10.35849792      4.07396314 H
atom       7.18781523     10.51037408      4.96917561 H
atom       3.44390620      6.40229218      3.94070736 H
atom       4.30878733      4.93343705      4.05656461 H
atom       8.69592859      5.03192309      5.60550940 H
atom       9.27181102      6.58499182      6.22310198 H
atom      16.05267830      1.65079785      4.36758721 N
atom      17.21183775     -0.39106610      4.81158604 N
atom      18.33493642      1.71067115      5.08585947 N
atom      17.15218421      3.65020374      4.60987390 N
atom      15.01579767     -0.37347036      4.07247873 N
atom      19.38877203     -0.29174352      5.55447987 N
atom      17.19329414      2.30182965      4.68790245 C
atom      16.11986246      0.30387764      4.43853813 C
atom      18.28047894      0.36325110      5.13402768 C
atom      16.47374638      4.03104907      3.93720372 H
atom      18.02231600      4.18156774      4.75152799 H
atom      14.11994879      0.11580265      4.15452353 H
atom      14.96155937     -1.36496146      4.28777569 H
atom      19.48286707     -1.29272765      5.31563243 H
atom      20.24606059      0.24681182      5.52728245 H
atom      16.51206672     10.90405736      0.98307754 N
atom      17.67335334     12.94487708      1.42720817 N
atom      18.79405381     10.84187243      1.70149717 N
atom      17.60919598      8.90343544      1.22557295 N
```

```
atom      15.47724576     12.92912838      0.68779239 N
atom      19.85039266     12.84282891      2.17021676 N
atom      17.65183272     10.25178203      1.30354210 C
atom      16.58068287     12.25090978      1.05405116 C
atom      18.74107040     12.18937135      1.74963641 C
atom      16.93021120      8.52354923      0.55301466 H
atom      18.47889222      8.37117449      1.36694464 H
atom      14.58129653     12.44001685      0.76960010 H
atom      15.42332961     13.92054066      0.90364881 H
atom      19.94604300     13.84353702      1.93130175 H
atom      20.70691801     12.30315364      2.14231495 H
atom       5.76846229      4.59690229      0.94280438 N
atom       6.94726558      6.62938465      1.38033658 N
atom       7.96977358      4.51439039      1.87344089 N
atom       6.78116123      2.58410286      1.38183902 N
atom       4.80539644      6.62663354      0.48940550 N
atom       9.05649406      6.49839768      2.29349943 N
atom       6.85383710      3.93354837      1.39839589 C
atom       5.86783668      5.94296952      0.95868570 C
atom       7.95531025      5.86328967      1.84191945 C
atom       6.13257829      2.19928375      0.68510097 H
atom       7.63634993      2.04531147      1.58027046 H
atom       3.89750464      6.15697046      0.55286608 H
atom       4.76293986      7.62539687      0.67068779 H
atom       9.15091595      7.52164834      2.21974601 H
atom       9.72527692      5.96741947      2.83520384 H
atom      15.28802457      4.62140149      2.41009463 N
atom      14.12909679      6.66336310      1.96587663 N
atom      13.00624331      4.56165951      1.69031435 N
atom      14.18850114      2.62207765      2.16718374 N
atom      16.32484460      6.64559323      2.70579815 N
atom      11.95273445      6.56409190      1.22124380 N
atom      14.14756402      3.97044525      2.08908254 C
atom      15.22089426      5.96833380      2.33924534 C
atom      13.06071508      5.90910262      1.64244871 C
atom      14.86661875      2.24106920      2.84004136 H
atom      13.31846483      2.09075073      2.02485330 H
atom      17.22076838      6.15639657      2.62406984 H
atom      16.37935133      7.63710645      2.49064068 H
atom      11.85841532      7.56503384      1.46008610 H
atom      11.09542583      6.02549435      1.24747884 H
atom       4.53643822     10.87698050      2.44381581 N
atom       3.35958122     12.91082433      2.00798947 N
atom       2.33432747     10.79718798      1.51453310 N
atom       3.52112786      8.86548984      2.00479172 N
atom       5.50182876     12.90565012      2.89768040 N
atom       1.25000009     12.78286975      1.09569114 N
atom       3.44994121     10.21504809      1.98867298 C
atom       4.43850941     12.22319178      2.42869854 C
atom       2.35036478     12.14608698      1.54654254 C
atom       4.16940272      8.47977569      2.70142185 H
atom       2.66531090      8.32762660      1.80677520 H
atom       6.40959922     12.43567679      2.83340832 H
atom       5.54459859     13.90464548      2.71792213 H
```

```
atom       1.15673494     13.80624900      1.17098101 H
atom       0.57987925     12.25296523      0.55466359 H
```

```
# Botari et al. 2017, Figure 2b, Table S8
# Crystalline melamine-melem, adduct 2, C36N64H48 (Sattler et al., 2009)
# Final structure after total-energy minimisation of atomic position and
#   unit cell parameters using DFT-PBE+TS.
lattice_vector      7.35267197     -0.00029104      0.10917412
lattice_vector     -0.00026266      7.46128647      0.00175424
lattice_vector      0.03859389     -0.00019784     24.81148861
atom       5.04952344      2.61551037      1.09196750 C
atom       5.48449520      3.75462984     -1.01875989 C
atom       5.55538049      3.72109968      3.03788232 C
atom       4.54639129      1.66471361     -0.94549392 C
atom       5.51761889      3.73804913      0.38722458 N
atom       5.11662498      2.59328674      2.41405439 N
atom       4.53389008      1.59502748      0.41116815 N
atom       5.03117212      2.69663256     -1.67798559 N
atom       5.54816109      3.71942454      4.36839102 N
atom       4.02951211      0.64305752     -1.61498626 N
atom       5.35834307      2.83459883      4.87820212 H
atom       3.61220865     -0.17600693     -1.13202677 H
atom       4.08707936      0.63309410     -2.62952820 H
atom       6.02380552      4.84450864      1.09045971 C
atom       6.43127330      5.84348812     -0.94645264 C
atom       5.99393554      4.84825570      2.41565825 N
atom       6.52678538      5.87117005      0.41095137 N
atom       5.90203525      4.82684890     -1.67316036 N
atom       6.90186471      6.88287790     -1.62240699 N
atom       5.78116287      4.58565876      4.88237584 H
atom       7.33058668      7.68033861     -1.11994889 H
atom       6.67344074      6.96804273     -2.62066039 H
atom       1.34647914      4.84470450     11.42617678 C
atom       1.88717023      3.75490489     13.53506333 C
atom       1.81387864      3.72136243      9.47848944 C
atom       0.94025580      5.84366075     13.46334949 C
atom       1.85333884      3.73842445     12.12909142 N
atom       1.37553148      4.84843638     10.10097537 N
atom       0.84372689      5.87130661     12.10600583 N
atom       1.47003630      4.82712507     14.18978245 N
atom       1.82041655      3.71977572      8.14798895 N
atom       0.47010641      6.88319123     14.13944846 N
atom       1.58756095      4.58623622      7.63427392 H
atom       0.04089990      7.68058281     13.63729944 H
atom       0.69859451      6.96840786     15.13757628 H
atom       2.32103183      2.61583190     11.42408811 C
atom       2.82528619      1.66490025     13.46116675 C
atom       2.25309644      2.59356696     10.10205771 N
atom       2.83716922      1.59536841     12.10454875 N
atom       2.34079995      2.69682158     14.19391225 N
atom       3.34249927      0.64325470     14.13046165 N
atom       2.01020822      2.83513601      7.63790796 H
atom       3.75930598     -0.17585291     13.64730689 H
atom       3.28332582      0.63226845     15.14495549 H
atom       2.34182190      4.85199374     23.83001553 C
atom       1.90660787      3.71280278     25.94066072 C
atom       1.83584433      3.74663214     21.88400049 C
```

```
atom       2.84484709      5.80269361     25.86754817 C
atom       1.87367102      3.72940529     24.53465488 N
atom       2.27465842      4.87437973     22.50793748 N
atom       2.85753447      5.87237667     24.51090949 N
atom       2.35980305      4.77080662     26.59994433 N
atom       1.84284477      3.74847597     20.55350210 N
atom       3.36175461      6.82425475     26.53717456 N
atom       2.03245775      4.63332713     20.04370101 H
atom       3.77909068      7.64334568     26.05432050 H
atom       3.30323646      6.83459665     27.55168074 H
atom       1.36753310      2.62302463     23.83131037 C
atom       0.95998675      1.62387623     25.86809907 C
atom       1.39746751      2.61936152     22.50611497 N
atom       0.86452010      1.59629405     24.51070427 N
atom       1.48901426      2.64052948     26.59493150 N
atom       0.48968145      0.58428567     26.54395295 N
atom       1.61001780      2.88219717     20.03954523 H
atom       0.06088277     -0.21314299     26.04149525 H
atom       0.71790958      0.49927382     27.54220466 H
atom       6.04265784      2.62296926     13.49583176 C
atom       5.50165299      3.71300028     11.38717141 C
atom       5.57552897      3.74600674     15.44375868 C
atom       6.44870420      1.62425916     11.45849750 C
atom       5.53591389      3.72945097     12.79315811 N
atom       6.01369019      2.61900525     14.82104843 N
atom       6.54526053      1.59643000     12.81582637 N
atom       5.91876140      2.64088354     10.73228517 N
atom       5.56918702      3.74743314     16.77426184 N
atom       6.91891151      0.58489633     10.78217871 N
atom       5.80237596      2.88101497     17.28784268 H
atom       7.34802792     -0.21257183     11.28426443 H
atom       6.69015386      0.49963811      9.78404560 H
atom       5.06818767      4.85187035     13.49838102 C
atom       4.56346285      5.80296807     11.46153969 C
atom       5.13625701      4.87391129     14.82041113 N
atom       4.55190976      5.87243412     12.81815958 N
atom       5.04766637      4.77106680     10.72853883 N
atom       4.04640269      6.82476895     10.79239202 N
atom       5.38011015      4.63223798     17.28439193 H
atom       3.62952613      7.64383391     11.27563925 H
atom       4.10406320      6.83516602      9.77782793 H
atom       5.48307801      7.47381688     17.68656620 C
atom       5.86723936      8.50417562     19.67541254 C
atom       5.73667948      8.62721977     18.34027389 N
atom       5.71921767      7.35331353     20.37621486 N
atom       6.17069780      9.61246136     20.37626691 N
atom       5.39584568      7.51842970     16.34620646 N
atom       6.22493749     10.50202550     19.89520217 H
atom       5.99259609      9.66053522     21.38115979 H
atom       5.70035835      8.36245045     15.85105233 H
atom       5.39074517      6.28578535     19.62200503 C
atom       5.28796047      6.27435116     18.28099226 N
atom       5.18367955      5.10596954     20.26218376 N
atom       4.53949213      4.45684580     19.82899813 H
```

```
atom       5.25281992      5.07838961     21.28593336 H
atom       5.28825292      6.64046650     15.82833474 H
atom       1.92996635      7.47509275     19.64272722 C
atom       2.02314355      6.28824077     17.70662347 C
atom       2.12560883      6.27602592     19.04768106 N
atom       1.69477866      7.35618549     16.95292507 N
atom       2.23025265      5.10883713     17.06579343 N
atom       2.01695890      7.51908645     20.98318050 N
atom       2.87369175      4.45888763     17.49884249 H
atom       2.16074397      5.08128807     16.04213455 H
atom       2.12374189      6.64081927     21.50075048 H
atom       1.54587397      8.50652209     17.65443583 C
atom       1.67599524      8.62876013     18.98969678 N
atom       1.24189680      9.61507438     16.95428084 N
atom       1.18693880     10.50421278     17.43603495 H
atom       1.42030101      9.66386692     15.94939987 H
atom       1.71122839      8.36260124     21.47840768 H
atom       1.90749219      7.45465897      7.23738035 C
atom       1.52437531      6.42395914      5.24850028 C
atom       1.65315397      6.30130475      6.58384343 N
atom       1.67381586      7.57453662      4.54759911 N
atom       1.22139871      5.31563959      4.54758500 N
atom       1.99428653      7.41013264      8.57781607 N
atom       1.16491089      4.42638437      5.02892581 H
atom       1.39983222      5.26716573      3.54274889 H
atom       1.68865672      6.56642238      9.07281225 H
atom       2.00143175      8.64232251      5.30189061 C
atom       2.10360115      8.65397110      6.64292839 N
atom       2.20697007      9.82214760      4.66129569 N
atom       2.85021460     10.47244522      5.09415298 H
atom       2.13779163      9.84939800      3.63755220 H
atom       2.10136180      8.28817823      9.09565356 H
atom       5.46174040      7.45420348      5.28078088 C
atom       5.36761835      8.64134674      7.21662494 C
atom       5.26476846      8.65320364      5.87565275 N
atom       5.69622530      7.57363867      7.97049625 N
atom       5.16111120      9.82095479      7.85742620 N
atom       5.37546574      7.41013181      3.94033392 N
atom       4.51712591     10.47059313      7.42465034 H
atom       5.23005328      9.84821745      8.88116651 H
atom       5.26774916      8.28822348      3.42265301 H
atom       5.84520842      6.42306916      7.26930940 C
atom       5.71629142      6.30070492      5.93397555 N
atom       6.14691883      5.31451455      7.97032938 N
atom       6.20277194      4.42518325      7.48902444 H
atom       5.96805375      5.26632739      8.97512039 H
atom       5.68075135      6.56644086      3.44514384 H
```

```
# Botari et al. 2017, Figure 2c, Table S8
# Crystalline melamine-melem, adduct 3, C84N144H96 (Sattler et al., 2009)
# Final structure after total-energy minimisation of atomic position and
#   unit cell parameters using DFT-PBE+TS.
lattice_vector     14.36162509     -0.00001771     -0.00013131
lattice_vector      0.00201504     25.71422165      0.00002679
lattice_vector     -0.68837151      0.00017117      8.20221118
atom       1.34672241      4.97276253      1.00685026 C
atom       5.00029856      5.63204694      3.69368140 C
atom       3.46908164      9.03596027      1.03306731 C
atom       3.16620545      5.22041781      2.36611326 C
atom       4.32976383      7.36680768      2.35243278 C
atom       2.39151150      7.02498173      0.94010928 C
atom       0.33592827      4.23108261      0.56674005 N
atom       5.83154927      5.18586025      4.63655608 N
atom       3.51577142     10.30842050      0.64473430 N
atom       2.20409578      4.42933106      1.90648649 N
atom       4.01137080      4.79462277      3.29627034 N
atom       5.20311660      6.89250341      3.23477610 N
atom       4.40752249      8.61826327      1.92162874 N
atom       2.48922244      8.26678347      0.49148086 N
atom       1.42232414      6.23010555      0.50276228 N
atom       3.29799388      6.53504281      1.88778844 N
atom      -0.36829470      4.68999604     -0.02987942 H
atom       0.15996336      3.30098304      0.95226989 H
atom       5.79459893      4.19833106      4.92946562 H
atom       6.72458614      5.70172068      4.72153063 H
atom       2.80177315     10.63859296     -0.01059852 H
atom       4.18993201     10.95262004      1.07186147 H
atom       8.52852779     17.83012877      1.00685341 C
atom      12.18204356     18.48947262      3.69379303 C
atom      10.65077550     21.89339917      1.03325219 C
atom      10.34800284     18.07777923      2.36614948 C
atom      11.51153214     20.22418549      2.35249873 C
atom       9.57316026     19.88244472      0.94033419 C
atom       7.51779444     17.08840582      0.56663191 N
atom      13.01322634     18.04334524      4.63675825 N
atom      10.69750546     23.16585725      0.64493173 N
atom       9.38596190     17.28665681      1.90642234 N
atom      11.19315654     17.65201717      3.29633629 N
atom      12.38489599     19.74990025      3.23483574 N
atom      11.58930725     21.47563188      1.92168096 N
atom       9.67079729     21.12428186      0.49180383 N
atom       8.60398782     19.08755526      0.50295983 N
atom      10.47972996     19.39243537      1.88789475 N
atom       6.81338824     17.54731356     -0.02976774 H
atom       7.34192464     16.15825500      0.95207604 H
atom      12.97632497     17.05581234      4.92964921 H
atom      13.90625819     18.55923398      4.72175227 H
atom       9.98355685     23.49603786     -0.01043956 H
atom      11.37181629     23.81000130      1.07192984 H
atom       5.49242253     17.83045763      3.09427237 C
atom       1.83878612     18.48969448      0.40746853 C
atom       3.37013623     21.89362668      3.06800470 C
```

```
atom       3.67304499     18.07817353      1.73487197 C
atom       2.50946211     20.22452021      1.74857960 C
atom       4.44771861     19.88270025      3.16092904 C
atom       6.50331881     17.08879024      3.53416798 N
atom       1.00753129     18.04348334     -0.53540495 N
atom       3.32352650     23.16614623      3.45618020 N
atom       4.63503962     17.28703423      2.19461908 N
atom       2.82766758     17.65226428      0.80494395 N
atom       1.63598024     19.75015457      0.86637841 N
atom       2.43161985     21.47592119      2.17951152 N
atom       4.34987356     21.12442524      3.60969854 N
atom       5.41672290     19.08772137      3.59852652 N
atom       3.54159748     19.39297143      2.21276471 N
atom       7.20764944     17.54762824      4.13072156 H
atom       6.67914964     16.15866113      3.14864503 H
atom       1.04444020     17.05595646     -0.82829881 H
atom       0.11447311     18.55935444     -0.62048451 H
atom       4.03751092     23.49635265      4.11142510 H
atom       2.64932536     23.81033865      3.02902741 H
atom      12.67246998      4.97312070      3.09407815 C
atom       9.01889204      5.63232877      0.40721160 C
atom      10.55037722      9.03638443      3.06752800 C
atom      10.85305385      5.22080480      1.73474060 C
atom       9.68967990      7.36726972      1.74813056 C
atom      11.62775812      7.02536100      3.16072326 C
atom      13.68337351      4.23148439      3.53397205 N
atom       8.18761472      5.18605004     -0.53560887 N
atom      10.50385045     10.30893283      3.45563165 N
atom      11.81507789      4.42968652      2.19445438 N
atom      10.00765346      4.79484176      0.80486089 N
atom       8.81625842      6.89291132      0.86586100 N
atom       9.61194638      8.61873262      2.17891286 N
atom      11.52998090      8.26712781      3.60939414 N
atom      12.59675380      6.23038489      3.59833345 N
atom      10.72159824      6.53561122      2.21260883 N
atom      14.38753995      4.69033918      4.13069326 H
atom      13.85924636      3.30134435      3.14848771 H
atom       8.22442991      4.19848188     -0.82840129 H
atom       7.29464089      5.70201534     -0.62083418 H
atom      11.21781918     10.63912144      4.11090849 H
atom       9.82971273     10.95314796      3.02843275 H
atom      12.32907257     20.74157223      7.19530412 C
atom       8.67551755     20.08245339      4.50839681 C
atom      10.20679968     16.67834010      7.16872119 C
atom      10.50962251     20.49399126      5.83598505 C
atom       9.34610681     18.34757646      5.84946929 C
atom      11.28431216     18.68932894      7.26187333 C
atom      13.33989556     21.48320315      7.63542861 N
atom       7.84423778     20.52872656      3.56560044 N
atom      10.16013663     15.40584377      7.55695310 N
atom      11.47171328     21.28505826      6.29568877 N
atom       9.66442954     20.91985980      4.90589164 N
atom       8.47274866     18.82193579      4.96716544 N
atom       9.26836711     17.09608100      6.28017189 N
```

```
atom      11.18661345     17.44749681      7.71040170 N
atom      12.25343866     19.48421360      7.69935008 N
atom      10.37788389     19.17930854      6.31416341 N
atom      14.04410464     21.02425738      8.23204971 H
atom      13.51589172     22.41331003      7.24994269 H
atom       7.88116774     21.51628189      3.27275549 H
atom       6.95122127     20.01283100      3.48055573 H
atom      10.87410170     15.07565268      8.21229197 H
atom       9.48598690     14.76165503      7.12978492 H
atom       5.14742431      7.88434521      7.19509448 C
atom       1.49382454      7.22502756      4.50826587 C
atom       3.02503193      3.82116257      7.16894002 C
atom       3.32801737      7.63663059      5.83571794 C
atom       2.16435843      5.49030083      5.84954697 C
atom       4.10269692      5.83209016      7.26176194 C
atom       6.15824040      8.62603629      7.63516870 N
atom       0.66255844      7.67120691      3.56540525 N
atom       2.97833466      2.54870941      7.55728174 N
atom       4.29005122      8.42776248      6.29543616 N
atom       2.48281254      8.06241935      4.90559427 N
atom       1.29093741      5.96462151      4.96728375 N
atom       2.08654026      4.23888237      6.28044481 N
atom       4.00491303      4.59033435      7.71048576 N
atom       5.07181613      6.62701117      7.69919777 N
atom       3.19635005      6.32195091      6.31390906 N
atom       6.86262473      8.16716426      8.23162310 H
atom       6.33414765      9.55613709      7.24961759 H
atom       0.69953434      8.65871604      3.27244727 H
atom      -0.23051141      7.15536532      3.48047089 H
atom       3.69225263      2.21857934      8.21271590 H
atom       2.30411876      1.90451672      7.13021439 H
atom       8.18351694      7.88399141      5.10756436 C
atom      11.83700990      7.22474169      7.79456094 C
atom      10.30562519      3.82073116      5.13412649 C
atom      10.00276677      7.63623572      6.46714119 C
atom      11.16626130      5.48982217      6.45359235 C
atom       9.22808263      5.83168065      5.04113897 C
atom       7.17265896      8.62567638      4.66760635 N
atom      12.66826811      7.67097650      8.73742411 N
atom      10.35221007      2.54820869      4.74596040 N
atom       9.04088123      8.42741553      6.00723690 N
atom      10.84822762      8.06222878      7.39695806 N
atom      12.03975481      5.96422327      7.33576544 N
atom      11.24412846      4.23842818      6.02263929 N
atom       9.32595110      4.58996317      4.59235438 N
atom       8.25920205      6.62671148      4.60335622 N
atom      10.13401607      6.32130869      5.98953676 N
atom       6.46832575      8.16682929      4.07106348 H
atom       6.99680629      9.55580033      5.05313769 H
atom      12.63145065      8.65853905      9.03021274 H
atom      13.56127315      7.15503518      8.82259188 H
atom       9.63826808      2.21803165      4.09065137 H
atom      11.02642341      1.90401675      5.17308744 H
atom       1.00334675     20.74141288      5.10803237 C
```

```
atom       4.65687893     20.08208455      7.79491994 C
atom       3.12556047     16.67819995      5.13427992 C
atom       2.82269402     20.49363385      6.46744484 C
atom       3.98619728     18.34723494      6.45382091 C
atom       2.04805893     18.68917964      5.04130770 C
atom      -0.00753312     21.48309334      4.66816090 N
atom       5.48810633     20.52830823      8.73781205 N
atom       3.17210773     15.40568289      4.74608573 N
atom       1.86071174     21.28478837      6.00771656 N
atom       3.66807899     20.91956353      7.39735345 N
atom       4.85962571     18.82157969      7.33609474 N
atom       4.06401611     17.09583310      6.02287773 N
atom       2.14591574     17.44746902      4.59248738 N
atom       1.07907026     19.48417443      4.60371529 N
atom       2.95412611     19.17883001      5.98956148 N
atom      -0.71170371     21.02428180      4.07141775 H
atom      -0.18339776     22.41320625      5.05372929 H
atom       5.45124197     21.51585161      9.03066790 H
atom       6.38111415     20.01238929      8.82301053 H
atom       2.45811238     15.07552259      4.09080410 H
atom       3.84622475     14.76144035      5.17326653 H
atom      12.22711512     11.33672459      0.85955032 C
atom      14.19071301     11.23413857      2.05017550 C
atom      13.13016286     13.35128313      1.46063990 C
atom      14.19047623     15.28918190      2.05007581 C
atom      11.25359344     10.69823273      0.22770274 N
atom      14.19044114     16.62172210      2.04988789 N
atom      13.14569970     14.67843776      1.44159809 N
atom      13.22950697     10.58814901      1.39844450 N
atom      14.19061729     12.64461172      2.05018989 N
atom      12.11770222     12.69110258      0.91703042 N
atom      10.55037791     11.25021892     -0.26282699 H
atom      11.33989859      9.70052506     -0.03919347 H
atom      13.46922537     17.11144135      1.52787784 H
atom      16.15430416     11.33700693      3.24078142 C
atom      15.25095084     13.35145967      2.63974918 C
atom      17.12794505     10.69857070      3.87249915 N
atom      15.23525817     14.67861467      2.65871012 N
atom      15.15202025     10.58829262      2.70187259 N
atom      16.26348373     12.69140956      3.18342863 N
atom      17.83112603     11.25056152      4.36307556 H
atom      17.04163647      9.70084237      4.13931243 H
atom      14.91198083     17.11161953      2.57124639 H
atom       5.04669633     24.19384122      0.86029582 C
atom       7.01042421     24.09137383      2.05078063 C
atom       5.94974199     26.20845545      1.46125010 C
atom       7.01031049     28.14641222      2.05005881 C
atom       4.07318450     23.55530501      0.22847001 N
atom       7.01031318     29.47895236      2.04969440 N
atom       5.96532051     27.53561095      1.44197902 N
atom       6.04917559     23.44533596      1.39915329 N
atom       7.01024038     25.50184484      2.05079541 N
atom       4.93722812     25.54822131      0.91776643 N
atom       3.36995908     24.10727046     -0.26207874 H
```

```
atom       4.15959031     22.55763404     -0.03856240 H
atom       6.28907632     29.96864787      1.52767379 H
atom       8.97428324     24.19439631      3.24106145 C
atom       8.07088421     26.20877387      2.63981962 C
atom       9.94792495     23.55603431      3.87287867 N
atom       8.05531541     27.53593144      2.65839097 N
atom       7.97190009     23.44563429      2.70236078 N
atom       9.08354178     25.54877628      3.18334001 N
atom      10.65120016     24.10805441      4.36330081 H
atom       9.86161648     22.55834284      4.13985419 H
atom       7.73218335     29.96886493      2.57058863 H
atom      15.81071600     14.37791559      7.34210004 C
atom      13.84709379     14.48034336      6.15149916 C
atom      14.90770529     12.36329508      6.74121273 C
atom      13.84739778     10.42530010      6.15207292 C
atom      16.78423461     15.01647191      7.97388283 N
atom      13.84747337      9.09276133      6.15253886 N
atom      14.89217953     11.03614555      6.76044360 N
atom      14.80827913     15.12641482      6.80318035 N
atom      13.84723407     13.06987049      6.15158958 N
atom      15.92017280     13.02354128      7.28471430 N
atom      17.48744933     14.46450554      8.46443536 H
atom      16.69785012     16.01416850      8.24081133 H
atom      14.56861341      8.60317180      6.67479767 H
atom      11.88352680     14.37731239      4.96086635 C
atom      12.78692558     12.36292535      5.56208944 C
atom      10.90987554     15.01567733      4.32909140 N
atom      12.80263215     11.03576568      5.54331360 N
atom      12.88575668     15.12610750      5.49976497 N
atom      11.77440495     13.02290523      5.01829226 N
atom      10.20671568     14.46365447      3.83851609 H
atom      10.99609801     16.01342360      4.06233072 H
atom      13.12585482      8.60273544      5.63143232 H
atom       8.62899203      1.52062245      7.34198129 C
atom       6.66519148      1.62307618      6.15159725 C
atom       7.72588885     -0.49398354      6.74112523 C
atom       6.66537431     -2.43195371      6.15225988 C
atom       9.60252341      2.15916777      7.97376582 N
atom       6.66542454     -3.76449431      6.15269859 N
atom       7.71036008     -1.82113392      6.76032817 N
atom       7.62647618      2.26912529      6.80317733 N
atom       6.66529073      0.21260431      6.15175393 N
atom       8.73848835      0.16625368      7.28444084 N
atom      10.30579997      1.60722965      8.46427092 H
atom       9.51609165      3.15683532      8.24082105 H
atom       7.38664538     -4.25411608      6.67482675 H
atom       4.70143072      1.52006094      4.96117576 C
atom       5.60478034     -0.49433586      5.56249136 C
atom       3.72777026      2.15841359      4.32937428 N
atom       5.62040872     -1.82149669      5.54383586 N
atom       5.70377034      2.26882213      5.49995051 N
atom       4.59223076      0.16566510      5.01876827 N
atom       3.02455999      1.60636269      3.83889014 H
atom       3.81404758      3.15611007      4.06243385 H
```

```
atom       5.94358926     -4.25447977      5.63184433 H
atom       5.87534532     13.48698203      2.08301543 C
atom       7.00984046     11.52183207      2.05056914 C
atom       4.69081729     14.15157251      2.12334747 N
atom       5.80707032     12.14747382      2.03825239 N
atom       7.00971823     10.18692914      2.05042374 N
atom       7.01010510     14.23006215      2.05063788 N
atom       3.87695231     13.62876819      2.44845282 H
atom       4.68834988     15.16671646      2.25626013 H
atom       7.89824334      9.67620655      2.04204105 H
atom       8.14468798     13.48677970      2.01828123 C
atom       9.32937467     14.15111069      1.97791326 N
atom       8.21273104     12.14725783      2.06302083 N
atom      10.14298208     13.62817899      1.65235026 H
atom       9.33198313     15.16625342      1.84502623 H
atom       6.12110496      9.67637184      2.05887702 H
atom      13.05715615     26.34403679      2.08285210 C
atom      14.19151757     24.37880927      2.05066264 C
atom      11.87268604     27.00868445      2.12306748 N
atom      12.98880482     25.00453192      2.03810160 N
atom      14.19135320     23.04391704      2.05065139 N
atom      14.19189547     27.08707747      2.05059154 N
atom      11.05882167     26.48593872      2.44823413 H
atom      11.87033478     28.02383918      2.25593659 H
atom      15.07984978     22.53316344      2.04236731 H
atom      15.32642800     26.34373834      2.01837178 C
atom      16.51109653     27.00805720      1.97804541 N
atom      15.39440854     25.00421840      2.06321858 N
atom      17.32473810     26.48513182      1.65255176 H
atom      16.51368503     28.02319651      1.84512293 H
atom      13.30276300     22.53334399      2.05891011 H
atom       7.80057071     12.22742670      6.11874640 C
atom       6.66608303     14.19257510      6.15112429 C
atom       8.98512638     11.56287958      6.07848795 N
atom       7.86884122     13.56693520      6.16348816 N
atom       6.66620426     15.52748097      6.15119669 N
atom       6.66585545     11.48434135      6.15107045 N
atom       9.79893556     12.08568884      5.75326867 H
atom       8.98760667     10.54773386      5.94559956 H
atom       5.77768295     16.03819221      6.15971196 H
atom       5.53122924     12.22759586      6.18350999 C
atom       4.34656904     11.56323403      6.22397860 N
atom       5.46318193     13.56711903      6.13875253 N
atom       3.53291029     12.08617628      6.54941051 H
atom       4.34395590     10.54808734      6.35686122 H
atom       7.55480666     16.03803637      6.14283746 H
atom      14.98042695     -0.62962421      6.11911747 C
atom      13.84602965      1.33558051      6.15120890 C
atom      16.16491409     -1.29424271      6.07894167 N
atom      15.04875321      0.70988270      6.16379976 N
atom      13.84617866      2.67047435      6.15110573 N
atom      13.84570193     -1.37268742      6.15140808 N
atom      16.97874841     -0.77148248      5.75371468 H
atom      16.16728622     -2.30939988      5.94609506 H
```

```
atom      12.95767817      3.18121269      6.15945948 H
atom      12.71115521     -0.62936884      6.18361867 C
atom      11.52650084     -1.29371125      6.22398985 N
atom      12.64314887      0.71014923      6.13871967 N
atom      10.71283769     -0.77078962      6.54942064 H
atom      11.52391325     -2.30885112      6.35691990 H
atom      14.73476311      3.18106032      6.14289667 H
```

g-t-C6N9H3

```
# Botari et al. 2017, Figure S3, Table S9
# g-t-C6N9H3, C12N18H6 (Melissen et al., 2015)
# Final structure after total-energy minimisation of atomic position and
#   unit cell parameters using DFT-PBE+TS.
lattice_vector      8.61797335      0.00002782     -0.00049715
lattice_vector     -4.30871509      7.46276913     -0.00058062
lattice_vector     -0.00076617     -0.00684167      6.67766256
atom      -0.84772979      4.01001894      1.66903909 C
atom      -1.35374555      5.23846585      1.66886264 N
atom       3.35075589      0.00633087      1.66944768 N
atom       2.33489312      0.00634305      1.66955526 H
atom       1.27299468      4.72849022      1.66881484 C
atom      -0.40962099      6.20576849      1.66882697 C
atom       5.15635993      3.44636332      5.00754875 C
atom       3.03563553      2.72789101      5.00775997 C
atom       4.71825232      1.25061389      5.00777533 C
atom       3.89927571      1.26964237      1.66917630 C
atom       3.46125831      3.46544949      1.66887136 C
atom       5.58191253      2.74688752      1.66879504 C
atom       0.40935564      6.18673963      5.00742202 C
atom       0.84737374      3.99093434      5.00770241 C
atom      -1.27328216      4.70949536      5.00779765 C
atom       0.46208636      3.67599443      1.66902060 N
atom       0.90727030      6.02975282      1.66879193 N
atom       5.66237568      2.21791727      5.00773549 N
atom       3.84654391      3.78038837      5.00754332 N
atom       3.40135964      1.42662852      5.00781452 N
atom       5.21617186      1.44559518      1.66890650 N
atom       2.95521177      2.23698423      1.66925050 N
atom       4.77104562      3.79940377      1.66870917 N
atom      -0.90753945      6.01078781      5.00769131 N
atom       1.35342226      5.21940025      5.00734145 N
atom      -0.46241204      3.65698173      5.00786908 N
atom       2.64125362      4.57187263      1.66849969 N
atom       0.95787533      7.45005224      5.00715261 N
atom      -2.64157531      4.55283623      5.00779127 N
atom       1.66737786      2.88451012      5.00803988 N
atom      -1.66776669      2.90351855      1.66930586 N
atom       7.45795008      2.02367624      1.66897494 H
atom       3.14902507      5.45172166      1.66811457 H
atom       1.15959773      2.00466584      5.00841822 H
atom       5.46865665      5.43273533      5.00712647 H
atom       6.28245334     -0.01272591      5.00761422 H
```

References

(1) Blum, V.; Gehrke, R.; Hanke, F.; Havu, P.; Havu, V.; Ren, X.; Reuter, K.; Scheffler, M. Ab initio molecular simulations with numeric atom-centered orbitals. *Computer Physics Communications* **2009**, *180*, 2175–2196.

(2) Havu, V.; Blum, V.; Havu, P.; Scheffler, M. Efficient O (N) integration for all-electron electronic structure calculation using numeric basis functions. *Journal of Computational Physics* **2009**, *228*, 8367–8379.

(3) Ren, X.; Rinke, P.; Blum, V.; Wieferink, J.; Tkatchenko, A.; Sanfilippo, A.; Reuter, K.; Scheffler, M. Resolution-of-identity approach to Hartree–Fock, hybrid density functionals, RPA, MP2 and GW with numeric atom-centered orbital basis functions. *New Journal of Physics* **2012**, *14*, 053020.

(4) Levchenko, S. V.; Ren, X.; Wieferink, J.; Johanni, R.; Rinke, P.; Blum, V.; Scheffler, M. Hybrid functionals for large periodic systems in an all-electron, numeric atom-centered basis framework. *Computer Physics Communications* **2015**, *192*, 60–69.

(5) Ihrig, A. C.; Wieferink, J.; Zhang, I. Y.; Ropo, M.; Ren, X.; Rinke, P.; Scheffler, M.; Blum, V. Accurate localized resolution of identity approach for linear-scaling hybrid density functionals and for many-body perturbation theory. *New Journal of Physics* **2015**, *17*, 093020.

(6) Knuth, F.; Carbogno, C.; Atalla, V.; Blum, V.; Scheffler, M. All-electron formalism for total energy strain derivatives and stress tensor components for numeric atom-centered orbitals. *Computer Physics Communications* **2015**, *190*, 33–50.

(7) Perdew, J. P.; Burke, K.; Ernzerhof, M. Generalized Gradient Approximation Made Simple. *Physical Review Letters* **1996**, *77*, 3865–3868.

(8) Tkatchenko, A.; Scheffler, M. Accurate Molecular van der Waals Interactions from Ground-State Electron Density and Free-Atom Reference Data. *Physical Review Letters* **2009**, *102*, 073005.

(9) Heyd, J.; Scuseria, G. E.; Ernzerhof, M. Erratum: "Hybrid functionals based on a screened Coulomb potential" [J. Chem. Phys. 118, 8207 (2003)]. *The Journal of Chemical Physics* **2006**, *124*, 219906.

(10) Ambrosetti, A.; Reilly, A. M.; DiStasio, R. A., Jr.; Tkatchenko, A. Long-range correlation energy calculated from coupled atomic response functions. *The Journal of Chemical Physics* **2014**, *140*, 18A508.

(11) McQuarrie, D. *Statistical Mechanics*; University Science Books: Mill Valley, California, 2000.

(12) NIST-JANAF Table – Ammonia. http://kinetics.nist.gov/janaf/html/H-083.html, Accessed: 2016-09-13.

(13) Chase, M. W. *NIST-JANAF Themochemical Tables*, 4th ed.; J. Phys. Chem. Ref. Data; 1998; Vol. Monograph 9.

(14) Haar, L.; Gallagher, J. S. Thermodynamic properties of ammonia. *Journal of Physical and Chemical Reference Data* **1978**, *7*.

(15) Joos, G.; Bartels, J.; ten Bruggencate, P. *Landolt-Börnstein: Zahlenwerte und Funktionen aus Physik, Chemie, Astronomie, Geophysik und Technik - 6. Auflage*; Springer Verlag: Berlin Heidelberg New York, 1952.

(16) Borge, J. Reviewing Some Crucial Concepts of Gibbs Energy in Chemical Equilibrium Using a Computer-Assisted, Guided-Problem-Solving Approach. *Journal of Chemical Education* **2015**, *92*, 296–304.

(17) Jürgens, B.; Irran, E.; Senker, J.; Kroll, P.; Müller, H.; Schnick, W. Melem (2,5,8-Triamino-tri-s-triazine), an Important Intermediate during Condensation of Melamine Rings to Graphitic Carbon Nitride: Synthesis, Structure Determination by X-ray Powder Diffractometry, Solid-State NMR, and Theoretical Studies. *Journal of the American Chemical Society* **2003**, *125*, 10288–10300.

(18) Fina, F.; Callear, S. K.; Carins, G. M.; Irvine, J. T. S. Structural Investigation of Graphitic Carbon Nitride via XRD and Neutron Diffraction. *Chemistry of Materials* **2015**, *27*, 2612–2618.

(19) Chamorro-Posada, P.; Vázquez-Cabo, J.; Sánchez-Arévalo, F. M.; Martín-Ramos, P.; Martín-Gil, J.; Navas-Gracia, L. M.; Dante, R. C. 2D to 3D transition of polymeric carbon nitride nanosheets. *Journal of Solid State Chemistry* **2014**, *219*, 232–241.

(20) Dante, R. C.; Martn-Ramos, P.; Snchez-Arvalo, F.; Huerta, L.; Bizarro, M.; Navas-Gracia, L. M.; Martn-Gil, J. Synthesis of crumpled nanosheets of polymeric carbon nitride from melamine cyanurate. *Journal of Solid State Chemistry* **2013**, *201*, 153 – 163.

(21) Tyborski, T.; Merschjann, C.; Orthmann, S.; Yang, F.; Lux-Steiner, M. C.; Schedel-Niedrig, T. Crystal structure of polymeric carbon nitride and the determination of its process-temperature-induced modifications. *Journal of Physics: Condensed Matter* **2013**, *25*, 395402.

(22) Lotsch, B. V.; Döblinger, M.; Sehnert, J.; Seyfarth, L.; Senker, J.; Oeckler, O.; Schnick, W. Unmasking Melon by a Complementary Approach Employing Electron Diffraction, Solid-State NMR Spectroscopy, and Theoretical Calculations—Structural Characterization of a Carbon Nitride Polymer. *Chemistry - A European Journal* **2007**, *13*, 4969–4980.

(23) Gracia, J.; Kroll, P.; Chemie, A.; Rwth, T. H. Corrugated layered heptazine-based car-

bon nitride: the lowest energy modifications of C3N4 ground state. *Journal of Materials Chemistry* **2009**, *19*, 3013.

(24) Melissen, S.; Le Bahers, T.; Steinmann, S. N.; Sautet, P. Relationship between Carbon Nitride Structure and Exciton Binding Energies: A DFT Perspective. *The Journal of Physical Chemistry C* **2015**, *119*, 25188–25196.

(25) Tyborski, T.; Merschjann, C.; Orthmann, S.; Yang, F.; Lux-Steiner, M.-C.; Schedel-Niedrig, T. Crystal structure of polymeric carbon nitride and the determination of its process-temperature-induced modifications. *Journal of Physics: Condensed Matter* **2013**, *25*, 395402.

(26) Algara-Siller, G.; Severin, N.; Chong, S. Y.; Björkman, T.; Palgrave, R. G.; Laybourn, A.; Antonietti, M.; Khimyak, Y. Z.; Krasheninnikov, A. V.; Rabe, J. P.; Kaiser, U.; Cooper, A. I.; Thomas, A.; Bojdys, M. J. Triazine-Based Graphitic Carbon Nitride: a Two-Dimensional Semiconductor. *Angewandte Chemie International Edition* **2014**, *53*, 7450–7455.

(27) Sattler, A.; Schnick, W. On the Formation and Decomposition of the Melonate Ion in Cyanate and Thiocyanate Melts and the Crystal Structure of Potassium Melonate, K 3[C 6N 7(NCN) 3]. *European Journal of Inorganic Chemistry* **2009**, *2009*, 4972–4981.

(28) Wirnhier, E.; Döblinger, M.; Gunzelmann, D.; Senker, J.; Lotsch, B. V.; Schnick, W. Poly(triazine imide) with intercalation of lithium and chloride ions [(C3N3)2(NH(x)Li(1-x))3LiCl]: a crystalline 2D carbon nitride network. *Chemistry – A European Journal* **2011**, *17*, 3213–21.

(29) Pickard, C. J.; Salamat, A.; Bojdys, M. J.; Needs, R. J.; McMillan, P. F. Carbon nitride frameworks and dense crystalline polymorphs. *Phys. Rev. B* **2016**, *94*, 094104.

(30) Perdew, J. P.; Ruzsinszky, A.; Csonka, G. I.; Vydrov, O. A.; Scuseria, G. E.; Con-

stantin, L. A.; Zhou, X.; Burke, K. Restoring the Density-Gradient Expansion for Exchange in Solids and Surfaces. *Phys. Rev. Lett.* **2008**, *100*, 136406.

PCCP

ROYAL SOCIETY OF CHEMISTRY

PAPER

View Article Online
View Journal

Cite this: DOI: 10.1039/d0cp06063a

What does graphitic carbon nitride really look like?†

Sigismund T. A. G. Melissen, [a] Tangui Le Bahers, [b] Philippe Sautet [cd] and Stephan N. Steinmann *[b]

Received 23rd November 2020,
Accepted 8th January 2021

DOI: 10.1039/d0cp06063a

rsc.li/pccp

Graphitic carbon nitrides (g-CNs) have become popular light absorbers in photocatalytic water splitting cells. Early theoretical work on these structures focused on fully polymerized g-C_3N_4. Experimentally, it is known that the typically employed melamine polycondensation does not go toward completion, yielding structures with ~15 at% hydrogen. Here, we study the conformational stability of "melon", with the $[C_6N_9H_3]_n$ structural formula using DFT. Referencing to a 2D melon sheet, B3LYP-dDsC and PBE-MBD computations revealed the same qualitative trend in stability of the 3D structures, with several of them within 5 kJ mol^{-1} per tecton. Fina's orthorhombic melon is the most stable of the studied conformers, with Lotsch' monoclinic melon taking an intermediate value. Invoking a simple Wannier–Mott-type approach, Fina's and Lotsch' structures exhibited the lowest optical gaps (2.8 eV), within the error margin of the experimental value (2.7 eV). All conformers yielded gaps below that of the monolayer's (3.2 eV), suggesting Jelley-type ("J") aggregation effects.

1 Introduction

As an alternative to photovoltaics, solar energy can be stored in the form of chemical bonds, counteracting the diurnal variation in solar power. To design chemical schemes allowing such storage, inspiration can be drawn from the photosynthetic process found in nature. Such schemes are commonly referred to as "artificial photosynthesis".[1]

An elegant route to perform artificial photosynthesis is by using graphitic carbon nitrides (g-CN), with general formula g-$C_xN_yH_z$, as photoharvester[2–8] in photocatalytic water splitting cells.[9,10] Its synthesis from basic petrochemicals is cheap and straightforward, while allowing a wide structural variety.[11] Furthermore, putting such compounds to use in renewable energy sources, instead of in fuels, is environmentally beneficial.[12]

In eqn (1) the formal reaction scheme from cyanamide to g-C_3N_4 is provided.[13]

$$n\mathrm{CN_2H_2(l)} \rightarrow \frac{n}{2}\mathrm{C_2N_4H_4(l)} \rightarrow \frac{n}{3}\mathrm{C_3N_6H_6(l)} \quad (1)$$

$$\rightarrow \frac{1}{6}[\mathrm{C_6N_9H_3}]_n\mathrm{(s)} + \frac{n}{2}\mathrm{NH_3(g)} \quad (2)$$

$$\rightarrow \frac{1}{3}[\mathrm{C_3N_4}]_n\mathrm{(s)} + \frac{n}{6}\mathrm{NH_3(g)} \quad (3)$$

In Fig. 1 the key species discussed in this study are depicted. The melamine core can be integrated directly as a tecton yielding gt-CNs (t for triazine). The melem core, however, yields the more stable gh-CNs (h for heptazine).

Following pioneering theoretical work by Liu and Prewitt in the late 1980s,[14,15] many computational studies have been devoted to fully detaminated CN. gt-C_3N_4,[16] gh-C_3N_4,[17–19] and other polymorphs[20,21] have been extensively studied, even though it is well known that these species are unstable,[22] decomposing at the synthesis temperature that would typically be required to produce them.[23] Furthermore, frequent presentation of these fully deaminated structures as flat,[18,24] rather than corrugated,[3,25] added further confusion to the research field. Finally, the community investigating the photocatalytic activity of these structures doubts that by increasing the degree of polycondensation, increasing photocatalytic activity should always be found: participation of N lone pairs in denser π-aromatic networks reduces their ability to bond to the noble metal cocatalyst that enables the half reaction leading to H_2, and defects – rather than always trapping electrons or holes –

[a] Université de Lyon, Université Claude Bernard Lyon 1, CNRS, Institut Lumière Matière, F-69622 Lyon, France
[b] Université de Lyon, Université Claude Bernard Lyon 1, Ecole Normale Supérieure de Lyon, CNRS, 46 allée d'Italie, F-69007 Lyon Cedex, France. E-mail: stephan.steinmann@ens-lyon.fr
[c] Department of Chemical and Biomolecular engineering, University of California, Los Angeles, Los Angeles, CA 90095, USA
[d] Department of Chemistry and Biochemistry, University of California, Los Angeles, Los Angeles, CA 90095, USA

† Electronic supplementary information (ESI) available: Energies for additional functionals and a comparison of computational unit cells to the experimental ones is provided. All structures are provided in POSCAR (Vienna Ab Initio Simulation Package (VASP)) format; subsequently in.gui (CRYSTAL14 format) and finally, for the 3D structures only, in.cif (Crystallographic) format. See DOI: 10.1039/d0cp06063a

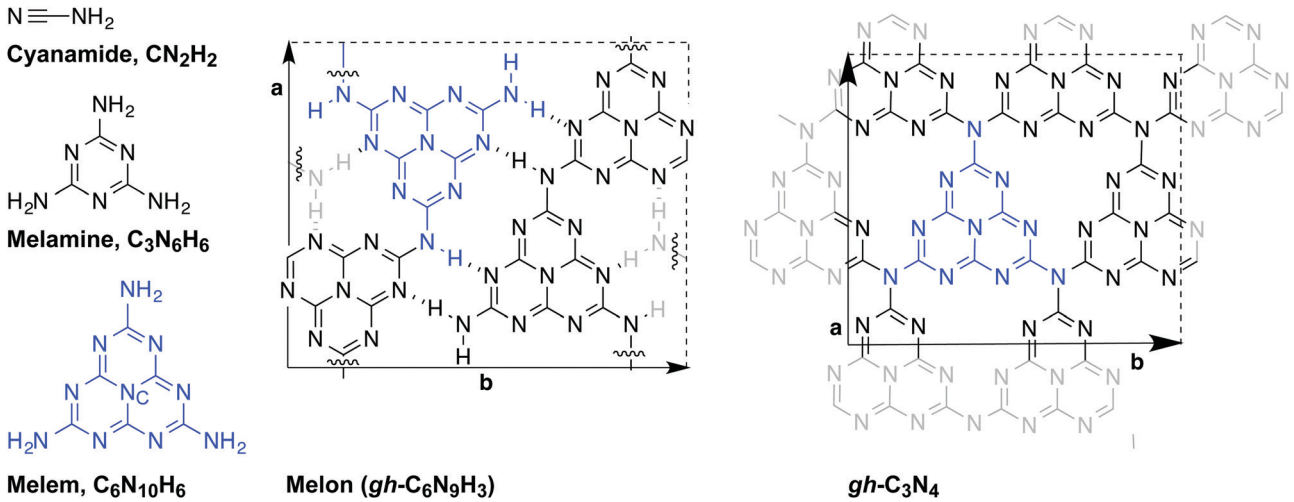

Fig. 1 Overview of structures involved in the CN synthesis process. Melem's core N atom is indexed C.

possibly enhance the reaction.[7,26–34] We reported earlier[22] that among the different polymeric species that form during CN synthesis, gh-$C_6N_9H_3$,[35] known as "melon" is the most stable one.

Melon can be synthesized using starting materials comprising a wider range of chemical elements than C, N and H alone, such as urea ($CO(NH_2)_2$)[36] and thiourea ($CS(NH_2)_2$).[37] Lotsch and co-workers[23,28,35] established the synthesis temperature range for the typical melamine precursor. Polymerization onset[28,38] occurs at 380 °C (in an open vessel). At the high end of this range crystalline[35] melon is produced (630 °C, closed vessel conditions). At higher temperatures the onset of material degradation is observed.[23,38] In practice, the experimental parameters are often compromises between these extremes.[38–40]

The stability of g-CN is largely due to the specific balance between steric repulsion, hydrogen bonding and the formation of a π-conjugated network. As can be understood from Fig. 1, the lone pairs in the hypothetical gh-C_3N_4 repel each other forcing a (partial) breaking of the overall π-conjugation, and causing the material to be corrugated. The hydrogen atoms in gh-$C_6N_9H_3$ stabilize several of these lone pairs, spatially separate others, and allow the formation of a flat, aromatic network overall.[22] The flat laminae themselves are interesting and can be integrated into other structures. Indeed, the van der Waals structures they can form are not just those that are created by stacking with itself, but also by interleaving other species.[41] Within this strategy, interleaving with molybdenum dichalcogenides to allow fast charge separation is of particular experimental[42] and theoretical interest.[43] Here, we focus on the question what particular lamination pattern between gh-$C_6N_9H_3$ layers yields the most stable form of melon.

In 2015, Fina *et al.*[40] published a neutron-scattering study of a melon conformer with a different packing structure from the one determined by Lotsch *et al.* in 2007.[35] Both Fina and Lotsch synthesized the conformers studied here from melamine in a sealed environment, the main differences in protocol being the temperature, 500 °C in Fina's case and 630 °C in Lotsch' and working in a sealed ampoule (Fina) or under ammonia (Lotsch). The influence of the synthesis conditions on the obtained polymorph and the significant impact that it can have on photoactivity, has been described before for other organic semiconductors.[44] Furthermore, the structure analysis temperature could also affect the particular crystal structure observed.[45]

In Fig. 2, the possible variations in stacking patterns studied here are provided. Essentially (Fig. 2a), the shaded layer below the reference layer can shift in the hydrogen bonding direction (corresponding to **b**) by $\mathbf{d}_H$, and/or in the covalent bonding direction by $\mathbf{d}_{Cov}$. Second (Fig. 2b and c), the stacking pattern can be ABAB, or AAAA. In the latter case, AA-stacking does not mean that the layers are sandwich stacked. Rather, π-aromatic systems such as those discussed here tend to shift slightly with respect to each other.[46] Finally, variations in interaromatic distances ($\mathbf{d}_{Ar-Ar}$), as well as in the lattice vectors within the aromatic plane are possible (arbitrarily referred to here as **a**, **b**), although these variations are typically smaller.

We study four important conformers reported in the literature. The first conformer is named "Lotsch", representing the first melon characterized. It has an AA stacking pattern and $\mathbf{d}_H = 0$. The structure determined from the aforementioned neutron scattering study is named "Fina", with $\mathbf{d}_H \neq \mathbf{d}_{Cov} \neq 0$ and AB-stacking. The third and fourth structures are included in Fina's comparison and here the same labels are adopted, namely S1 for the alternative monoclinic structure and S2 for the alternative triclinic structure. S1 has an AA stacking pattern and $\mathbf{d}_{Cov} = 0$. For S2, like Fina, $\mathbf{d}_H \neq \mathbf{d}_{Cov} \neq 0$, but the stacking pattern is AA. Included in the comparison are lastly 1D and 2D melon.[22]

A 2010 study[47] that combined theory (molecular mechanics level of theory[48]) and dedicated NMR experiments[49] of melon conformers suggested that configurations resembling Lotsch' – with $\mathbf{d}_{Cov} = 0$ – and Fina's – with $\mathbf{d}_H \gg \mathbf{d}_{Cov} > 0$ – to be the two prevalent ones within melon macrostructures. These authors further proposed that the proximity in energies of the structures was the reason that experimentally, no definitive ordering for the stacking direction is found, and indeed a random combination of the above stacking types is likely.

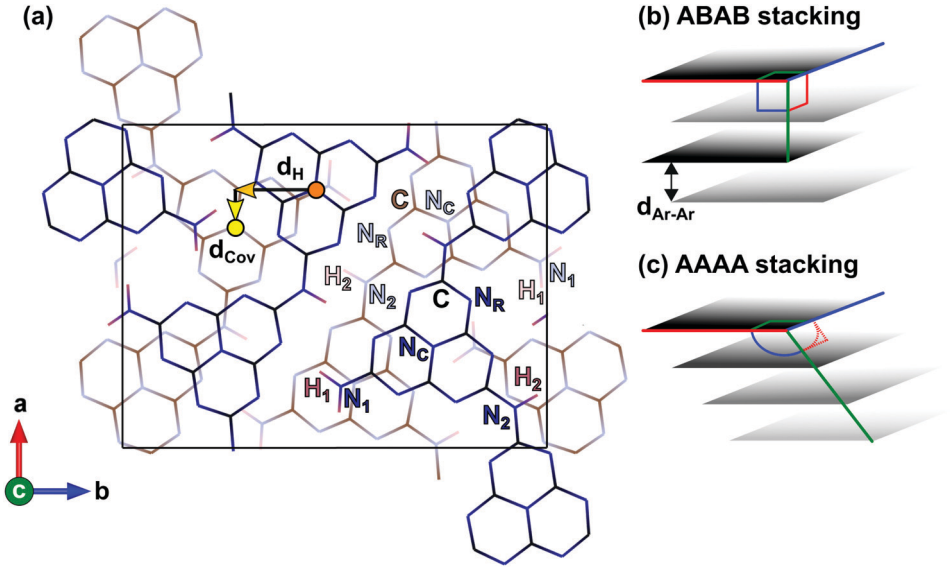

Fig. 2 Crystallography of melon. (a) Representation of an arbitrary melon bilayer. Black and brown: C; blue shades: N; pink shades: H. To guide the eye, chemically different atoms are marked, in particular the ring (R), core (C) nitrogen atoms and the primary (1) and secondary (2) amine groups are highlighted for a top and bottom heptazine subunit of choice. d_{Cov} is the distance the lower layer moves along the "covalent bonding direction" (*a*-direction) with respect to the top layer. d_H is the distance the lower layer moves along the "H-bonding direction" (*b*-direction) with respect to the top layer. Distances in the opposite direction of this choice of unit cell, are written with a minus sign. The distances are taken from N_C to the nearest next N_C (see Fig. 1). (b) One organizational form of the melon layers is by A–B–A–B stacking, leading to an orthorhombic structure. The distance between two layers is systematically referred to as d_{Ar-Ar}. (c) Alternatively, the layers organize following a systematic shift in the same direction, leading to a monoclinic or trigonal lattice.

We herein revisit the most important proposals for a crystalline structure of melon polymorphs by using state of the art hybrid DFT computations to differentiate the stability of the various melon conformers. Given the increasing use of the g-CN family of compounds for a variety of purposes,[50] such a comparative work using first principles approaches is timely.

2 Computational details

Following our earlier work,[22] DFT computations were performed using B3LYP,[51–53] which was proven earlier to yield accurate thermochemistry for g-CNs.

Geometry optimizations (freezing only the space group symmetry, thus leaving the cell constants fully, and the Wyckoff positions partially, free) and frequency computations – invoking the harmonic approximation – were performed with the Crystal 14 suite[54,55] starting from the geometries as they were provided in Lotsch' and Fina's original papers. Gatti's[56] all-electron 6-31G(d,p) basis set[57] was used for these calculations. The fundamental gaps were determined through subsequent single point calculations with the triple-ζ basis set by Peintinger *et al.*[58] The optical gaps were then determined by invoking a simple Wannier–Mott model.[59] Its combination with hybrid-DFT was described earlier by us,[60] and it has proved to yield good correspondence to experiment.[5,61–66]

Civalleri's "D*" variation[67,68] to the semi-empirical Grimme D2 framework[69] was used to describe dispersive interactions, with the scaling factor s_6 equal to 0.35. This scaling factor avoids the underestimation of non-covalent bond lengths often found in molecular crystals when using Civalleri's default scaling factor of 1.0. For these calculations, the electronic convergence criterion was set to 10^{-10} Ha.[70]

The electronic energies were determined on the optimized structures using the PAW formalism to account for the ion-electron intraction[71] as implemented in VASP 5.4.1,[72–75] with "hard" pseudopotentials datemarked 06 Feb 2004. The wave function was expanded in a plane wave basis set, characterized by a cut-off energy of 600 eV. The use of plane waves has the additional benefit of being intrinsically free from the BSSE.[76,77] Dispersion interactions were refined by using the dDsC[78] and D3BJ[79] dispersion corrections. For comparison, PBE[80,81] computations with both MBD[82–84] and dDsC[78] (see Table S2 in the ESI†) long range corrections were performed. Vacuum layers of >15 Å were used to suppress spurious interactions for the 1D and 2D melon. An electronic convergence criterion of 10^{-6} eV was imposed. Gaussian smearing with $\sigma = 0.01$ eV was employed.

Because of the different basis sets and associated computational cost for the two codes, the *K*-point samplings[85] for the VASP calculations were different from those using Crystal 14 (*cf.* Table 1).[86] However, convergence tests at the PBE level of theory have shown the relative energies to be converged within 1 kJ mol^{-1} per tecton with the chosen setup in VASP. The optimized structures' symmetry was verified using the findsym code.[87]

3 Results and discussion

In Fig. 3 a visualization of every 3D crystallographic unit cell is provided and in Table 2, the numerical details of the obtained geometries are summarized. The only significant variations in geometry are the in-plane displacements of the different layers

Table 1 *K*-Point meshes used for the Brillouin zone integration

Species	C14 grid	VASP grid
Fina	4 × 4 × 4	2 × 2 × 2
$P2_1/a$	4 × 4 × 4	2 × 2 × 2
S1	4 × 4 × 4	2 × 2 × 2
S2	4 × 4 × 4	2 × 2 × 2
2D	4 × 4	2 × 2 (× 1)
1D	4	2 (× 1 × 1)

Table 2 Tabulation of geometrical results. Distances are reported in Å. Differences with respect to experiment are indicated by a percentage change

Species	Symmetry[a]	Z[b]	Stacking	d_{Ar-Ar}	d_H	d_{Cov}
1D	Polymer	2	—	—	—	—
2D	p2gg[c]	4	—	—	—	—
Fina	P.O.[d]	8	AB	3.21	+3.12 (+19%)	+1.45 (+11%)
S1	Monoclinic	4	AA	3.24	−3.45 (−21%)	0 (0%)
Lotsch	Monoclinic	4	AA	3.22	0 (0%)	3.43 (+27%)
S2	Primitive	4	AA	3.23	+1.10 (+7%)	−3.35 (−26%)

[a] Notes: under "symmetry" general crystallographic information is listed, *cf.* Fig. 3 and ESI. [b] Z is the number of formula units per cell.[88] [c] p2gg is the wallpaper group for this 2D structure. [d] P.O. stands for "pseudo-orthorhombic".

Table 3 Relative energies (in kJ mol^{-1} per tecton; the contribution of the dispersion correction is given in parentheses) and optical gaps (in eV)

	$\delta G_{th.}$[a]	$\Delta E_{el.}$	$\Delta E_{el.}$	$\Delta E_{el.}$	$\Delta E_{g,opt}$
	B3LYP-D*	B3LYP-D*	PBE-MBD	B3LYP-dDsC	B3LYP[b]
1D	−4	+100 (+8)	+94 (+23)	+97 (+35)	3.05
2D	0	0	0	0	3.22
Fina	+3	−46 (−36)	−68 (−77)	−96 (−116)	2.76
Lotsch	+5	−46 (−37)	−66 (−77)	−88 (−108)	2.83
S1	+5	−44 (−35)	−63 (−81)	−87 (−104)	3.08
S2	+5	−46 (−37)	−65 (−85)	−95 (−114)	3.03
Exp					2.7

[a] Notes: $\delta G_{th.}$ is the thermal correction which needs to be added to the electronic energy $\Delta E_{el.}$ in order to obtain the Gibbs free energy ΔG. When comparing the ΔG for the polymorphs, all methods shown here identify Fina as the most stable one. [b] The bandgaps are obtained using the Peintinger–Oliveira–Bredow basis set (*cf.* Computational details).

with respect to each other. The interlayer spacings and the lattice parameters associated to the individual melon layer vary negligibly. This is also seen when comparing the computational and experimental lattice parameters, independently if one considers B3LYP-D* or PBE-dDsC (see Table S2 in the ESI†).

In Table 3 the energetic results are summarized. Energies discussed here, unless specified otherwise, are in reference to those calculated with the most sophisticated approach used: the B3LYP-dDsC functional.[78] In contrast to the "*D**" dispersion correction, "dDsC" depends on the electronic density and has been successfully applied to various branches of chemistry, from homogeneous catalysis[78] to adsorption on metal surfaces.[89] In order to assess the importance of higher-order dispersion effects, we have also tested the MBD dispersion correction.[82] However, MBD is not parametrized for the hybrid functional B3LYP. Therefore, we use the generalized gradient approximation PBE-MBD,[82–84] which has been demonstrated to be accurate for crystal structure predictions.[90–92]

The formation of the H-bonding network upon going from 1D to 2D melon yields ∼95 kJ mol^{-1} stabilization per repeat unit ($C_6N_9H_3$ "tecton"). Stacking 2D melon yields a similar, additional stabilization. The stabilization energies due to stacking are relatively close for all four polymorphs. Nevertheless, the effect of dispersion is crucial for the relative stabilities, whereas the effect of the vibrational energy is almost negligible. Although differences in stability are negligible when using B3LYP-D*, B3LYP-dDsC evidences energetic differences up to ∼10 kJ mol^{-1} for the different polymorphs. For comparison, Table S1 in the ESI,† reports results for several more functionals.

Since the principal application of g-CN is as a light absorber in photocatalytic devices, and the primary quantity of interest for such light absorbers is the optical gap $E_{g,opt}$ (see ref. 93 for the definitions used here), the B3LYP optical gaps are provided in the rightmost column of Table 3. As can be seen from Fig. 5d in ref. 3, the conduction band is essentially flat for melon in the d_H and d_{Ar-Ar} directions, due to the compound's molecular character, yielding very slightly lower indirect gaps than direct gaps. The fundamental gap for all 3D structures is hence formally indirect, but within 0.15 eV of the direct one. It is direct for the 2D and 1D melon structures. The exciton binding energy was assumed to be 840 meV (see ref. 3) based on the Wannier–Mott model. This model to evaluate the exciton binding energy for carbon nitrides has proven its reliability compared to the more sophisticated, but also more resource consuming, Bethe–Salpeter equation.[4] This quantity was thus

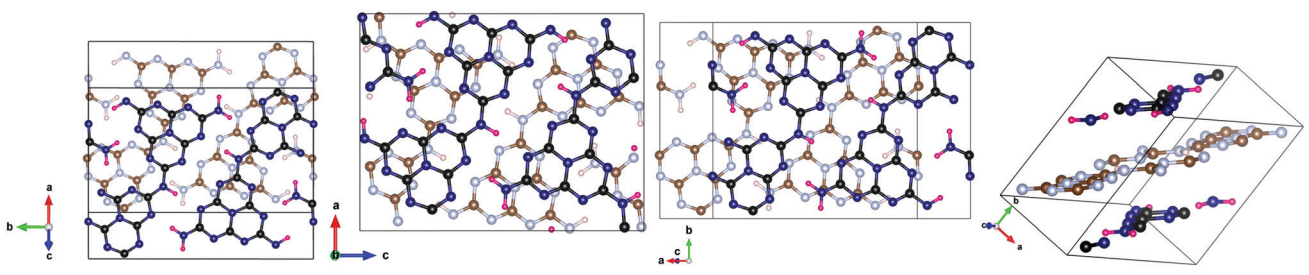

(a) Lotsch. $P2_1/$ (b) Fina. $P2_1/m$, (c) S1. $P2_1/a$, (d) S2. $\bar{P}_1$.

Fig. 3 Visualization of different crystals in a single unit cell. Black and brown: C; blue shades: N; pink shades: H. The computed unit cells are compared to the experimental ones in Table S2 (ESI†).

subtracted from the narrowest fundamental gap to obtain the optical band-gap ($E_{g,opt} \equiv (E_{CB}^{min} - E_{VB}^{max}) - E_b$). The optical gap for the monolayer was equal to 3.2 eV. The obtained 3D optical gaps range from 2.76 eV (Fina) to 3.08 eV (S1), with Lotsch' melon having a similar gap as Fina's (2.83 eV).

The S1 structure is predicted by all methods to be the least stable of the 3D structures and the Fina structure seems the most stable following the accurate methods, and hardly distinguishable energetically from the Lotsch and S2 structures for B3LYP-D*. Fina *et al.* suggest that the difference in packing between their structure and the structure found by Lotsch *et al.* could be due to the use of a sealed ampoule. Other subtle differences between their methods, such as synthesis time and temperature, could also lead to different structures.

The above results explain why it proves challenging to determine the crystallographic nature of melon with high certainty. First, the layers can slide with respect to each other, second, several minima are stable and third, the energetic differences between the structures are small. Together, these factors can also be seen as an explanation for the sometimes amorphous nature of melon.

Different polymorphs having similar formation energies is a common situation in crystal structure prediction of organic molecules. Reliably distinguishing polymorphs is challenging even for modern, dispersion corrected DFT approaches.[94] Given the small energetic difference for melon polymorphs obtained here, we stress the importance of combining theory and experiment in the determination of g-CN structures.

Researchers focusing on the photocatalytic quality, rather than structural perfection, of melon, could likely find melon that is overall amorphous, but contains crystalline domains like those found in Fina's and Lotsch's structures, possibly even with the "S2-domains" described here. We could expect that a scanning tunneling microscope image of crystalline domains of carbon nitrides could unveil "Moire" coincidence patterns helping the resolution of the structure as it was done for graphene supported materials.[95]

As for $E_{g,opt}$, our values are in agreement with the established experimental gap of 2.7 eV, especially when considering the limitations of the Wannier–Mott model. Furthermore, trends within a family, are better described by this model than the absolute values, suggesting that the gap of S1 and S2 should be significantly higher than for the Fina polymorph. A "Jelley"-type[96,97] or "J"-aggregation phenomenon such as that seen in fluorescent, aromatic dyes[98] could be the reason for the lowering of the gap in the 3D crystals with respect to the monolayer.[99] Indeed, the "ladder" and "staircase" organizations of the aromatic units – and with that of their dipole moments – observed here are known to lead to this type of photophysics.[100] This insight could be important to synthetic chemists developing new generations of carbon nitrides.

4 Conclusions

In summary, we have revisted the polymorphs of melon by density functional theory computations. When taking dispersion interactions accurately into account, our results consistently predict that the Fina polymorph is the most stable, even though other polymorphs are close (within 5 kJ mol^{-1} of tectons) in energy. These small energy differences rationalize the experimental observation of different polymorphs depending on the synthesis conditions and suggest that disordered melon structures might be the rule, rather than the exception. The Fina polymorph has also the lowest band-gap ($\sim$2.8 eV), in close agreement with experimental estimates. Since it is also the most stable polymorph, we conclude that it most closely represents the commonly produced "melon". However, the S2 polymorph with its 0.2 eV higher band-gap is close in energy, which suggests that it could be accessible *via* crystal-phase engineering if such a soft-UV band-gap is beneficial for a given application. The bulk band-gap is lowered by 0.2–0.4 eV compared to the 1D and 2D building blocks, indicating that it is a J-type aggregate in the solid state that is responsible for the photoabsorption properties.

Acronyms

B3LYP	Becke-3-parameter-Lee–Yang–Parr
BSSE	Basis set superposition error
CB	Conduction band
CN	Carbon nitride
DFT	Density functional theory
D3BJ	Grimme's D3 formalism with Becke–Johnson damping
GGA	Generalized gradient approximation
MBD	Many body dispersion
NMR	Nuclear magnetic resonance
PAW	Projector augmented-wave
PBE	Perdew–Burke–Ernzerhof exchange and correlation functional
ESI	Electronic supporting information
VASP	Vienna *ab initio* simulation package
VB	Valence band
WM	Wannier–Mott

Conflicts of interest

There are no conflicts to declare.

Acknowledgements

The authors gratefully acknowledge the computational resources provided by l' Institut du Développement et des Ressources en Informatique Scientifique (IDRIS, under project x2015080609) of the Centre National de la Recherche Scientifique (CNRS). The authors thank the SYSPROD project and AXELERA Pôle de Compétitivité for financial support (PSMN Data Center).

Notes and references

1 N. Lewis and G. Crabtree, *Basic Research Needs for Solar Energy Utilization*, Office of Science US Dept of Energy, 2005.
2 X. Wang, K. Maeda, A. Thomas, K. Takanabe, G. Xin, J. M. Carlsson, K. Domen and M. Antonietti, *Nat. Mater.*, 2009, **8**, 76–80.
3 S. Melissen, T. L. Bahers, S. N. Steinmann and P. Sautet, *J. Phys. Chem. C*, 2015, **119**, 25188–25196.
4 S. N. Steinmann, S. T. A. G. Melissen, T. Le Bahers and P. Sautet, *J. Mater. Chem. A*, 2017, **5**, 5115–5122.
5 M. K. Bhunia, S. T. A. G. Melissen, M. R. Parida, P. Sarawade, J.-M. Basset, D. H. Anjum, O. F. Mohammed, P. Sautet, T. Le Bahers and K. Takanabe, *Chem. Mater.*, 2015, **27**, 8237–8247.
6 X. Li, A. F. Masters and T. Maschmeyer, *ChemCatChem*, 2015, **7**, 121–126.
7 C. Butchosa, P. Guiglion and M. A. Zwijnenburg, *J. Phys. Chem. C*, 2014, **118**, 24833–24842.
8 R. Godin, Y. Wang, M. Zwijnenburg, J. Tang and J. Durrant, *J. Am. Chem. Soc.*, 2017, **139**, 5216–5224.
9 J. McEvoy and G. Brudvig, *Chem. Rev.*, 2006, **106**, 4455–4483.
10 B. A. Pinaud, J. D. Benck, L. C. Seitz, A. J. Forman, Z. Chen, T. G. Deutsch, B. D. James, K. N. Baum, G. N. Baum, S. Ardo, H. Wang, E. Miller and T. F. Jaramillo, *Energy Environ. Sci.*, 2013, **6**, 1983–2002.
11 S. Cao and J. Yu, *J. Phys. Chem. Lett.*, 2014, **5**, 2101–2107.
12 J. Ran, J. Zhang, J. Yu, M. Jaroniec and S. Z. Qiao, *Chem. Soc. Rev.*, 2014, **43**, 7787–7812.
13 F. K. Kessler, Y. Zheng, D. Schwarz, C. Merschjann, W. Schnick, X. Wang and M. J. Bojdys, *Nat. Rev. Mater.*, 2017, **2**, 17030.
14 A. Y. Liu and M. L. Cohen, *Science*, 1989, **245**, 841–842.
15 A. Y. Liu and M. L. Cohen, *Phys. Rev. B: Condens. Matter Mater. Phys.*, 1990, **41**, 10727–10734.
16 A. H. Reshak, S. A. Khan and S. Auluck, *RSC Adv.*, 2014, **4**, 6957–6964.
17 J. Gracia and P. Kroll, *J. Mater. Chem.*, 2009, **19**, 3013–3019.
18 S. Zuluaga, L.-H. Liu, N. Shafiq, S. M. Rupich, J.-F. Veyan, Y. J. Chabal and T. Thonhauser, *Phys. Chem. Chem. Phys.*, 2015, **17**, 957–962.
19 Y. Xu and S.-P. Gao, *Int. J. Hydrogen Energy*, 2012, **37**, 11072–11080.
20 H. Dong, A. R. Oganov, Q. Zhu and G.-R. Qian, *Sci. Rep.*, 2015, **5**, 9870.
21 C. J. Pickard, A. Salamat, M. J. Bojdys, R. J. Needs and P. F. McMillan, *Phys. Rev. B*, 2016, **94**, 094104.
22 S. T. A. G. Melissen, S. N. Steinmann, T. Le Bahers and P. Sautet, *J. Phys. Chem. C*, 2016, **120**, 24542–24550.
23 T. Botari, W. P. Huhn, V. W.-h. Lau, B. V. Lotsch and V. Blum, *Chem. Mater.*, 2017, **29**, 4445–4453.
24 W. Wei and T. Jacob, *Phys. Rev. B: Condens. Matter Mater. Phys.*, 2013, **87**, 085202.
25 J. Sehnert, K. Baerwinkel and J. Senker, *J. Phys. Chem. B*, 2007, **111**, 10671–10680.
26 P. Guiglion, C. Butchosa and M. A. Zwijnenburg, *J. Mater. Chem. A*, 2014, **2**, 11996.
27 P. Guiglion, C. Butchosa and M. A. Zwijnenburg, *Macromol. Chem. Phys.*, 2016, **217**, 344–353.
28 V. W.-h. Lau, M. B. Mesch, V. Duppel, V. Blum, J. Senker and B. V. Lotsch, *J. Am. Chem. Soc.*, 2015, **137**, 1064–1072.
29 V. W.-H. Lau, I. Moudrakovski, T. Botari, S. Weinberger, M. B. Mesch, V. Duppel, J. Senker, V. Blum and B. V. Lotsch, *Nat. Commun.*, 2016, **7**, 12165.
30 V. W.-H. Lau, V. W.-Z. Yu, F. Ehrat, T. Botari, I. Moudrakovski, T. Simon, V. Duppel, E. Medina, J. K. Stolarczyk, J. Feldmann, V. Blum and B. V. Lotsch, *Adv. Energy Mater.*, 2017, **7**, 1602251.
31 D. He, C. Zeng, C. Xu, N. Cheng, H. Li, S. Mu and M. Pan, *Langmuir*, 2011, **27**, 5582–5588.
32 H. Cheng, L. Chen, A. C. Cooper, X. Sha and G. P. Pez, *Energy Environ. Sci.*, 2008, **1**, 338–345.
33 S. Tao, L.-J. Yu, R. Pang, Y.-F. Huang, D.-Y. Wu and Z.-Q. Tian, *J. Phys. Chem. C*, 2013, **117**, 18891–18903.
34 X. Li, G. Hartley, A. J. Ward, P. A. Young, A. F. Masters and T. Maschmeyer, *J. Phys. Chem. C*, 2015, **119**, 14938–14946.
35 B. V. Lotsch, M. Döblinger, J. Sehnert, L. Seyfarth, J. Senker, O. Oeckler and W. Schnick, *Chem. – Eur. J.*, 2007, **13**, 4969–4980.
36 Y. Zhang, J. Liu, G. Wu and W. Chen, *Nanoscale*, 2012, **4**, 5300–5303.
37 G. Zhang, J. Zhang, M. Zhang and X. Wang, *J. Mater. Chem.*, 2012, **22**, 8083–8091.
38 X. Li, S. T. Melissen, T. Le Bahers, P. Sautet, A. F. Masters, S. N. Steinmann and T. Maschmeyer, *Chem. Mater.*, 2018, **30**, 4253–4262.
39 A. Schwarzer, T. Saplinova and E. Kroke, *Coord. Chem. Rev.*, 2013, **257**, 2032–2062.
40 F. Fina, S. K. Callear, G. M. Carins and J. T. S. Irvine, *Chem. Mater.*, 2015, **27**, 2612–2618.
41 J. Yi, W. El-Alami, Y. Song, H. Li, P. M. Ajayan and H. Xu, *Chem. Eng. J.*, 2020, **382**, 122812.
42 Y. Hou, A. B. Laursen, J. Zhang, G. Zhang, Y. Zhu, X. Wang, S. Dahl and I. Chorkendorff, *Angew. Chem., Int. Ed.*, 2013, **52**, 3621–3625.
43 S. Arra, R. Babar and M. Kabir, *Phys. Rev. Mater.*, 2019, **3**, 095402.
44 H. Chung and Y. Diao, *J. Mater. Chem. C*, 2016, **4**, 3915–3933.
45 Y. Abe, V. Savikhin, J. Yin, A. C. Grimsdale, C. Soci, M. F. Toney and Y. M. Lam, *Chem. Mater.*, 2017, **29**, 7686–7696.
46 S. M. Malathy Sony and M. N. Ponnuswamy, *Cryst. Growth Des.*, 2006, **6**, 736–742.
47 L. Seyfarth, J. Seyfarth, B. V. Lotsch, W. Schnick and J. Senker, *Phys. Chem. Chem. Phys.*, 2010, **12**, 2227–2237.
48 S. L. Mayo, B. D. Olafson and W. A. Goddard, *J. Phys. Chem.*, 1990, **94**, 8897–8909.
49 L. Seyfarth and J. Senker, *Phys. Chem. Chem. Phys.*, 2009, **11**, 3522–3531.
50 J. Liu, H. Wang and M. Antonietti, *Chem. Soc. Rev.*, 2016, **45**, 2308–2326.
51 A. D. Becke, *J. Chem. Phys.*, 1993, **98**, 5648–5652.

52 A. D. Becke, *Phys. Rev. A: At., Mol., Opt. Phys.*, 1988, **38**, 3098–3100.
53 C. Lee, W. Yang and R. G. Parr, *Phys. Rev. B: Condens. Matter Mater. Phys.*, 1988, **37**, 785–789.
54 R. Dovesi, R. Orlando, A. Erba, C. M. Zicovich-Wilson, B. Civalleri, S. Casassa, L. Maschio, M. Ferrabone, M. De La Pierre, P. D'Arco, Y. Noël, M. Causà, M. Rérat and B. Kirtman, *Int. J. Quantum Chem.*, 2014, **114**, 1287–1317.
55 R. Dovesi, V. R. Saunders, C. Roetti, R. Orlando, C. M. Zicovich-Wilson, B. Pascale, B. Civalleri, K. Doll, N. M. Harrison, I. J. Bush, P. D'Arco, M. Llunell, M. Causà and Y. Noël, *CRYSTAL14 User's Manual*, University of Torino, 2014.
56 C. Gatti, V. R. Saunders and C. Roetti, *J. Chem. Phys.*, 1994, **101**, 10686–10696.
57 R. Ditchfield, W. J. Hehre and J. A. Pople, *J. Chem. Phys.*, 1971, **54**, 724–728.
58 M. F. Peintinger, D. V. Oliveira and T. Bredow, *J. Comput. Chem.*, 2013, **34**, 451–459.
59 I. Pelant and J. Valenta, *Luminescence Spectroscopy of Semiconductors*, Oxford University Press, Oxford U.K., 2012.
60 T. Le Bahers, M. Rérat and P. Sautet, *J. Phys. Chem. C*, 2014, **118**, 5997–6008.
61 S. Melissen, F. Labat, P. Sautet and T. Le Bahers, *Phys. Chem. Chem. Phys.*, 2015, **17**, 2199–2209.
62 S. Petit, S. T. A. G. Melissen, L. Duclaux, M. T. Sougrati, T. Le Bahers, P. Sautet, D. Dambournet, O. J. Borkiewicz, C. Laberty-Robert and O. Durupthy, *J. Phys. Chem. C*, 2016, **120**, 24521–24532.
63 T. A. Kandiel, D. H. Anjum, P. Sautet, T. Le Bahers and K. Takanabe, *J. Mater. Chem. A*, 2015, **3**, 8896–8904.
64 T. Le Bahers, S. Haller, T. L. Mercier and P. Barboux, *J. Phys. Chem. C*, 2015, **119**, 17585–17595.
65 A. BaQais, A. Curutchet, A. Ziani, H. Ait Ahsaine, P. Sautet, K. Takanabe and T. Le Bahers, *Chem. Mater.*, 2017, **29**, 8679–8689.
66 A. Ziani, C. Le Paven, L. Le Gendre, F. Marlec, R. Benzerga, F. Tessier, F. Cheviré, M. N. Hedhili, A. T. Garcia-Esparza, S. Melissen, P. Sautet, T. Le Bahers and K. Takanabe, *Chem. Mater.*, 2017, **29**, 3989–3998.
67 B. Civalleri, C. M. Zicovich-Wilson, L. Valenzano and P. Ugliengo, *CrystEngComm*, 2008, **10**, 405–410.
68 D. Presti, A. Pedone, I. Ciofini, F. Labat, M. C. Menziani and C. Adamo, *Theor. Chem. Acc.*, 2016, **135**, 1–11.
69 S. Grimme, *J. Comput. Chem.*, 2006, **27**, 1787–1799.
70 1 Hartree or "Atomic Unit" $\hat{=}$ 27.211 eV $=\hat{}$ 2625.5 kJ mol^{-1}. 1 atm $\triangleq$ 1.01325 Pa.
71 G. Kresse and D. Joubert, *Phys. Rev. B: Condens. Matter Mater. Phys.*, 1999, **59**, 1758–1775.
72 G. Kresse and J. Hafner, *Phys. Rev. B: Condens. Matter Mater. Phys.*, 1993, **47**, 558–561.
73 G. Kresse and J. Hafner, *Phys. Rev. B: Condens. Matter Mater. Phys.*, 1994, **49**, 14251–14269.
74 G. Kresse and J. Furthmüller, *Comput. Mater. Sci.*, 1996, **6**, 15–50.
75 G. Kresse and J. Furthmüller, *Phys. Rev. B: Condens. Matter Mater. Phys.*, 1996, **54**, 11169–11186.
76 S. F. Boys and F. de Bernardi, *Mol. Phys.*, 1970, **19**, 553–566.
77 P. Jurečka, J. Černý, P. Hobza and D. R. Salahub, *J. Comput. Chem.*, 2007, **28**, 555–569.
78 S. N. Steinmann and C. Corminboeuf, *J. Chem. Theory Comput.*, 2011, **7**, 3567–3577.
79 S. Grimme, S. Ehrlich and L. Goerigk, *J. Comput. Chem.*, 2011, **32**, 1456–1465.
80 J. P. Perdew, K. Burke and M. Ernzerhof, *Phys. Rev. Lett.*, 1996, **77**, 3865–3868.
81 J. P. Perdew, K. Burke and M. Ernzerhof, *Phys. Rev. Lett.*, 1997, **78**, 1396.
82 A. Tkatchenko, R. A. DiStasio, R. Car and M. Scheffler, *Phys. Rev. Lett.*, 2012, **108**, 236402.
83 A. Ambrosetti, A. M. Reilly, R. A. DiStasio and A. Tkatchenko, *J. Chem. Phys.*, 2014, **140**, 18A508.
84 T. Bučko, S. Lebègue, T. Gould and J. G. Ángyán, *J. Phys.: Condens. Matter*, 2016, **28**, 045201.
85 H. J. Monkhorst and J. D. Pack, *Phys. Rev. B: Solid State*, 1976, **13**, 5188–5192.
86 J. Paier, M. Marsman, K. Hummer, G. Kresse, I. C. Gerber and J. G. Ángyán, *J. Chem. Phys.*, 2006, **124**, 154709.
87 H. T. Stokes and D. M. Hatch, *J. Appl. Crystallogr.*, 2005, **38**, 237–238.
88 L. Glasser, *J. Chem. Educ.*, 2011, **88**, 581–585.
89 S. Gautier, S. N. Steinmann, C. Michel, P. Fleurat-Lessard and P. Sautet, *Phys. Chem. Chem. Phys.*, 2015, **17**, 28921–28930.
90 J. G. Brandenburg and S. Grimme, *Acta Crystallogr., Sect. B: Struct. Sci., Cryst. Eng. Mater.*, 2016, **72**, 502–513.
91 N. Marom, R. A. DiStasio, V. Atalla, S. Levchenko, A. M. Reilly, J. R. Chelikowsky, L. Leiserowitz and A. Tkatchenko, *Angew. Chem., Int. Ed.*, 2013, **52**, 6629–6632.
92 L. Kronik and A. Tkatchenko, *Acc. Chem. Res.*, 2014, **47**, 3208–3216.
93 J.-L. Bredas, *Mater. Horiz.*, 2014, **1**, 17–19.
94 G. J. O. Beran, *Chem. Rev.*, 2016, **116**, 5567–5613.
95 B. Wang, M.-L. Bocquet, S. Marchini, S. Günther and J. Wintterlin, *Phys. Chem. Chem. Phys.*, 2008, **10**, 3530–3534.
96 E. E. Jelley, *Nature*, 1936, **138**, 1009–1010.
97 E. E. Jelley, *Nature*, 1937, **139**, 631–632.
98 Y.-Y. Liao, S. T. Melissen, J. Audibert, T. Vu, G. Clavier, R. Méallet-Renault, P. Retailleau, J. Lemaistre, V. Génot and R. Pansu, *ChemPhotoChem*, 2017, **2**, 72–80.
99 F. C. Spano and C. Silva, *Annu. Rev. Phys. Chem.*, 2014, **65**, 477–500.
100 W. J. Harrison, D. L. Mateer and G. J. T. Tiddy, *J. Phys. Chem.*, 1996, **100**, 2310–2321.

Supporting information for: What Does Graphitic Carbon Nitride Really Look Like?

Sigismund T.A.G. Melissen,[†] Tangui Le Bahers,[‡] Philippe Sautet,[¶,§] and Stephan N. Steinmann[*,‖]

[†] *Université de Lyon, Université Claude Bernard Lyon 1, CNRS, Institut Lumière Matière, F-69622 Lyon, France*

[‡] *Université de Lyon, Université Claude Bernard Lyon 1, Ecole Normale Supérieure de Lyon, CNRS, 46 allée d'Italie, F-69007 Lyon Cedex*

[¶] *Department of Chemical and Biomolecular engineering University of California, Los Angeles, Los Angeles, CA 90095, USA*

[§] *Department of Chemistry and Biochemistry University of California, Los Angeles, Los Angeles, CA 90095, USA*

[‖] *Univ Lyon, Ecole Normale SupÃlrieure de Lyon, CNRS UniversitÃl Lyon 1, Laboratoire de Chimie UMR 5182, 46 allÃle d'Italie, F-69364, LYON, France*

E-mail: stephan.steinmann@ens-lyon.fr

Contents

1 Additional Tables

Table S1: Relative energies (in kJ/mol per tecton) and the contribution of the dispersion corrections (in parenthesis). Note: (a) The thermal correction which needs to be added to ΔE in order to obtain the Gibbs free energy ΔG.

Species	ΔE_{therm} [a]	$\Delta E_{B3LYP\text{-}D3}$	$\Delta E_{B3LYP\text{-}dDsC}$	$\Delta E_{PBE\text{-}dDsC}$	$\Delta E_{PBE\text{-}MBD}$
1D	–4.2	+91 (+30)	+97 (+35)	+92 (+21)	+94 (+23)
2D	0	0	0	0	0
Fina	5.3	–92 (–112)	–96 (–116)	–81 (–90)	–68 (–77)
S1	5.3	–91 (–108)	–87 (–104)	–75 (–84)	–63 (–81)
Lotsch	4.9	–93 (–113)	–88 (–108)	–77 (–88)	–66 (–77)
S2	5.4	–94 (-112)	–95 (–114)	–79 (–89)	–65 (–85)

Table S2: Geometrical parameters of the investigated systems at the B3LYP-D* and PBE-dDsC level of theory and experiment. Lattice vectors are given in Å and angles in degrees.

Species	a/Å	b/Å	c/Å	α/°	β/°	γ/°
exp						
Fina	12.4	6.49	16.4	90.0	90.0	90.0
S1	16.4	12.4	3.3	90.0	98	90.0
Lotsch	12.4	16.7	3.31	90.0	92-115	90.0
S2	3.95	10.87	16.26	98.5	90.1	96.4
B3LYP-D*						
Fina	12.73	6.43	16.71	90.0	90.0	90.0
S1	16.76	12.73	4.73	90.0	43.2	90.0
Lotsch	12.71	16.74	4.69	90.0	136.7	90.0
S2	4.84	8.68	16.71	99.1	97.8	92.7
PBE-dDsC						
Fina	12.70	6.24	16.58	90.0	90.0	90.0
S1	16.66	12.71	4.66	90.0	42.7	90.0
Lotsch	12.67	16.61	4.61	90.0	137.4	90.0
S2	4.68	8.81	16.37	101.3	95.3	91.7

2 Coordinates

Here, the optimized structures are provided. In the first section, all structures are provided in POSCAR (VASP) format. In the second section, all structures are provided in .gui (Crystal14) format. In the last section, all structures are provided in .cif (Crystallographic) format.

2.1 Structures in POSCAR format

Fina, POSCAR format

```
Melon_3D_FINA_POSCAR_631Gdp_with_special
1.00000000000000
12.7337335436999997   0.0000000000000008    0.0025483719854600
-0.0000000000000000   6.4285279450299999    0.0000000000000000
 0.0033250456111200   0.0000000000000010   16.7106790624000006
   N    C    H
    72    48    24
Direct
  0.3690540828846025  0.2500000000000000  0.4907495353746967
  0.6309459171153975  0.7500000000000000  0.5092504646253033
  0.0170039441125525  0.2500000000000000  0.9918338676944174
  0.9829960558874475  0.7500000000000000  0.0081661323055826
  0.5168993495115970  0.2500000000000000  0.3224843272087980
  0.4831006504884030  0.7500000000000000  0.6775156727912020
  0.8689361955866985  0.2500000000000000  0.8217429136820016
  0.1310638044133015  0.7500000000000000  0.1782570863179984
  0.2243423519294012  0.2500000000000000  0.4058789566350001
  0.7756576480705988  0.7500000000000000  0.5941210433649999
  0.1614787772612019  0.2500000000000000  0.9067061504098319
  0.8385212227387981  0.7500000000000000  0.0932938495901681
  0.6608003439418013  0.2500000000000000  0.4077422823618022
  0.3391996560581987  0.7500000000000000  0.5922577176381978
  0.7244246562651000  0.2500000000000000  0.9065707542442780
  0.2755753437349000  0.7500000000000000  0.0934292457557220
  0.0496789837800833  0.2500000000000000  0.4635891134452024
  0.9503210162199167  0.7500000000000000  0.5364108865547976
  0.3358404614429986  0.2500000000000000  0.9639601650392891
  0.6641595385570014  0.7500000000000000  0.0360398349607109
  0.8354328502672033  0.2500000000000000  0.3507211565733996
  0.1645671497327967  0.7500000000000000  0.6492788434266004
  0.5496970864464998  0.2500000000000000  0.8489899102389984
  0.4503029135535002  0.7500000000000000  0.1510100897610016
  0.1987033039728985  0.2500000000000000  0.5458550393622019
  0.8012966960271015  0.7500000000000000  0.4541449606377981
  0.1871186745931013  0.2500000000000000  0.0466400906381566
  0.8128813254068987  0.7500000000000000  0.9533599093618434
  0.6870605609897993  0.2500000000000000  0.2676800842223983
  0.3129394390102007  0.7500000000000000  0.7323199157776017
  0.6988307754380969  0.2500000000000000  0.7665507164274032
  0.3011692245619031  0.7500000000000000  0.2334492835725968
  0.1762371383166013  0.2500000000000000  0.6859178991377988
  0.8237628616833987  0.7500000000000000  0.3140821008622012
  0.2102888015383968  0.2500000000000000  0.1865233227046019
  0.7897111984616032  0.7500000000000000  0.8134766772953981
  0.7106051714981021  0.2500000000000000  0.1277599310287982
  0.2893948285018979  0.7500000000000000  0.8722400689712018
  0.6760355336410981  0.2500000000000000  0.6266395038658032
  0.3239644663589019  0.7500000000000000  0.3733604961341968
  0.0743332937354708  0.2500000000000000  0.3289332304337975
  0.9256667062645292  0.7500000000000000  0.6710667695662025
  0.3110827003647003  0.2500000000000000  0.8291406344198009
  0.6889172996352997  0.7500000000000000  0.1708593655801991
  0.8101643785280999  0.2500000000000000  0.4855258376714033
  0.1898356214719001  0.7500000000000000  0.5144741623285967
  0.5744158556016998  0.2500000000000000  0.9837163599122221
  0.4255841443983002  0.7500000000000000  0.0162836400877779
  0.0103294876729407  0.2500000000000000  0.7388044746825031
  0.9896705123270593  0.7500000000000000  0.2611955253174969
  0.3757770448408024  0.2500000000000000  0.2394329202254966
```

0.6242229551591976	0.7500000000000000	0.7605670797745034
0.8760090931773021	0.2500000000000000	0.0751171812690714
0.1239909068226979	0.7500000000000000	0.9248828187309286
0.5104222140202026	0.2500000000000000	0.5737213389762985
0.4895777859797974	0.7500000000000000	0.4262786610237015
0.0270540615395518	0.2500000000000000	0.5996221351292021
0.9729459384604482	0.7500000000000000	0.4003778648707979
0.3591429575972001	0.2500000000000000	0.0999302010486289
0.6408570424027999	0.7500000000000000	0.9000697989513711
0.8590376602712979	0.2500000000000000	0.2147305126332029
0.1409623397287021	0.7500000000000000	0.7852694873667971
0.5270523993644005	0.2500000000000000	0.7130808913466993
0.4729476006355995	0.7500000000000000	0.2869191086533007
0.3433991885645966	0.2500000000000000	0.6330907351042967
0.6566008114354034	0.7500000000000000	0.3669092648957033
0.0427810053921220	0.2500000000000000	0.1341493345375966
0.9572189946078780	0.7500000000000000	0.8658506654624034
0.5428463255084992	0.2500000000000000	0.1802213717970034
0.4571536744915008	0.7500000000000000	0.8197786282029966
0.8435111342354986	0.2500000000000000	0.6793816010246019
0.1564888657645014	0.7500000000000000	0.3206183989753981
0.2402478171560034	0.2500000000000000	0.6227552009833985
0.7597521828439966	0.7500000000000000	0.3772447990166015
0.1454882810805032	0.2500000000000000	0.1236107882311970
0.8545117189194968	0.7500000000000000	0.8763892117688030
0.6458111797522008	0.2500000000000000	0.1904973855260010
0.3541888202477992	0.7500000000000000	0.8095026144739990
0.7404860494189975	0.2500000000000000	0.6894171364728976
0.2595139505810025	0.7500000000000000	0.3105828635271024
0.4022970108994031	0.2500000000000000	0.5666300106820970
0.5977029891005969	0.7500000000000000	0.4333699893179030
0.9841644807218728	0.2500000000000000	0.0680419981326068
0.0158355192781272	0.7500000000000000	0.9319580018673932
0.4844725576773996	0.2500000000000000	0.2463723953125978
0.5155274423226004	0.7500000000000000	0.7536276046874022
0.9023272200737225	0.2500000000000000	0.7455578213656011
0.0976727799262775	0.7500000000000000	0.2544421786343989
0.1174338988571009	0.2500000000000000	0.4006218278071998
0.8825661011428991	0.7500000000000000	0.5993781721928002
0.2680511481369976	0.2500000000000000	0.9011741535673679
0.7319488518630024	0.7500000000000000	0.0988258464326321
0.7673443253991010	0.2500000000000000	0.4133781478569034
0.2326556746008990	0.7500000000000000	0.5866218521430966
0.6171284787057019	0.2500000000000000	0.9121256107274220
0.3828715212942981	0.7500000000000000	0.0878743892725780
0.2656301785464024	0.2500000000000000	0.4784709522108983
0.7343698214535976	0.7500000000000000	0.5215290477891017
0.1201944202890033	0.2500000000000000	0.9795612646602407
0.8798055797109967	0.7500000000000000	0.0204387353397593
0.6199083048107994	0.2500000000000000	0.3347308046560968
0.3800916951892006	0.7500000000000000	0.6652691953439032
0.7657864170676021	0.2500000000000000	0.8336580094033010
0.2342135829323979	0.7500000000000000	0.1663419905966990
0.0897377125690966	0.2500000000000000	0.5356724213594006
0.9102622874309034	0.7500000000000000	0.4643275786405994
0.2960128922282976	0.2500000000000000	0.0360901895089185
0.7039871077717024	0.7500000000000000	0.9639098104910815
0.7957445846765978	0.2500000000000000	0.2781504432525992
0.2042554153234022	0.7500000000000000	0.7218495567474008
0.5898014035611965	0.2500000000000000	0.7768858584077023
0.4101985964388035	0.7500000000000000	0.2231141415922977
0.0717660538316878	0.2500000000000000	0.6708745088755990
0.9282339461683122	0.7500000000000000	0.3291254911244010
0.3142320066841009	0.2500000000000000	0.1711636866692032
0.6857679933158991	0.7500000000000000	0.8288363133307968
0.8143866789339000	0.2500000000000000	0.1431712246892971
0.1856133210661000	0.7500000000000000	0.8568287753107029
0.5719294131751980	0.2500000000000000	0.6414296551670020
0.4280705868248020	0.7500000000000000	0.3585703448329980
0.1201106798921998	0.2500000000000000	0.2788571689037980
0.8798893201078002	0.7500000000000000	0.7211428310962020
0.2648094836766006	0.2500000000000000	0.7790665483990011
0.7351905163233994	0.7500000000000000	0.2209334516009989
0.7636183051596035	0.2500000000000000	0.5356562831151024
0.2363816948403965	0.7500000000000000	0.4643437168848976
0.6198610865650025	0.2500000000000000	0.0340192580028571
0.3801389134349975	0.7500000000000000	0.9659807419971429
0.9945527037838104	0.2500000000000000	0.3251423303947973
0.0054472962161896	0.7500000000000000	0.6748576696052027
0.3912014323675024	0.2500000000000000	0.8257782952452004
0.6087985676324976	0.7500000000000000	0.1742217047547996
0.8902236008812991	0.2500000000000000	0.4896498308878989
0.1097763991187009	0.7500000000000000	0.5103501691121011
0.4944992778356010	0.2500000000000000	0.9875904382336813
0.5055007221643990	0.7500000000000000	0.0124095617663187
0.0494532054029193	0.2500000000000000	0.7922222790575972
0.9505467945970807	0.7500000000000000	0.2077777209424028

```
  0.3362528381559997  0.2500000000000000  0.2929302690465008
  0.6637471618440003  0.7500000000000000  0.7070697309534992
  0.8363370381118003  0.2500000000000000  0.0219080205323010
  0.1636629618881997  0.7500000000000000  0.9780919794676990
  0.5499793706286979  0.2500000000000000  0.5204320051558966
  0.4500206293713021  0.7500000000000000  0.4795679948441034
```

$P2_1/a$ POSCAR format

```
hi
   1.00000000000000
    12.6971164520999995    0.0000000000000007   -0.4970005017450000
    -0.0000000000000001   16.7404692558000008   -0.0000000000000000
    -3.2993394650700001    0.0000000000000003    3.3469337249200000
   N    C    H
    36    24    12
Direct
  0.4342392685459018  0.4155848451634014  0.0193855121180704
  0.0657607314540982  0.9155848451634228  0.9806144878819296
  0.5657607314540982  0.5844151548365986  0.9806144878819296
  0.9342392685459018  0.0844151548365772  0.0193855121180704
  0.2859499088769013  0.5002704244394991  0.0080714632251500
  0.2140500911230987  0.0002704244395346  0.9919285367748572
  0.7140500911230987  0.4997295755605009  0.9919285367748500
  0.7859499088769013  0.9997295755604654  0.0080714632251428
  0.1161216668538003  0.4426487406227011  0.0270435816544179
  0.3838783331461997  0.9426487406227011  0.9729564183455892
  0.8838783331461997  0.5573512593772989  0.9729564183455821
  0.6161216668538003  0.0573512593772989  0.0270435816544108
  0.2654124323132976  0.3606561678314009  0.0264752135597632
  0.2345875676867024  0.8606561678314009  0.9735247864402368
  0.7345875676867024  0.6393438321685991  0.9735247864402368
  0.7654124323132976  0.1393438321685991  0.0264752135597632
  0.2453849208707979  0.2209326236124980  0.0346389691824669
  0.2546150791292021  0.7209326236124980  0.9653610308175331
  0.7546150791292021  0.7790673763875020  0.9653610308175331
  0.7453849208707979  0.2790673763875020  0.0346389691824669
  0.1345111352583999  0.5769800808649990  0.0054929971208608
  0.3654888647416001  0.0769800808650132  0.9945070028791392
  0.8654888647416001  0.4230199191350010  0.9945070028791392
  0.6345111352583999  0.9230199191349868  0.0054929971208608
  0.0806654624185299  0.1674469884301999  0.0370290722379067
  0.4193345375814985  0.6674469884301999  0.9629709277620933
  0.9193345375814701  0.8325530115698001  0.9629709277620933
  0.5806654624185015  0.3325530115698001  0.0370290722379067
  0.0999274964283501  0.3068114285205965  0.0498105223104872
  0.4000725035716997  0.8068114285205965  0.9501894776895128
  0.9000725035716499  0.6931885714794035  0.9501894776895128
  0.5999274964283003  0.1931885714794035  0.0498105223104872
  0.4153450381691997  0.2736476162114982  0.0444561019038474
  0.0846549618308430  0.7736476162114982  0.9555438980961526
  0.5846549618308003  0.7263523837885018  0.9555438980961526
  0.9153450381691570  0.2263523837885018  0.0444561019038474
  0.3092196880579010  0.2838325171538969  0.0340528675486382
  0.1907803119420990  0.7838325171538969  0.9659471324513618
  0.6907803119420990  0.7161674828461031  0.9659471324513618
  0.8092196880579010  0.2161674828461031  0.0340528675486382
  0.4718952823813964  0.3399405489905973  0.0367102089646778
  0.0281047176186178  0.8399405489905973  0.9632897910353222
  0.5281047176186036  0.6600594510094027  0.9632897910353222
  0.9718952823813822  0.1600594510094027  0.0367102089646778
  0.1806699162910022  0.5055198182448990  0.0145943880716572
  0.3193300837089978  0.0055198182448564  0.9854056119283428
  0.8193300837089978  0.4944801817551010  0.9854056119283428
  0.6806699162910022  0.9944801817551436  0.0145943880716572
  0.3300737541843972  0.4280050695317001  0.0182335597250898
  0.1699262458156028  0.9280050695317286  0.9817664402749102
  0.6699262458156028  0.5719949304682999  0.9817664402749102
  0.8300737541843972  0.0719949304682714  0.0182335597250898
  0.1578741043903023  0.3707376295959008  0.0320165202630065
  0.3421258956096977  0.8707376295959008  0.9679834797369935
  0.8421258956096977  0.6292623704040992  0.9679834797369935
  0.6578741043903023  0.1292623704040992  0.0320165202630065
  0.1430818640805995  0.2356539841409031  0.0418250110284291
  0.3569181359194005  0.7356539841409031  0.9581749889715709
  0.8569181359194005  0.7643460158590969  0.9581749889715709
  0.6430818640805995  0.2643460158590969  0.0418250110284291
  0.1757443426118996  0.6272651393136996  0.9894579049193908
  0.3242556573881004  0.1272651393136996  0.0105420950806092
  0.8242556573881004  0.3727348606863004  0.0105420950806092
  0.6757443426118996  0.8727348606863004  0.9894579049193908
  0.0558904777603075  0.5803189789875987  0.0111080083687796
```

```
  0.4441095222396996  0.0803189789876484  0.9888919916312204
  0.9441095222396925  0.4196810210124013  0.9888919916312204
  0.5558904777603004  0.9196810210123516  0.0111080083687796
  0.1222385815684035  0.1142480384961004  0.0430643634022729
  0.3777614184315965  0.6142480384961004  0.9569356365977271
  0.8777614184315965  0.8857519615038996  0.9569356365977271
  0.6222385815684035  0.3857519615038996  0.0430643634022729
```

S1, POSCAR format

```
  Hi
   1.000000000000000
    16.7560758569000008    0.0000000000000010    0.3889506231090000
     0.0000000000000000   12.7367938635000009    0.0000000000000000
     3.3786711390900002    0.0000000000000003    3.3214704421399999
   N    C    H
    36    24    12
Direct
  0.4182844750068995  0.4267125351003003  0.9807475408473820
  0.0817155249931218  0.9267125351002719  0.0192524591526180
  0.5817155249931005  0.5732874648996997  0.0192524591526180
  0.9182844750068782  0.0732874648997281  0.9807475408473820
  0.4994032602001965  0.2830474918384027  0.0019877438788782
  0.0005967397998390  0.7830474918384027  0.9980122561211218
  0.5005967397998035  0.7169525081615973  0.9980122561211147
  0.9994032602001610  0.2169525081615973  0.0019877438788782
  0.4373546274160987  0.1081381254264002  0.0285559087941394
  0.0626453725839013  0.6081381254264002  0.9714440912058606
  0.5626453725839013  0.8918618745735998  0.9714440912058606
  0.9373546274160987  0.3918618745735998  0.0285559087941394
  0.3602366514384983  0.2563211747015970  0.0004846562533345
  0.1397633485615017  0.7563211747015970  0.9995153437466726
  0.6397633485615017  0.7436788252984030  0.9995153437466726
  0.8602366514384983  0.2436788252984030  0.0004846562533274
  0.2250919648111989  0.2323685072667985  0.9801781021910188
  0.2749080351888011  0.7323685072667985  0.0198218978089812
  0.7749080351888011  0.7676314927332015  0.0198218978089812
  0.7250919648111989  0.2676314927332015  0.9801781021910188
  0.5746459039051004  0.1338506925651970  0.0136364323913227
  0.9253540960949209  0.6338506925651970  0.9863635676086773
  0.4253540960948996  0.8661493074348030  0.9863635676086773
  0.0746459039050791  0.3661493074348030  0.0136364323913227
  0.1658875851692017  0.0671957391464773  0.0144081619721277
  0.3341124148307983  0.5671957391464986  0.9855918380278723
  0.8341124148307983  0.9328042608535227  0.9855918380278723
  0.6658875851692017  0.4328042608535014  0.0144081619721277
  0.2993310188353036  0.0844841725859808  0.0406297093320802
  0.2006689811646964  0.5844841725860022  0.9593702906679198
  0.7006689811646964  0.9155158274140192  0.9593702906679198
  0.7993310188353036  0.4155158274139978  0.0406297093320802
  0.2772945602997012  0.4001118637130006  0.9770854508954088
  0.2227054397002988  0.9001118637130006  0.0229145491045912
  0.7227054397002988  0.5998881362869994  0.0229145491045912
  0.7772945602997012  0.0998881362869994  0.9770854508954088
  0.2862888236404970  0.2974134118135012  0.9861806082765483
  0.2137111763595030  0.7974134118135012  0.0138193917234517
  0.7137111763595030  0.7025865881864988  0.0138193917234517
  0.7862888236404970  0.2025865881864988  0.9861806082765483
  0.3423998540773994  0.4592016468467008  0.9801661753024220
  0.1576001459226006  0.9592016468466582  0.0198338246975780
  0.6576001459226006  0.5407983531532992  0.0198338246975780
  0.8423998540773994  0.0407983531533418  0.9801661753024220
  0.5031124963715996  0.1763114355693034  0.0114818780667605
  0.9968875036284359  0.6763114355693034  0.9885181219332395
  0.4968875036284004  0.8236885644306966  0.9885181219332395
  0.0031124963715641  0.3236885644306966  0.0114818780667605
  0.4281283809837007  0.3238540811411994  0.9941608191700482
  0.0718716190163278  0.8238540811411994  0.0058391808299518
  0.5718716190162993  0.6761459188588006  0.0058391808299589
  0.9281283809836722  0.1761459188588006  0.9941608191700482
  0.3663535262462005  0.1475923778239974  0.0225111723702298
  0.1336464737537995  0.6475923778239974  0.9774888276297702
  0.6336464737537995  0.8524076221760026  0.9774888276297702
  0.8663535262462005  0.3524076221760026  0.0225111723702298
  0.2336465840079995  0.1285466362091015  0.0134518729248825
  0.2663534159920005  0.6285466362091015  0.9865481270751175
  0.7663534159920005  0.8714533637908985  0.9865481270751175
  0.7336465840079995  0.3714533637908985  0.0134518729248825
  0.6272506581366031  0.1797448095452978  0.0009505595977544
  0.8727493418633969  0.6797448095452978  0.9990494404022456
  0.3727493418633969  0.8202551904547022  0.9990494404022456
  0.1272506581366031  0.3202551904547022  0.0009505595977544
```

```
  0.5791588743391003  0.0539661805157579  0.0118582640761176
  0.9208411256608784  0.5539661805158005  0.9881417359238824
  0.4208411256608997  0.9460338194842421  0.9881417359238824
  0.0791588743391216  0.4460338194841995  0.0118582640761176
  0.1151464850046011  0.1061299086168006  0.0021299523181852
  0.3848535149953989  0.6061299086168006  0.9978700476818148
  0.8848535149953989  0.8938700913831994  0.9978700476818148
  0.6151464850046011  0.3938700913831994  0.0021299523181852
```

S2, POSCAR format

```
Hi
   1.00000000000000
     4.7247995723700003   -0.3300690995270000   -0.1707838361170000
     0.1209360489830000    8.9798520228500003   -0.3397386322170000
    -1.1417356344400000   -2.4690329267000002   16.2825099185000006
   N    C    H
    36    24    12
Direct
  0.2767855142498021  0.4271092770874034  0.4152831334688969
  0.7232144857501979  0.5728907229125966  0.5847168665311031
  0.0551679054991325  0.0722316688895717  0.9166126195967976
  0.9448320945008675  0.9277683311104283  0.0833873804032024
  0.0651033591076100  0.2839976800600965  0.4999810231419985
  0.9348966408923900  0.7160023199399035  0.5000189768580015
  0.4291884346889034  0.2184110787980984  0.0009167036030817
  0.5708115653110966  0.7815889212019016  0.9990832963969183
  0.6519498023908028  0.1129336684446969  0.4423400931465977
  0.3480501976091972  0.8870663315553031  0.5576599068534023
  0.7268020918212983  0.3895226466142034  0.9421526009903189
  0.2731979081787017  0.6104773533857966  0.0578473990096811
  0.8739303177371980  0.2608508117448025  0.3606133943586016
  0.1260696822628020  0.7391491882551975  0.6393866056413984
  0.3416914843670966  0.2422509862077007  0.8608180800278973
  0.6583085156329034  0.7577490137922993  0.1391819199721027
  0.6968237841207028  0.2356346820689978  0.2200992442685035
  0.3031762158792972  0.7643653179310022  0.7799007557314965
  0.2494215865346021  0.2615206739040019  0.7205408251298024
  0.7505784134653979  0.7384793260959981  0.2794591748701976
  0.8391798713037986  0.1322010659499000  0.5760140167904026
  0.1608201286962014  0.8677989340501000  0.4239859832095974
  0.8108423538867982  0.3669227008963034  0.0769749815879806
  0.1891576461132018  0.6330772991036966  0.9230250184120194
  0.3077826668572001  0.0726910853789988  0.1665253299488967
  0.6922173331427999  0.9273089146210012  0.8334746700511033
  0.5241907714138989  0.4289775567059024  0.6672255410745009
  0.4758092285861011  0.5710224432940976  0.3327744589254991
  0.4658758533973000  0.0959511649821181  0.3073310141675023
  0.5341241466027000  0.9040488350178819  0.6926689858324977
  0.6342438391716030  0.4119924217963984  0.8062791189331975
  0.3657561608283970  0.5880075782036016  0.1937208810668025
  0.0806324484922172  0.4050642477386006  0.2738187466400035
  0.9193675515077828  0.5949357522613994  0.7261812533599965
  0.9711200519970831  0.0920272956109400  0.7735187925451967
  0.0288799480029169  0.9079727043890600  0.2264812074548033
  0.8844967202671015  0.3013327627128035  0.2836613560063981
  0.1155032797328985  0.6986672372871965  0.7163386439936019
  0.1842121558765015  0.1981717778404999  0.7836310933890971
  0.8157878441234985  0.8018282221595001  0.2163689066109029
  0.2646072521262965  0.4630908215769978  0.3400561565535014
  0.7353927478737035  0.5369091784230022  0.6599438434464986
  0.9179050727622808  0.0355781493912204  0.8404170847412971
  0.0820949272377192  0.9644218506087796  0.1595829152587029
  0.8540167071381006  0.1778578067325967  0.5050124407566017
  0.1459832928618994  0.8221421932674033  0.4949875592433983
  0.6519597447441967  0.3232064790323008  0.0055942078015079
  0.3480402552558033  0.6767935209676992  0.9944057921984921
  0.0768312876742101  0.3256122151711978  0.4276896984808971
  0.9231687123257899  0.6743877848288022  0.5723103015191029
  0.2743592826981001  0.1763085908928019  0.9286188837194231
  0.7256407173018999  0.8236914091071981  0.0713811162805769
  0.6613567447967981  0.1543529744099033  0.3708135111342017
  0.3386432552032019  0.8456470255900967  0.6291864888657983
  0.5710546554471989  0.3505814872503024  0.8704294004433990
  0.4289453445528011  0.6494185127496976  0.1295705995566010
  0.4947198956496024  0.1359684136405974  0.2352231321087999
  0.5052801043503976  0.8640315863594026  0.7647768678912001
  0.4718625876494968  0.3666295417890026  0.7352762888506987
  0.5281374123505032  0.6333704582109974  0.2647237111493013
  0.9851787673907921  0.1744191025337969  0.6258687545632995
  0.0148212326092079  0.8255808974662031  0.3741312454367005
  0.7723000981129005  0.3191490157695966  0.1268422102323967
```

```
  0.2276999018870995  0.6808509842304034  0.8731577897676033
  0.6802065089045968  0.0526987166018031  0.5791215303831976
  0.3197934910954032  0.9473012833981969  0.4208784696168024
  0.9832656155695005  0.4412694021708035  0.0794645320051117
  0.0167343844304995  0.5587305978291965  0.9205354679948883
  0.3324734676979020  0.1136011313950007  0.1133874480904993
  0.6675265323020980  0.8863988686049993  0.8866125519095007
  0.3966941115813967  0.3853407757070997  0.6134360669896992
  0.6033058884186033  0.6146592242929003  0.3865639330103008
```

2D, POSCAR format

```
Melon_2D_POSCAR_20A_BOX_631Gdp_with_spec
   1.00000000000000
    12.7325024485000000    0.0000000000000008    0.000
    -0.0000000000000000   16.7956456289000009    0.000
     0.0000000000000000    0.0000000000000000   20.000
   N    C    H
    36    24    12
Direct
  0.4277944259999984  0.4148490720000026  0.9999139648871989
  0.9277944255999984  0.0851509284999992  0.0000860351128011
  0.5722055740000016  0.5851509279999974  0.0000860351128011
  0.0722055744000016  0.9148490715000008  0.9999139648871989
  0.2830928970000031  0.4993404729999966  0.9998638540520020
  0.7830928970000031  0.0006595274180015  0.0001361459479980
  0.7169071029999969  0.5006595270000034  0.0001361459479980
  0.2169071029999969  0.9993404725840023  0.9998638540520020
  0.1083179920000035  0.4420461340000017  0.9998881472190035
  0.6083179920000035  0.0579538662999965  0.0001118527809965
  0.8916820079999965  0.5579538659999983  0.0001118527809965
  0.3916820079999965  0.9420461337000035  0.9998881472190035
  0.2574031739999967  0.3599714079999998  0.9998954550190007
  0.7574031739999967  0.1400285920000002  0.0001045449809993
  0.7425968260000033  0.6400285920000002  0.0001045449809993
  0.2425968260000033  0.8599714079999998  0.9998954550190007
  0.2348598040000027  0.2205929049999966  0.9999255585049980
  0.7348598040000027  0.2794070950000034  0.0000744414950020
  0.7651401959999973  0.7794070950000034  0.0000744414950020
  0.2651401959999973  0.7205929049999966  0.9999255585049980
  0.1331077780000030  0.5761186300000034  0.9998116310559979
  0.6331077780000030  0.9238813699000019  0.0001883689440021
  0.8668922219999970  0.4238813699999966  0.0001883689440021
  0.3668922219999970  0.0761186300999981  0.9998116310559979
  0.0692568282999986  0.1677587100000011  0.9999971001389270
  0.5692568280000003  0.3322412899999989  0.0000028998610730
  0.9307431717000014  0.8322412899999989  0.0000028998610730
  0.4307431719999997  0.6677587100000011  0.9999971001389270
  0.0856430814000007  0.3065224099999995  0.9999508521096985
  0.5856430810000006  0.1934775900000005  0.0000491478903015
  0.9143569185999993  0.6934775900000005  0.0000491478903015
  0.4143569189999994  0.8065224099999995  0.9999508521096985
  0.4022794270000034  0.2732128219999979  0.9999047065106978
  0.9022794270999981  0.2267871780000021  0.0000952934893022
  0.5977205729999966  0.7267871780000021  0.0000952934893022
  0.0977205729000019  0.7732128219999979  0.9999047065106978
  0.2992003960000034  0.2832064669999994  0.9999132048519002
  0.7992003960000034  0.2167935330000006  0.0000867951480998
  0.7007996039999966  0.7167935330000006  0.0000867951480998
  0.2007996039999966  0.7832064669999994  0.9999132048519002
  0.4608436359999999  0.3392510139999985  0.9999480514647985
  0.9608436358000034  0.1607489860000015  0.0000519485352015
  0.5391563640000001  0.6607489860000015  0.0000519485352015
  0.0391563641999966  0.8392510139999985  0.9999480514647985
  0.1761774240000022  0.5047927330000022  0.9998557197479983
  0.6761774240000022  0.9952072669300023  0.0001442802520017
  0.8238225759999978  0.4952072669999978  0.0001442802520017
  0.3238225759999978  0.0047927330699977  0.9998557197479983
  0.3244409970000035  0.4271219150000007  0.9998804481249977
  0.8244409970000035  0.0728780852000028  0.0001195518750023
  0.6755590029999965  0.5728780849999993  0.0001195518750023
  0.1755590029999965  0.9271219147999972  0.9998804481249977
  0.1482879060000002  0.3701983340000012  0.9999085186376035
  0.6482879060000002  0.1298016659999988  0.0000914813623965
  0.8517120939999998  0.6298016659999988  0.0000914813623965
  0.3517120939999998  0.8701983340000012  0.9999085186376035
  0.1306728039999996  0.2355217539999970  0.9999607288438028
  0.6306728039999996  0.2644782460000030  0.0000392711561972
  0.8693271960000004  0.7644782460000030  0.0000392711561972
  0.3693271960000004  0.7355217539999970  0.9999607288438028
  0.1788118600000033  0.6261946990000027  0.9997961385420027
  0.6788118600000033  0.8738053020000009  0.0002038614579973
```

```
  0.8211881399999967  0.3738053009999973  0.0002038614579973
  0.3211881399999967  0.1261946990000027  0.9997961385420027
  0.0531356185000007  0.5800141929999967  0.9998663121710010
  0.5531356190000025  0.9199858065000015  0.0001336878289990
  0.9468643814999993  0.4199858070000033  0.0001336878289990
  0.4468643809999975  0.0800141934999985  0.9998663121710010
  0.1086396620000016  0.1145546629999998  0.9999757606757029
  0.6086396620000016  0.3854453370000002  0.0000242393242971
  0.8913603379999984  0.8854453370000002  0.0000242393242971
  0.3913603379999984  0.6145546629999998  0.9999757606757029
```

1D, POSCAR format

```
Melon_1D_POSCAR_20A_BOX_631Gdp_with_spec
   1.00000000000000
    13.7957847100999995    0.0000000000000000    0.0000000000000000
     0.0000000000000000   20.0000000000000000    0.0000000000000000
     0.0000000000000000    0.0000000000000000   20.0000000000000000
   N    C    H
    18    12     6
Direct
  0.1667807669999988  0.9678681898000008  0.0469277532000021
  0.0825875664000009  0.8712281079999968  0.0115274149000015
  0.9959074685899978  0.9694450580999998  0.0466805171000004
  0.3376540530000014  0.9694445772000009  0.0466806883000004
  0.2509735559999982  0.8712277910000026  0.0115277144999979
  0.0792115702000018  0.0613448450000007  0.0867008641000027
  0.2543504799999994  0.0613442606000021  0.0867016433000032
  0.1667814990000025  0.1497089209999984  0.1263192890000013
  0.4167803779999986  0.8769248500000018  0.0040541151600024
  0.4959076569999965  0.9692073833000023  0.9609177844000030
  0.6667807560000014  0.9676258876000006  0.9606714813999986
  0.5825872770000018  0.8711861399999989  0.9966138712499983
  0.8376537819999967  0.9692076376000003  0.9609204365999986
  0.7509731820000027  0.8711861829999989  0.9966150484999972
  0.5792114959999992  0.0608871091000012  0.9203960992999995
  0.7543505740000001  0.0608875276999967  0.9203977008999971
  0.6667811209999996  0.1490314130000030  0.8802910530000005
  0.9167801724999975  0.8769247769999993  0.0040563740500019
  0.0785383967999991  0.0006712217319986  0.0603126942000003
  0.1667805900000019  0.9014543063000033  0.0235531566000020
  0.0027837594800033  0.9083325836000000  0.0209522382000031
  0.2550232549999976  0.0006709770350000  0.0603128122999976
  0.3307773940000018  0.9083323983999989  0.0209516939999972
  0.1667810829999965  0.0883203595000026  0.0988443601999975
  0.5027837989999995  0.9082384008999966  0.9869845608999981
  0.5785383979999992  0.0003565362329994  0.9471105894999994
  0.6667804450000006  0.9013441115999967  0.9844182271000008
  0.7550233190000029  0.0003566922639990  0.9471117877999973
  0.8307769999999977  0.9082384712000007  0.9869864393999990
  0.6667811129999990  0.0877977004000030  0.9081093958999986
  0.9167807238999970  0.8263798489999985  0.0041944329599986
  0.1031545359999981  0.1724771769999975  0.1356503860000018
  0.2304088070000034  0.1724760139999972  0.1356518540000025
  0.4167798929999975  0.8263799220000010  0.0041922542200012
  0.7304081790000012  0.1717467120000009  0.8708323899999968
  0.6031538909999981  0.1717459110000021  0.8708308790000032
```

2.2 Structures in .gui format

Fina, .gui format

```
   3   1   2 E -5.7833181922602E+03 DE-1.6E-08( 28)
  0.127337335437E+02  0.776635721440E-15  0.254837198546E-02
 -0.130205882973E-17  0.642852794503E+01  0.785097899967E-19
  0.332504561112E-02  0.101919047805E-14  0.167106790624E+02
  4
  0.100000000000E+01  0.000000000000E+00 -0.123259516441E-31
  0.000000000000E+00  0.100000000000E+01  0.000000000000E+00
  0.000000000000E+00  0.000000000000E+00  0.100000000000E+01
  0.000000000000E+00  0.000000000000E+00  0.000000000000E+00
 -0.100000000000E+01  0.000000000000E+00  0.123259516441E-31
```

```
-0.122464679915E-15  0.100000000000E+01 -0.122464679915E-15
 0.000000000000E+00  0.000000000000E+00 -0.100000000000E+01
-0.651029414865E-18  0.321426397251E+01  0.392548949984E-19
-0.100000000000E+01  0.000000000000E+00  0.123259516441E-31
 0.000000000000E+00 -0.100000000000E+01  0.000000000000E+00
 0.000000000000E+00  0.000000000000E+00 -0.100000000000E+01
 0.000000000000E+00  0.000000000000E+00  0.000000000000E+00
 0.100000000000E+01  0.000000000000E+00 -0.123259516441E-31
 0.122464679915E-15 -0.100000000000E+01  0.122464679915E-15
 0.000000000000E+00  0.000000000000E+00  0.100000000000E+01
-0.651029414865E-18  0.321426397251E+01  0.392548949984E-19
72
   6      3.057997331968      1.607131986257     -6.303404523503
   6      1.853020016525      1.607131986257      2.065990969036
   6     -4.509512648714      1.607131986257      3.182438066877
   6     -3.305614199772      1.607131986257     -5.190711892751
   6      5.121301967258      1.607131986257     -7.240881604316
   6     -0.201419040267      1.607131986257      1.136987638762
   6      6.169963658174      1.607131986257      4.118284644187
   6     -1.244585185908      1.607131986257     -4.252150493662
   6      1.496704062899      1.607131986257      6.694962055120
   6      3.412963296025      1.607131986257     -1.650763908765
   6     -2.961200866613      1.607131986257      6.907236667026
   6     -4.875676120004      1.607131986257     -1.469416415994
   6      3.384054852528      1.607131986257      7.996251447563
   6      1.530455761679      1.607131986257     -0.341238846610
   6     -4.838873373538      1.607131986257      5.592610433864
   6     -2.982966452094      1.607131986257     -2.780284482789
   6      1.141152210303      1.607131986257     -7.759000461391
   6      3.769469296675      1.607131986257      0.603845925145
   6     -2.600009170685      1.607131986257      4.647562269468
   6     -5.224101491768      1.607131986257     -3.729434153034
   6      0.912755449709      1.607131986257     -5.499727566820
   6      4.001915771098      1.607131986257      2.861062215101
   6     -2.363074521774      1.607131986257      2.392015374961
   6     -5.452129053294      1.607131986257     -5.993044836874
   1      1.530384606311      1.607131986257      4.660198740480
   1      3.371278791192      1.607131986257     -3.691273170773
   1     -3.011565480755      1.607131986257     -7.760101215975
   1     -4.840474517706      1.607131986257      0.567516167068
   1     -0.068283305472      1.607131986257      5.433335251077
   1      4.980875506586      1.607131986257     -2.910366067083
   1     -1.399560353359      1.607131986257     -8.528577636552
   1      6.296780779176      1.607131986257     -0.206112035875
   1      0.629033070086      1.607131986257     -3.471980785814
   1      4.282728050913      1.607131986257      4.895920610999
   1     -2.083967702497      1.607131986257      0.365680825900
   1     -5.732037369061      1.607131986257     -8.015053670383
   7      4.697743073662      1.607131986257     -8.508980589624
   7      0.216496540760      1.607131986257     -0.136418283765
   7     -6.150602683033      1.607131986257      5.387700974463
   7     -1.669524275571      1.607131986257     -2.979130959379
   7      2.858065298090      1.607131986257      6.783084690256
   7      2.055917516309      1.607131986257     -1.558592071001
   7     -4.317922276689      1.607131986257      6.812786013800
   7     -3.509413654851      1.607131986257     -1.561968409348
   7      0.634140397127      1.607131986257      7.747015492117
   7      4.276383115130      1.607131986257     -0.601394269065
   7     -2.094388070909      1.607131986257      5.860369309563
   7     -5.734539430600      1.607131986257     -2.524628684504
   7      2.528724874346      1.607131986257     -7.588564315073
   7      2.382874423756      1.607131986257      0.779864434082
   7     -3.983997383196      1.607131986257      4.472318492726
   7     -3.835784886664      1.607131986257     -3.901863546333
   7      2.243112422525      1.607131986257     -5.248076068953
   7      2.678381764579      1.607131986257      3.117467277452
   7     -3.684651827484      1.607131986257      2.134217718777
   7     -4.126518632935      1.607131986257     -6.239933007431
   7      0.947634073851      1.607131986257      5.496887075608
   7      3.960676101331      1.607131986257     -2.854383268570
   7     -2.419026870990      1.607131986257     -8.597696384328
   7     -5.419329239058      1.607131986257     -0.273195230185
   7      0.130664456636      1.607131986257     -4.364728272727
   7      4.785840886241      1.607131986257      4.002044306546
   7     -1.578617401275      1.607131986257      1.254943133303
   7     -6.235570471596      1.607131986257     -7.124653521813
   7      0.343167936258      1.607131986257     -6.690517059716
   7      4.573562998633      1.607131986257      1.670816748212
   7     -1.794262885060      1.607131986257      3.587933457031
   7     -6.023342745771      1.607131986257     -4.795818387979
   7      4.371533776281      1.607131986257     -6.130427861806
   7      0.545207976053      1.607131986257      2.241835497802
   7     -5.820673835238      1.607131986257      3.010456506661
   7     -1.993753590009      1.607131986257     -5.358149958606
```

$P2_1/a$, .gui format

```
   3   1   2 E -2.8916590116591E+03 DE 1.0E-10( 71)
 0.126979868482E+02  0.690566271567E-15 -0.468715797446E+00
-0.120367831600E-15  0.167371449136E+02 -0.353611766341E-16
-0.329236477339E+01  0.290781543338E-15  0.334032352102E+01
 4
 0.100000000000E+01  0.000000000000E+00 -0.222044604925E-15
 0.123259516441E-31  0.100000000000E+01  0.123259516441E-31
 0.000000000000E+00  0.000000000000E+00  0.100000000000E+01
 0.000000000000E+00  0.000000000000E+00  0.000000000000E+00
-0.100000000000E+01  0.000000000000E+00  0.222044604925E-15
-0.122464679915E-15  0.100000000000E+01 -0.298506990459E-15
 0.000000000000E+00  0.000000000000E+00 -0.100000000000E+01
 0.634899342412E+01  0.836857245676E+01 -0.234357898723E+00
-0.100000000000E+01  0.000000000000E+00  0.222044604925E-15
-0.123259516441E-31 -0.100000000000E+01 -0.123259516441E-31
 0.000000000000E+00  0.000000000000E+00 -0.100000000000E+01
 0.000000000000E+00  0.000000000000E+00  0.000000000000E+00
 0.100000000000E+01  0.000000000000E+00 -0.222044604925E-15
 0.122464679915E-15 -0.100000000000E+01  0.298506990459E-15
 0.000000000000E+00  0.000000000000E+00  0.100000000000E+01
 0.634899342412E+01  0.836857245676E+01 -0.234357898723E+00
18
   6      0.521665369000      4.750502748258      3.306273209870
   6      2.578561668334      5.690189463963      3.239583695147
   6      2.245381051536     -8.275601547364     -0.034888707435
   6      0.838451626440      7.164056351287      3.247407233266
   6      1.898917093427      6.205029740639      0.033947985230
   6      1.678801547643      3.943628266459      0.070099895064
   7      2.157360790131      6.956521618553      3.202100193248
   7      0.311611930246     -8.363354001611      3.234560421537
   7      1.385049588241      7.408801562068      0.038414745832
   7      3.282716367986      6.036488811406     -0.035960751192
   7      3.001570209113      3.697427202764     -0.003756706919
   7      1.688849054233     -7.079659440515     -0.045724329541
   7      0.902062134564      2.801769353712      0.082545913261
   7      1.104428774512      5.134753649273      0.119665586402
   7      1.834883486644      4.580250263324      3.289623922487
   1      2.265112359369     -6.237664803828     -0.118888990046
   1      0.671917952906     -7.024172965055      0.009530475265
   1      1.409993182503      1.911091045191      0.082423092108
```

S1, .gui format

```
   3   1   2 E -2.8916560987187E+03 DE 8.6E-11( 71)
 0.167572417171E+02  0.104931238299E-14  0.377158690172E+00
 0.214996594033E-16  0.127336342423E+02  0.179189746922E-16
 0.337663121126E+01  0.294738444724E-15  0.331878052147E+01
 4
 0.100000000000E+01  0.000000000000E+00  0.000000000000E+00
 0.000000000000E+00  0.100000000000E+01  0.123259516441E-31
 0.000000000000E+00  0.000000000000E+00  0.100000000000E+01
 0.000000000000E+00  0.000000000000E+00  0.000000000000E+00
-0.100000000000E+01  0.000000000000E+00  0.000000000000E+00
-0.122464679915E-15  0.100000000000E+01 -0.507265313324E-16
 0.000000000000E+00  0.000000000000E+00 -0.100000000000E+01
 0.837862085854E+01  0.636681712114E+01  0.188579345085E+00
-0.100000000000E+01  0.000000000000E+00  0.000000000000E+00
 0.000000000000E+00 -0.100000000000E+01 -0.123259516441E-31
 0.000000000000E+00  0.000000000000E+00 -0.100000000000E+01
 0.000000000000E+00  0.000000000000E+00  0.000000000000E+00
 0.100000000000E+01  0.000000000000E+00  0.000000000000E+00
 0.122464679915E-15 -0.100000000000E+01  0.507265313324E-16
 0.000000000000E+00  0.000000000000E+00  0.100000000000E+01
 0.837862085854E+01  0.636681712114E+01  0.188579345085E+00
18
   6      1.373462709733      3.789161887718     -3.256851996808
   6      2.295698466527      5.849044150154     -3.255657352212
   6     -4.912997760158      2.242957332803      3.169374799393
   6      3.777485694027      4.123469311122     -3.177178704584
   6      2.835884674998      1.879615758440     -3.105593088666
   6      0.581433364005      1.639188634595     -3.185949129453
   7      3.568723522324      5.433737745899     -3.225496637806
   7      4.997861562051      3.602539545942     -3.124357001620
   7      4.045662863338      1.375933403295     -3.058545815289
   7      2.660425310947      3.264546659161     -3.181513647372
   7      0.326740637349      2.961655722479     -3.300205604089
   7     -3.708135165692      1.699999756316      3.203430355043
   7      2.825726443085      0.857737851273      0.110418194031
   7      1.773432500153      1.077096199934     -3.070237868739
```

```
   7      1.193530593011      5.097337335111     -3.290193377398
   1     -2.868202618136      2.282462548982      3.181487430844
   1     -3.641242635243      0.682016675924      3.198848197734
   1      1.933764853731      1.353309557100      0.050304470639
```

S2, .gui format

```
   3   1   1 E -2.8916593606854E+03 DE 1.0E-10( 73)
  0.481848877294E+01 -0.313144365534E+00 -0.272739127308E+00
  0.145782279636E+00  0.867913772870E+01 -0.230330572336E+00
 -0.149404169984E+01 -0.217497080094E+01  0.164965529405E+02
  2
  0.100000000000E+01  0.000000000000E+00  0.000000000000E+00
  0.000000000000E+00  0.100000000000E+01  0.000000000000E+00
  0.000000000000E+00  0.000000000000E+00  0.100000000000E+01
  0.000000000000E+00  0.000000000000E+00  0.000000000000E+00
 -0.100000000000E+01  0.000000000000E+00  0.000000000000E+00
  0.000000000000E+00 -0.100000000000E+01  0.000000000000E+00
  0.000000000000E+00  0.000000000000E+00 -0.100000000000E+01
  0.000000000000E+00  0.000000000000E+00  0.000000000000E+00
 36
    6     -0.948432057984      2.055743182214      4.645432187921
    6      1.251442368914      2.110396328899     -3.666838776254
    6      0.824227214177      3.216872164150      5.433623633766
    6     -0.128716752061      0.645919803223     -2.624617640009
    6     -1.429902980462      0.497997531787      8.325654945406
    6     -1.626102153994      2.887158851459      0.109237706786
    6     -0.225201138548      1.886530960385      6.959931212699
    6      1.475156803020      1.571673193680     -1.299795385337
    6     -2.170007994049      0.657833518810      6.172905655032
    6     -1.814978085334      3.446422849480     -2.101814747493
    6      2.033455304321      0.545482671895      3.719144725267
    6     -2.088011196588      3.905928777469     -4.307890105294
    1      0.516206273873      2.328371522637     -6.209975959042
    1     -1.233808001975      2.565107876841      2.082417195118
    1     -0.898589631779      1.471972870697     -6.876335647488
    1     -0.135246057843      3.664431523482      1.214174263485
    1      1.425335550723      0.673446135507      1.761729897350
    1     -2.411078204521     -4.326388682676     -6.070639641495
    7      0.765027324061      2.738249125051      6.680391431049
    7      0.429789711929      0.751963889195     -1.417238129046
    7     -0.390346992406      1.364712069822      8.162277303594
    7      2.118433948462      1.735796220842     -0.158893279683
    7      2.496077645296     -0.174784967688      7.090028134422
    7     -1.167897992408      3.582517882635     -0.969568621836
    7     -1.114936814990      1.536521808609      5.924072899829
    7      1.901589230097      2.279415814932     -2.447900055920
    7     -1.774100192560      1.688551683851      3.666577312478
    7      1.667846585203      2.777951190487     -4.739445901623
    7     -0.115129533168      2.117667136715     -6.987231164613
    7     -0.963830703902      3.070376315644      1.234350653109
    7      1.219887272791      0.209926449930      2.654430164087
    7     -1.871688376928     -4.100217762743     -5.229229381279
    7      1.788385374393      0.047209503677      4.920257773615
    7     -1.409340273325      4.101655536410     -3.189762695087
    7      0.026545759426      2.916550354805      4.405017221449
    7      0.228598493178      1.271034577035     -3.751955850912
```

2D, .gui format

```
   2   1   2 E -2.8915892342465E+03 DE 1.1E-10( 67)
  0.127325346371E+02  0.779642889420E-15  0.000000000000E+00
 -0.502747107234E-17  0.167944365802E+02  0.000000000000E+00
  0.000000000000E+00  0.000000000000E+00  0.500000000000E+03
  4
  0.100000000000E+01  0.000000000000E+00  0.000000000000E+00
  0.000000000000E+00  0.100000000000E+01  0.000000000000E+00
  0.000000000000E+00  0.000000000000E+00  0.100000000000E+01
  0.000000000000E+00  0.000000000000E+00  0.000000000000E+00
  0.100000000000E+01  0.000000000000E+00 -0.122464679915E-15
  0.122464679915E-15 -0.100000000000E+01  0.000000000000E+00
  0.000000000000E+00  0.000000000000E+00 -0.100000000000E+01
  0.636626731856E+01  0.839721829010E+01  0.000000000000E+00
 -0.100000000000E+01  0.000000000000E+00  0.000000000000E+00
  0.000000000000E+00 -0.100000000000E+01  0.000000000000E+00
  0.000000000000E+00  0.000000000000E+00 -0.100000000000E+01
```

```
 0.000000000000E+00  0.000000000000E+00  0.000000000000E+00
-0.100000000000E+01  0.000000000000E+00  0.122464679915E-15
-0.122464679915E-15  0.100000000000E+01  0.000000000000E+00
 0.000000000000E+00  0.000000000000E+00  0.100000000000E+01
 0.636626731856E+01  0.839721829010E+01  0.000000000000E+00
18
   6      3.809501911592      4.756387326080     -0.001124276182
   6      5.867611093156      5.697759553710     -0.000850153475
   6      2.242874895853     -8.316425614532     -0.001569281921
   6      4.130750265174      7.173594493673     -0.001338641653
   6      1.887940944680      6.217303996404     -0.000914765531
   6      1.663771053819      3.955272344272     -0.000418670650
   7      5.446715853918      6.967434822135     -0.001171273440
   7      3.604237392771      8.386523468794     -0.001607534897
   7      1.379030565788      7.424035035418     -0.001076916020
   7      3.277243121007      6.045632666798     -0.001169857008
   7      2.990304932981      3.704668095038     -0.000959040903
   7      1.694144383358     -7.118639646038     -0.001938671289
   7      0.881738149920      2.817175740328      0.000181535975
   7      1.090351960995      5.147805801682     -0.000387466893
   7      5.121941864305      4.588582922793     -0.001110657324
   1      2.275275173564     -6.277054172264     -0.001909039610
   1      0.675835163141     -7.053838166707     -0.001335436379
   1      1.383186083433      1.923569341726     -0.000137111132
```

1D, .gui format

```
  1   1   1 E -1.4457186125671E+03 DE 1.3E-10( 59)
 0.137948836966E+02  0.000000000000E+00  0.000000000000E+00
 0.000000000000E+00  0.500000000000E+03  0.000000000000E+00
 0.000000000000E+00  0.000000000000E+00  0.500000000000E+03
 1
 0.100000000000E+01  0.000000000000E+00  0.000000000000E+00
 0.000000000000E+00  0.100000000000E+01  0.000000000000E+00
 0.000000000000E+00  0.000000000000E+00  0.100000000000E+01
 0.000000000000E+00  0.000000000000E+00  0.000000000000E+00
36
   6      1.083272170075      0.014019798038      1.211821559755
   6      2.300718157654     -1.968670519954      0.472370367668
   6      0.038286029435     -1.830839648319      0.419850643605
   6      3.518131938515      0.014064245650      1.211754678801
   6      4.563148150377     -1.830793393405      0.419818074031
   6      2.300691678914      1.763657385823      1.989682568914
   6     -6.859140945050     -1.832685352773     -0.261125929106
   6     -5.814131299707      0.007806170251     -1.063160261901
   6     -4.596716337180     -1.970883430744     -0.313014293415
   6     -3.379273436020      0.007778145502     -1.063190778052
   6     -2.334289892213     -1.832722999639     -0.261144588087
   6     -4.596692501329      1.753125284955     -1.850631052399
   1     -1.148005991519     -3.469671152746      0.083869334178
   1      1.422899758283      3.443073516669      2.734043803166
   1      3.178464952458      3.443118282402      2.733963803887
   1      5.749454687424     -3.469625432404      0.083896321705
   1     -3.718898339344      3.428309303175     -2.604467845378
   1     -5.474467976781      3.428337112263     -2.604427018878
   7      2.300706847501     -0.641462653449      0.942869841381
   7      1.139259528458     -2.572735709149      0.230798493386
   7     -0.056678075694     -0.609295181765      0.936125446631
   7      4.658090217691     -0.609223299957      0.936034172773
   7      3.462186728956     -2.572711002362      0.230780400882
   7      1.092583689619      1.225567677570      1.743864739308
   7      3.508805109129      1.225625878327      1.743766696111
   7      2.300685329669      2.988269832191      2.546031266135
   7      5.749450756994     -2.458739205170      0.081092908606
   7      6.840797049880     -0.613959361692     -0.784022162110
   7     -4.596706434265     -0.646260040804     -0.790743630975
   7     -5.758183380603     -2.573581160622     -0.068090083490
   7     -2.239324797201     -0.614010501785     -0.784070285916
   7     -3.435257121491     -2.573601060455     -0.068101326470
   7     -5.804805378366      1.216458052684     -1.601751608091
   7     -3.388584930468      1.216420361611     -1.601803451344
   7     -4.596685864693      2.974625222432     -2.413780134028
   7     -1.148005243138     -2.458785162347      0.081089328716
```

2.3 Structures in .cif format

Fina, .cif format

```
# CIF file
# This file was generated by FINDSYM
# Harold T. Stokes, Branton J. Campbell, Dorian M. Hatch
# Brigham Young University, Provo, Utah, USA

data_findsym-output

_symmetry_space_group_name_H-M 'P 1 21/m 1'
_symmetry_Int_Tables_number 11

_cell_length_a      12.73400
_cell_length_b       6.42900
_cell_length_c      16.71100
_cell_angle_alpha   90.00000
_cell_angle_beta    90.0
_cell_angle_gamma   90.00000

loop_
_space_group_symop_operation_xyz
x,y,z
-x,y+1/2,-z
-x,-y,-z
x,-y+1/2,z

loop_
_atom_site_label
_atom_site_type_symbol
_atom_site_fract_x
_atom_site_fract_y
_atom_site_fract_z
_atom_site_occupancy
N1  N   -0.36905   0.25000  -0.49075   1.00000
N2  N   -0.01700   0.25000   0.00817   1.00000
N3  N    0.48310   0.25000  -0.32248   1.00000
N4  N    0.13106   0.25000   0.17826   1.00000
N5  N   -0.22434   0.25000  -0.40588   1.00000
N6  N   -0.16148   0.25000   0.09329   1.00000
N7  N    0.33920   0.25000  -0.40774   1.00000
N8  N    0.27558   0.25000   0.09343   1.00000
N9  N   -0.04968   0.25000  -0.46359   1.00000
N10 N   -0.33584   0.25000   0.03604   1.00000
N11 N    0.16457   0.25000  -0.35072   1.00000
N12 N    0.45030   0.25000   0.15101   1.00000
N13 N   -0.19870   0.25000   0.45414   1.00000
N14 N   -0.18712   0.25000  -0.04664   1.00000
N15 N    0.31294   0.25000  -0.26768   1.00000
N16 N    0.30117   0.25000   0.23345   1.00000
N17 N   -0.17624   0.25000   0.31408   1.00000
N18 N   -0.21029   0.25000  -0.18652   1.00000
N19 N    0.28939   0.25000  -0.12776   1.00000
N20 N    0.32396   0.25000   0.37336   1.00000
N21 N   -0.07433   0.25000  -0.32893   1.00000
N22 N   -0.31108   0.25000   0.17086   1.00000
N23 N    0.18984   0.25000  -0.48553   1.00000
N24 N    0.42558   0.25000   0.01628   1.00000
N25 N   -0.01033   0.25000   0.26120   1.00000
N26 N   -0.37578   0.25000  -0.23943   1.00000
N27 N    0.12399   0.25000  -0.07512   1.00000
N28 N    0.48958   0.25000   0.42628   1.00000
N29 N   -0.02705   0.25000   0.40038   1.00000
N30 N   -0.35914   0.25000  -0.09993   1.00000
N31 N    0.14096   0.25000  -0.21473   1.00000
N32 N    0.47295   0.25000   0.28692   1.00000
N33 N   -0.34340   0.25000   0.36691   1.00000
N34 N   -0.04278   0.25000  -0.13415   1.00000
N35 N    0.45715   0.25000  -0.18022   1.00000
N36 N    0.15649   0.25000   0.32062   1.00000
C1  C   -0.24025   0.25000   0.37725   1.00000
C2  C   -0.14549   0.25000  -0.12361   1.00000
C3  C    0.35419   0.25000  -0.19050   1.00000
C4  C    0.25951   0.25000   0.31058   1.00000
C5  C   -0.40230   0.25000   0.43337   1.00000
C6  C    0.01584   0.25000  -0.06804   1.00000
C7  C   -0.48447   0.25000  -0.24637   1.00000
C8  C    0.09767   0.25000   0.25444   1.00000
C9  C   -0.11743   0.25000  -0.40062   1.00000
C10 C   -0.26805   0.25000   0.09883   1.00000
C11 C    0.23266   0.25000  -0.41338   1.00000
C12 C    0.38287   0.25000   0.08787   1.00000
C13 C   -0.26563   0.25000  -0.47847   1.00000
C14 C   -0.12019   0.25000   0.02044   1.00000
```

```
C15 C    0.38009   0.25000  -0.33473   1.00000
C16 C    0.23421   0.25000   0.16634   1.00000
C17 C   -0.08974   0.25000   0.46433   1.00000
C18 C   -0.29601   0.25000  -0.03609   1.00000
C19 C    0.20425   0.25000  -0.27815   1.00000
C20 C    0.41020   0.25000   0.22311   1.00000
C21 C   -0.07177   0.25000   0.32912   1.00000
C22 C   -0.31423   0.25000  -0.17116   1.00000
C23 C    0.18561   0.25000  -0.14317   1.00000
C24 C    0.42807   0.25000   0.35857   1.00000
H1  H   -0.12011   0.25000  -0.27886   1.00000
H2  H   -0.26481   0.25000   0.22093   1.00000
H3  H    0.23638   0.25000   0.46434   1.00000
H4  H    0.38014   0.25000  -0.03402   1.00000
H5  H    0.00545   0.25000  -0.32514   1.00000
H6  H   -0.39120   0.25000   0.17422   1.00000
H7  H    0.10978   0.25000  -0.48965   1.00000
H8  H   -0.49450   0.25000   0.01241   1.00000
H9  H   -0.04945   0.25000   0.20778   1.00000
H10 H   -0.33625   0.25000  -0.29293   1.00000
H11 H    0.16366   0.25000  -0.02191   1.00000
H12 H    0.45002   0.25000   0.47957   1.00000
```

S1, .cif format

```
# CIF file
# This file was generated by FINDSYM
# Harold T. Stokes, Branton J. Campbell, Dorian M. Hatch
# Brigham Young University, Provo, Utah, USA

data_findsym-output

_symmetry_space_group_name_H-M 'P 1 21/c 1'
_symmetry_Int_Tables_number 14

_cell_length_a      11.64133
_cell_length_b      12.73700
_cell_length_c      11.79379
_cell_angle_alpha   90.00000
_cell_angle_beta    23.31663
_cell_angle_gamma   90.00000

loop_
_space_group_symop_operation_xyz
x,y,z
-x,y+1/2,-z+1/2
-x,-y,-z
x,-y+1/2,z+1/2

loop_
_atom_site_label
_atom_site_type_symbol
_atom_site_fract_x
_atom_site_fract_y
_atom_site_fract_z
_atom_site_occupancy
N1  N   -0.18268  -0.07329  -0.23560   1.00000
N2  N    0.00079  -0.21695   0.49980   1.00000
N3  N   -0.09673  -0.39186  -0.34062   1.00000
N4  N   -0.27904  -0.24368  -0.08120   1.00000
N5  N    0.43036  -0.26763   0.34455   1.00000
N6  N    0.16293  -0.36615   0.26243   1.00000
N7  N    0.34618  -0.43280   0.48793   1.00000
N8  N   -0.36071  -0.41552   0.06138   1.00000
N9  N   -0.46833  -0.09989   0.19103   1.00000
C1  C   -0.44124  -0.20259   0.15495   1.00000
C2  C   -0.33503  -0.04080  -0.00737   1.00000
C3  C    0.01771  -0.32369   0.47918   1.00000
C4  C   -0.14958  -0.17615  -0.27854   1.00000
C5  C   -0.24478  -0.35241  -0.12157   1.00000
C6  C    0.48075  -0.37145   0.28561   1.00000
H1  H    0.25545  -0.32025   0.11730   1.00000
H2  H    0.17018  -0.44603   0.25066   1.00000
H3  H    0.23242  -0.39387  -0.34757   1.00000


# end_of_file
```

S2, .cif format

```
# CIF file
# This file was generated by FINDSYM
# Harold T. Stokes, Branton J. Campbell, Dorian M. Hatch
# Brigham Young University, Provo, Utah, USA

data_findsym-output

_symmetry_space_group_name_H-M 'P -1'
_symmetry_Int_Tables_number 2

_cell_length_a      16.50800
_cell_length_b       8.98700
_cell_length_c       4.73900
_cell_angle_alpha   86.85800
_cell_angle_beta    84.60200
_cell_angle_gamma  100.81600

loop_
_space_group_symop_operation_xyz
x,y,z
-x,-y,-z

loop_
_atom_site_label
_atom_site_type_symbol
_atom_site_fract_x
_atom_site_fract_y
_atom_site_fract_z
_atom_site_occupancy
N1  N    0.41528   0.42711  -0.27679   1.00000
N2  N   -0.08339   0.07223  -0.05517   1.00000
N3  N    0.49998   0.28400  -0.06510   1.00000
N4  N    0.00092   0.21841  -0.42919   1.00000
N5  N    0.44234   0.11293   0.34805   1.00000
N6  N   -0.05785   0.38952   0.27320   1.00000
N7  N    0.36061   0.26085   0.12607   1.00000
N8  N   -0.13918   0.24225  -0.34169   1.00000
N9  N    0.22010   0.23563   0.30318   1.00000
N10 N  -0.27946   0.26152  -0.24942   1.00000
N11 N  -0.42399   0.13220   0.16082   1.00000
N12 N   0.07698   0.36692   0.18916   1.00000
N13 N   0.16653   0.07269  -0.30778   1.00000
N14 N  -0.33277   0.42898   0.47581   1.00000
N15 N   0.30733   0.09595  -0.46588   1.00000
N16 N  -0.19372   0.41199   0.36576   1.00000
N17 N   0.27382   0.40506  -0.08063   1.00000
N18 N  -0.22648   0.09203   0.02888   1.00000
C1  C    0.28366   0.30133   0.11550   1.00000
C2  C   -0.21637   0.19817  -0.18421   1.00000
C3  C    0.34006   0.46309  -0.26461   1.00000
C4  C   -0.15958   0.03558   0.08210   1.00000
C5  C   -0.49499   0.17786   0.14598   1.00000
C6  C    0.00559   0.32321   0.34804   1.00000
C7  C    0.42769   0.32561  -0.07683   1.00000
C8  C   -0.07138   0.17631  -0.27436   1.00000
C9  C    0.37081   0.15435   0.33864   1.00000
C10 C  -0.12957   0.35058   0.42895   1.00000
C11 C   0.23522   0.13597  -0.49472   1.00000
C12 C  -0.26472   0.36663  -0.47186   1.00000
H1  H   -0.37413   0.17442   0.01482   1.00000
H2  H    0.12684   0.31915   0.22770   1.00000
H3  H   -0.42088   0.05270   0.31979   1.00000
H4  H    0.07946   0.44127   0.01673   1.00000
H5  H    0.11339   0.11360  -0.33247   1.00000
H6  H   -0.38656   0.38534  -0.39669   1.00000


# end_of_file
```